Université de Montréal

Mechanism and Prediction of Post-Operative Atrial Fibrillation Based on Atrial Electrograms

par

Feng Xiong

Institut de génie biomédical
Département de physiologie
Faculté de Médecine

Thèse présentée à la Faculté des études supérieures
en vue de l'obtention du grade de Philosophiae Doctor (Ph.D.)
en génie biomédical

Mars 2012

Université de Montréal
Faculté des études supérieures

Cette thèse intitulée:

Mechanism and Prediction of Post-Operative Atrial Fibrillation Based on Atrial Electrograms

Présentée par :
Feng Xiong

A été évaluée par un jury composé des personnes suivantes :

Dr Pierre Savard, président-rapporteur
Dr Alain Vinet, directeur de recherche
Dr Damien Garcia, membre du jury
MD Paul Dorian, examinateur externe
MD Isabelle Greiss, représentant du doyen de la FES

Abstract

Atrial fibrillation (AF) is an abnormal heart rhythm (cardiac arrhythmia). In AF, the atrial contraction is rapid and irregular, and the filling of the ventricles becomes incomplete, leading to reduce cardiac output. Atrial fibrillation may result in symptoms of palpitations, fainting, chest pain, or even heart failure. AF is an also an important risk factor for stroke. Coronary artery bypass graft surgery (CABG) is a surgical procedure to restore the perfusion of the cardiac tissue in case of severe coronary heart disease. 10% to 65% of patients who never had a history of AF develop AF on the second or third post CABG surgery day. The occurrence of postoperative AF is associated with worse morbidity and longer and more expensive intensive-care hospitalization. The fundamental mechanism responsible of AF, especially for post-surgery patients, is not well understood. Identification of patients at high risk of AF after CABG would be helpful in prevention of postoperative AF. The present project is based on the analysis of cardiac electrograms recorded in patients after CABG surgery. The first aim of the research is to investigate whether the recordings display typical changes prior to the onset of AF. A second aim is to identify predictors that can discriminate the patients that will develop AF.

Recordings were made by the team of Dr. Pierre Pagé on 137 patients treated with CABG surgery. Three unipolar electrodes were sutured on the epicardium of the atria to record continuously during the first 4 post-surgery days. As a first stage of the research, an automatic and unsupervised algorithm was developed to detect and distinguish atrial and ventricular activations on each channel, and join together the activation of the different channels belonging to the same cardiac event. The algorithm was developed and optimized on a training set, and its performance assessed on a test set. Validation software was developed to prepare these two sets and to correct the detections over all recordings that were later used in the analyses. It was complemented with tools to detect, label and validate normal sinus beats, atrial and ventricular premature activations (PAA, PVC) as well as episodes of arrhythmia.

Pre-CABG clinical data were then analyzed to establish the preoperative risk of AF. Age, serum creatinine and prior myocardial infarct were found to be the most important predictors. While the preoperative risk score could to a certain extent predict who will develop AF, it was not correlated with the post-operative time of AF onset.

Then the set of AF patients was analyzed, considering the last two hours before the onset of the first AF lasting for more than 10 minutes. This prolonged AF was found to be usually triggered by a premature atrial PAA most often originating from the left atrium. However, along the two pre-AF hours, the distribution of PAA and of the fraction of these coming from the left atrium was wide and inhomogeneous among the patients. PAA rate, duration of transient atrial arrhythmia, sinus heart rate, and low frequency portion of heart rate variability (LF portion) showed significant changes in last hour before the onset of AF. Comparing all other PAA, the triggering PAA were characterized by their prematurity, the small value of the maximum derivative of the electrogram nearest to the site of origin, as well as the presence of transient arrhythmia and increase LF portion of the sinus heart rate variation prior to the onset of the arrhythmia.

The final step was to compare AF and Non-AF patients to find predictors to discriminate the two groups. Five types of logistic regression models were compared, achieving similar sensitivity, specificity, and ROC curve area, but very low prediction accuracy for Non-AF patients. A weighted moving average method was proposed to design to improve the accuracy for Non-AF patient. Two models were favoured, selected on the criteria of robustness, accuracy, and practicability. Around 70% Non-AF patients were correctly classified, and around 75% of AF patients in the last hour before AF. The *PAA* rate, the fraction of *PAA* initiated in the left atrium, *pNN50*, the atrio-ventricular conduction time, and the correlation between the latter and the heart rhythm were common predictors of these two models.

Key words:
Coronary artery bypass graft surgery, Postoperative Atrial Fibrillation, Atrial Electrogram, statistical analysis, predictor.

Résumé

La fibrillation auriculaire (FA) est une arythmie touchant les oreillettes. En FA, la contraction auriculaire est rapide et irrégulière. Le remplissage des ventricules devient incomplet, ce qui réduit le débit cardiaque. La FA peut entraîner des palpitations, des évanouissements, des douleurs thoraciques ou l'insuffisance cardiaque. Elle augmente aussi le risque d'accident vasculaire. Le pontage coronarien est une intervention chirurgicale réalisée pour restaurer le flux sanguin dans les cas de maladie coronarienne sévère. 10% à 65% des patients qui n'ont jamais subi de FA, en sont victime le plus souvent lors du deuxième ou troisième jour postopératoire. La FA est particulièrement fréquente après une chirurgie de la valve mitrale, survenant alors dans environ 64% des patients. L'apparition de la FA postopératoire est associée à une augmentation de la morbidité, de la durée et des coûts d'hospitalisation. Les mécanismes responsables de la FA postopératoire ne sont pas bien compris. L'identification des patients à haut risque de FA après un pontage coronarien serait utile pour sa prévention. Le présent projet est basé sur l'analyse d'électrogrammes cardiaques enregistrées chez les patients après pontage un aorte-coronaire. Le premier objectif de la recherche est d'étudier si les enregistrements affichent des changements typiques avant l'apparition de la FA. Le deuxième objectif est d'identifier des facteurs prédictifs permettant d'identifier les patients qui vont développer une FA.

Les enregistrements ont été réalisés par l'équipe du Dr Pierre Pagé sur 137 patients traités par pontage coronarien. Trois électrodes unipolaires ont été suturées sur l'épicarde des oreillettes pour enregistrer en continu pendant les 4 premiers jours postopératoires. La première tâche était de développer un algorithme pour détecter et distinguer les activations auriculaires et ventriculaires sur chaque canal, et pour combiner les activations des trois canaux appartenant à un même événement cardiaque. L'algorithme a été développé et optimisé sur un premier ensemble de marqueurs, et sa performance évaluée sur un second ensemble. Un logiciel de validation a été développé pour préparer

ces deux ensembles et pour corriger les détections sur tous les enregistrements qui ont été utilisés plus tard dans les analyses. Il a été complété par des outils pour former, étiqueter et valider les battements sinusaux normaux, les activations auriculaires et ventriculaires prématurées (PAA, PVA), ainsi que les épisodes d'arythmie.

Les données cliniques préopératoires ont ensuite été analysées pour établir le risque préopératoire de FA. L'âge, le niveau de créatinine sérique et un diagnostic d'infarctus du myocarde se sont révélés être les plus importants facteurs de prédiction. Bien que le niveau du risque préopératoire puisse dans une certaine mesure prédire qui développera la FA, il n'était pas corrélé avec le temps de l'apparition de la FA postopératoire.

Pour l'ensemble des patients ayant eu au moins un épisode de FA d'une durée de 10 minutes ou plus, les deux heures précédant la première FA prolongée ont été analysées. Cette première FA prolongée était toujours déclenchée par un PAA dont l'origine était le plus souvent sur l'oreillette gauche. Cependant, au cours des deux heures pré-FA, la distribution des PAA et de la fraction de ceux-ci provenant de l'oreillette gauche était large et inhomogène parmi les patients. Le nombre de PAA, la durée des arythmies transitoires, le rythme cardiaque sinusal, la portion basse fréquence de la variabilité du rythme cardiaque (LF portion) montraient des changements significatifs dans la dernière heure avant le début de la FA.

La dernière étape consistait à comparer les patients avec et sans FA prolongée pour trouver des facteurs permettant de discriminer les deux groupes. Cinq types de modèles de régression logistique ont été comparés. Ils avaient une sensibilité, une spécificité et une courbe opérateur-receveur similaires, et tous avaient un niveau de prédiction des patients sans FA très faible. Une méthode de moyenne glissante a été proposée pour améliorer la discrimination, surtout pour les patients sans FA. Deux modèles ont été retenus, sélectionnés sur les critères de robustesse, de précision, et d'applicabilité. Autour 70% patients sans FA et 75% de patients avec FA ont été correctement identifiés dans la dernière heure avant la FA. Le taux de *PAA*, la fraction des PAA initiés dans l'oreillette gauche, le *pNN50*, le temps de conduction auriculo-ventriculaire, et la corrélation entre

ce dernier et le rythme cardiaque étaient les variables de prédiction communes à ces deux modèles.

Mots-clés :
Pontage coronarien, fibrillation auriculaire postopératoire, électrogramme auriculaire, analyse statistique, facteurs de prédiction.

Contents

Table List

Chapter 1

Chapter 3

Chapter 4

Chapter 5

Figure List

Chapter 1

Chapter 2

Chapter 3

Chapter 4

Chapter 5

Chapter 6

Abbreviation List

A	atrial
AA	time interval between consecutive atrial activations
AAMean	mean of AA
AAStd	standard deviation of AA series
ACE	angiotensin-converting enzyme
AEG	atrial electrogram
AF	atrial fibrillation
ANP	atrial natriuretic peptides
ANS	autonomic nervous system
ArrhyDuration	arrhythmia duration
AV	time interval between consecutive atrial and ventricular activations
AV	atrioventricular
BTI	Basic Time Interval
CABG	coronary artery bypass graft surgery
CANS	Cardiac Autonomic Nervous System
CAP	cell action potential
CHF	congestive heart failure
COPD	chronic obstructive pulmonary disease
COPD	chronic obstructive pulmonary disease
CorrAA_AV	Correlation of *AA* series and *CTAV* series
CorrAA_CTA	Correlation of *AA* series and *CTA* series
CorrAV_CTA	Correlation of AV series and CTA series
CPB	cardiopulmonary bypass time
CRP	C-reative protein
CTA	intra-atrial conduction time
CTAStd	standard deviation of *CTA* series
CTAV	atrio-ventricular conduction time

CTAVMean	mean of *CTAV*
CTAVStd	standard deviation of *CTAV*
DC	Deviation Cohort
DF	discrimination function
dv/dt	the maximum slopes of negative deflections of each atrial activation
ECG	electrocardiogram
ERP	refractory period
FFRW	far field R-waves
FFT	Fast Fourier transformation
FN	False Negative
FP	False Positive
HF	high frequency, 0.15-0.4 Hz
HRV	heart rate variability
HT	hypertension
ICD	implantable cardioverter-defibrillator
LF	low frequency, 0.04-0.15 Hz
LPAA	*PAA* initiated from left atrium
LPAAFraction	LPAA fraction
LVEF	left ventricular ejection fraction
LVEF	left ventricular ejection insufficiency
MAP	monophasic action potential
MI	Myocardial Infarct
Non-AF	without atrial fibrillation
NSAIDs	nonsteroidal anti-inflammatory drugs
PAA	premature atrial activation
PAC	premature atrial complex
pNN50	Proportion of successive with a difference > 50ms
P-Prem	Position value of the prematurity of each triggering PAA
$Prem_{abs}$	absolute prematurity
$Prem_{rel}$	relative prematurity
PreopRisk	Preoperative risk score obtained by logistic regression

PVA	premature ventricular activation
rMSSD	root mean square of difference between successive AA
ROC	Receiver Operating Characteristics
RPAA	*PAA* initiated from right atrium
R_{PAA}	PAA rate
R_{PAA}^{L}	Left PAA rate
R_{PVA}	*PVA* rate
SA	sinoatrial
SAPD	signal-averaged P-wave duration
TN	True Negative
TP	True Positive
UW vs. W	unweighted vs. weighted
V	ventricular
VA	time interval between consecutive ventricular and atrial activations
VV	time interval between consecutive ventricular activations

Acknowledgements

I would like to acknowledge Dr. Alain Vinet, who served as mentor, supervised me and supported me during my M.Sc., Ph.D. study and the research work in Hôpital du Sacré-Coeur. He encouraged me, and believed me to be able to overcome the difficulties. He shared enormous time with me on the project. His strong theoretical background, scientific spirit, and patient supervision, made my research work advanced further. He set a good example for me to be a researcher. I am very fortunate and grateful to have him as my mentor.

I also wish to thank Dr Pierre Pagé, for his contribution of the clinical data of the project, and the sharing his clinical experience related to this project. I appreciated very much the help of Dr Aimé-Robert Leblanc for his good suggestion about the project, especially in detection part of the electrograms study.

I would also like to acknowledge Dr Yalin Yin and Mr. Bruno Dubé. Dr Yin taught me so much cardiac electrophysiology and clinical knowledge about atrial fibrillation. He also revised the dissertation. Bruno did a big part of work in the detection and identification. They both contributed in a major way to the success of this research.

There are numerous others who contributed to this project in different stages and ways. Dr Pierre Savard, Dr Michael Guevara shared their ideas in the research proposal. I am also grateful to Dr Réginald Nadeau for his revision of the dissertations.

This project would not have been possible without the support of Centre biomédecine, Hôpital du Sacré-Coeur. I do appreciate the help and support from the working staff and students in the research center.

I would never forget all the people who helped, supported me during the time of my study.

Chapter 1 Introduction

1.1 Post-operative Atrial Fibrillation

The cardiovascular system transports and distributes essential substances to each part of the body and removes by-products of metabolism. The heart consists of two pumps in series: the right ventricle propels blood to exchange of oxygen and carbon dioxide within the lungs and the left ventricle propels blood to all other tissues of the body. The functions of different cardiac chambers must be precisely controlled and electrically synchronized. In normal resting heart rhythm, the heart rate varies from 60 to 100 beats per minute. Normal electrical activation is initiated in the sinoatrial (SA), from which the impulse propagates in the atria and then induces the atrial contraction. The wave of excitation ultimately reaches the atrioventricular (AV) node. Conduction is slow in the AV node, which provides a delay between the atrial and ventricular depolarization that assures a complete filling of the ventricles. Then the impulse spreads rapidly across the ventricles through the Purkinje fibers to make them contract [1, 2].

.

Atrial fibrillation (AF) is a cardiac arrhythmia, involving the two atria. During AF, the atrial contraction is rapid and irregular. The filling of the ventricles becomes incomplete, and their frequency, which is limited by the refractory period of the AV node, may become very rapid and irregular, leading to reduce of cardiac output [3-5]. The regular electrical impulses travelling from the sinoatrial node are replaced by disorganized and rapid electrical impulses, which result in irregular heartbeats [6]. Atrial fibrillation may result in symptoms of palpitations, fainting, chest pain, or even heart failure. In addition, the erratic motion of the atria leads to blood stagnation, which increases the risk of formation of blood clots that may travel from the heart to the brain and other areas. AF is

generally explained by the phenomenon of reentry, in which the propagation of an activation front becomes self-sustained. Two scenarios have been proposed: uncoordinated multiple wavelets of excitation circulating throughout the atria or fibrillatory conduction front generated by a single mother rotor [5, 7].

Coronary artery bypass graft surgery (CABG) is a surgical procedure performed to relieve angina and restore the blood flow. Arteries or veins from elsewhere in the patient's body are grafted from the aorta to the coronary arteries to bypass atherosclerotic narrowing and improve the blood supply to the coronary circulation supplying the myocardium [5, 8-11]. Despite the increased rate of percutaneous coronary intervention, CABG is still a common surgery. In Ontario for example, around 8,0000 interventions have been performed each year from 1998 to 2004 [12]. About 500,000 CABG operations are performed annually in the United States. 10% to 65% of patients who never had a history of AF develop AF on the second or third post CABG surgery day [13-15]. The patients undergoing valve surgery or combined valve and CABG have higher incidence of postoperative AF than patients having CABG alone. AF is especially common after mitral valve surgery, occurring in as many as 64% of patients. The occurrence of postoperative AF is associated with worse morbidity and longer and more expensive intensive-care hospitalization [16-19]. There is evidence that AF associates with adverse events: patient discomfort, the need for additional medications and treatments, decrease in cardiac output, hypotension, and congestive heart failure. The most serious complication of AF is stroke. The prolongation of stay in hospital leads to negative social and economic aftereffects. In the United States, the cost for the intensive care against postoperative AF is substantial, with annual estimated expenditures exceeding 1 billion US dollars [20]-[21].

Although the understanding of cardiac arrhythmias has advanced considerably during the last half century, it is only during the last 20 years that the pathology of AF has become a popular topic for physicians and researchers in the cardiology field. The fundamental mechanism responsible of AF, especially for post-surgery patients, is not well understood. Prophylactic medical therapy decreases the incidence of postoperative AF

after CABG. The most effective preventive methods, either medical prevention or preventive pacing, require additional nursing and medical resources and expense. Prophylaxis of the whole patient population undergoing GABG is not an optimal choice. Unless the pathophysiological mechanisms of AF are identified, the design of adequate strategy of prevention will remain problematic. Identification of patients at high risk of AF after CABG would be very helpful and cost-effective [20] [9, 10, 19].

Therefore, the aim of the present research is to investigate to which extent multi-channel unipolar atrial electrograms (AEG) can be used to predict the onset of AF and discriminate AF from non-AF patients

1.2 Review of the Literature

In the last 20 years with the development and maturing of the CABG operation, more and more researchers and physicians turn toward research of mechanism, prediction and management of AF [7, 20-27]. Many studies aimed to develop methods of AF prediction based on the analysis of ECG, with focus on different aspects such as P wave duration, autonomic balance, non-linear analysis or advanced signal processing [24, 28-35]. However, so far, there is not adequate explanation for why some patients develop postoperative AF whereas others remain in sinus rhythm. The next section will discuss the current development and hypotheses regarding the electrophysiological mechanisms, the prevention, the treatment and the prediction of AF.

1.2.1 Electrophysiological Mechanism

Publications are still controversial regarding the mechanisms responsible for the onset of post-CABG AF as well as the identification of patients at risk [7, 11, 20, 21, 36-38]. However, all forms of AF are believed to share common basic electrophysiological mechanisms, while some studies indicated possible localized pathoelectrophysiological mechanisms [37-43]

The search for AF mechanism could be traced as early in 1907 when Winterberg proposed that multiple rapidly firing foci located throughout the atria led to occurrence of AF [44]. GR Mines and WE Garrey advanced independently the concept of reentry, whereby the conduction of an excitation front around a closed circuit can become self-sustained. They then proposed that AF or VF could be caused by 'multiple-simultaneous-reentrant circuits' coexisting in the tissue [7, 45, 46]. In a later 1924 review paper, Garrey stated that its original proposal did "not mean, and never was intended to mean that multiple circuits were fixed in their isolated paths and independent of each other,…, but it was intended to convey the idea that impulses looped back upon its old path, completing a circuit now here, now there. Such reentrant circuit can exist side by side transiently" [47]. Until the mid 20'th century, the debate between the multiple foci and multiple reentries hypotheses, as well as on the exact nature of these reentries (unique or multiple, fixed or transient) was still open [48]. In 1959, Moe and Abildskov, in fact revisiting the arguments of Garrey, proposed that the occurrence of AF was fundamentally different from multiple ectopic discharges [3]. Afterwards, Moe put forward the 'multiple wavelets hypothesis', which differed from the fixed multiple-circuit-reentry concept. It states that multiple independent wavelets circulate around functionally refractory tissue without returning to their initial starting points. Some wavelets are able to propagate through tissues of adequate excitability and maintain themselves with or without producing daughter wavelets. They exemplified their multiple wavelets hypothesis by a two dimensional cellular automata model [49]. From then, Moe's theory was more generally accepted compared to the foci origination theory. The idea of Moe's theory, in brief, is that atrial fibrillation was considered to be a fundamentally turbulent and self-sustaining process, occurring in inhomogeneous excitable medium. The process could be initiated by an impulse propagating through the medium at a time when some of its components have recovered while others remain partially or fully refractory as a result of a preceding activation [3, 49]. The mother wave hypothesis, in which a one or a few anchored or locally meandering high frequency reentries result in complex patterns of propagation, has been proposed as an alternative to the multiple wavelet hypothesis [44]. Nowadays, both scenarios are considered to occur, suggesting that they may require different types of intervention.

Reentry can occur around an anatomical obstacle, in which case it can be labeled as closed circuit reentry. Two-dimensional simulation plans of the depolarization front along one direction and the reentry are showed in Figure 1.1. However, both mother wave and multiple-wavelet AF implicitly refer to functional reentry which does not necessitate an unexcitable core. An example of reentry induced by premature stimulation is a two-dimensional model cardiac tissue is showed in Figure 1.1. There exist two competing models of functional reentry in cardiac tissue: the leading circle which is a qualitative model based on experimental observations [50], the spiral wave model, based on theoretical considerations and numerical simulations of ionic models[7, 51, 52]. The latter provides a more realistic representation of the electrical properties of the tissue and a more correct prediction of state of the core around which propagation takes place [53]. In the classical view of closed circuit and leading circle reentry, the wavelength of reentrant wavelets, the product of the conduction velocity and refractory period, is the main determinant of the persistence of AF. The wavelength determines the size of each functional reentry circuit and limits the number of simultaneous reentry wavelets that can exist during fibrillation. The relation becomes more complex in the spiral model, since it involves the curvature of the front and the electronic effect during repolarization [53]. Nevertheless, both models predict that the shortening of the refractory period (ERP) has a crucial role in increasing wavelets number and is a major determinant in sustaining of AF [54].

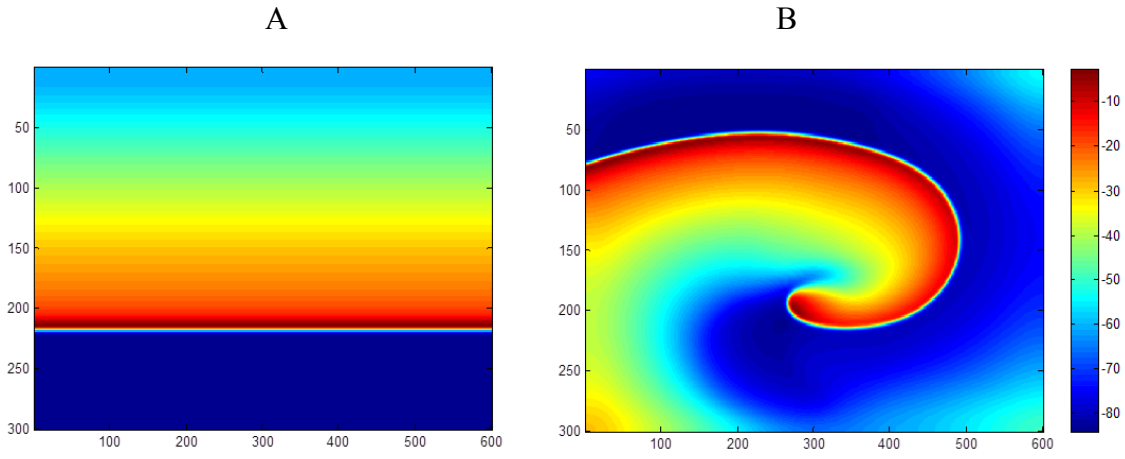

Figure 1. 1 A) A normal plane depolarization front travelling along the vertical direction; B) reentry. It was induced by applying a second stimulus covering half of the plane in the

horizontal direction. The abscissa and ordinate are the coordinate of the tissue in the unit of pixel. The color stands for the membrane potential, corresponding values indicated in the color bar (*mv*). (Figure provided by Elhacene Matene, student of Dr. V. Jacquemet, Centre de recherche de l'Hôpital du Sacré-Cœur and Institut de Génie biomédical, Université Montréal. It shows a simulation of reentry in a model of atrial tissu).

Patients developing postoperative AF are speculated to have a vulnerable heterogeneous substrate prone to develop AF, such as non-uniform and dissimilar refractoriness, a depolarizing wave front becomes fragmented when encountering both refractory and excitable myocardium. This allows wave fronts to return and stimulate previously refractory but now repolarized myocardium, which can lead to self-sustained propagation or reentry [55, 56]. However, other elements such as the slope of the action potential restitution curve, the curvature of the wave front and the distribution of gap junctions also contribute to the dynamics and stability of reentry [54, 57]. Han et al. proposed that dispersion of recovery of excitability in the atria or ventricles of the heart predispose to the development of both atrial and ventricular arrhythmias [58, 59]. Comtois et al. also explained that the difference of adjacent atrial cells can predispose to pulse conduction reentry [53]. Beside, fibrosis has been strongly associated with the presence of heart diseases/arrhythmias. It was recently considered to alter atrial electrical conduction and excitability and provides a substrate for AF onset and perpetuation [60, 61].

Although the pathological substrate may favors the incidence of AF, ectopic focal activation is a mechanism to trigger the AF [62]. Ectopic foci can be found in many areas of the atrium including the pulmonary veins, the superior cava, the coronary sinus ostium, as well as the posterior and anterior left atrium [63-65]. In Holter ECG monitoring, a triggering premature atrial complex (PAC) was present in more than 90% percent of AF episodes. According to the polarity of the ectopic P-wave, triggering PACs were left atrial origin in 74.3%, right atrial in 15.3%, not determined in 10.4% of cases. Frequency of PACs was significantly higher in the hour preceding the onset of AF. Among PAC, two-thirds had a left atrial origin [66].

The intrinsic cardiac autonomic nervous system is also believed to play a role in the occurrence and maintenance of AF. Heterogeneous electrophysiological properties could

be due to autonomic innervations [34, 37, 67]. It is reported that either vagal nerve activation or sympathetic nerve stimulation, both could facilitate the occurrence of AF. Either vagal stimulation or acetylcholine administration decreases the atrial refractory period in a spatially heterogeneous way [68, 69]. In addition, vagal stimulation promotes both the production of PAA and their propensity to start AF [7, 70]. Sympathetic stimulation can also promote the initiation of AF. Sympathetic nerve stimulation also shortens atrial refractoriness in a comparable degree. The difference between vagal and sympathetic stimulation might lie in the more spatially heterogeneous effect of vagal nerve activation. Two major patterns of AF initiation can be observed. AF occurring after a slowing heart rate, thought to be triggered by a dominant parasympathetic tone that frequently occurs in patients with normal hearts. Adrenergic-induced AF is more frequent in older patients with structural heart disease, and typically occurs during exercise [71, 72]. The possible implication of the autonomic nervous system in postoperative AF was discussed in many publications, and the atrial electrophysiological effects caused by autonomic nervous system stimulation are complex, sometimes even controversial [20, 33, 71, 73, 74]. Amar reported an increase both in heart rate and in heart rate variability (HRV) prior to the onset of postoperative AF. These findings are consistent with parasympathetic resurgence competing with increasing sympathetic activity as a triggering mechanism for postoperative AF [33]. It has been put forward that elevated norepinephrine levels suggested that sympathetic activation may be important in the pathogenesis of post CABG AF. Sympathetic activation, however, is highest the first 24 hours after operation, whereas the onset of AF usually occurs between the second and third postoperative days [75]. Some findings suggested divergent autonomic conditions to occur before arrhythmia onset, which could be either heightened sympathetic or parasympathetic tone, or event dysfunctional autonomic heart rate control, with higher or lower measures of heart rate variable [71, 76].

1.2.2 Risk Factors: Preoperative, Intraoperative, and Postoperative of Postoperative AF

Many risk factors for postoperative AF have been identified, but the results of different studies have often been inconsistent. This might be due to the factors as: 1. the mechanism of AF is complex and multi-factorial; 2. most studies are observational and retrospective, with varying inclusion criteria. This is illustrated in Table 1.1, which shows the patients characteristics in four studies on post-operative AF. The distribution of preoperative factors found to be related to AF occurrence in some studies is not even reported in others (empty boxed if not available). Table 1.2 compares the risk score (a risk index to indicate risk degree, definition seen in [77]) or odds ratio associated to different variables in these same four studies. It shows that using different data and/or study population can leads to very different results. The following reviews current knowledge on the preoperative, intraoperative and postoperative risk factors.

Preoperative Risk Factors

The following variables have been reported as potential preoperative and perioperative risk factors: age, sex, right coronary artery stenosis of 90% or higher, left ventricular abnormality as ejection fraction, enlargement, hypertrophy; dilation, aortic atherosclerosis, hypokalemia, history of atrial fibrillation, valvular disease, CHF(congestive heart failure), vascular disease, neurological event, diabetes, any MI(myocardial infarction), hypertension or chronic obstructive pulmonary disease (COPD), prior CABG surgery or valve surgery, previous congestive heart failure, and preopeative absorption of beta-blockers, angiotensin-converting enzyme (ACE) inhibitors, calcium channel blockers, amiodarone, or nonsteroidal anti-inflammatory drugs (NSAIDs) [17, 36, 38, 75, 76, 78-80].

Age has a significant relation with the incidence of postoperative AF. The incidence rate of post-CABG AF is more than 50% for patients older than 80 years, but less than 5% for those that are less than 50 years [76, 81]. The association could be attributable to age-related structural changes in the atrium such as dilation, muscle atrophy and fibrosis. Patients with a history of AF appear to have the underlying substrate conducive to the development of AF and may be more susceptible to postoperative AF [77, 82]. This

would be consistent with the concepts of electrical remodeling and "AF begets AF" that is supported by numerous clinical and experimental studies [7].

Men appear more likely to develop AF after CABG than women [83, 84]. Sex differences in ion-channel expression and hormonal effects on autonomic tone may explain this difference between genders However, there exist conflicting reports, in which male gender was not an independent predictor of AF [80].

Hypertension was regarded as a predictor of postoperative AF, and this may be related to increased fibrosis and dispersion of atrial refractoriness [85, 86]. However, such a relation was not found in another study involving a larger number of patients [87].

Chronic obstructive pulmonary disease (COPD) is a predictor of AF after cardiac surgery. It might be related to fact that COPD patients have frequent premature atrial contractions that can act as a trigger for the initiation of AF [84].

The right coronary artery also conveys the blood supply to the right atrium, the sinoatrial node and the atrioventricular node. Patients with a total occlusion or severe stenosis of the proximal right artery had postoperative AF more often when retrograde cardioplegia was used. In other studies, obstructive disease in the sinoatrial nodal and atrioventricular nodal arteries was more common in patients developing AF after CABG than in those who remained in sinus rhythm. Stenosis of the sinoatrial artery or the right coronary artery has been found to be independent predictors of AF after CABG by other investigators [14, 88].

Many studies showed that obesity, or body mass index and metabolic syndrome are risk factors of postoperative AF [13, 89-93]. Echahidi demonstrated that obesity was a powerful and independent risk factor for the occurrence of postoperative AF in patients older than 50 years. In a younger population, obesity was not a risk factor whereas metabolic syndrome remained an independent risk factor [13] .

There was also the study about preoperative renal function associated with the risk of atrial fibrillation after surgery [94, 95]. It was found the patients measured higher level of serum creatinine, were more risky to develop postoperative AF.

Several studies have examined the relationship between left atrial dysfunction [96, 97]. Leung found that the patients subsequently developing post-operative AF had a larger LA and LA appendage area, and lower LA ejection fraction measured in the pre-bypass period. Their results demonstrate that some of the structural and functional changes in the atria common to chronic AF in the elderly population are also prevalent in surgical patients who develop post-operative AF, suggesting that both may share similar pathophysiology. LA enlargement was also found to be a predictor of postoperative AF either in CABG patients [98] after cardiac valvular surgery [99]. However, Zaman et al. did not find any difference in the size of LA between the patients who had AF and those who remained in sinus rhythm. Their study included only 64 patients and was subgroup of a larger study population [100].

Some studies proposed that preoperative withdrawal of beta-adrenergic blockers was associated with increased risk for postoperative AF [80, 101]. The withdraw effect is characterized by an increased plasma concentration of catecholamine that may increase the incidence of AF. It has been demonstrated that the bioavailability of perioperative metoprolol (beta-adrenergic blockers) is markedly reduced when administered in tablet early after CABG. The poor absorption of oral beta blocker immediately cardiac surgery may further strengthen the withdrawal effect [102]. The prophylaxis with moderate doses of amiodarone in the postoperative period of cardiac surgery (coronary artery bypass grafting and/or valve surgery), was shown to reduce the incidence of AF in high risk patients with high risk patients, raising the possibility that it could also be protective for a larger class of patients [103].

Table 1.1 Baseline Characters of Patients of Study Population

	Mathew [77]	Zaman [100]	Amar [104]	Auer [80]
Age(mean, SD), years		(p<0.0005)	(p<0.0001)	(p=0.008)
AF	67.8(8.2, n=976)	65.9(n=92)	68(9,n=508)	67.5(9.1,n=99)
Non-AF	61.8(9.8, n=2117)	61.7(n=234)	62(11, n=1.045)	63.7(11.4,n=154)
Incidence of AF	32.27%	28.22%		
Men, No. (%)		(p=0.084)	(p=0.63)	(p=0.29)
AF	770(78.9, DC)	81(88)	336(66)	55(55.5)
Non-AF	1682(79.5, DC)	187(80)	704(67)	98(63)
SAPD(ms)		(p<0.0005)	(p=0.02)	
AF		158	117±17	
Non-AF		145	115±18	
LVEF, %		(p=0.751)		
AF		56		
Non-AF		56		
Left atrial size, cm*		(p=0.831)		
AF		3.8		
Non-AF		3.9		
History, No. (%)				
Atrial fibrillation			(p<0.0001)	
AF	142(14.6, DC)		57(11)	
Non-AF	126(6.0, DC)		27(3)	
Valvular disease				
AF	271(27.8, DC)			
Non-AF	316(14.9, DC)			
Myocardial Infarction			(p=0.48)	
AF	612(62.7, DC)		265(52)	
Non-AF	1334(63.0, DC)		525(50)	
COPD			(p=0.13)	
AF	137(14.0, DC)		46(9)	
Non-AF	183(8.6, DC)		72(7)	
Hypertension (%)			(p=0.17)	(p=0.68)
AF	668(68.4, DC)		371(73)	(60.6)

Non-AF	1348(63.7, DC)		728(70)	(64)
Diabetes(%)			(p=0.19)	(p=0.12)
AF	303(31.1, DC)		167(33)	(19.2)
Non-AF	660(31.2, DC)		379(36)	(28.6)
Preop. treatment, No.(%)				
β-Blockers			(p=0.05)	
AF	645(66.1, DC)	54(59)	239(47)	
Non-AF	1480(69.9, DC)	164(70)	547(52)	
Calcium channel blockers				
AF				
Non-AF	391(40.1, DC)			
ACE inhibitors	768(36.3, DC)			
AF				
Non-AF	447(45.8, DC)			
	875(41.3, DC)			
Cross-clamp, mean(SD),min		(p=0.306)	(p=0.33)	
AF	69.5(35.1, DC)	45	63 ± 22	
Non-AF	61.8(29.3, DC)	43	64 ± 22	
Heart valve surgery(%)				(P<0.0001)
AF				62.6
Non-AF				33.1
RCA graft(% of CABG)				(P=0.08)
AF				58.1
Non-AF				72.3
CPB time, mean(SD), min				
AF	108.6(45.7, DC)			
Non-AF	98.7(39.8, DC)			
Pre-operative Q-waves, n(%)		(p=0.506)		
AF		31(34)		
Non-AF		70(30)		
RCA stenosis, n(%)		(p=0.212)		
AF		55(60)		
Non-AF		122(52)		
CPB time, min		(p=0.025)		
AF		81		

Non-AF		74		
Grafts>3, n(%) *AF* *Non-AF*		(p=0.040) 31(34) 53(23)		
Preoperative creatinine >125 μ mol/L, n(%) *AF* *Non-AF*		(p=0.260) 22(23) 43(18)		
Postoperative Low cardiac output, n(%) *AF* *Non-AF*			<0.0001 36(7) 24(2)	
Postoperative complications(%) *AF* *Non-AF*				(p<0.05) 12.1 5.8

DC: Derivation Cohort;

ACE: angiotensin converting enzyme;

SAPD: signal-averaged P-wave duration;

LVEF: left ventricular ejection fraction;

CPB=cardiopulmonary bypass time.

Table 1.2 Multivariable Predictors of Postoperative Atrial Fibrillation

	Mathew [77]	Zaman [100]	Amar [104]	Auer [80]
	Risk Score, (R.S., p)	Odds Ratio (O.R., p)	Odds Ratio (O.R., p)	Odds Ratio (O.R., 95% CI, p)
Age, y <30 (R.S.) 30-39(R.S.) 40-49(R.S.) 50-59(R.S.) 60-69(R.S.) 70-79(R.S.) ≥80(R.S.) (R.S., Risk Score)	p<0.001 6 12 18 24 30 36 42	1.53(<0.0005) (per 5-y increase)	1.1 (p<0.0001) (per year incre.)	2.6(1.2-3.9) <0.01
Medical history AF(R.S.), p COPD(R.S.), p	 7(<0.001) 4(.009)		3.7(p<0.0001, O.R.)	
Concurrent valve surgery	6(<.001)			2.8(1.1-3.5) <0.01
Withdrawal of treatment β-Blockers ACE inhibitors	 6(<.001) 5(<0.001)			
Preop. and postop. treatment β-Blockers ACE inhibitors	 -7(<0.001) -5(<0.001)			
Postop. β-Blockers treatment	-11(<0.001)			

Other treatment Potassium supplementation NSAIDs	-5(<0.001) -7(<0.001)			
SAPD>155ms		5.37(<0.0005)		
p-wave duration >110ms			1.3(p=0.02)	
Male sex		2.88(0.0092)		
Postoperative low cardiac output (O.R.)			3.0(p=0.0001)	
Postoperative complication				1.9(1.0-7.5) <0.05
Non-use preoperative beta-adrenergic blocker				1.7(1.1-4.9) <0.05

O.R.: odds ratio

Intraoperative Risk Factors

Auer proposed that the type of surgery may affect the risk of AF after cardiac surgery [80], and higher risk of postoperative AF and mortality were observed after mitral valve surgery [105].

Whether the risk of AF is different for On-pump versus off-pump CABG is still contentious. Murphy reported a lower incidence of AF after off-pump than on-pump CABG [106] , while Topal found that on-pump no significant difference as long as the operating time did not exceed a certain duration [107].

The association between the duration of aortic cross-clamp and the risk postoperative AF also remains controversial. Mathew proposed that the risk was increased by prolonged cross-clamp [108], an observation contradicted by the study of Salaria el al [109].

Postoperative Risk Factors

Many studies have considered the association of inflammation with the occurrence of postoperative AF [110-113]. C-reactive protein (CRP) is the classic acute phase reactant. During severe inflammation or infection, its blood levels may increase up to 500 times to 1,000 times above normal. The reason why inflammation markers in atrial fibrillation may become high after CABG is a puzzling problem. The peak levels of C-reactive protein (CRP) were paralleled to the incidence of postoperative AF. In the general population, CRP was also higher in patients with AF than those who do not develop [114]. The reported efficacy of anti-inflammatory drugs such as steroids in the prevention of AF supports the association between AF and inflammation [115]. However, Ahlsson found that postoperative AF has no correlation to CRP level in heart surgery patients [116].

Postoperative pneumonia and mechanical ventilation for more than 24 hours have been shown to be independent postoperative predictors of AF [75]. Another study reported that low postoperative mixed venous oxygen saturation and the need for postoperative

mechanical circulatory support were also independent predictors of post-CABG AF [117].

1.2.3 Prophylaxis and Postoperative AF Treatment

The prevention of post-cardiac surgery AF arouses much interest because of its high incidence and the associated morbidity, mortality, and cost. Prophylactic drug administration has been shown to decrease the incidence of post-CABG atrial fibrillation and Prophylactic appears to be more effective than postoperative administration [103, 118-120]. The most promising drugs include β-blockers, amiodarone and calcium channel blocker, which are also administered for a wide range of ventricular and supraventricular arrhythmias [118]. The effectiveness of beta-blockers in the prevention of AF after cardiac surgery has been demonstrated in numerous studies [120, 121]. Indeed, according to the recent guideline, beta-blocker prophylaxis should be given to every patients undergoing cardiac surgery when there is no contraindications.

If AF does occur after cardiac surgery, the guidelines recommend managing patients as non-surgical AF patients [122, 123]. Two management strategies are available to treat AF after CABG: rate control or rhythm control. For patients who less urgently require sinus rhythm restoration, β-blockers are considered as the first-line therapy. When β-blockers alone inadequately control the heart rate, calcium channel blockers may be administered [122]. Infusion of amiodarone can also be used for adequate rate control in AF. For hemodynamically unstable, highly symptomatic patients or for those having a contraindication to anticoagulation, rhythm management is preferred. These patients should undergo urgent electrical cardioversion to sinus rhythm.

1.2.4 Methods for Predicting Postoperative Atrial Fibrillation

Many studies aim to develop methods for the prediction of postoperative. Risk stratification would be very useful either to optimize the prophylactic antiarrhythmic treatment in high risk patients, or to limit drugs administration in low risk subjects. The

works published so far managed to achieve good results in terms of sensitivity and specificity. However, since these methods were not completely reliable, their clinical application is still limited. Methods were based on ECG analysis in the time or frequency domain, or on the measure of biochemical markers such as atrial natriuretic peptides [15, 24, 28, 31, 124, 125].

It is generally believed that an abnormal prolongation of P wave duration on the ECG reflects the presence of intra-atrial conduction defects [24, 29-32, 126-133]. A slowed conduction may promote the development of arrhythmia by shortening the wavelength necessary to sustain reentry. P wave dispersion is also considered as a predictor for AF after CABG. The main limitations of the methods based on P wave duration come from the fact that there is no accepted definition of normal duration. Beside, the use of different methods to measure of P wave duration makes the comparison of the results achieved by various groups difficult. P wave delineation is more difficult to implement than QRS complex one, mainly owing to the low signal-to-noise ratio and the shape variability of the P wave [134].

The autonomic nervous system (ANS) has been recognized as a potential contributor to the initiation of AF [20, 33, 37, 67, 69, 71, 73, 82]. Perturbation the sympathovagal balance has been hypothesized to be associated to AF. The notion that certain ranges of frequencies in the power spectrum of the heart rhythm may be indicative of either sympathetic or parasympathetic tone has stimulated the of heart rate variability (HRV) as a diagnostic tool. The parasympathetic influence on heart rate is mediated via release of acetylcholine by the vagus nerve. Higher sympathetic /parasympathetic tone usually related with higher/lower heart rate [2]. The efferent vagal activity is a major contributor to the high frequency component. More controversial is the interpretation of the low frequency component, which is considered by some as a marker of sympathetic modulation (especially when expressed in normalized units) and by others as a parameter that includes both sympathetic and vagal influences. This discrepancy is due to the fact that in some conditions associated with sympathetic excitation, a decrease in the absolute power of the LF component has been observed [135]. Divergent results have been

reported the link between heart rate variability (HRV) and post-cardiac surgery AF. Dimmer et al. observed a shift in the autonomic balance, with a loss of vagal tone and a moderate increase in sympathetic tone, before the onset of AF [71], while Hogue et al., performing HRV analysis after CABG surgery, observed either lower or higher values of different frequencies content before AF. They concluded that their patients could have either heightened sympathetic or vagal tone or dysfunctional autonomic heart rate control before AF onset [136]. Marco Bettoni concluded that the occurrence of AF greatly depended on the variation of the autonomic tone, with a primary increase in adrenergic tone followed by an abrupt shift toward vagal predominance [137]. David Amar et al evaluated autonomic change preceding AF after thoracotomy. They found a significant increase in HRV and heart rate prior to the onset of AF, consistent with vagal resurgence competing in a background of increasing sympathetic activity as a mechanism to trigger AF [33].

Recent studies have shown that the new nonlinear measures, particularly fractal analysis methods of heart rate dynamics, could perform better than traditional analysis methods as a predictor of sudden cardiac death in post-infarction populations [134, 138]. Altered short-term fractal properties of heart rate dynamics have also been shown to precede the onset of ventricular tachyarrhythmias in patients with heart disease. Approximate entropy, a measure of complexity of heart rate variability has been used to predict the onset of paroxysmal atrial fibrillation. However, these methods have not been applied yet to post- CABG AF [134].

Currently, most electrophysiological methods to predict the onset of postoperative AF are based on the ECG. The intrinsic limitation of P wave studies is that P wave cannot give precise information of atrial activity. P wave is a complex expression of the whole electrical activity in left and right atrium, and it cannot give a detail picture of the electrical propagation in the atrium. Furthermore, the criteria of calibration of P wave sets quite rely on the individuals, which may explain the discrepancies between the published articles [134]. Authors also use different methods to choose subjects, to treat the

premature beats, saturations periods, etc., which further contribute to the differences between their results.

A M Pichlmaier et al utilized the monophasic action potential continuously recorded from the epicardial surface to predict the onset of atrial fibrillation after cardiac surgery [139]. They found that the morphological changes in the MAP could be good indicators that the atrial rhythm is likely to become unstable and to deteriorate to AF, and concluded that epicardium MAP recording could be a valid tool for detecting imminent AF after cardiac surgery.

Atrial natriuretic peptides (ANP) are produced primarily in the cardiac atria. The dominant stimulus controlling their release is the increase of the atrial wall tension, reflecting rising intravascular volume. Different studies have examined the possible link between ANP level and AF [15, 124, 140, 141]. Hakala et al. found that, in the univariate analysis, high ANP level were associated with the development of postoperative AF. However, ANP did not appear in forward conditional multivariate analysis in which only age and left atrial enlargement were left as independent predictors. In their cohort, ANP level did not act as an independent predictor because it was correlated to age. They concluded that the wide variation in the peptide levels observed in their cohort renders the implementation of this measure in clinical practise superfluous [15].

1.3 Analysis on Atrial Electrograms (AEG) to Study the Mechanism and Prediction

1.3.1 Hypothesis and Objectives

Postoperative AF is the most common complication after surgery. Its mechanisms are not fully understood. Both “structural” and “electrical” remodelling of the atrium may act to promote AF [142]. The remodeling may involve pathological alterations in the structure, function and geometry of the atria, such as changes of the atrial electrical and contractile properties or in the amount and the composition of the extracellular matrix,

which may facilitate the induction of AF. Studies on the induction of AF by neural stimulation in canine preparation have shown that the autonomic can be involved. [143]. Pichlmaier also noticed significant change of MAP waveforms prior to the onset of AF [139]. Our study relies on the analysis of three channels unipolar electrograms recorded on the atria (AEG). The advantage to use AEG rather than ECG is that AEG can provide some measures relevant to the occurrence of AF that are difficult or even impossible to obtain from ECG. For example, AF is often preceded by multiple atrial premature activations [62, 66]. Simultaneous recording of unipolar electrograms from different sites can supply more precise information on the origin of these premature activations. The hypotheses guiding our analyses are:

1) The onset of AF after CABG is preceded by typical changes that are reflected in the time series derived from the AEG.

2) These time series, in addition for pre-CABG risk factors, can be used to discriminate patients with and without AF, and predict the onset of AF soon enough to allow for prophylactic interventions

1.3.2 Choice of Subjects

Patients admitted for CABG surgery at Hôpital du Sacré-Coeur de Montréal (HSC) and Institut de Cardiologie de Montréal (ICM) were screened. Patients were excluded if they were not in sinus rhythm at admission, were taking class I or III antiarrhythmic drugs or digoxin, had a prior history of AF, were diagnosed for congestive heart failure, were receiving hemodialysis, or had a permanent pacemaker. We realized that these exclusions criteria were meant to avoid such confounding effects as the effect of class I drugs on conduction times and atrial ectopy or the parasympathicomimetic effects of digoxin. Informed written consent was obtained. A total of 137 patients were included, 108 from HSC and 29 from ICM.

The criteria to decide a patient belonging to AF group, it is upon whether the patient develop sustained atrial fibrillation with duration longer than 10 minutes after CAGB surgery [101]. Among these 137 patients, 41 patients developed at least sustained AF lasting for 10 minutes or more after the CABG surgery. Herein, these 41 patients were classified as AF patients. Among AF group, the distribution of the first sustained AF duration time was very inhomogeneous, with a minimum value of 10 minutes, maximum duration time of 3732 minutes. 75% of AF group patients have the fist sustained AF duration time between 150 and 650 minutes. Among remaining 96 patients classified as Non-AF group, some of them had very short transient supraventricular arrhythmias, from several second to 2 or 3 minutes, and with a maximum duration close to 5 minutes.

1.3.2 Study Plan

AEG were recorded continuously during the first four post-operative days. The First task was to detect, distinguish and validate the markers corresponding to the atrial and ventricular activation on each channel. The markers of the three channels belonging to the same cardiac event had to be grouped together and the nature of each event (e.g. normal sinus beat, premature atrial or premature ventricular beat) resolved. Then, different time series were constructed, reflecting either the intra-beat or inter-beat dynamics. Finally, statistical analysis of the time series characteristics was performed to discriminate the AF group (patients with AF ≥ 10 minutes) and non-AF group and obtain predictors.

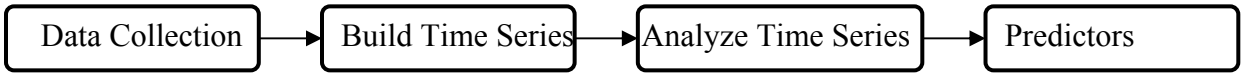

Figure 1. 2 Flow chart of the project research method

Results are presented in the three following chapters. Chapter 2 presents the methods of activation and events detection and labeling. In chapter 3, the time series of AF patients are analyzed to see if changes occur in the two hours before the onset of the first long lasting AF. In chapter 4, AF and Non-AF are compared regarding their preoperative risk

factors. In chapter 5, the preoperative predictors and AEG time series are used together to discriminate AF and Non-AF patients. The final chapter summarizes the results and draws the conclusions over the whole studies.

1.3.3 Statistical Methods

In the following chapters, diverse statistical methods were used to analyze the preoperative data as well as the time series extracted from the electrograms. Two softwares, Matlab (The MathWorks Inc, Mass, USA) and SPSS (IBM), were used for the analysis. The main statistical methods used in the analysis are explained below.

1. Repeated measures analysis of variance (ANOVA)

Repeated measures ANOVA test the equality of the means as any ANOVA. It is used when the measurement of dependent variable is repeated under different condition for each subject [144]. The sphericity assumption of repeated measures ANOVA means that the variances of the differences between all combinations of the groups are assumed to be equal. If sphericity is violated, then the variance calculations may be distorted, which could result in an inflated F-ratio [145]. In the project, Huynh-Feldt correction was applied to assess the significance of the F-ratio.

2. Logistic regression

Logistic regression is widely used to model the outcomes of a categorical dependent variable based on one or more predictor variables. The probabilities describing the possible outcome of a single trial are modeled as a function of explanatory variables through the logistic function. For binary outcome (y=0, 1), the probability for a subject i to get the reference outcome (y=1) is given by:

$$P_i = \frac{e^{\sum_j \beta_j x_{ij}}}{1 + e^{\sum_j \beta_j x_{ij}}}$$

in which $x_{i,j}$ is the value of the j'th independent variable for patient i, and β_j the value of the parameters. In the project, the logistic regression was done using either SPSS or an in-house Matlab program in which part of code was originally contributed as freeware by Britt Anderson (http://brittlab4.uwaterloo.ca). A Conditional forward stepwise method was used, of the predictor selection was used with p value criterion for variables to enter and remain in the model usually set at 0.05 and 0.10 respectively

Parameters are obtained by maximum likelihood estimation. The likelihood function is

$$L = \prod_i P_i^{w_i y_i} (1 - P_i)^{w_i (1 - y_i)}$$

where y_i is the outcome (0 or 1) of the i'th subject and w_i the weight that can be given to the observation (1 by default). The significance of the contribution of each variable included in the model is assessed by a chi-square test over the improvement that it brings to the likelihood functio[146], [147]. The logistic regression provides a value P_i (probability of having y=1) for each patient. In logistic regression, the patient would be assigned to outcome 0 or 1 if P_i is less or greater than 0.5 respectively

However, P_i can also be treated as a propensity score. In that case, an arbitrary threshold between 0 and 1 can be selected to allocate each subject to one of the outcomes. For each value of the threshold, the sensitivity (number of subjects with y=1 correctly classified) and specificity (number of subjects with y=0 correctly classified) can be computed. The set of [1-specificity, sensitivity] for all values of the threshold can be plotted together as a ROC (receiver operating characteristic) curve. The area under the curve measures the probability that a randomly selected pair of y=1 and y=0 subjects would be correctly classified (i.e. score of subject with y=1 > score of subject with y=0), such that the scores do not provide any discrimination if the area ≤ 0.5. The significance of the discrimination can be evaluated from the excess of the area beyond 0.5 [148]. Methods and the software

also exist to compare different ROC curves based on their difference of area (http://www.medcalc.org/manual/comparison_of_roc_curves.php). Upon stepwise logistic regression, it is expected that the ROC curves associated to successive significant improvement of the maximum likelihood ratio by addition of new variables would also bring significant changes of the ROC area. As we will see in the next chapters, it may occur that the two tests differ because they are based on different concepts.

3. Survival analysis and Cox regression model

Survival analysis is generally defined as a set of methods for analyzing data where the outcome is the time elapsed until the occurrence of an event of interest. The Cox model is a statistical technique for exploring the relationship between the temporal evolution of the proportion of surviving subjects and several explanatory variables whose values are distributed among the subjects [149].

Consider S(t), the survival curve giving the proportion of subject for which the event has not yet occurs at time t. The hazard function is defined as:

$$h(t) = -\frac{dS/dt}{S(t)}$$

The proportional hazard Cox model postulates that the hazard function with a set of variable $X=[x_1,\ldots,x_n]$ is expressed as:

$$h(t/X) = h_0(t)e^{\sum_i \beta_i x_i}$$

A positive β_i coefficient means that the hazard increases with x_i higher and thus that the prognosis is worse.

4. Cluster analysis

Cluster analysis is a set of techniques to separate a set of subjects in different groups (also called cluster) based on some index of similarity. It can be achieved by various algorithms that differ in the choice of the index of similarity and the way the index calculated between clusters [**150**]. Since diverse methods has been used in different phases of our study, details will be given in the sections where they appear.

Chapter 2 Detection, Validation and Time Series Building of AEG

The aim of the project is to study how time series extracted from 3-channel atrial unipolar electrograms (AEG) can help to predict the onset of AF in post-CABG patients. As seen in Figure 2.1, the morphology of the signals is very different from standard ECG. The local atrial activations (A) are brief with amplitude most often larger than the deflections associated to the far-field ventricular activation (V). Since standard ECG timing methods were ineffective, the first task was to develop an automatic and unsupervised algorithm (Find AV) to automatically detect and distinguish A and V activations. To develop the algorithm and assess its performance, sets of activation times were required for which both the temporal position and the labeling (A or V) of the markers were validated. Validation software was elaborated and implemented (Validate AV) for this purpose, which was also later used to validate all the results of the automatic timing prior to the analysis.

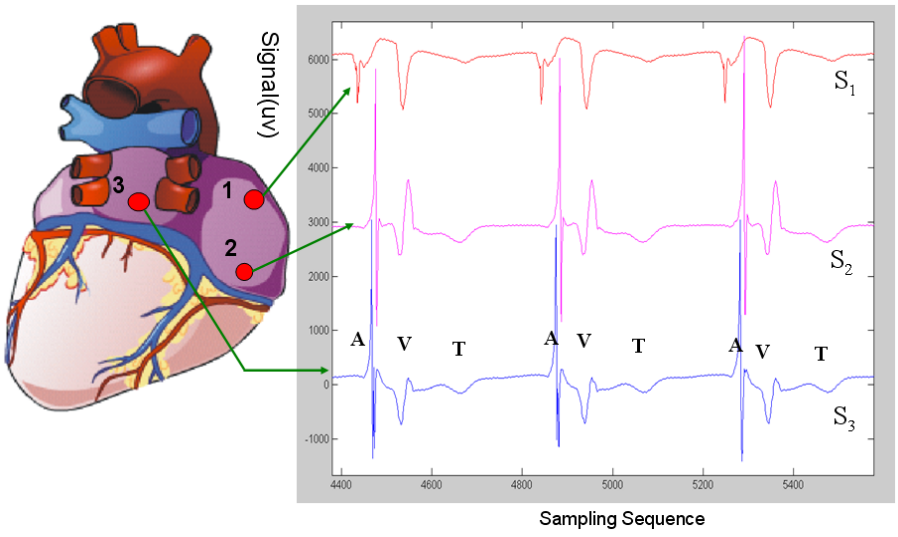

Figure 2. 1 Posterior view of the heart showing the 3 electrodes sutured to the right (S_1, S_2) and left (S_3) atrium and their electrograms. The atrial (A) and ventricular activations (V) are indicated for three beats, as well as the ventricular T wave (T).

Because the electrodes are distributed in the two atriums, their A activations in a cardiac beat are not simultaneous. Hence, atrial and ventricular activations of the different channels belonging to the same cardiac beat must be grouped together. Different types of events must also be distinguished, such as normal sinus beats, premature atrial or ventricular activations, atrial activations that do not reach the ventricles, as well as runs of ventricular or atrial arrhythmias. Software for automatic beat formation and labeling (Form Beat), complemented by a validation tool (Validate Beat), was also developed. The flowchart in Figure 2.2 resumes the different steps of the process leading to the activation markers that are needed for the construction of the time series used in the analysis. This chapter presents some details on each stage of the processing. We have been associated closely to development of Find AV. We have designed and implemented Validate AV, Form Beat and Validate Beat, and have performed most of the validation of the data.

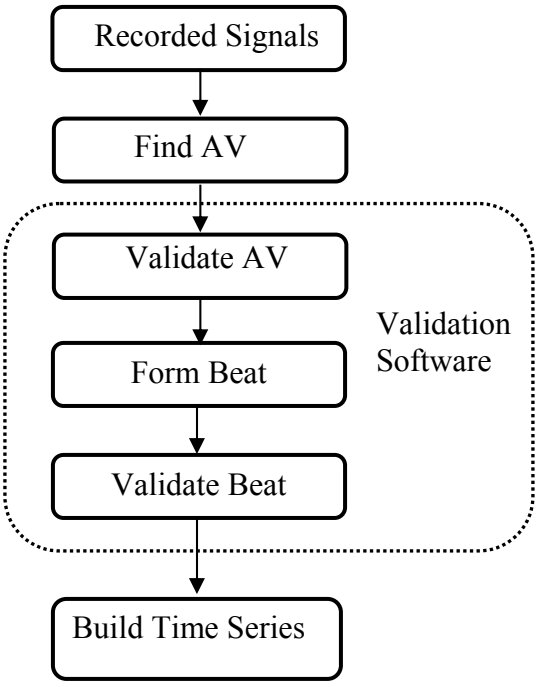

Figure 2. 2 Flow chart of building time series from AEG

2.1 Data Collection

Recordings were made by the team of Dr. Pierre Pagé on patients on which he had performed CABG surgery at the Hôpital du Sacré-Coeur de Montreal or at the Institut de Cardiologie de Montréal. The protocol was approved by the Ethics Committee of Hôpital du Sacré-Coeur de Montréal. Recordings were made for the first 4 consecutive days following CABG using a modified (class III) three-channel Holter digital recorder with 16 bits encoding, providing a ± 5 mV input range with 0.16 μV resolution (Burdick, model 6632). The sampling rate was set at 500 Hz per channel. This setting was chosen such that batteries and the storage memory card had to be changed only once every 24 hours. Three atrial unipolar electrodes (ETHICON model TPW40) were sutured on the epicardium of the atria and connected to the positive poles of the Holter by wires fixed on the patient's thoracic wall. The three negative poles of the Holter were connected together to serve as a reference electrode positioned on the lateral side of the thigh.

Then recordings were transferred to a PC for off-line analysis. A short stretch of signal is shown in Figure 2.1, in which A and V activations are identified. More than 100 patients were recorded. In the course of the project, five different configurations of electrodes were used, which are shown in Figure 2.3.

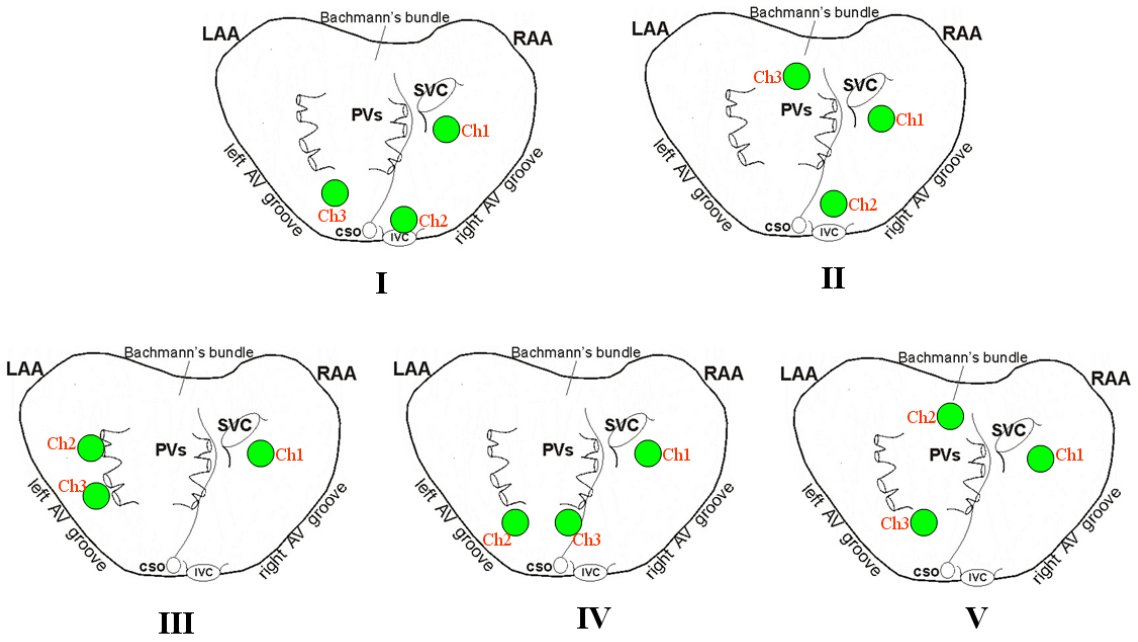

Figure 2. 3 The five spatial configurations of unipolar electrodes on the posterior atria. LAA: Left Atrial Appendage. RAA: Right Atrial Appendage. LA: Left Atrium. RA: Right Atrium. PV: Pulmonary Vein. SVC: Superior Vena Cava. IVC: Inferior Vena Cava.

The number of patients of the five recording configuration were 49 (I, 35.8%), 6 (II, 4.4%), 2 (III, 1.5%), 62 (IV, 45.3%) and 18 (V, 13.1%). All recordings methods have one electrode near the sinus node, where the electricity pulse normally initiates and at least another close to the pulmonary veins, from where the ectopic beats are known to often originate. All configurations thus allow discriminating whether an ectopic beat was produced from the left or right and give similar total conduction times for normal sinus beats.

2.2 Detection and Classification of Atrial and Ventricular Activations

2.2.1 Detection Challenges

AEG recorded both the local A and the far field V activations. Because the positions of the electrodes on the atrial epicardium were not the same among the patients and their health status were different and varied during the recordings, so the morphology of the signals were usually very different between patients, channels and even in time within one channel. The challenge of activation detection was further enhanced by the possible disproportion of the amplitudes between the channels, the presence of artifacts related to the movement of the subjects or to poor contact and polarization of the electrodes, as well as bouts of saturation. Some of these difficult circumstances are illustrated in Figure 2.4.

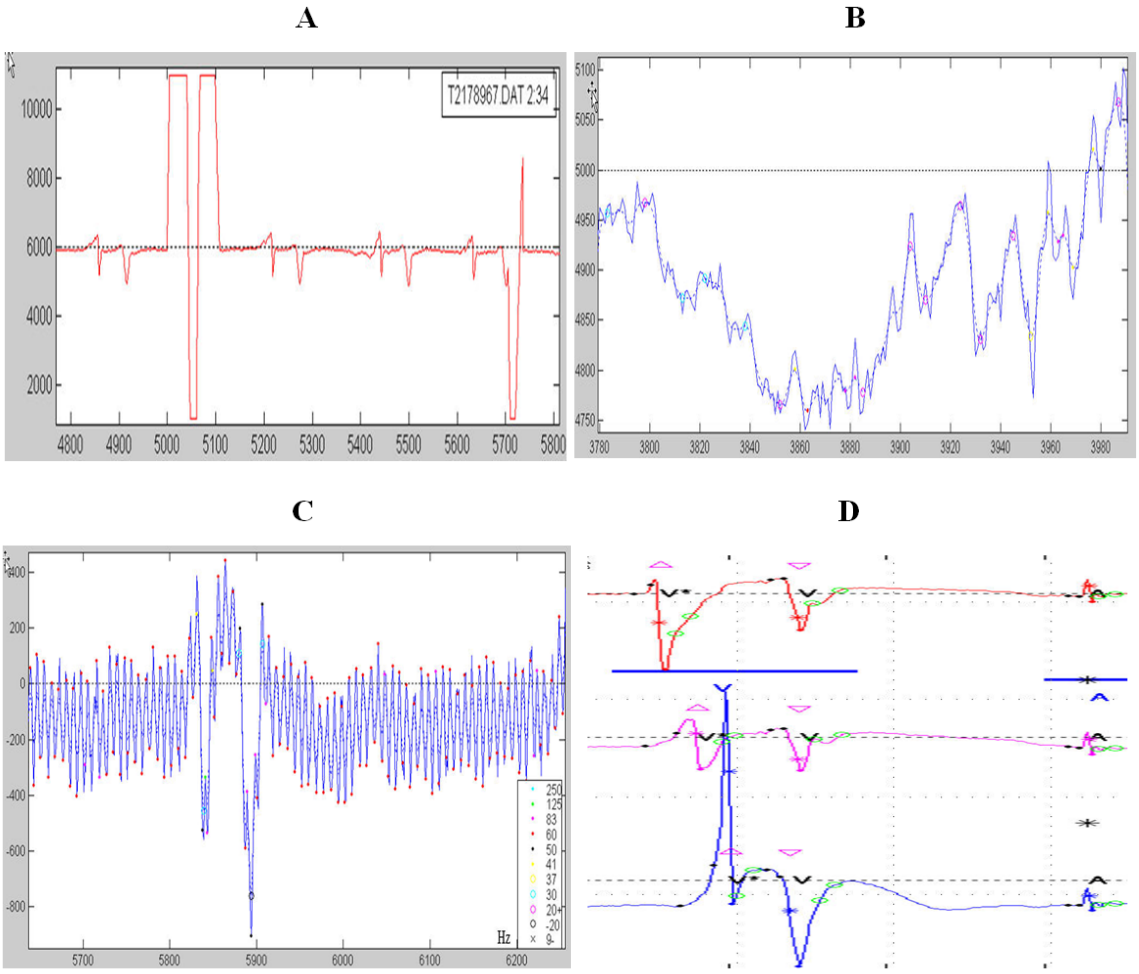

Figure 2. 4 Four example of difficulties encountered in the detection process: A) Holter device saturation, B) Baseline wandering, C) Noise in signal, D) Disproportion within and between channels.

Assuming a normal heart rate of 75 beats/min, the analysis of the recordings necessitates the determination of 27,000 markers/hr (60 min/h * 75 b/min* 3 channels * 2 markers (A, V)/beat), which made mandatory the development of a reliable automatic and unsupervised method of A and V timing and discrimination.

2.2.2 A and V Detection and Discrimination

The detection of algorithm was developed using a validated test set of ~46,000 markers from 19 patients, and its final performance assessed from ~1.6 millions validated markers coming from 27 patients. In this section, we only describe the main original features of the method whose flowchart is presented in Figure 2.5. For more details, the reader is referred to the article "Automatic detection and classification of human epicardial atrial unipolar electrograms" [151] included in Annexe II.

The detection of the activations was done on a pseudo-energy computed from the square of the derivative of the signals, a quantity commonly used for ECG processing [152, 153]. A global energy, constructed by adding the energy of the three channels, was used to identify the A or V global events and set their limits. Afterward, activations of the individual channels were located by analyzing their own energy within these limits. Ideally, each local and global event should be associated with an isolated bell-shaped peak of the energy functions, such as shown in Figure 2.6. To reach this result, the energies must be computed as a moving average to remove the notches associated with the zero-crossing of the derivatives and obtain a function whose amplitude remains high during the activation. Optimal averaging windows were determined, specific to the global and individual channel energy (given by eq. 2, 3, 4, 5 in paper). This was the first specificity of the method.

A second originality of the method was the pre-processing of the derivatives prior to the computation of the energy. Two sample-by-sample functions were computed from the raw signal to quantify saturation and baseline wandering (QoS^{Sat} in flowchart), as well as the local high frequency noise content (QoS^{35}). QoS^{Sat} was convoluted with the

derivative, while QoS^{35} triggers conditional low-pass filtering of the derivative along noisy segments. Another function (QoS^{art}), which provided a sample-by-sample measure of the density of the low frequency fluctuations, was used to adjust the threshold of detection.

Typically, high energy events corresponding to A activations are followed by lower energy V events. The detection of the Global events relied on a two-step process. In the first step, an adaptive sample-by-sample threshold function was constructed from the distribution of the minima and maxima of the global energy in an interval around each point. Once high amplitude events had been detected using this threshold function (energy > threshold for at least 40 ms), the energy was blanked in the intervals associated to each global event, and detection was repeated with a new threshold function whose computation also took into account the density of low frequency fluctuations measured by QoS^{art} (See Figure 2.6). The dual detection process, involving time-varying adapting threshold, was another original feature of the method.

The detection of global events and their temporal delineation was followed by the detection of the events in each individual channel. Within the time limit of each global event, the threshold was fixed to a fraction of the maximum energy of each channel, which depended on the type of global detection (first or second pass) associated to the interval and on the local density of fluctuation (i.e. QoS^{art}). At the end of this step of the processing, there was a sequence of temporally delineated global events, each associated with local events detected on the individual channels.

The last innovative aspect of the algorithm was the method to discriminate A from V events. Because A activations corresponded to sharp deflections produced by the travelling of activation fronts beneath the electrodes, they usually had higher frequency content than the far-field V events. The discrimination was based on the comparison of the energy computed from the [6, 90] (I^{90}) and [6, 25] (I^{25}) Hz band-pass filtered derivatives. The I^{25}/I^{90} ratio is usually lower for A than V events (See Figure 2.7). The

ratio discriminating threshold was based on a moving average of the ratio computed from event to event (See Figure 2.8).

Similar rules were applied for both global and individual channel events, based on the global or channel energy respectively. The final diagnosis (A or V) of the global and associated local events was completed with test of coherence over their labels. Finally, the temporal markers of local events, which would be needed to build the time series to be analyzed, were put at the location where the cumulative energy within the limits of an event reaches 50%.

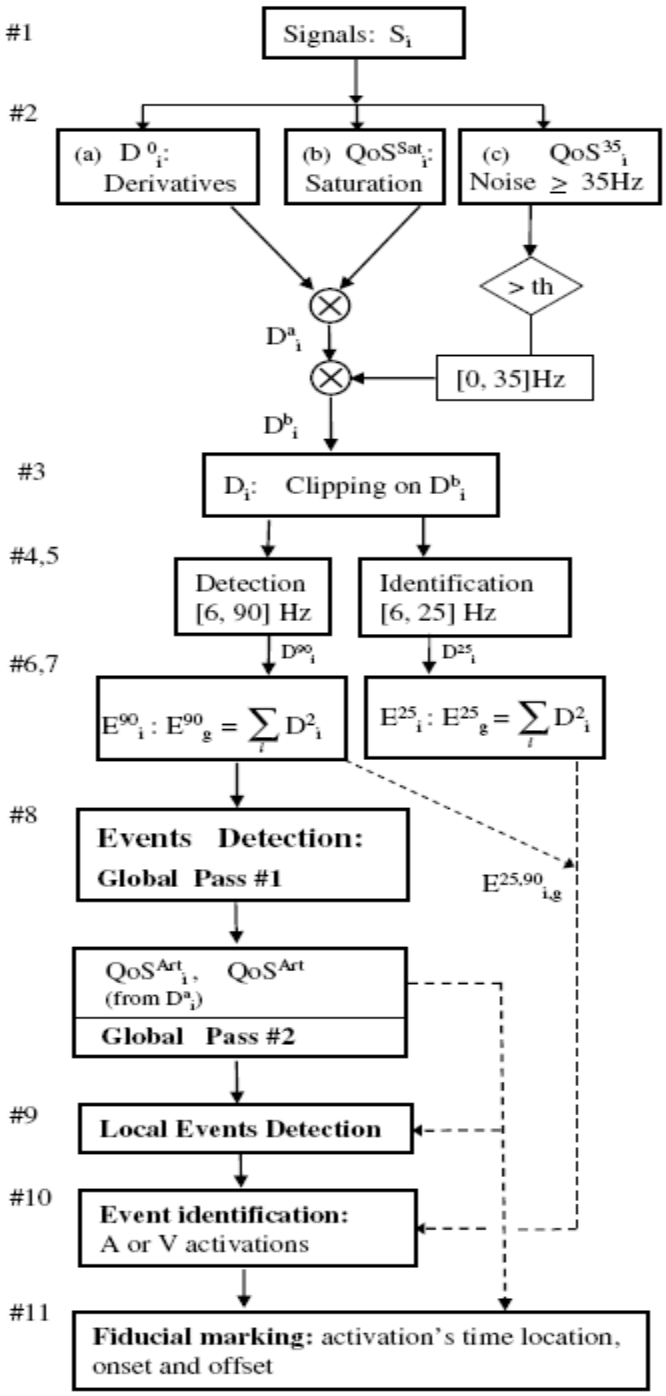

Figure 2. 5 Detection and labelling algorithm (From the paper [151] with permission of the editor). The acronyms in the figure refer to variables that are defined in the paper presented in Annexe I**.**

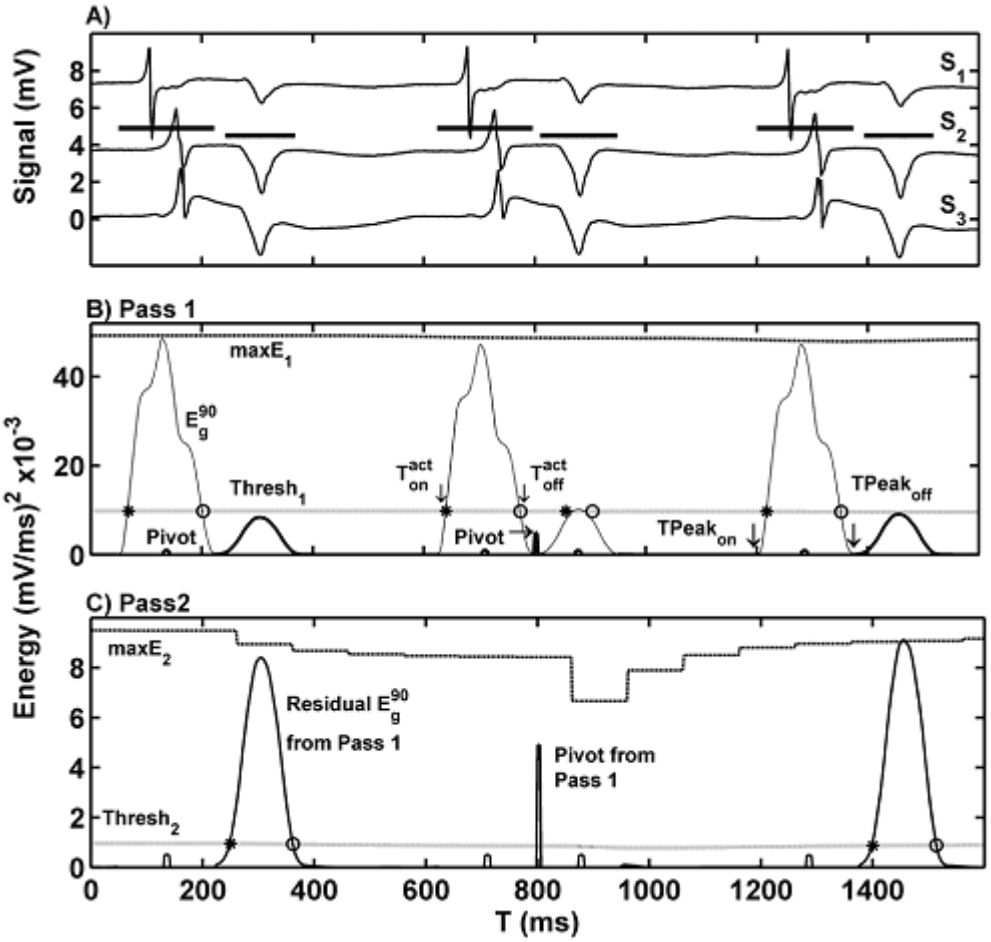

Figure 2. 6 Detection of global activations (step 8).a) Original signals S_1, S_2, and S3. The horizontal lines show the extent of the global activations, from their onset ($TPeak_{on}$) and to their offset ($TPeak_{off}$). b) Pass 1: events are segments with $E^{90}_g \geq Thresh_1$ (gray line) for at least 40 ms, from T^{act}_{on}(*) to T^{act}_{off} (o). The upper dash line $maxE_1$ is the maximum of energy used to calculate the threshold (line labelled $Thresh_1$). $TPeak_{on}$ and $TPeak_{off}$, used to delineate the extent of the global in panel A, are the first minimum before T^{act}_{on} and after T^{act}_{off} respectively. Each event is removed and replaced by a 3 samples pivot with an amplitude = 5% of energy at T^{act}_{on}. If the limits of two events are separated by less than 50ms, as the two events in the middle of the panel, a pivot in inserted in the middle, with an amplitude = 50% of energy at the first T^{act}_{on}. c) Pass 2: The residual E^{90}_g is analyzed as in Pass 1, with the new threshold $Thresh_2$ (gray line), calculated from the updated $maxE_2$ function (upper dash line, Eq. 2.8) (from the paper [151] with permission of the editor)

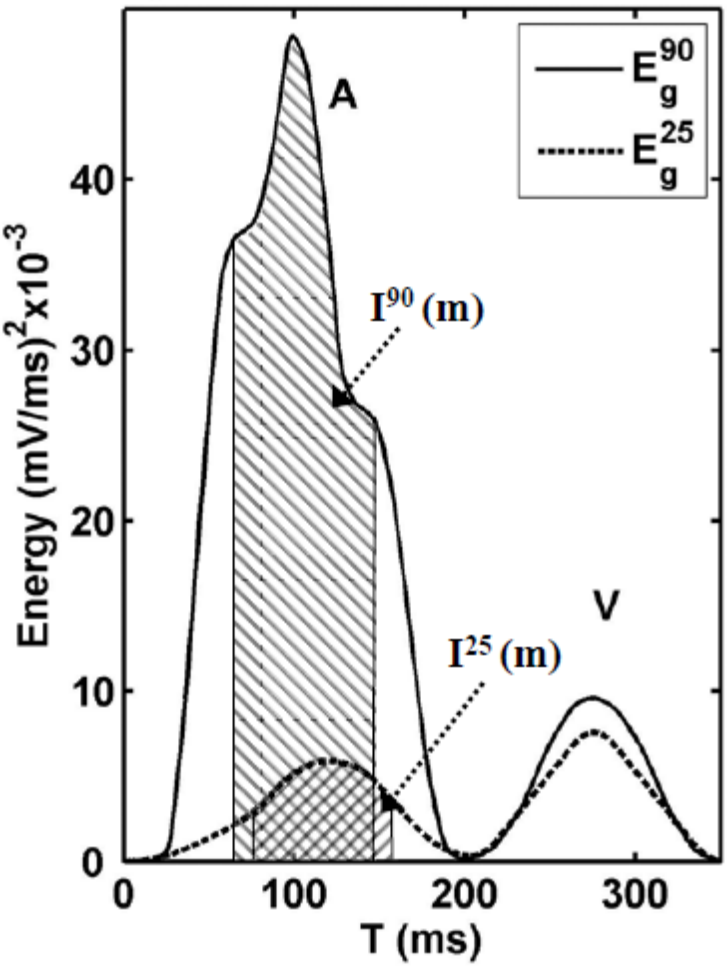

Figure 2. 7 E_g^{90} (continuous line) and E_g^{25} (dash line).I90 and I25 are the integral on a ±40ms interval around the maximum of E90 and E25 respectively. The ratio R=100 I25/ I90 is used to calculate the threshold to discriminate A and V events. (From the paper [151] with permission of the editor)

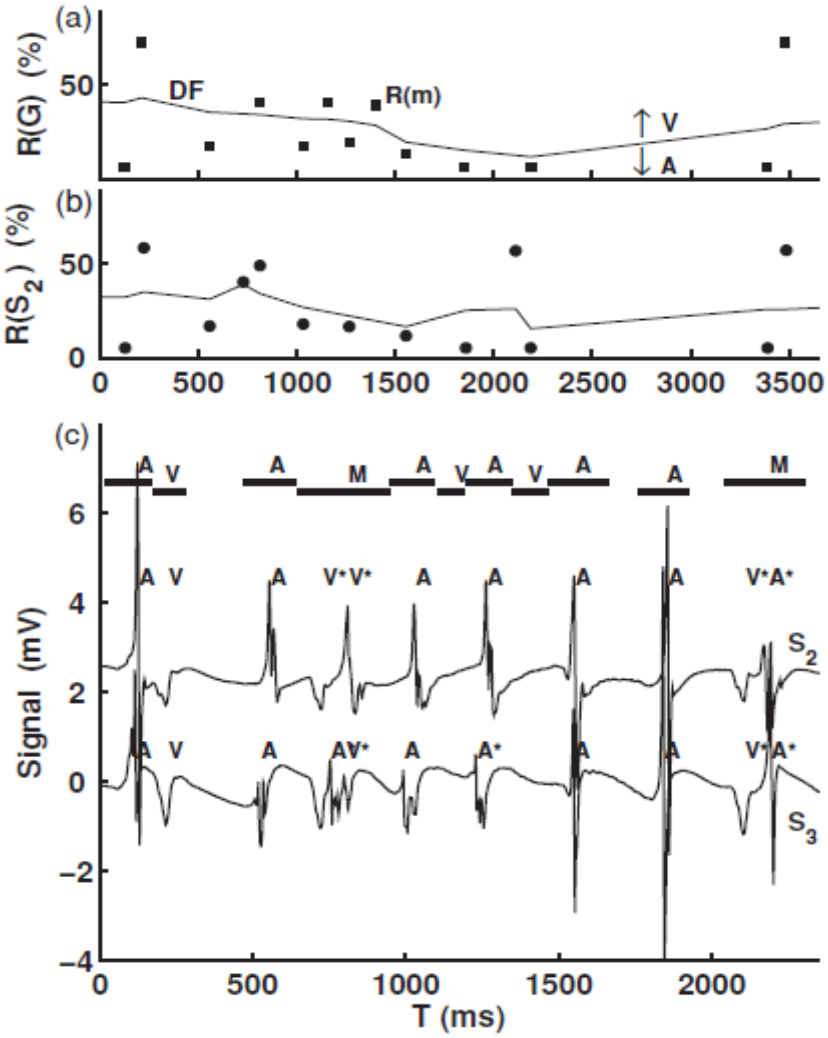

Figure 2. 8 Detection and identification in a sequence containing a salvo of atrial premature activations. a) Discriminating function (continuous line, DF) and of a sequence of R ratio (described in Figure 2.7) for global events, showing discrimination of A (under DF) and V (over DF). When an activation is missed (3 V in that example), DF, which also depends on past values, maintains the discrimination. b) The DF function for channel S_2 shown in the panel c. Even if one V is detected after 4 successive A, the discrimination is maintained. c) A and V detection and discrimination for a salvo of premature atrial activation (PAA) whose energy was highly depressed. All the PAA's were correctly detected and labelled as A, even when much depressed as in channel S_3 (only 2 channel shown for clarity). In S_2, the first fusion beat was detected, but the depressed A was labelled as a possible V. In S_3, the three fusion beats were labelled as A (from the paper [151] with permission of the editor)

2.2.3 Detection Results

As described in the Annexe, the final algorithm was tested on a set of 1,593,697 validated activations that were also classified as normal A or V activations (A, V) or premature atrial or ventricular activations. (PAA, PVA). These were from 2-hours recordings from 29 patients taken just before the onset of their first prolonged (> 30 min) AF. They were selected because it was a moment where the heart rhythm was known to become more irregular, and where activation would be more difficult to detect. 99.92% of the activations were detected, and among these, 99.91% of the A and 99.75% of the V activations were correctly labeled. In the subset of the 39705 PAA, 99.85% were detected and 99.21% were correctly classified as A. The false positive rate was 0.34%. The detailed results can be found in Table 1 and 2 of the article in the Annexe. In summary, an automatic and unsupervised detection and labeling method had been successfully developed.

2.3 Validation

The timing software provided a list of global events with their temporal limits, and the temporal location of the activations detected on each channel within the limits of each global. The global events were labeled as A or V if the global and all markers of the three channels received the same label (A or V). The global could also be classified as mixed when there were discrepancies between the global and some local labels. The Validate AV software permitted to change, delete or add makers on selected channels, to correct or modify their labels including the addition of new labels (such as premature atrial or ventricular activation, PAA, PVA, or other user defined categories). It also allowed to suppress existing global activations, to modify their limits and/or labels, to merge global activations (e.g. when delayed atrial activation in one channel ended up in a separate global), or create new global activations with specific user defined signatures (e.g. stretch of signal associated to atrial flutter, AF, or other atrial or ventricular arrhythmias).

The basic functions of the software are:

1. Location of dubious global or local markers for manual editing.
2. Deletion, repositioning or relabeling of activations based on waveform analysis;
3. New timing also based on waveform analysis.

Herein, we just describe the main features of the software. Details were given in a user manual and it is available at the Sacré-Coeur hospital research center. The software was written in Matlab (MathWorks Inc).

2.3.1 Selection of the Interval to Validate

The choice of markers or intervals to validate is based on the examination of time series computed from individual channels or global activations. For individual channels, the user can display AA, VV, AV and VA time series, (i.e. time between successive A and/or V markers). For global activations, these time series, calculated from the mean values of the markers within each global, are also available. Panels showing the sequence of the type of global activations (A, V or Mixed) and of the number of activations within these global events can also be selected. Any number of these time series can be displayed in the main or supplementary panels (see Figure 2.9).

To help locating problematic intervals, points lying beyond two standard deviations of the mean value are highlighted by red dots. Clicking on a position in any of these panels display the three channels over an adaptable interval centered on the selected location. Beside, the chosen location is indicated in all panels. As seen in Figure 2.9, the signals, the positions and labels of each marker, as well as the extent and label of each global appear in the main panel.

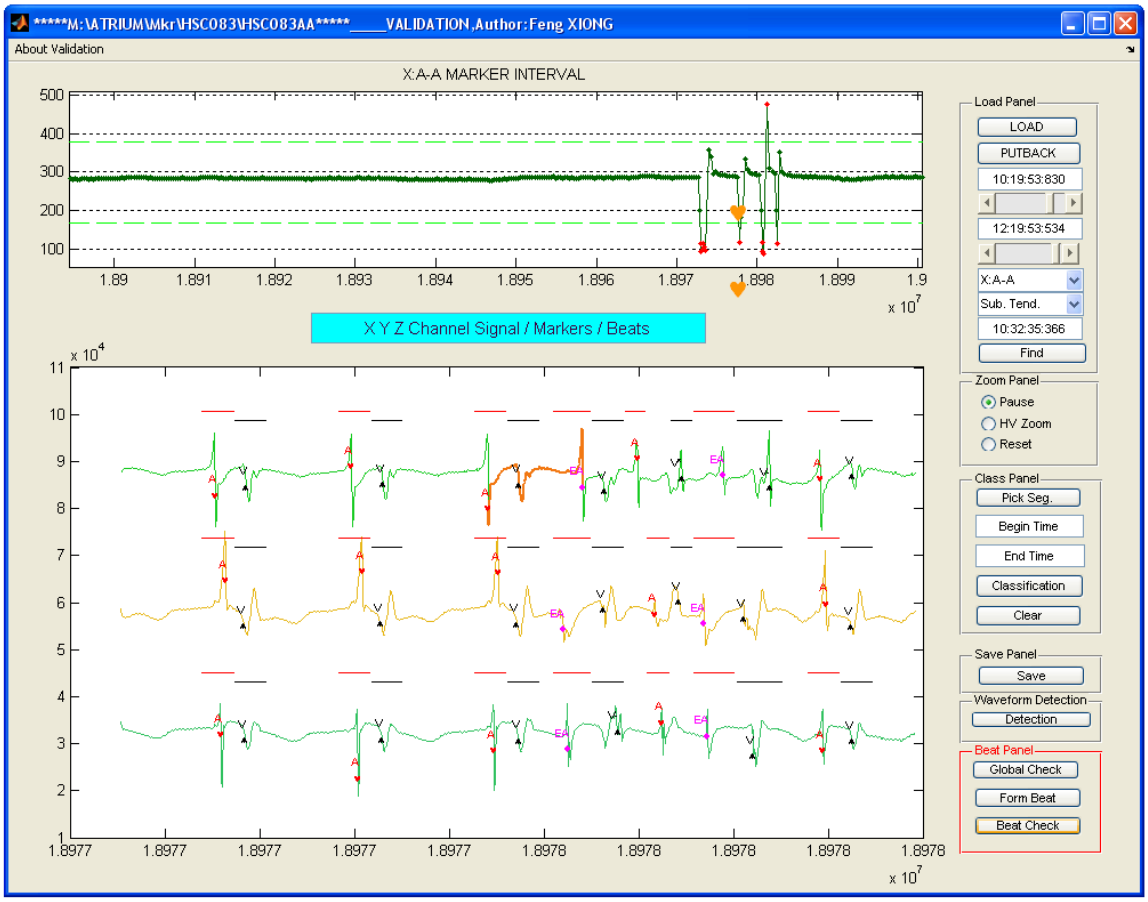

Figure 2. 9 Principal interface of the validation software. The upper panel shows the tendencies, in this case AA of an electrode. Lines showing the mean value ± 2 standard deviations are displayed and outliers are highlighted by red dots. The orange heart shape dot indicated the position that is selected for examination. The lower panel shows the signal of three channels, the A and V markers, and the extent and labels of the global (A red, V green) in an adjustable interval around the location selected in the upper panel. The operation control menus and buttons appear on the right of the figure.

2.3.2 Correction of Individual Local or Global Event

Once a problematic detection area has been identified, the following functions are available: Change the signature of the local or global markers, remove or add markers. It

is also possible to define new global events bringing together new and/or existing markers. All displayed time series are immediately updated after any modification. As shown in Figure 2.10, global events can receive labels such as atrial fibrillation, atrial flutter and ventricular tachycardia. For these, two distinct global events are necessarily given the same label, to locate the beginning and end of the arrhythmia. The same method is used to delineate intervals where the quality of the signals does not allow reliable detections.

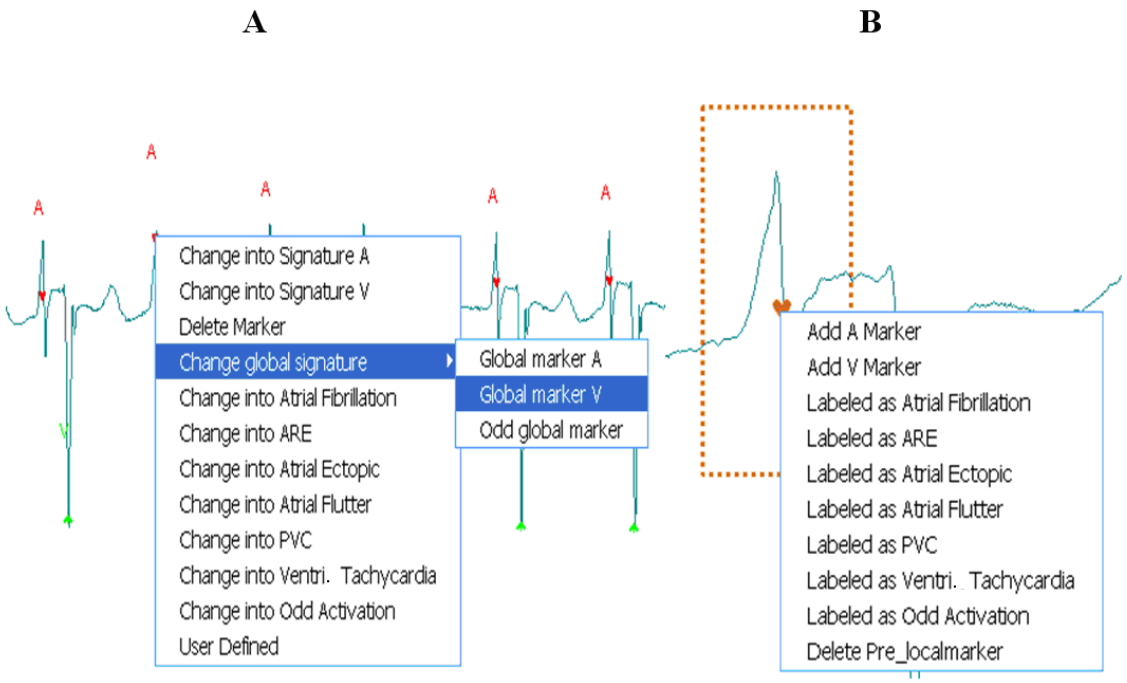

Figure 2.10 The context menu serves to remove or to change the label of the markers or modify their location. B) Pop-up menu for adding a marker.

2.3.3 Template Matching

Template matching, another option allows a waveform analysis of all or a few types of markers from a channel in a preselected time interval. The user first chooses the duration of the signal around each marker to be included in the waveform. The intervals preceding and following the markers are set independently. Afterwards, cluster analysis is performed on the waveforms using criteria that are described in the next section. At the

end of the process, the reference waveform and the number of member of each cluster are reported (See Figure 2.11). From there, all the markers belonging to a specific cluster can be deleted or relabeled. Any cluster can also be selected for further processing. The position of the marker in the template can be changed, which is applied to all members of the cluster. If the waveform is chosen long enough, other markers can also appear in some or all members of the cluster (e.g. V before or after waveform driven by A activation, see Figure 2.11). These secondary markers can be removed, added, or relabeled, and then such modification can be applied to all events in the cluster.

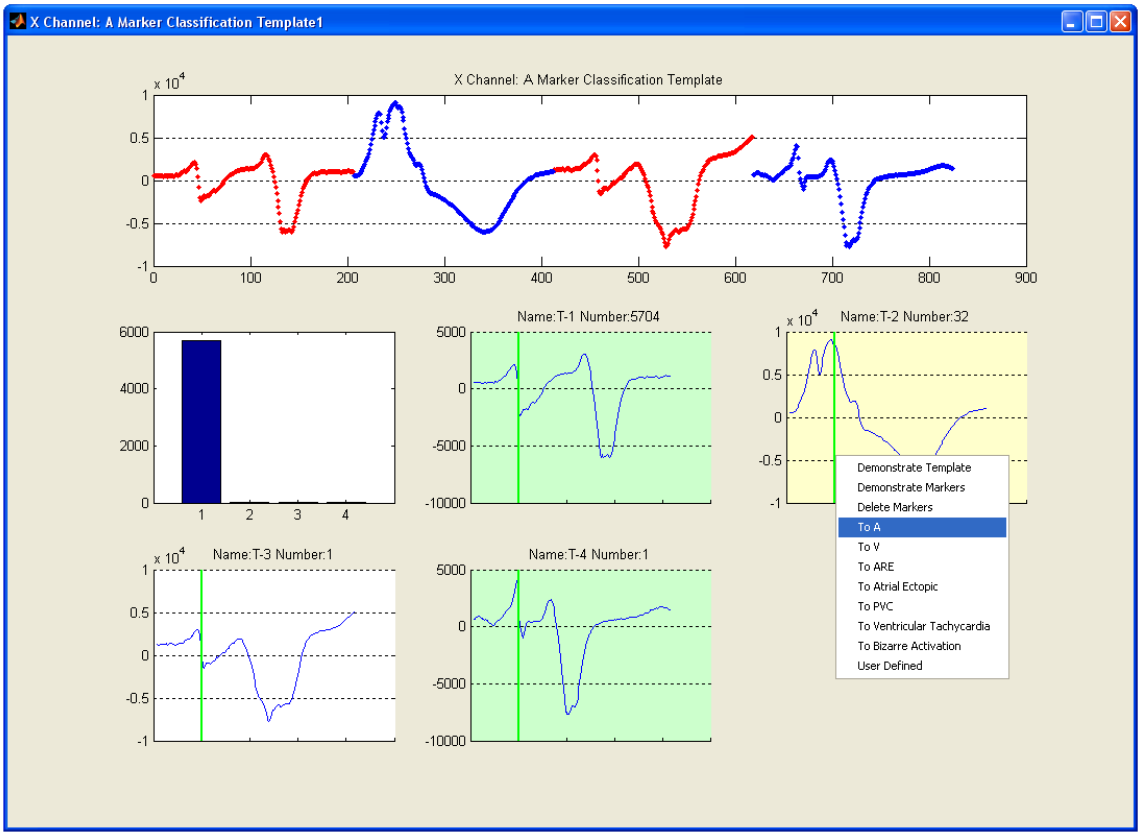

Figure 2. 11 Classification in selected time interval and pop-up menu providing choices for group modification of the attributes of markers in a cluster.

2.3.4 Classification Algorithm

The classification theory has been much developed in the past thirty years with the introduction of artificial neural networks and advanced signal and image processing

methods. Several algorithms have been proposed for classification of ECG beats and reported results that left room for improvement. [154-168]. One major problem is the wide variations in the morphologies of ECG waveforms within and among patients. For example, an ECG beats classifier which performs well for a given training database often fails miserably when presented with different patient's ECG. Such an inconsistency is a major hurdle preventing fully automated ECG processing systems to be widely used clinically. Our classification method is very general and fast implementing, based on template matching.

Cluster analysis requires a measure of distance between the objects to be compared, and a rule to group together objects considered as similar [169]. In our case, the objects are N-samples waveforms ($X = \{x_i = 1, N\}$), corresponding stretches of signal around the markers selected for analysis. We use two measures of distance between waveform X and Y.

1. **Pearson's correlation coefficient**

$$r(X,Y) = \frac{\sum_{i=1}^{N} (x_i - \bar{x})(y_i - \bar{y})}{\sqrt{\sum_{i=1}^{N} (x_i - \bar{x})^2} \sqrt{\sum_{i=1}^{N} (y_i - \bar{x})^2}} \qquad (2.1)$$

Statisticians in medical data analysis generally refer to a correlation close to zero as indicating 'no correlation', a correlation between 0 and 0.3 as 'weak', a correlation between 0.3 to 0.6 as 'moderate', a correlation between 0.6 and 1.0 as 'strong', and a correlation of 1.0 as 'perfect' [170]. In our program, the value for clustering can be selected by the user, but is set at a default value of 0.8. This measure is independent of the baseline and amplitude of the signals.

2. **Minimum distance**

Alternatively, the Euclidean distance

$$D_E^2 = \|X - Y\|^2 = (X - Y)^T (X - Y) = \sum_{i=1}^{n} (x_i - y_i)^2 \tag{2.2}$$

is also often used in pattern classification. We have implemented a variant that has been used in ECG classification[171]. It started by setting a threshold $\theta > 0$ to define

$$X1 : X1 = X + \theta$$
$$X2 : X2 = X - \theta \tag{2.3}$$

The choice of θ is done through an interactive panel (See Figure 2.12) on which the first waveform to analyze is displayed.

Then, Y belongs to the same class X if

$$D_E^2(X1, Y) = (X1 - Y)^T (X1 - Y) = \sum_{i=1}^{n} (x_i + \theta - y_i)^2 < n\theta^2 \tag{2.4}$$

Or

$$D_E^2(X2, Y) = (X2 - Y)^T (X2 - Y) = \sum_{i=1}^{n} (x_i - \theta - y_i)^2 < n\theta^2 \tag{2.5}$$

Note that the vector taken as a reference does not matter since $D_E(X_1, Y) = D_E(X, Y_2)$ and $D_E(X_2, Y) = D_E(X, Y_1)$.

Classification:

Considering a set of waveforms $\{X_1, X_2, \cdots, X_N\}$, the algorithm of the classification proceeds as follow: Choose the metric to compare waveforms (correlation and/or distance), and set the required threshold (r_{thr} and/or θ). If both metrics are selected, a waveform will be included in a cluster as soon as one of the criteria is satisfied.

1. Set the reference waveform $Z_1=X_1$;

2. Calculate $r(Z_1, X_2)$ and/or $D_E(Z_1, X_2)$. If the criterion on r or D_E is met, put X_2 in cluster Z_1. Otherwise, create a new cluster with $Z_2=X_2$;

Then for $X_{i=2,N}$

3. Apply step 2 to X_i using the reference waveform of each existing cluster Z_1 to Z_K and stopping the search as soon as the clustering criterion is fulfill. Otherwise create a new cluster Z_{K+1} with reference waveform X_i;

4. Sort the order of the existing clusters according to their number of member, and their order of creation for ties.

More complex algorithms could have been implemented. However, we kept this simple cluster-seeking algorithm because it ends up being very efficient in our context of validation. Figure 2.12, is an example of a first reference waveform, which is used to set the clustering criteria θ. Figure 2.13 shows the reference waveforms of the cluster found in a stretch of signal.

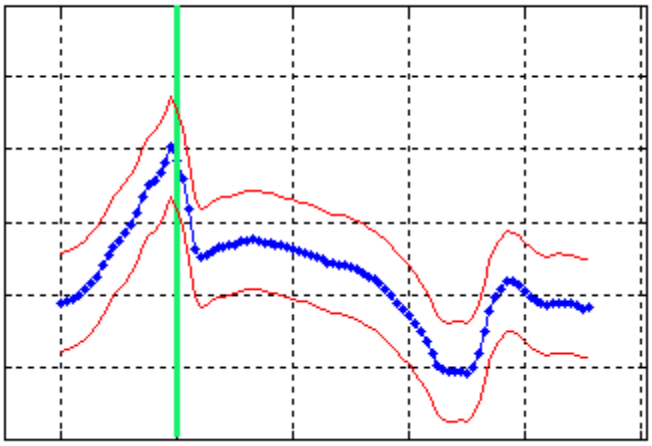

Figure 2. 12 Signal (blue line) around the position of a selected marker (green), and boundaries (red) set by choosing θ.

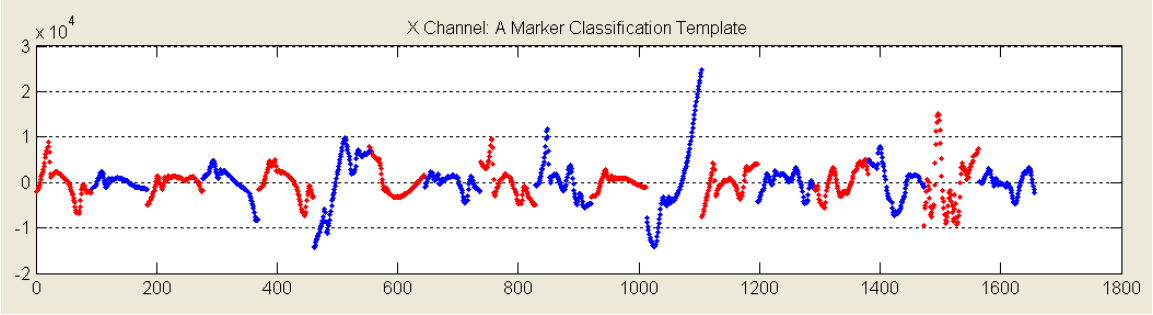

Figure 2. 13 The set of reference waveforms of the clusters.

2.3.5 Template Driven Timing

A template driven timing module is also integrated to the Validate AV software. The module is based on linear adaptive filtering method [172]. It is used to localize the segments of the signal that are similar to the template. Any stretch H(n) of the signal X can be picked a template. Then H is convoluted with the portion of X selected for analysis to produce a new function Z (Figure 2.14).

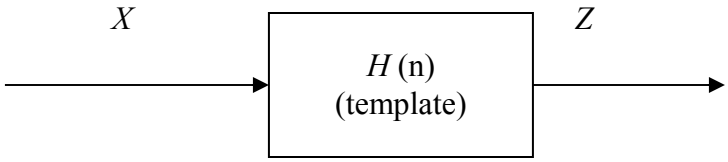

Figure 2. 14 Adaptive filtering method $Z = H * X$

Figure 2.14 shows an example where an atrial activation was chosen as template from a signal X (Figure 2.16), to produce the output Z (Figure 2.17). Then a threshold can be selected to detect activation similar to H.

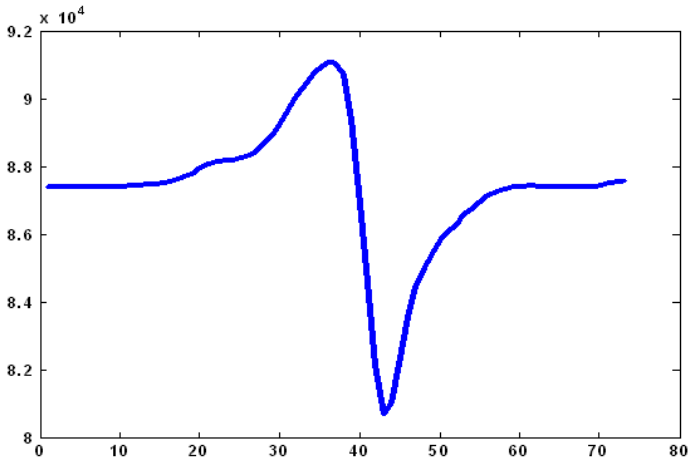

Figure 2. 15 One atrial activation chosen as the filter (template H)

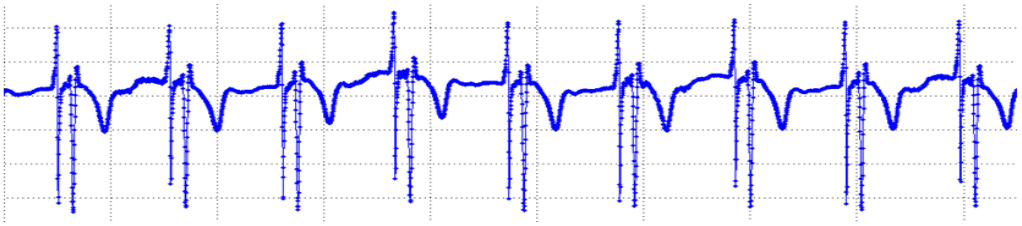

Figure 2. 16 The signal X as input of filtering

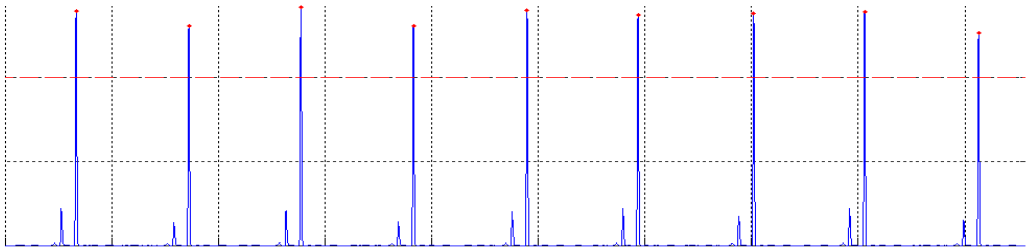

Figure 2. 17 The output of the convolution of H with X. Maximum beyond an adjustable threshold (red hatched line) localizes the position of similar waveform to H in X

2.4 Beat Formation

Once local and global activations are validated, the final processing step is to form beats, in which atrial and ventricular events belonging to the same cardiac cycle are linked together, and where final identification are given to all events. The analysis is performed on successive frames of five minutes. This is done because, as explained below, premature activations are identified with reference to the mean atrial frequencies, which needed to be updated. The procedure is as follows:

1. For each global ventricular activation, search for the closest immediate (i.e. without any other intercalated event) global atrial activation. The search is done in 5 sec. windows both before and after the ventricular global, allowing for the detection of retrograde activation of the auricles by premature ventricular activation.
2. For all the couples formed at step 1, calculate the absolute value of the time distances between the V and the associated atrial activation (D_{AV}, Figure 2.18),

build the D_{AV} cumulative distribution, and remove the first and last deciles of the distribution before computing the mean value (MD_{AV}). The distribution is truncated to get rid of possible outliers.

3. Couples in which $D_{AV} \leq 3*MD_{AV}$ are joined together and define events which are consider as AV cardiac beats. All other global are considered as isolated events.
4. From AV consecutive cardiac beats, get the time series of coupling times *AA* (difference between the time of the first atrial activation in each beat, most often A1A1, as in Figure 2.19).
5. For beats in which the atrial activations precede the ventricular activation (as in Figure 2.18), extract the atrial firing order of the three channels and identify the most frequent order, which corresponds to that of normal sinus beats. Calculate the mean coupling time ($MeanAA_{ref}$) from consecutive beats of this class.
6. Finally, each beat or isolated global is labeled as:
   i) SNAC(Sinus normal activation): beats formed by an atrial global followed by a ventricular global for which the atrial firing order belongs to the most frequent group and $AA \geq 0.7* MeanAA_{ref}$;
   ii) PAA (Premature Atrial Activation): beats formed by an atrial global followed by a ventricular global for which the atrial firing order is not the most frequent and/or $AA<0.7\ MeanAA_{ref}$;
   iii) PVC (premature ventricular conduction): beats formed by an ventricular global followed by an atrial global;
   iv) BA/BV (Blocked atrial/ventricular conduction): isolated atrial or ventricular activation;
   v) ARE (atrial retrograde conduction): isolated mixed global, holding both atrial and ventricular activations;
   vi) VT (ventricular tachycardia), AF (atrial fibrillation), AFL (atrial flutter), SATUE (invalid interval): as described in section 2.3.2, the beginning and end of these kinds of intervals are labeled by the user in the validation step. All global activations between these limits are then put together to define either an invalid or arrhythmia episode.

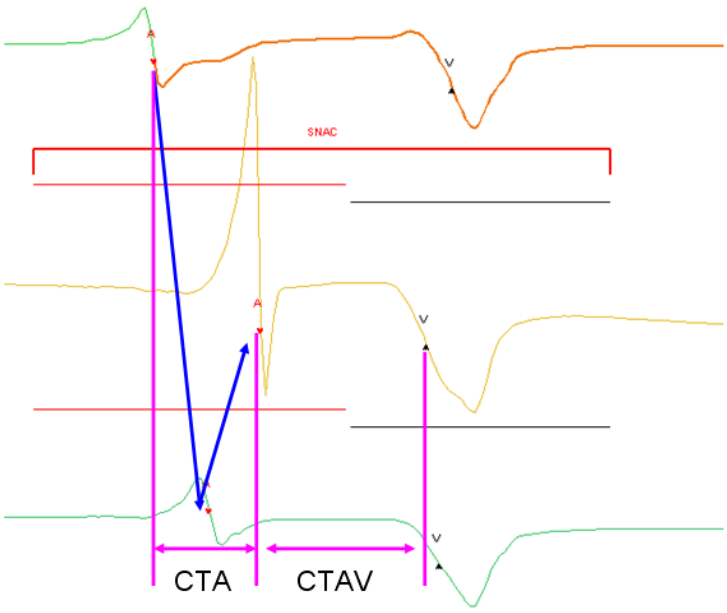

Figure 2. 18 Intra-Atrial conduction time (CTA), atrial firing order, an atrio-ventricular conduction time (CTAV)

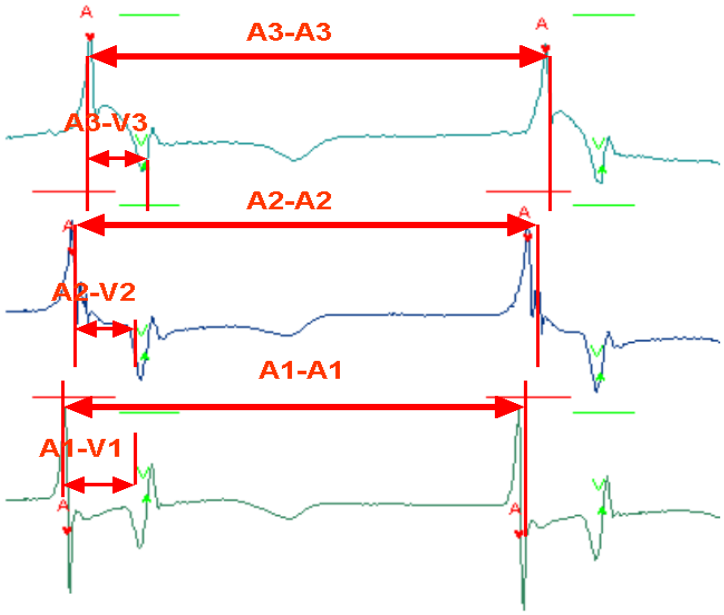

Figure 2. 19 AA intervals of two consecutive beats with the same order of atrial firing

2.5 Validate Beat

As for global and local activations, the results of the Form Beat software have to be validated. This is done by the module Validate Beat that offers five main functions (Figure 2.20):

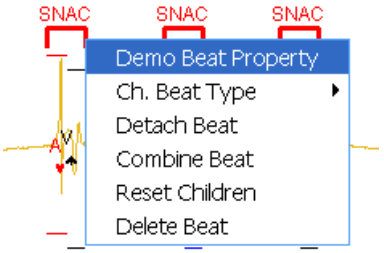

Figure 2. 20 The main menu of Validate Beat.

1. Demo Beat: the information of any particular beat can be displayed and edited. as shown in Figure 2.21;

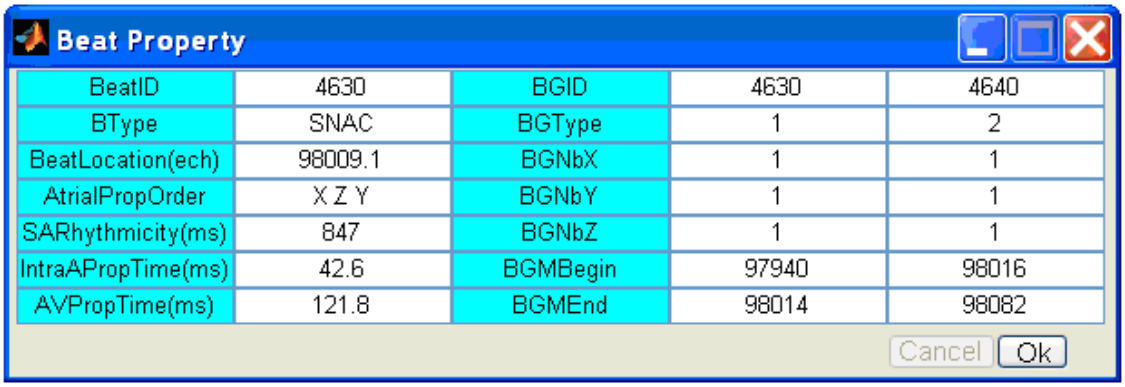

Figure 2. 21 Indices of a beat, which can be edited.

2. Change Beat Type

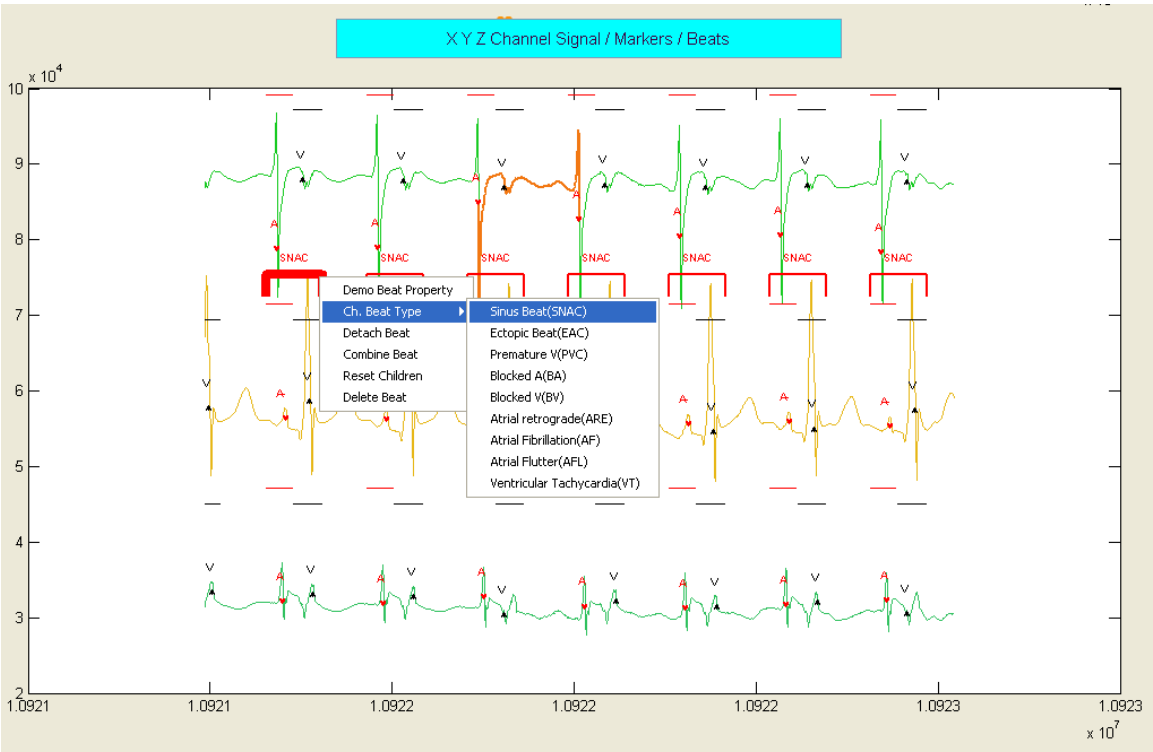

Figure 2. 22 Interactive panel to perform beat modification.

3. Detach Beat: uncombined global activations linked in a beat or arrhythmia, such that they become available for the formation of new events;
4. Combine Beat: combine two consecutive events into one beat;
5. Reset Children: reset the beat information if the local markers or global markers information has been modified;
6. Delete Beat: delete the existing beats if local or global markers have been deleted;

Actions 2 to 6 can be performed in an interactive panel shown in Figure 2.22. Figure 2.23 shows an example a final validated sequence of events.

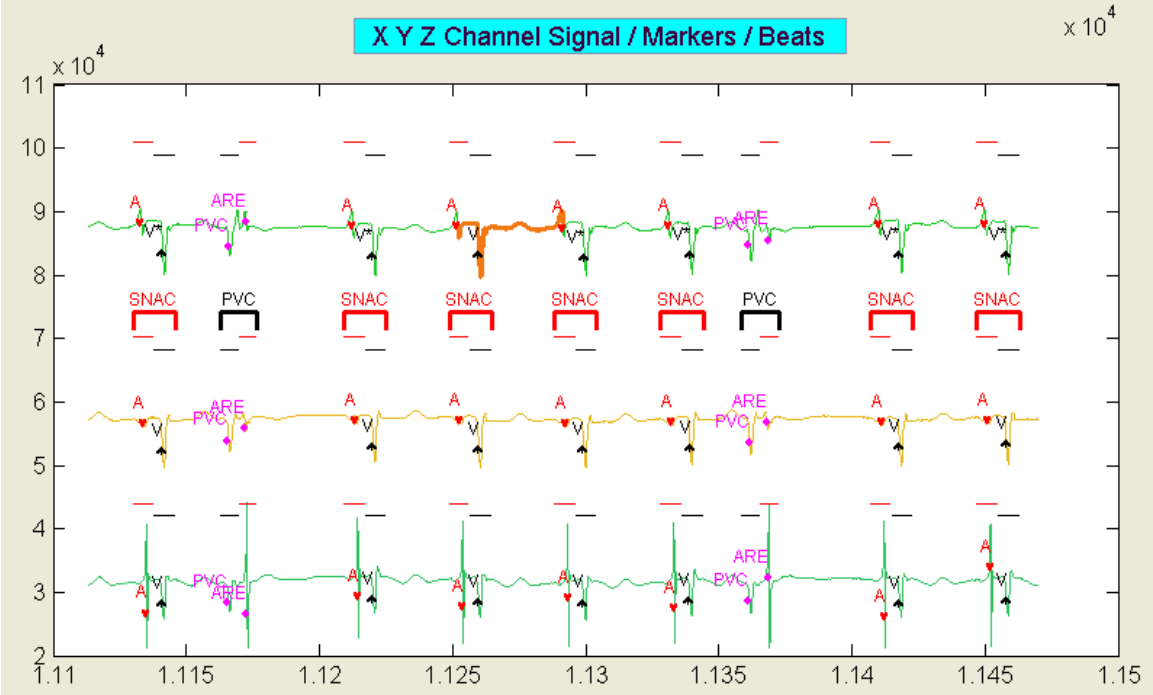

Figure 2. 23 After detection and validation, the activations of three channels are grouped into beats with a label corresponding to their type (Normal sinus beat, PAA…)

2.6 Beat Time Series Building

Different time series were built from the validated markers and events. The following section provides a definition of the variables and how they are computed.

1. PAA(premature atrial activation) related measures

The origin (left or right, LPPA, RPAA) of the PAA is set by the location of the first activated channel in the beat.

PAA Rate: The total (R_{PAA}), left (R_{PAA}^{L}) and right (R_{PAA}^{R}) rate: number of PAA occurring in a reference period (e.g. 5 minutes) divided by the time without atrial and ventricular arrhythmia during the reference period.

PAA proportion (P_{PAA} , P_{PAA}^{L} , P_{PAA}^{R}): corrected number of PAA in a reference period (CN_i= rate in the i'th period* duration of the period) divided by CN_T, the sum of the CN_i. Anova was performed on the Freeman-Tukey arc-sine transformed proportion [173]

$$F\text{-}T(P_{PAA,I}) = \frac{1}{2}\left[\arcsin\left(\sqrt{\frac{CN_I}{CN_T+1}}\right)+\arcsin\left(\sqrt{\frac{CN_I+1}{CN_T+1}}\right)\right] \approx \arcsin\left(\sqrt{P_{PAA,I}}\right)$$

Besides, in the few instances where the total number of Right PAA was zero, P_{PAA}^{R} was set to $\sin^2$ (F-T (P_{PAA}^{R})=0);

LPAA Fraction (*LPAAFraction*): the number of LPAA in the reference period divided the total number of PAA in the period. Anova was also performed using the Freeman-Tukey transformed fraction. When the total number of PAA was 0, then LPAAFraction was set as 0.5.

2. Sinus atrial rhythm related measures

In events defined as normal sinus beats, the first atrial activation always occurs in the same channel, which is used to calculated *AA* (ms), the time interval between successive normal sinus beats. The following measures are also computed in each reference time interval (most often, 5 minutes):

Mean (*AAMean*) and Standard deviation of AA (*AAStd*);

rMSSD : Root mean square of difference between successive *AA* ;

*pNN*50 : Proportion of successive *AA* with a difference > 50ms;

3. PAA prematurity

Two measure of PAA prematurity are used in the analysis

$Prem_{abs,}$ the absolute prematurity: the time from the previous activation to the premature activation calculated from the electrode first activated in the PAA.

$Prem_{rel,}$ the relative prematurity: $Prem_{abs}$ divided by the mean AA interval of the normal sinus beats in the minute before the PAA.

4. Premature ventricle activation (*PVA*) related measured.

PVA rate (R_{PVA}): The total number of *PVA* in the reference period of time (e.g. 5 minutes) divided by the duration of the interval without of atrial or ventricular arrhythmia;

5. Arrhythmia Duration(*ArrhyDuration*)

ArrhyDuration : Duration of all arrhythmias during in each reference period. An episode of arrhythmia was considered to occur when there was more than 3 consecutive atrial or ventricular ectopic beats. In these cases, the first ectopic beat was kept as a PAA or PVC, while the other was joined in an arrhythmia.

6. Intra-atrial conduction time (*CTA*) related measures

For all events, *CTA* is computed as the time between the first and last atrial activation. Then, the Mean (*CTAMean*) and standard deviation (*CTAStd*) are computed from normal sinus beats in each reference time interval.

7. AV node conduction time (*CTAV*)

Atrio-ventricular conduction time (*CTAV* , ms) correspond to the time elapsed between the last atrial activation and the following ventricular activation within each beat. Then, the mean (*CTAVMean*) and standard deviation (*CTAVStd*) of CTAV are computed from normal sinus beats in each reference time interval.

8. Local derivative (dv/dt)

dv/dt (mV/ms): the maximum slopes of negative deflections of each atrial activation ($\max\left|-dv/dt\right|$);

9. CANS (Cardiac Autonomic Nervous System) measures from spectral analysis of AA

Five minutes *AA* time series of normal sinus beats were analyzed by Fast Fourier transformation (*FFT*). All events different from normal sinus beats were excluded, as well as normal sinus beats immediately following a PAA. The resulting time series was interpolated with a fixed time step of 1 second and convoluted with a Hamming window [174]. Then following a common rule, the power contained in low (LF: 0.04-0.15) and high frequency (HF: 0.15-0.40 Hz) was computed [175-178]. The following quantities were considered:

Low Frequency (*LF*) component: The summation of low-frequency spectrum (*LF* :0.04-0.15 HZ);
High Frequency (*HF*) component: The summation of high-frequency spectrum (*HF* :0.15-0.4 HZ).
LF Portion: *LF/ (LF+HF);*
HF Portion: *HF/ (LF+HF)*;
LF HF Ratio: *LF*/*HF*.

10. Correlation of conduction time series

The following Pearson correlation of normal sinus beats time series were built within each five-minute interval:

CorrAA _ AV : Correlation of *AA* series and *CTAV* series;

$CorrAA\_CTA$: Correlation of AA series and CTA series;

$CorrAV\_CTA$: Correlation of AV series and CTA series.

2.7 Discussion

2.7.1 Recording

Although methods were devised to continuously monitor the noise level of the signals in order to activate conditional filtering and adjust the detection thresholds, a few recordings had to be excluded because the quality was too poor to provide reliable time series. Different configurations of electrodes were used. Although their sequence of activations in a beat differed, all of them allowed to decide whether ectopic beats were originating from the left or right atrium and provided similar measure of atrial and atrio-ventricular conduction times for normal sinus beats. Because the number and position of the electrodes in the left atrium was changed, the measure of the prematurity of left atrium premature activation was probably the variable that could be the most affected by the change of configuration. It is acknowledged that would have been more appropriate to get data from a single recording configuration. Nevertheless, we decided to keep and analyze all patients together because of the limited number of subjects, especially among patients with episodes of AF.

2.7.2 Detection

The final performance of the detection algorithm was assessed using more than 1.5 million validated markers taken in the 2 hours before the onset of a prolonged AF, a period that most often encloses complex rhythms. The problem of detection and labelling in our project was somewhat similar to that encountered in the analysis of signals recorded by ICD or pacemaker, i.e., to capture activations during atrial ectopy,

tachycardia, and fibrillation and avoid false detections caused by noise or far-field R-waves (FFRW). The top panel of Figure 2.24 is an example where the plot of activation amplitude versus dV/dt_{min} shows a continuous spectrum, thus invalidating separation by clustering. In the bottom panel of Figure 2.24, PAA and V activations fall in between two separated clusters of atrial activations. In both cases, our method based on energy frequency content was able to correctly label most of the activations.

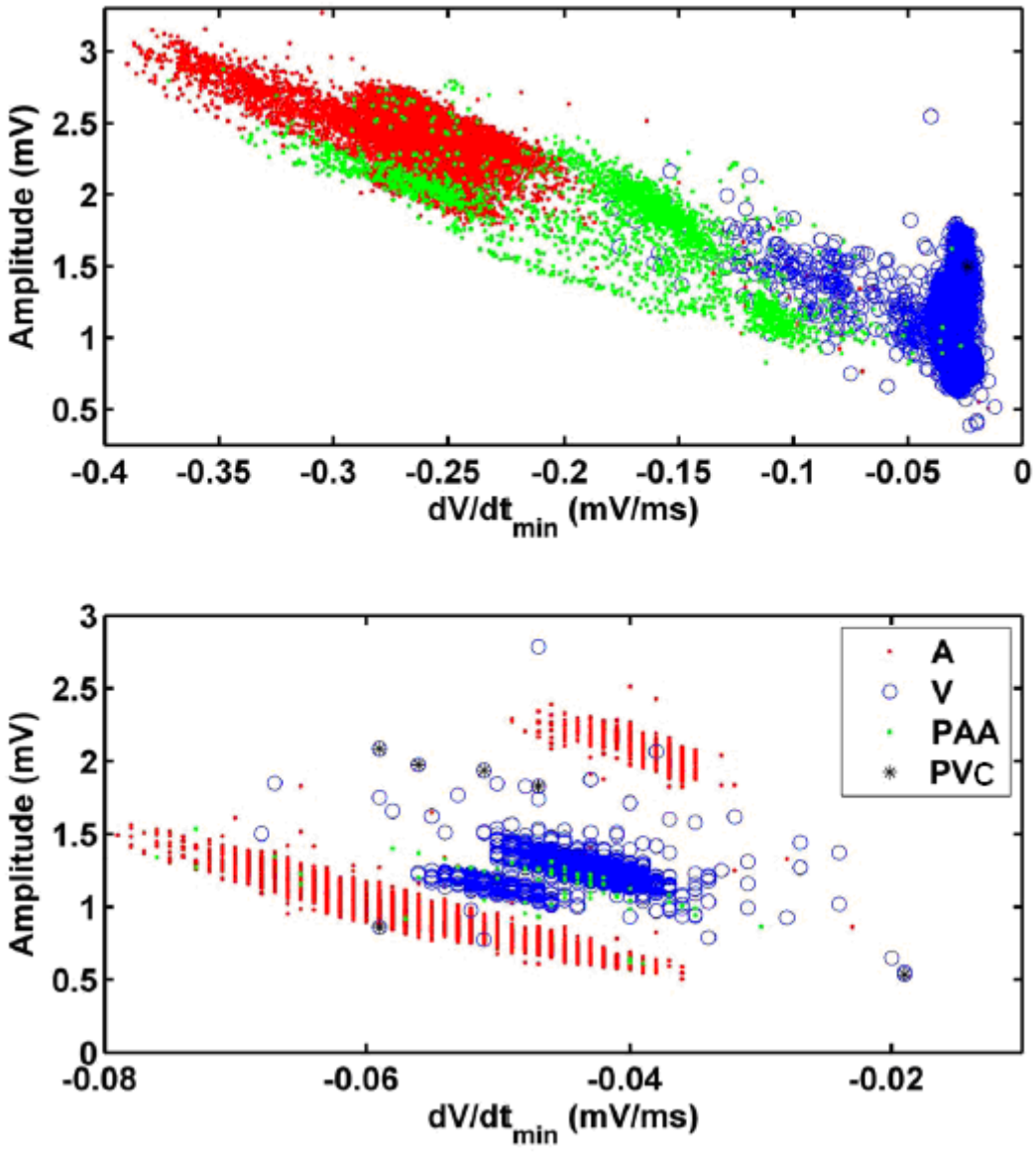

Figure 2. 24 Dispersion of the activations Amplitude vs. dV/dt_{min} from two channels from different patients. All activations from 2hr recording prior to AF onset are shown: A (red

dot), V (blue circle) and PAA (green dot), PAC (black star). Top panel: the distribution forms a continuous cluster, with PAA spread between A and V. Bottom panel: PAA and V are in a cluster between two separated clusters of A.

Another study proposed to use A and V wave templates to detect and label the activations [179]. However, this study ignored highly changing conditions and inter-individual variability, as well as the complex rhythms that frequently arise just before AF. That makes the template approach less appropriate for our work.

The problem of faulty detections due to noise was handled by continuous monitoring of the quality of the signal to guide local filtering and threshold adjustment. The signal was also blanked during episodes of saturation and clipped to equilibrate the amplitude of the different channels. This brought an improvement of the false positive and false negative detections by a factor 4 and 3.5 respectively. The parameters adjusting the threshold as a function of the quality of the signals were optimized to detect PAA and PVC even at the expense of some false positive. These can also be adjusted for other requirements or different types of signals.

2.7.3 Validation software

The development of the validation software (Validate AV) was mandatory to obtain both the training and evaluation sets of A and V activations needed for the development and assessment of the automatic timing algorithm. Beside, much emphasis was put on strengthening the method to detect PAA and PVC that firstly had to be authenticated manually. After the development of the algorithm, validation was still needed to correct missed or mistaken global or local activations and defined episodes of arrhythmia prior to the analyses. Along with the progress of the project, new functions were added, such as the automatic formation and labeling of beats, as well as associated tools of validation. The final result is user-friendly interactive software specifically adapted for multichannel AEG analysis, with no commercial equivalent. It is acknowledged that the final manual validation of the activation times, beats and beats types is to some extent operator dependent, which may have so impact on the reproducibility of the resulting time series.

To reduce the inter- and intra-user differences, a proper training of the validation software is strongly suggested. The optimal method which will compare the results obtained by different users to reach a consensus would be too much time-consuming.

The classification module is an important part of validation software. Diverse methods of ECG analysis have been proposed, based on artificial neural networks or signal processing methods [153, 159, 161, 162]. Classification is usually performed by feature extraction from raw data waveforms, or from compressed waveforms constructed by principal component analysis [180, 181], independent component analysis [182], or wavelet analysis [183-185]. Class formation then relies on some measure of similarity. Since the markers of activation were already available, we found that the option to define the extent of the waveform both before and after the markers very useful for analysis and classification. Our clustering method, using either correlation coefficient or minimum distance without prior processing, was at once simple, fast and reliable.

The initial purpose of the classification module was to validate the identification of A or V activations. Then the module was strengthened to validate the detection of cardiac beats. In addition, once the templates of the classes were defined, they could be used to delete, move, positioned or label any number of markers simultaneously for all events belonging to a chosen cluster. This much improved the efficiency and the speed of the validation process especially in time periods enclosing many of detection errors.

The grouping of neighboring global atrial and ventricular activations within cardiac beats was based on the computation of the mean $CTAV$ over 80% of the adjacent pairs in each five minutes period. Even for normal sinus beats, $CTAV$ was found to range from 50 to 100 ms among different time interval and patients. Finally, we have chosen 3 times the mean $CTAV$ as an upper bound for beat formation. This criterion was appropriate for most beats, except during arrhythmia episodes such as atrial fibrillation, atrial flutter and ventricular tachycardia. In these types of episodes, especially with long lasting time, $CTAV$ could become very irregular, with complex and even asynchronous A-to-V or V-to-A activations ratio. This is why all intervals of arrhythmia were defined manually. The

automatic detection of atrial retrograde activation was also often difficult. For activations presumably starting in the Hiss or Purkinje system, some atrial activations were often close or even within the ventricular activation, such that they could be included in the same mixed global event. Sometimes, the waveform of atrial retrograde looked like premature ventricular activation. The morphology of atrial retrograde beats also frequently varied from beat to beat and channel to channel.

The detection and identification of PAA was imperative because of their suspected relation with the occurrence of AF. The detection was maximized by the two-step process of detection, both with moving threshold. They were identified by either their prematurity or their firing sequence with respect to the normal sinus beats. They were assumed to originate from the atria where the first activated channel was located. Obviously, this remains an approximation since the time for the activation front to reach an electrode is not only related to its distance from the ectopic focus, but also depends on the conduction speed and the conduction path.

2.7.4 Time Series Building

Our basic hypothesis was that the onset of AF could be linked to the distribution and prematurity of PAA, as well as to the presence of a proarrhythmic substratum. Therefore, variables related to these two factors were computed. Some were used to typify each PAA: localization, prematurity, intra atrial and atrio-ventricular conduction times, dv/dt of the first activated channel. Others were considered to characterize the state of the substratum: density of PAA, PVC and duration of transient arrhythmia; diverse measures computed during normal sinus rhythm.

The use of AEG gives access to information that is difficult or impossible to obtain from ECG. The value of local derivative (dv/dt) associated to each atrial activation, which is related to the local pulse propagation velocity, provides a measure of the local excitability of the tissue. The atrial firing sequence permits at least a partial identification of the

location of the ectopic focus, which would have been difficult to be known from three channels ECG Holter recordings. The intra-atrium conduction time (CTA), although it does not correspond to the full time needed for the front to cover both atria, is a more reliable and stable measure that the duration of P wave which is often difficult to evaluate from the low amplitude ECG. This is also true for AA and $CTAV$.

Both sympathetic and parasympathetic stimulation can shorter refractory period of action potential of the cardiac myocytes, possibly causing substrate conduction inhomogeneous property and then facilitating electricity reentry. AA LF and HF power components obtained by FFT analysis were analyzed both in absolute and normalized units. The LF/HF ration has been proposed to be an index of sympathovagal balance. The dynamics of autonomic nervous system tone can be studied to find if imbalance occurs before the occurrence of AF.

Neural modulation can produce changes in $AA, CTA, CTAV$ time series. The correlation between these time series might provide some measure of the state of cardiac autonomic nervous system, complementary to those provide by the spectral analysis of the AA. Since the cardiac autonomic nervous system feeds the sinus node, the auricles and the AV node, positive or negative correlation between any of these time series might indicate either an imbalance or concordance of the autonomic input between these structures and/or a dominance of the rhythm dependent properties in the atrial tissue or AV node.

2.8 Summary

1.An automatic algorithm to detect and identify complex AEG signals was presented. The algorithm was unique, robust, and gave results at a high level, and solved the prerequisite problem of our study with good performance.

2.Validation software was designed to validate the AV detection results, form beats and validate beats. It provided an intuitive tool to investigate the signal and tendencies of conduction time series, to validate the detect markers and form beats. The embedded functions in the software also allowed unsupervised classification to automatically modify markers and beats. These strengthened the validation performance of the software.

3.Time series were built for the purpose of identifying predictors of postoperative atrial fibrillation.

Chapter 3 Analysis of Premature Atrial Activation and Time Analysis before Onset of AF

This chapter studies the temporal evolution of various indices before to first protracted episode of AF (> 10 minutes [101]). If there is no significant change prior to the onset of AF, it would be useless to monitor the patients to detect impending AF.

It is generally acknowledged most AF are preceded by premature atrial activations (PAA) that frequently originate from the pulmonary vein [62, 186-188]. Waktare et al. have shown an increase of ectopic activity before the onset of paroxysmal AF [189, 190]. Increasing frequency of supraventricular ectopic beats and of 'warning' short transient atrial arrhythmias also occur before the onset of postoperative AF [186, 187]. It was thus mandatory to first examine if there was an increased incidence of PAA close to the onset of AF.

In many patients in our study, a large number of PAAs were recorded all over the two hours before the AF. Although PAAs preceded the onset of AF, the occurrence of PAA was not bound to trigger an episode of AF. J. M. Leung has proposed that impairment of left atrial function is an important risk factor of post-operative AF [96]. More generally, patients developing AF are speculated to have heterogeneous spatial distribution of excitability and repolarization [7, 191-193]. This raises the possibility that substrate properties may evolve toward a state that facilitates the incidence of AF. The analysis presents both univariate and multivariate analyses of the temporal evolution of indicators of the state of the atrial tissue, while the last section examines if the triggering PAAs that occur just before the onset of AF are endowed with specific properties.

Initially, the choice to analyze the two hours before the onset of AF was guided by previous studies in which the same period was considered [33, 136]. We decided that, at the end of the analysis of AF patients, this period would be considered appropriate if significant changes were found between some periods close to the AF onset and the others, while in the further periods the time series could be considered as constant. If the periods further from the AF had not been diagnosed as constant, we would have extended the analysis to a longer time period. As demonstrated in the chapter, we found significant changes to occur in the first hour before AF, but none in the second hour. As a consequence, the two hours period was used for all analysis. Among the 41 patients with AF, 11 patients were excluded because the quality of their signals (such as too much noise, or lost of contact by at least one electrode) precluded a complete and reliable analysis. Among the 30 remaining patients, there were 24 men (age: 69.9 ± 6.3) and 6 women (age: 74.6 ± 2.1).

3.1 PAA Analysis

3.1.1 Number of LPAA (Left PAA) vs. RPAA (Right PAA)

All long lasting AF (>10 minutes) episodes were immediately preceded by one or more premature atrial activations that originated from the left atrium (*LPAA*) for 26 patients and from the right atrium (*RPAA*) for 3 patients. For one patient recorded with the second configuration described in chapter 2, the origin was ambiguous because the electrode positioned in the left atrium was most often activated firstly even in regular rhythm. Since many analyses were performed considering PAA either a left or a right PAA, this patient was discarded.

The number of *LPAA* was greater than the number of *RPAA* for 25/26 of the patients whose AF was triggered from the left atrium, and 2/3 of patients triggered from the right atrium (Figure 3.1). However, the proportion of *LPAA* (i.e. *LPAA*/ *LPAA*+*RPAA*) was very inhomogeneous.

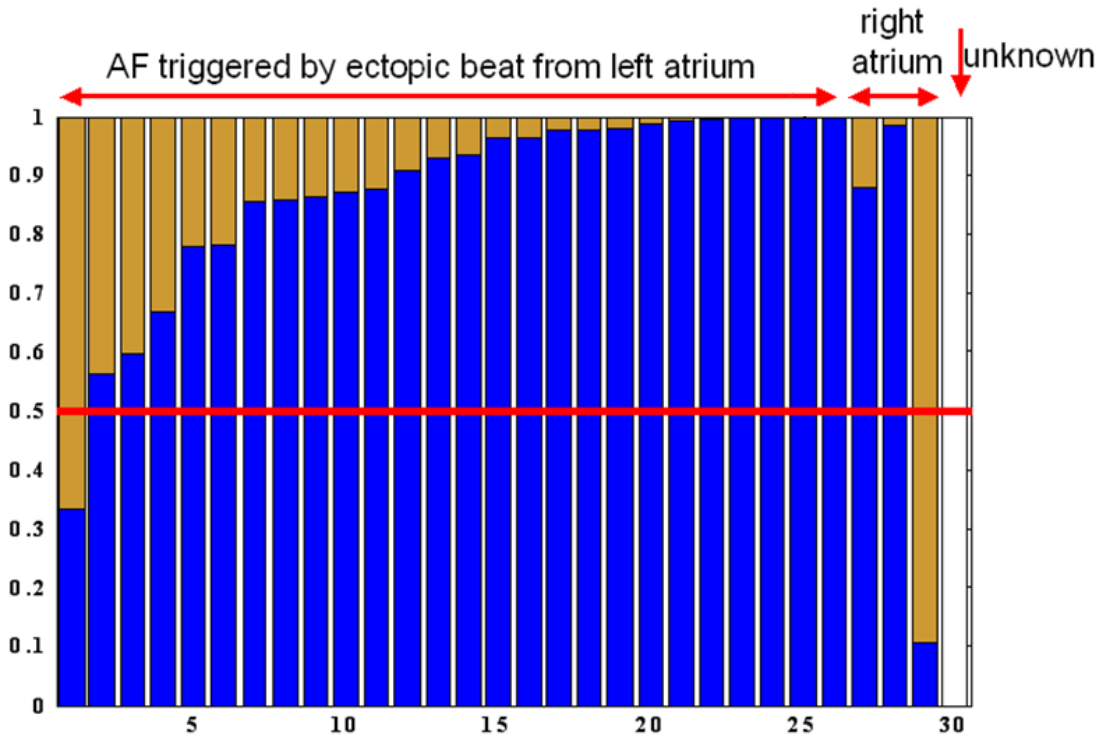

Figure 3.1 Proportion of *LPAA* (blue) and *RPAA* (golden) in the second hour before AF onset. The abscissa represents the identification (ID) number of the patients in the analysis. The ordinate is the proportion of *LPAA* (blue) and *RPAA* (gold) among the total *PAA* number within each patient. Patients with ID 1 to 26 and 27 to 29 had their AF triggered by PAA from left and right atrium respectively, while the origin of a subset of PAA including the trigger was unknown for the patient with ID 30. Homogeneity of proportion was rejected by χ^2 test, using either the mean number (patients 1-29, P <0.0001, patients 1-26 P<0.0001) or the mean proportion of left and right PPA (patients 1-29, P <0.0001, patients 1-26 P<0.0001) as null hypothesis. Both variables were examined because of the huge dispersion in the number of PAA among the patients.

The rate of PAA (R_{PAA} = nb. PAA/ minute without arrhythmia) was also highly variable among the patients: [$R_{PAA,\min}$ $R_{PAA,\text{median}}$ $R_{PAA,\max}$] = [0.02, 0.7, 37.90/min] in the two hours; [0.03, 0.95, 38.11/min] in last 30 minutes; [0.2, 2.36, 35.80/min] in last 5 min before AF.

3.1.2 Temporal Trend of PAA and Arrhythmia

Temporal Trend

The temporal evolution of *LPPA* and *RPAA* was studied by considering their incidence in successive 5 minutes intervals. Analysis was performed either by considering for each patient either the rate within each interval (R^{L}_{PAA}, R^{R}_{PAA} = number of PAA in 5 minutes/(5 min-duration of arrhythmias), Figure 3.2 A) or by the proportion of the total 2hr *LPAA* or *RPAA* in each 5 minute interval (P^{L}_{PAA}, P^{R}_{PAA} = number of PAA in 5 minutes/ total number of PAA, Figure 3.2 B). Either from the aspect of rate or proportion, *LPAA* shows an increasing trend over the time. Each method has its own drawback, the former being driven by the patients with the highest numbers of PAA, while the latter can be distorted by patients with a small number of PAA concentrated in a few intervals.

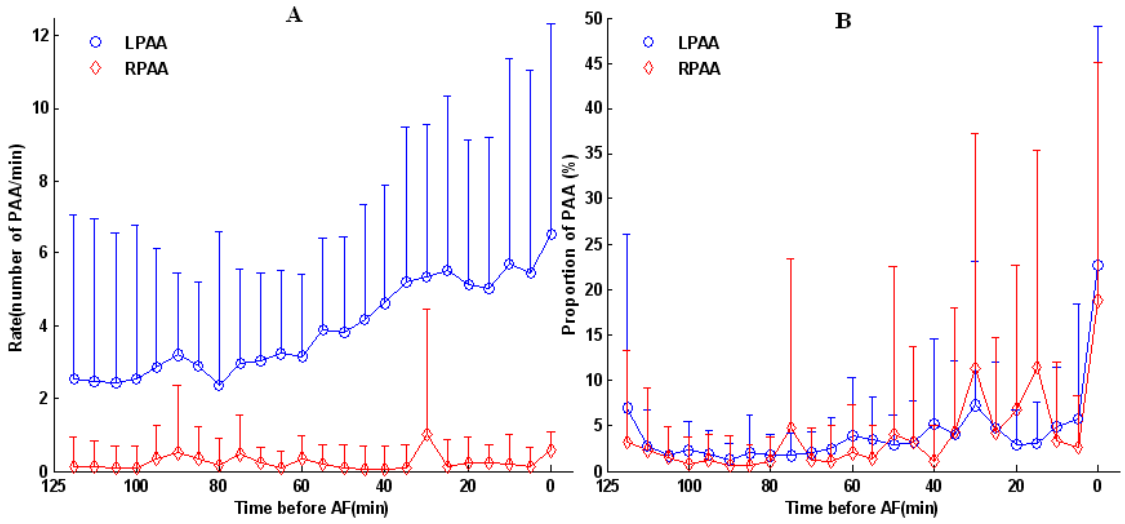

Figure 3.2 Mean value and standard deviation of A) PAA Rate (R^{L}_{PAA}, R^{R}_{PAA}, in Panel A) and B) PAA Proportion (P^{L}_{PAA}, P^{R}_{PAA}, in Panel B) within each 5 minutes before AF. Left atrium: blue line and circle; Right atrium: red line and diamond.

Analysis of the Rates **(R^{L}_{PAA}, R^{R}_{PAA})**

Because the temporal trends of R^{L}_{PAA} and R^{R}_{PAA} were significantly different (Anova time*L-R interaction, p=0.001, Huynh-Feldt criteria), they were analyzed separately. Only R^{L}_{PAA} showed a significant time effect (p=0.048, Huynh-Feldt criterion). Post-hoc analysis was done using different sets of orthogonal contrasts. The difference between the first and second hour was the only significant contrast (p=0.034) and it remained significant even after removing the last five minutes. No contrast (linear or other) restricted to the last hour, the last 20 or 10 minutes was even close to being statistically significant. The non-significance of the R^{L}_{PAA} linear increase in the second hour may seem surprising upon the examination of the Figure 3.2 A. As explained below, it stems from the heterogeneity of the profiles among the patients.

Analysis of Proportion **(** P^{L}_{PAA}, P^{R}_{PAA} **)**

Since P^{L}_{PAA} and P^{R}_{PAA} both sum to 1, analysis was performed by removing the first 5 minutes. As mentioned in Chapter 2**,** all ANOVAs' on proportions were performed using the Freeman-Tukey transformation. Taken together, P^{L}_{PAA} and P^{R}_{PAA} shows a significant time effect, with or without the last five minutes (p=0.003, p=0.045 respectively), but no significant left-right difference or interaction. Post-hoc analysis with different sets of orthogonal contrasts showed a significant difference between the first and second hour, both with and without the last 5 minutes before AF ($p<0.001$, p=0.003 for both right and left taken separately). Within the last hour, all significant contrasts were a consequence of the high increase in the last 5 minutes for P^{L}_{PAA} as well as P^{R}_{PAA}.

Patterns of Temporal Evolution

The analysis of rate and proportion both concluded to an increase of PAA in the last hour before AF (left and right for proportion, left only for rate). However, the lack of significant contrast within the second hour also suggests that there were different patterns of evolution among the patients. The patterns were classified by cluster analysis of the

sequences of 5 minutes values in the last hour. The correlation between the mean sequence of each cluster was used as a measure of similarity, with a threshold of 0.576 to stop the aggregation (threshold corresponding to p=0.05 significance level for sample size of 12). Correlation was chosen because it compares the profiles, irrespective of their relative amplitudes.

Figure 3.3 A presents the mean profiles R^{L}_{PAA} of the clusters obtained from the analysis. The largest cluster, gathering 11/29 patients, shows an increase of the PAA rate beginning 15 minutes before AF and culminating in the last 5 min. However, the rate of the members of this cluster was generally smaller than those of other clusters. This explains why a similar trend was seen in the evolution of the mean proportions (Figure 3.3) but not in the mean rates (Figure 3.2 A). The other three clusters, for a total of 7 patients, displayed a sharp rise of the rates from 40 to 30 minutes before AF. Together, all these clusters are responsible for the linear trend of the mean rate in Fig 3.2 A. Finally, three other patients rather showed a progressive decrease of the PAA rates during last hour. The remaining 8 patients, who did not belong to any cluster, had isolated bursts of PAA in one or a few intervals.

For R^{R}_{PAA} , the most important cluster, gathering 9 patients, with another cluster of 3 patients, showed an abrupt increase of PAA in the last 5 minute. 5 patients in this cluster also had a marked increase of R^{L}_{PAA} in the last 5 minutes. Globally, 19/29 patients showed a high rate of RPAA in the last 5 minutes, which may have been preceded by bursts in one or a few intervals within the last hour. The correlation between the profile of right and left PAA within either the last hour or half hour was highly variable, being beyond 0.5 for only 10 (1hr) or 5 patients (1/2 hour) respectively.

Finally, the rate of *PVA* was also analyzed. For most patients, there were random fluctuations of the rate of *PVA* within the 2 hours, with only a few patients showing an increase before AF. 4 patients had higher rate of *PVA* than PAA without any significant time trend. For these, some *PVA* may have induced PAA by retrograde propagation.

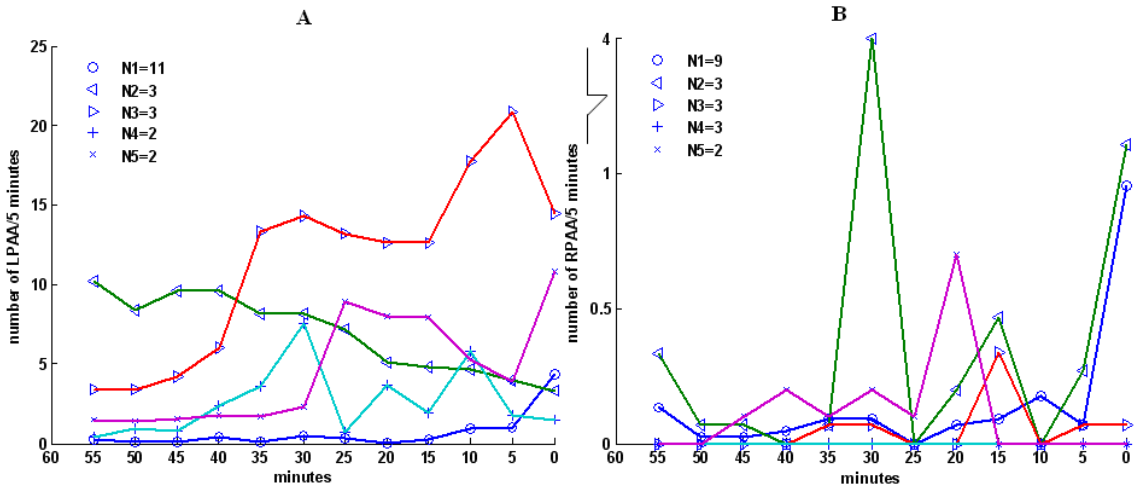

Figure 3.3 Mean patterns associated to the clusters obtained by the analysis of five minutes (A) R^{L}_{PAA} and (B) R^{R}_{PAA} . The number of patient within each cluster is indicated. The abscissa axis is the time before the onset of AF (min).

Non-sustained Arrhythmia

As shown in Figure 3.4 A, the duration of transient atrial arrhythmias increased in the last 30 minutes, with an abrupt rise in the last 5 minutes where it reached a mean duration of 10.03 seconds. These non-sustained arrhythmias were made of short runs of ectopic activations and/or atrial tachycardia. Figure 3.4 B shows the main clusters identified using correlation. 23/29 of the patients were in the biggest cluster, presenting an abrupt jump of the arrhythmia duration time in the last five minutes, and a minor increase in the last 25 minutes. The other patients had burst of arrhythmias distributed in the last hour before the onset of AF.

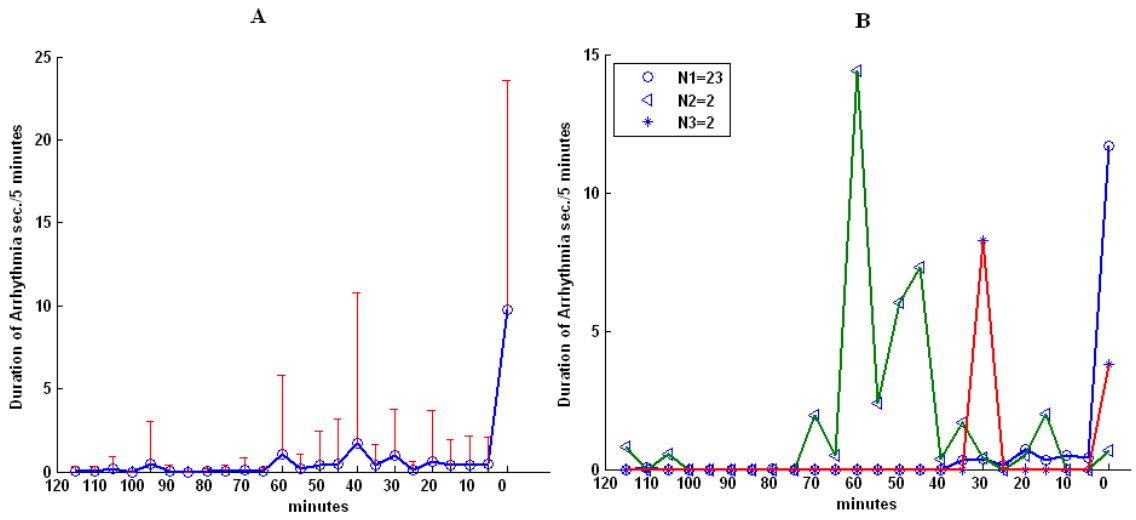

Figure 3.4 A) mean and standard deviation of the duration of arrhythmia (*ArrhyDuration*) by 5 minutes interval; B) Mean clusters profile of arrhythmia duration.

3.2 Post-hoc Analysis of Raw Data and Position Data

The methods used to analyze the PAA rate and the arrhythmia duration (repeated measures ANOVA analysis of values calculated within each 5 minutes, followed by post-hoc contrasts and finally cluster analysis), were also employed for the other variables. These variables were $AAMean$, $AAStd$, $rMSSD$, $PNN50$, $CTAMean$, $CTAVMean$, LF , HF , LF/HF , $LF/(LF+HF)$, $CorrAA\_AV$, $CorrAA\_CTA$, $CorrAV\_CTA$. They were calculated keeping only the sinus beats within each interval. These variables were considered as indices of the state of the tissue. The significance of the time effect was assessed for the raw data as well as the position data.

As described in Methods, position data were obtained by allocating to each data point of a patient its position in the cumulative distribution of the values obtained by this patient. Hence, for measures such as *AA*, *CTA* or *CTAV*, the position of each data point was obtained from the 2hr time series, and the mean position calculated within each time interval. For measures like PAA rate, arrhythmia duration, *AAStd* (standard deviation) or LF (low frequency content of the *AA* time series), the values were obtained from the raw

data within each five minutes interval, and position was allocated with respect the set of 24 values obtained from the two hours. Then, these position data were analyzed like raw data.

As seen in Table 3.1, among all indices, only the PAA Rate (R_{PAA}), the arrhythmia duration, the mean period of sinus rhythm (AA), the low frequency proportion of the AA variation (*LFPortion*= *LF*/(*LF*+*HF*) or alternatively *LF*/*HF* ratio) had significant (P<0.05) or close to significant (P<0.10) time effects for raw and position data. Table 3.2 shows the results of the post-hoc contrast analysis for these variables. In nearly all instances, the significance was higher for position than raw data.

The details of the AA and LF portion last hour evolution are presented in Figure 3.5 and Figure 3.6 respectively. The mean AA and the mean position AA showed a slight decreasing trend during the last hour (Figure 3.5 A). This heart rate acceleration was associated with the largest cluster, including 15/29 patients (Figure 3.5 B, blue line). A group of 3 patients oscillated from 680 msec. to 740 msec. in the last hour (red) and a cluster of 5 patients displayed a slightly increasing AA (green). In both these clusters, AA reached a maximum close to the onset of AF. The last cluster of 3 patients did not show much change (cyan). The other three patients that did not belong to any cluster had isolated fluctuations of AA.

The mean and position *LFPortion* (Figure 3.6 A) exhibited an increasing trend starting about 20 minutes before AF and peaking in the last 5 minutes. Despite the complexity of the profiles (Figure 3.6 B), three clusters including 17 patients showed a LF portion increase (blue, green, red), especially in the last 30 minutes. The other three profiles including 9 patients (cyan, yellow, violet) did not show any regular trend. Other 3 patients did not belong to any cluster and showed sharp and isolated burst of LF increase.

Table 3.1 Test within subject effects: (One-Way Within-Subjects ANOVA)

	P (*raw*)	*P* (*position*)
R_{PAA} (PAA Rate)	0.035	0.007
ArrhyDuration (Arrhythmia Duration)	0.030	0.009
AAMean (AA Mean)	0.002	0.004
$LF/(LF+HF)$ (LF Portion)	0.025	0.087

Table 3.2 Post-Hoc Analysis of Raw and Position Data of Specific Variables with Significant Time-effects in 2-pre AF Hours

(The upward arrow stands for the increasing trend over the contrasted comparison periods, and the downward arrow stands for the decreasing trend over those periods)

	R_{PAA}		*ArrhyDuration*		*AAMean*		$LF/(LF+HF)$	
	raw	position	raw	position	raw	position	raw	position
[120 60] Vs. [60 0]	0.019 ⇧	0.007 ⇧	0.016 ⇧	0.009 ⇧	0.001 ⇩	0.024 ⇩		
[60 30] Vs. [30 0]					0.084 ⇩			
[30 15] Vs. [15 0]						0.019 ⇩	0.069 ⇧	0.026 ⇧
[10 5] Vs. [5 0]		<0.001 ⇧	0.010 ⇧	0.010 ⇧			0.001 ⇧	<0.001 ⇧

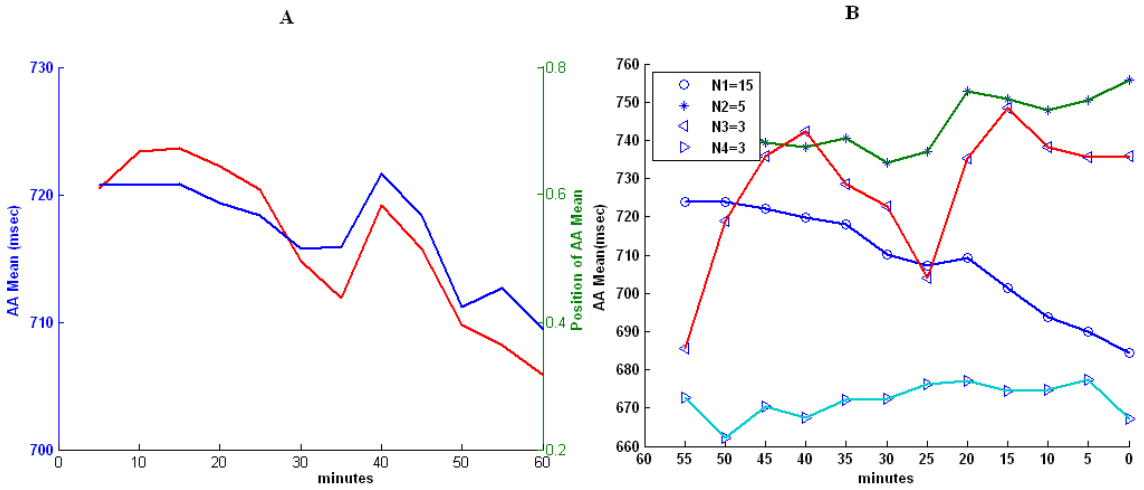

Figure 3.5 A) evolution of mean of the raw (blue) and position *AAMean* (red) in the last hour before AF. B) Cluster analysis of *AAMean* during the last hour before AF. Mean patterns of the clusters were plotted, and the number of patients associated to each cluster is indicated.

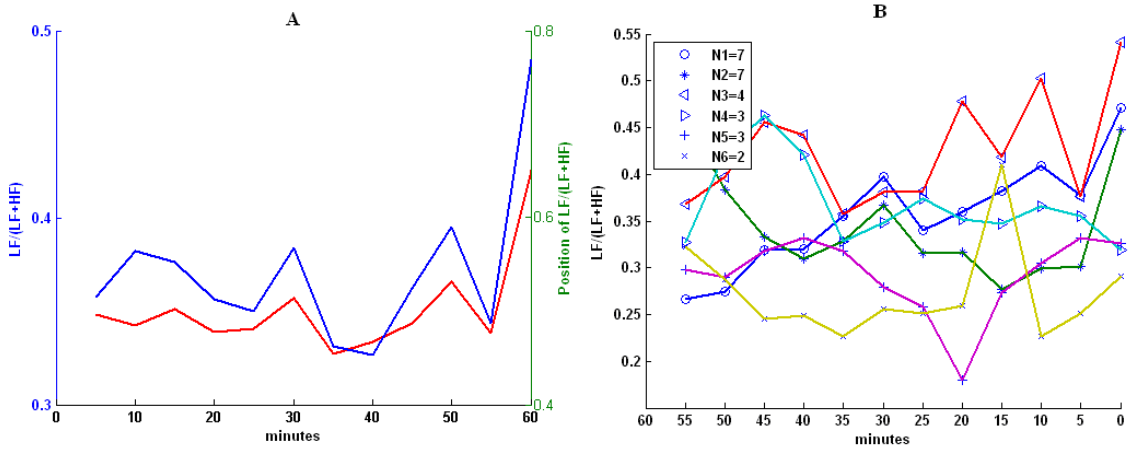

Figure 3. 6 A) evolution of mean of the raw (blue) and position *LFPortion* (red) in the last hour before AF. B) Cluster analysis of *LFPortion* during the last hour before AF.

3.3 Discrimination of Trigger from Non-Trigger Period

In an alternative approach, the power to identify the period close to AF was assessed by logistic regression. The analysis was repeated for both raw and position data dividing the 2 pre-AF hours in equal time periods of 5, 10, 15, 20, 30 and 60 minutes (variables analyzed in Sections 3.1 and 3.2). The power of these variables to discriminate the last period just before AF (triggering period) from the others (non-triggering periods) was assessed using forward conditional stepwise logistic regression ($p<.05$ entrance criteria). The scores of the resulting logistic model were used to build a ROC (Receiver Operating Characteristic) curve and select the optimal cut-off point.

Figure 3.7 shows the classification obtained for five minutes periods. The performance was much better with position than raw data although the same variables were selected in both cases. Similar results were obtained for all the partitions of the two hours: same selection of variables, but superior discrimination with position data.

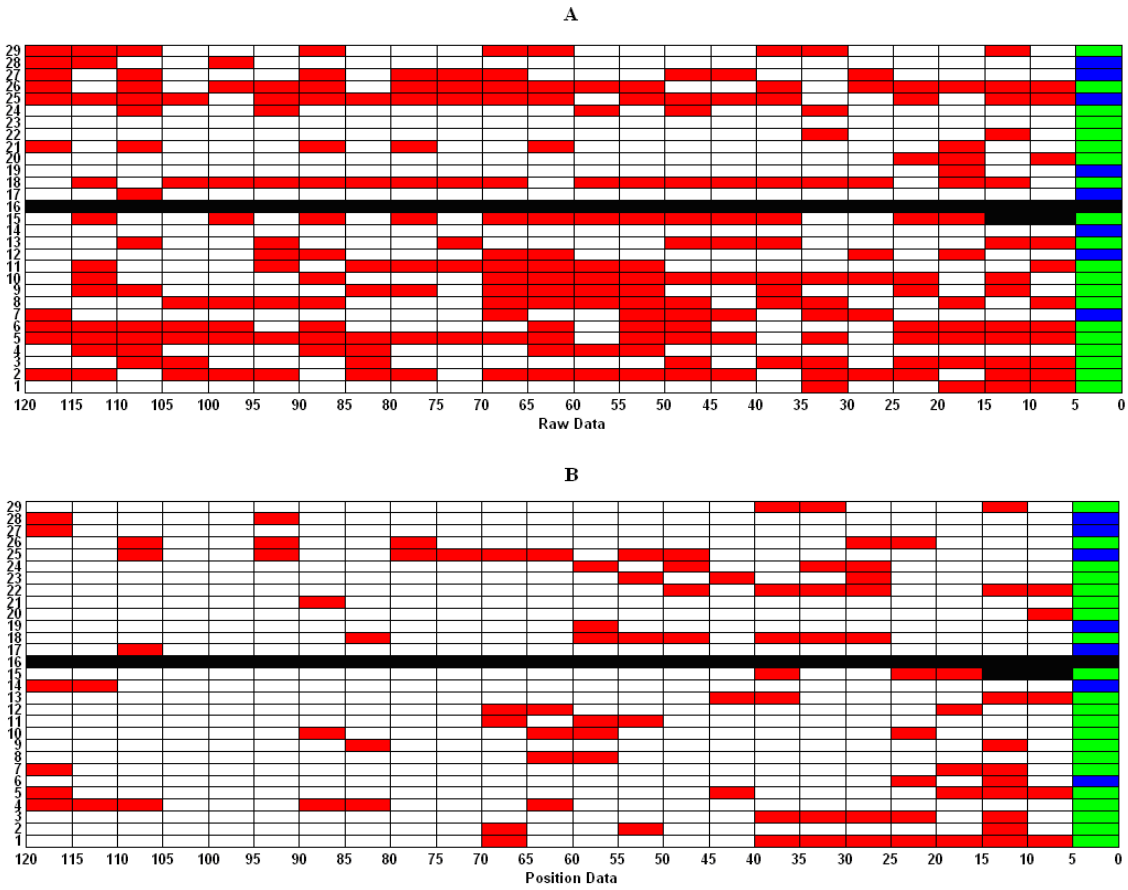

Figure 3.7 Comparison of prediction of the trigger period (last interval before AF) using raw variables (A) and position variable (B) for five minutes intervals. Green color box stands for true positive, blue for false negative, red for false positive, and white for true negative, black for the period with missing values because of insufficient number of sinus beats in five minutes. The abscissa is the time from the onset of AF, and the ordinate is the patient identity.

The results of the logistic model with the position data for different time divisions are shown in Figure 3.8. Panel A gives the variables kept in the model for each time partition, the color code indicating whether higher (red) or lower values (green) were predictive of the triggering period. Globally, seven variables were selected at least once, while R_{PAA} (PAA rate), $ArrhyDuration$ (Arrhythmia Duration), $AAMean$ (means AA) and $LF/(LF+HF)$ (LF Portion) were more often present. Globally, the results indicated that the onset AF tended to be preceded by an increased number of PAA and transient

arrhythmia episodes, on a background of accelerated sinus rhythm and a relative increase of its low frequency fluctuations. However, the changes were more informative when normalized using the distribution of values within each patient (position vs. raw data). The sensitivity and specificity (correct classification of the trigger and non-trigger interval respectively) remained between 65% and 85%, the total predictivity reaching a maximum for 30 to 60 minutes intervals. (Figure 3.8 B)

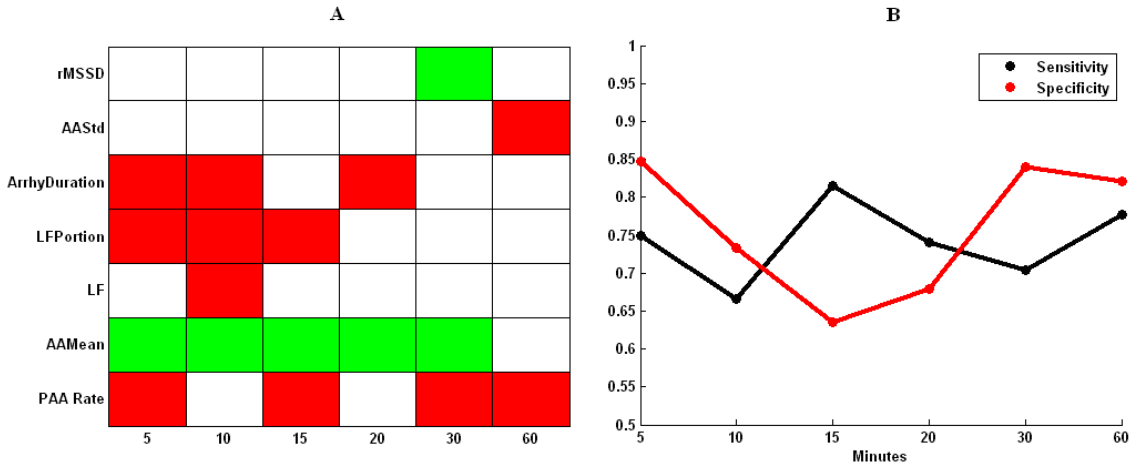

Figure 3.8 A) Sign of estimated coefficient of predictors in the logistic model (red: positive coefficient, green: negative coefficient) for different partitions of 2 hours intervals before AF. B) Sensitivity (red) and specificity (black) of each model with cutting point calculated from the ROC curve.

Table 3.3 The p value from univariate and multivariate logistic regression model with position data and 5 minutes partition

	Univariate (p Value)	Multivariate (p<0.05)
R_{PAA}	<0.001	0.002
ArrhyDuration	<0.001	0.045
AAMean	0.002	0.010
AAStd	0.576	
rMSSD	0.810	
pNN50	0.794	

LF	<0.001	
HF	0.016	
LFPortion	<0.001	0.001
HFPortion	<0.001	
LF/HF	<0.001	
CTAVMean	0.631	
CTAVStd	0.489	
CTAMean	0.632	
CTAStd	0.558	
CorrAA_AV	0.279	
CorrAA_CTA	0.316	
CorrAV_CTA	0.732	

Table 3.3 gives the results of the univariate and multivariate logistic regression for 5 minutes position data. Four variables were entered in the multivariate model in the following order*: RPAA, LFPortion, Arrhythmia Duration, AAMean*. Figure 3.9 shows the ROC curve associated with the successive models: I, R_{PAA};II, $LFPortion + R_{PAA}$; III: $LFPortion + R_{PAA} + ArrhyDuration$; IV: $LFPortion + R_{PAA} + ArrhyDuration + AAMean$. It is evident that the predictor R_{PAA} plays the most important role, achieving around 65% sensitivity and specificity. Then the other two predictors *LFPortion* and *ArrhyDuration* made some sensitivity improvements. The predictor of *AAMean*, finally introduced in the model, further improved the prediction, to reach a sensitivity of 72% and a specificity of 85%. Table 3.4 show the results of the comparison of AUC (area under ROC curve) differences using the method described in section 1.3.3. The methodology of the calculation of the Standard Error of the Area Under the Curve (AUC) and of the difference between two AUCs is the method of DeLong et al. [194]. The method employed the nonparametric approach to compare the areas under correlated ROC curves, by using the theory on generalized Mann-Whitney U-statistics for comparing distributions of values from the two samples [195]. The asymptotic normality and the

expression for the variance of the Mann-Whitney statistic was derived from theory developed for generalized U-statistics by Hoeffding [194]. Once the distribution of the variance, the distribution was defined, the standard deviation, and the confidence interval automatically followed.

In the table, the standard error The results of this test much differed from those of the logistic regression since none of the variables entered after R_{PAA} were diagnosed to bring a significant AUC difference.

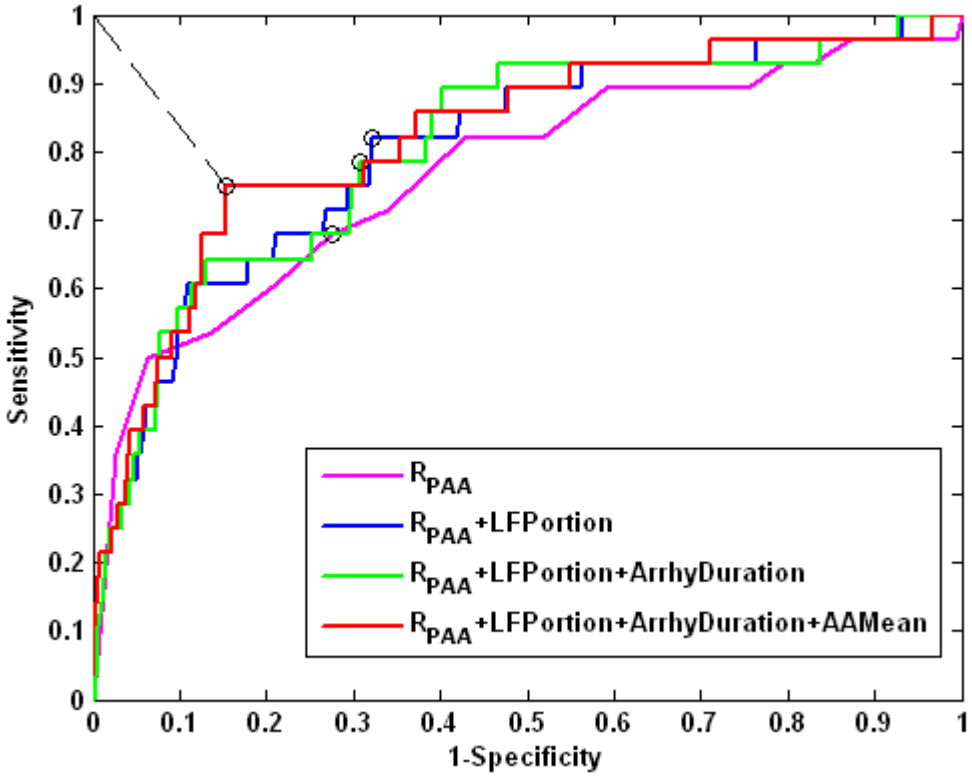

Figure 3.9 ROC curves of Model I, II, III, and IV. The circles indicated the best cut off points for each model.

Table 3. 4 The comparison of AUC (area under ROC curve) among the four methods, including the area difference, the standard error, the significance of the difference and the confidence interval.

	I vs. II	I vs. III	I vs. IV	II vs. III	II vs. IV	III vs. IV
Difference of AUC	0.0328	0.0353	0.0506	0.00256	0.0178	0.0152
S.E.	0.0415	0.0351	0.0471	0.00723	0.0211	0.0233
95% Confidence Interval	-0.0408 to 0.114	-0.0335 to 0.104	-0.0417 to 0.143	-0.0116 to 0.017	-0.0236 to 0.0592	-0.0305 to 0.0610
Significance Level	0.4301	0.3147	0.2830	0.7233	0.3992	0.5137

3.4 Characteristics of PAA Eliciting Occurrence of AF

In the second phase analysis, we examined whether the trigger PAA occurring just before the onset of AF were endowed with specific properties.

3.4.1 Prematurity

The arrhythmogeneity of an activation is often linked to its degree of prematurity [186]. For each PAA, the absolute prematurity ($Prem_{abs}$ = Time from the previous activation to the premature activation, evaluated at the electrode first activated in the PAA) and the relative prematurity ($Prem_{rel}$ = absolute prematurity/ mean AA interval of the sinus beats in the minute before the PAA) were calculated. Position value of the prematurity of each triggering PAA (*P-Prem*) was obtained by finding its location in the cumulative

distribution of the prematurity of all PAAs within each patient. The distribution of the *P-Prem* of the trigger PAA among the patients was similar for $Prem_{abs}$ and $Prem_{rel}$. As seen in Figure 3.10 A, the trigger $P\text{-}Prem_{abs}$ and $P\text{-}Prem_{rel}$ were among the 5% most premature for about 40% patients, but were spread uniformly for the others such that $P\text{-}Prem_{abs,rel}$ ≤ 0.5 for about 75% of the patients.

It was suspected that the accumulation of PAA close to the onset of AF might make the substrate so prone to arrhythmia that any PAA could then act as a trigger. However, there was a low correlation between the prematurity of the trigger PAA and the rate of PAA in the last 5 minutes ($P\text{-}Prem_{abs}$, r= 0.15, $P\text{-}Prem_{rel}$, r= 0.24). In fact, the three patients with the highest rates of the PAA (> 28/min, at least twice higher than all others patients) were responsible for this low level of correlation. As seen in Figure 3.10 B, not very premature trigger PAA could occur for different rates of PAA, which suggests that information on the substrate must also be taken into account.

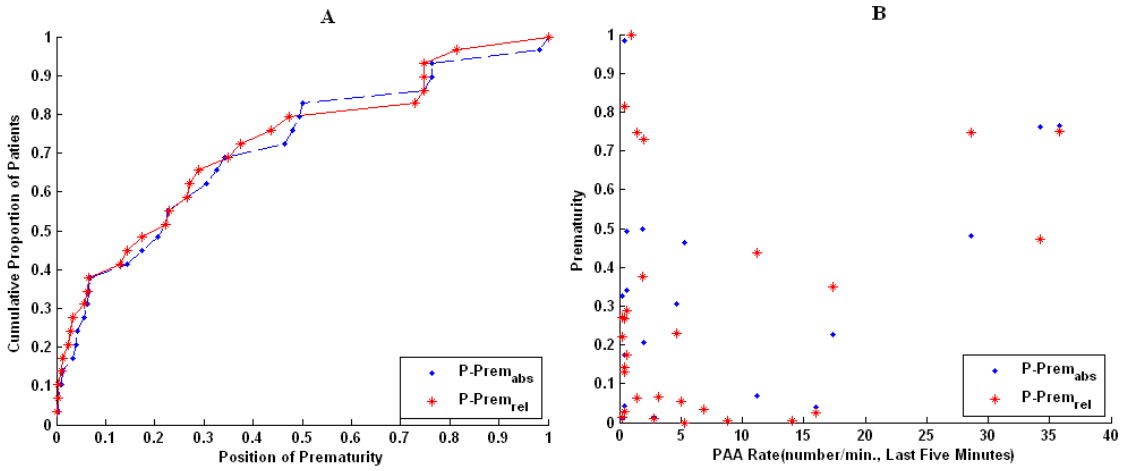

Figure 3.10 A) Cumulative distribution among the patients of the normalized absolute ($P\text{-}Prem_{abs,}$ point) and relative ($P\text{-}Prem_{rel,}$ star) prematurity of the triggering PAA. The abscissa is the value of $P\text{-}Prem_{abs}$ and $P\text{-}Prem_{rel}$, the ordinate is the cumulative proportion of patients for which the trigger PAA has $P\text{-}Prem_{abs}$ and $P\text{-}Prem_{rel} \leq$ the corresponding value on the abscissa. B) Relation between PAA rate and $P\text{-}Prem_{abs}$ and $P\text{-}Prem_{rel}$. The

abscissa is the PAA rate in last five minutes (number/min.), and the ordinate is the absolute (*P-Prem*$_{abs,}$ point) and relative (*P-Prem*$_{rel,}$ star) prematurity of triggering PAA.

3.4.2 Intra-atrial Propagation Time (CTA) of PAA

Intra-atrial conduction time (*CTA*) was measured as the time between the first and last activation for each PAA. The definition of *CTA* in our project, however different from the definition of intra-atrial time in traditional ECG analysis, in fact measured the intervals between detected markers for the first and last activations within a beat. As seen in the example presented in Figure 3.11 A, the *CTA* of left and right PAAs were often very different (paired t-test between mean *CTA* of *LPAA* and *RPAA* of each patient, $p<0.0001$), such that they could not be pooled together for analysis. Even considering only *LPAA* (or *RPAA*), the dispersion of the *CTA* values was huge and the distribution was complex and multi-modal. The example of Figure 3.11 B shows a LPAA bimodal distribution, suggesting at least two different ectopic foci. Hence, CTA might depend on multiple factors such as prematurity, previous sinus rhythm, changes in the relative position of ectopic focus and of the conduction path across the atria, which explains why it was not a useful variable to discriminate trigger from non-trigger PAA.

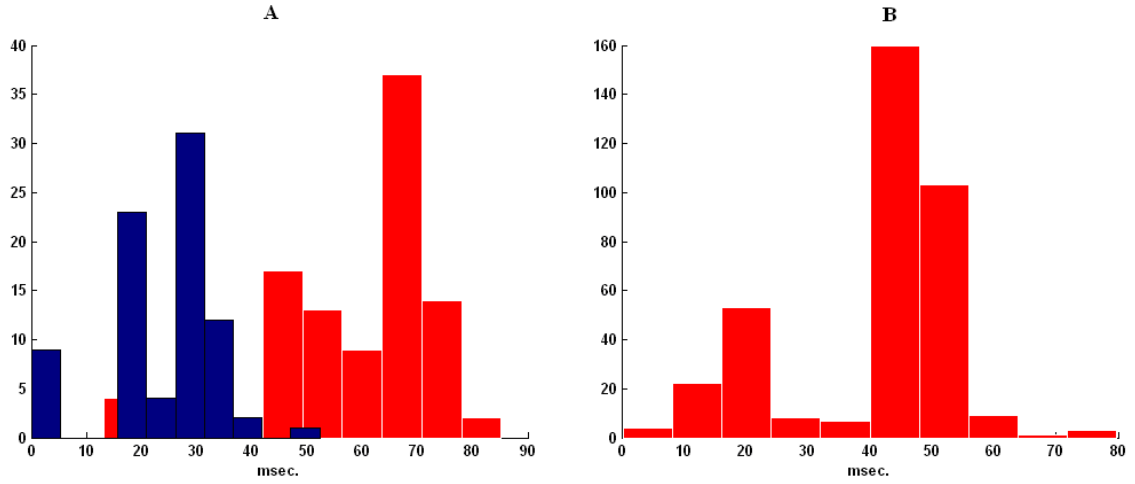

Figure 3.11 A) Histogram of *CTA* distribution of *LPAA* and *RPAA* of one patient (*LPAA*, red color; *RPAA*, blue color). B) Histogram of *CTA* of *LPAA* of one patient, *CTA* varying from around 10 to 80 msec.

3.4.3 Local Derivative (*Dvdt*)

The maximum derivative of unipolar electrogram (*Dvdt* $=|dV/dt|_{max}$) depends on the extracellular current associated with the passage of the activation front close to the electrode. It is related to the local excitability of the tissue, the propagation speed, form of wave front, the thickness of cardiac tissue beneath the electrode, the electrode-heart contact and resistance and the intra and extracellular resistivity [196-198]. We analyzed the *Dvdt* of the first activated channel for each PAA. Since first activations could occur on different channels, a normalization procedure was needed to bring the data together within each patient. For each channel, the *Dvdt* of all PAAs were collected, outliers were removed when bigger than 10 times the mean value, and the normalized derivatives within each channel were calculated as *NDvdt*=(*Dvdt*-min(*Dvdt*))/(max(*Dvdt*)-min(*Dvdt*)). Afterward, the *NDvdt* of the first activated channel was selected for each PAA and a position was assigned to each data point with the usual distribution method. Figure 3.12 A shows the distribution of the trigger PAA *NDvdt* among the patients. It was less than 0.2 for 60% of the patient. Low *NDvdt* might be a consequence of prematurity and/or high frequency activation prior to the PAA, which would be translated by a positive correlation between *NDvdt* and both the prematurity and the mean sinus beats AA for the minute before the PAA. Figure 3.12 B shows the distribution of these correlations, among which around 60% were located in region I where both correlations were positive.

To remove the effect of *AA* and Prematurity, the residues of the linear regression of *NDvdt* with *AA* and prematurity were also analyzed. For each patient, the residues were ranked from the most negative to the most positive to obtain the position of the trigger PAA. As seen in Figure 3.12 C, the residue was the most negative for ~30% of the patients and below 0.5 for 85%. Hence, the *NDvdt* of the triggering PAA was often lower than what would be expected from its prematurity and previous sinus rhythm, which suggests that it may occur in tissue with enhanced depression of excitability.

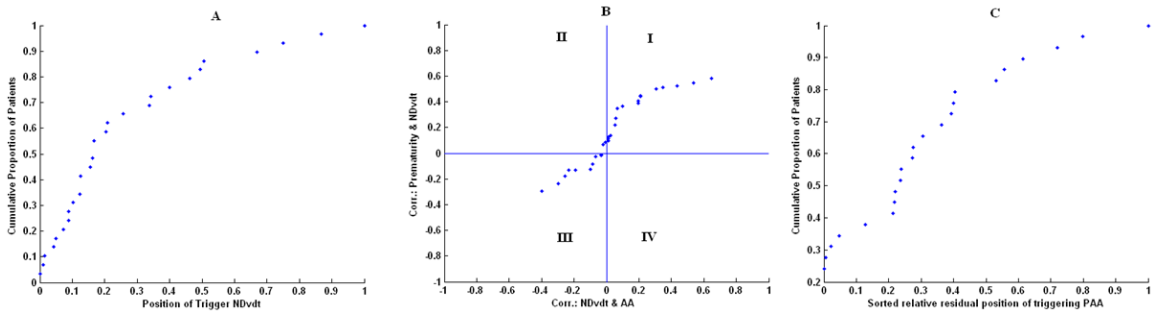

Figure 3.12 A) Cumulative distribution among the patients of the position of *NDvdt* of the triggering PAA. The abscissa is the position of *NDvdt* of triggering PAA, and the ordinate is the proportion of patients having *NDvdt* of the trigger PAA with position ≤ to each level indicated by the abscissa; B) The contrast plot of correlations: the abscissa is the correlation between *NDvdt* and prematurity, and the ordinate is the correlation between *NDvdt* and *AA*; C) Cumulative distribution of the trigger *NDvdt* residue position. Residue of regression of *Ndvdt* with *AA* and Prematurity were obtained and ranked in each patient (see text).

3.4.4 Cardiac Autonomic Neural Balance

In order to characterize the substrate associated with each PAA, the normal sinus beats in the 5 minutes preceding PAA were analyzed. Position data were calculated from the distribution of all sinus beat, as in the section of temporal evolution. Figure 3.13 shows the result of analysis for *AAMean* and *LFPortion=LF*/(*LF+HF*), the two variables that brought a significant contribution to the discrimination of AF onset time in the previous section. *LFPortion* were calculated from the sinus beats AA time series for the five minutes preceding each PAA, and the position values were obtained from the distribution of these *LFPortion* values within each patient.

Figure 3.13 A shows the distribution of the values associated with the triggering PAA among the patients. For *AAMean*(blue line), the position of trigger PAA was less than 0.3 for 55% of the patients. For the remaining 45% patients, the position of the trigger was

spread uniformly from 0.3 to 1.0. The distribution of the trigger *LFPortion* was somewhat a mirror image of the *AAMean*. A group gathering ~40% of the patients had a trigger *LFPortion* above 0.9, 4 patients (~13%) had a low value below 0.15, the remnant being spread between these values. The scatter plot (Figure 3.13 B) did not show a significant correlation between *LFPortion* and *AAMean* of the trigger PAA'a (correlation coefficient 0.052, p= 0.788). This suggests that *AAMean* and *LFPortion* bring different non-redundant information on the state of the substrate. Hence, the relative high heart rate and high portion of LF components represents different meanings. The *LFPortion* might mainly represent the fluctuation of heart rate, while the higher heart rate is attributed to comparative increase of sympathetic tone.

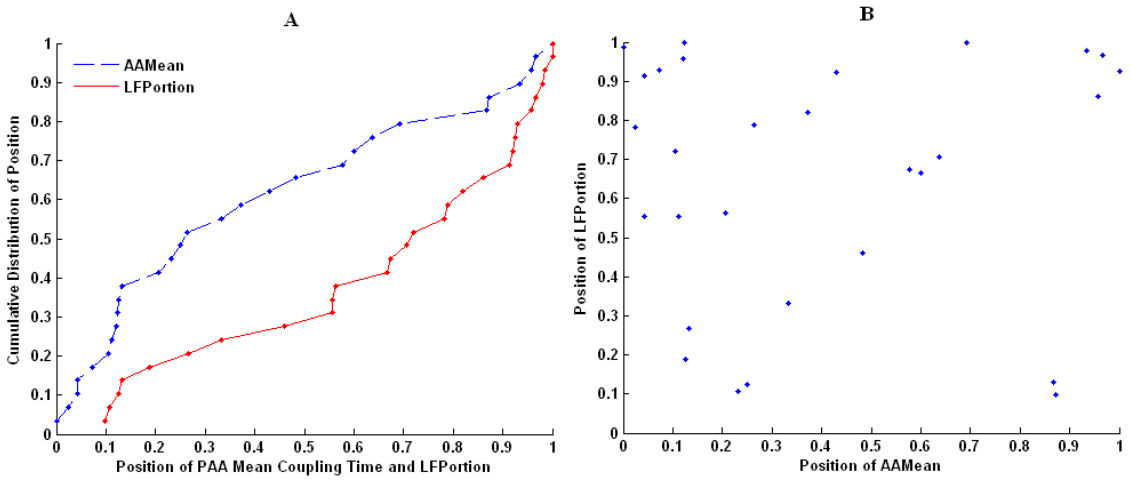

Figure 3.13 A) The cumulative distribution among the patients of the *AAMean* (continuous red line) and *LFPortion* (broken blue line) trigger PAA position. The abscissa is position of the trigger PAA, and the ordinate is the proportion of patients having a triggering PAA with a position ≤ to each level indicated by the abscissa. B) Scatter plot of *MeanAA* vs. *LFPortion* positions of the triggering PAA among the patients.

3.5 Uniqueness of PAA Eliciting AF

Forward conditional logistic regression was used to discriminate trigger PAA (set as 1, 1 by patient) from other PAA (set as 0, number varying among patients). As for the temporal analysis of section 3.3, the analysis was repeated for both raw and position data. The selected variables were the same for both sets of data, but position data again provided a better discrimination. In this section, we report only the results obtained with the position data. The positions (with respect to the distribution of values among PAA in each patient) of PAA were used as independent variables, namely $Prem_{abs}$, *CTAMean*, *CTAVMean*, *NDvdt*, *AAMean*, *AAStd*, *LF*, *HF*, *LFPortion*, *LF/HF*, *ArrhyDuration* and R_{PAA}, which were either significant predictors in univariate logistic regression analysis, or closely related to the substrate of PAA.

Bootstrapping was used to get around to problem of the obvious discrepancy between the numbers of triggering (1 for each patient) and non-triggering PAA. Analysis was performed including from 5 to 100% of non-triggering PAA. For each sampling percentage < 100%, the analysis was repeated on 200 random samples. Figure 3.14 A displays, for each sampling percentage, the ratio of the 200 samples for which each variable was included in the logistic model. Clearly, four variables were always included irrespective of the sampling percentage: *ArrhyDuration*, $Prem_{abs}$, *NDvdt*, and *LFPortion*. Mean value and standard deviation of the sensitivity, specificity and the area under ROC curve are plotted in Panel B of Figure 3.14. These three indices did not vary much as a function of the sampling frequency. Hence, additional analyses were performed using all non-triggering PAA.

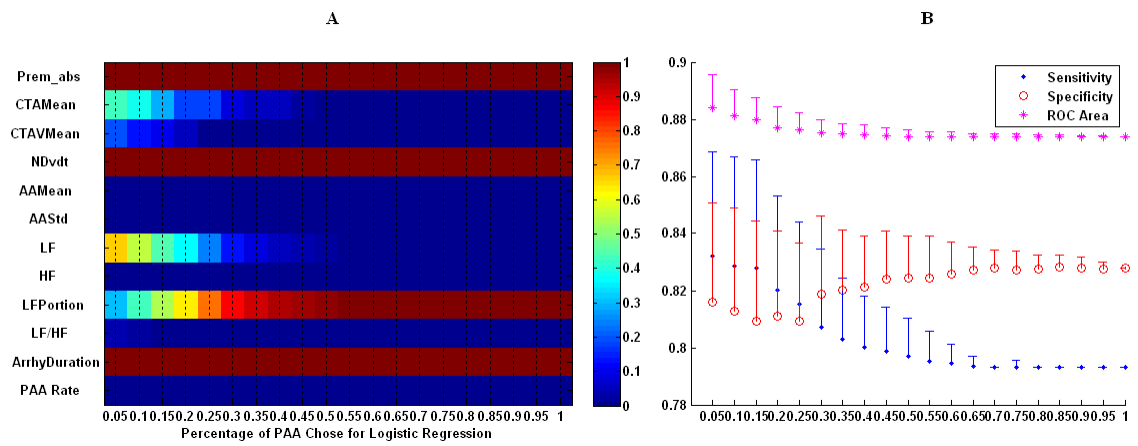

Figure 3.14 A) For each percentage of non-triggering PAA included in the sample, the ratio of the 200 runs in which each variable was included in the logistic model. The color bar indicate the value of the ratio; B) Mean value and standard deviation of sensitivity, specificity, and ROC curve area over the 200 runs for each percentage of non-triggers PAA.

The discrimination power of each variable was also measured by using the statistical significance of its parameter in the univariate logistic regression. Since most patients had their triggering PAA on the left atrium, analysis was repeated for these patients considering their LPAA only. Besides, analysis was also done separately in the subset of these patients with high (N>100) and low number (N<=100) of PAA to verify if the predictive power of the variables was different in these subgroups.

Figure 3.15 shows the results for the four groups of patients: all patients (Tot), patients triggered from the left atrium considering only their *LPAA* (LeLe) and among these, those with high or low *LPAA* rate (LeHi, LeLow). Figure 3.15 A gives the discriminating power of each individual variable (p of the null hypothesis/0.2, set as 1 if bigger than 1, such that the usual $p \leq .05$ level of significance corresponds to $p/0.2 \leq .25$). For all patients taken together, all variables, except *AAMean* and *CTAMean*, could individually bring a significant contribution. *AAMean* also became significant when the analysis was restricted to the LeLe group (*LPAA* from patients with AF triggered by *LPAA*). Within this group of patients, *CTAVMean*, R_{PAA} and *ArrhyDuration* provided a significant

discrimination only in the low *LPAA* rate group (LeLow), while *NDvdt* and *LFPortion* were significant only for the high rate group.

Figure 3.15 B gives the variables that were selected by the conditional forward logistic regression, using a cut-off point of 0.05 or .1 for inclusion. *ArrhyDuration*, $Prem_{abs}$, *LFPortion* and *NDvdt* were selected in both the total and LeLe groups. *ArrhyDuration* and $Prem_{abs}$ were selected in the LeLo groups, *LFPortion* and *NDvdt* in the LeHi group.

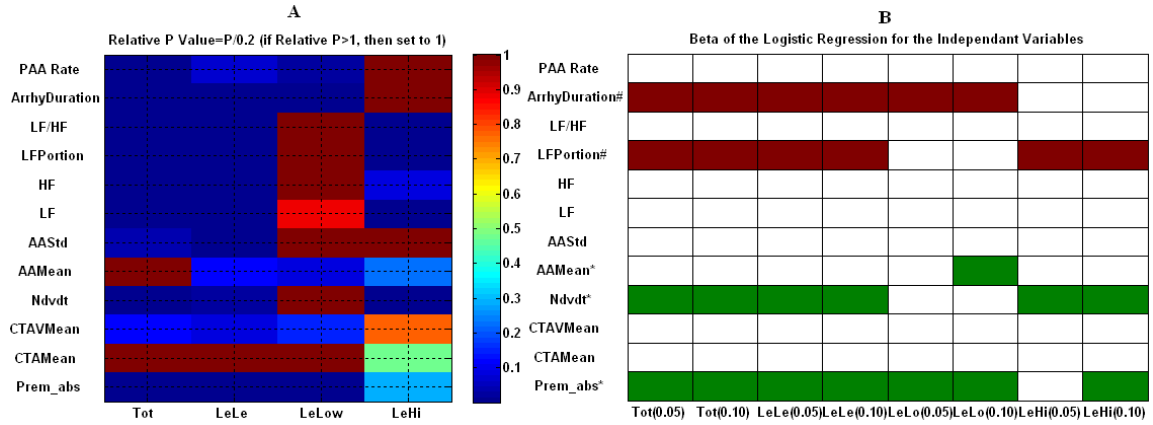

Figure 3. 15 A) Relative P value of each independent variable in the logistic regression for four groups of patients (P/0.2, set to a maximum of 1); B: Beta values of variables of in the final forward conditional logistic model on different group PAA with significant level for entering the variables as 0.05 and 0.10, green stands for negative parameter, and red stands for positive parameters, white indicates non-significant predictor. (Tot, total PAA; LeLe, *LPAA* from patients with AF triggered by *LPAA*; LeLo, *LPAA* with PAA number<100; LeHi with PAA number>100)

3.6 Discussion

3.6.1 Time Evolutionary Risk Factors

Previous studies on post-CABG AF have considered intervals of two hours, one hour, thirty minutes, or even a few minutes before the onset of the arrhythmia [134, 139, 188].

Besides, different durations of AF were considered. We initially chose two hours to investigate if monitoring could be useful to detect changes associated with impending AF. Significant differences were found for subsets of variables between the first and second hour, within the second hour, but never during the first hour (Table 3.1, 3.2). Therefore, we conclude that the 2 hours interval was an appropriate time frame for our study.

AEG provides the local prematurity of PAA and helps to determine the origin of PAA. Prematurity is a local measure, in contrast to coupling time measured from QRS which is a global measure that includes intra-atrial and atrio-ventricular conduction time. AF was initiated by *LPAA* for 87.6% of the patients, and the proportion of *LPAA* was greater than *RPAA* in all except two patients (Fig. 3.2). This differs from the result of Frost et al. who found the trigger PAA to originate from the left atrium in only 8 of 14 post-CABG patients. However, they were using only two epicardial electrodes and were considering the first >30 s AF, while we chose >10 minutes AF [186].

In this chapter, position data were calculated from all information recorded in the two hours and ended up to improve the discrimination of periods close to AF relative to raw data. This indicates that changes measured relative to the state of the patients might be more relevant that raw values. However, position data were less effective than raw or other forms of normalized data in the comparison of AF and Non-AF patients presented in Chapter 5.

Most patients had more *LPAA* than *RPAA*. Ashar reported that AF triggers most frequently originate in the carina region of the pulmonary veins [199, 200]. However, was the 26/30 dominance of trigger *LPPA* simply a consequence of their greater incidence among the total PAA, or did *LPAA* stems from a more arrhythmogenic substrate to have greater potential to trigger AF? Here we give a discussion of the difference of *LPAA* and *RPAA* in the substrate point of view. On average, *LPAA* had lower prematurity, *Dvdt*, *NDvdt*, and longer *CTA* (Table 3.4). As shown in Figure 3.16,

such differences in mean value are found in 13 to 20 patients, together lower $Prem_{abs,\ rel}$ and lower *CTA* in 15 patients.

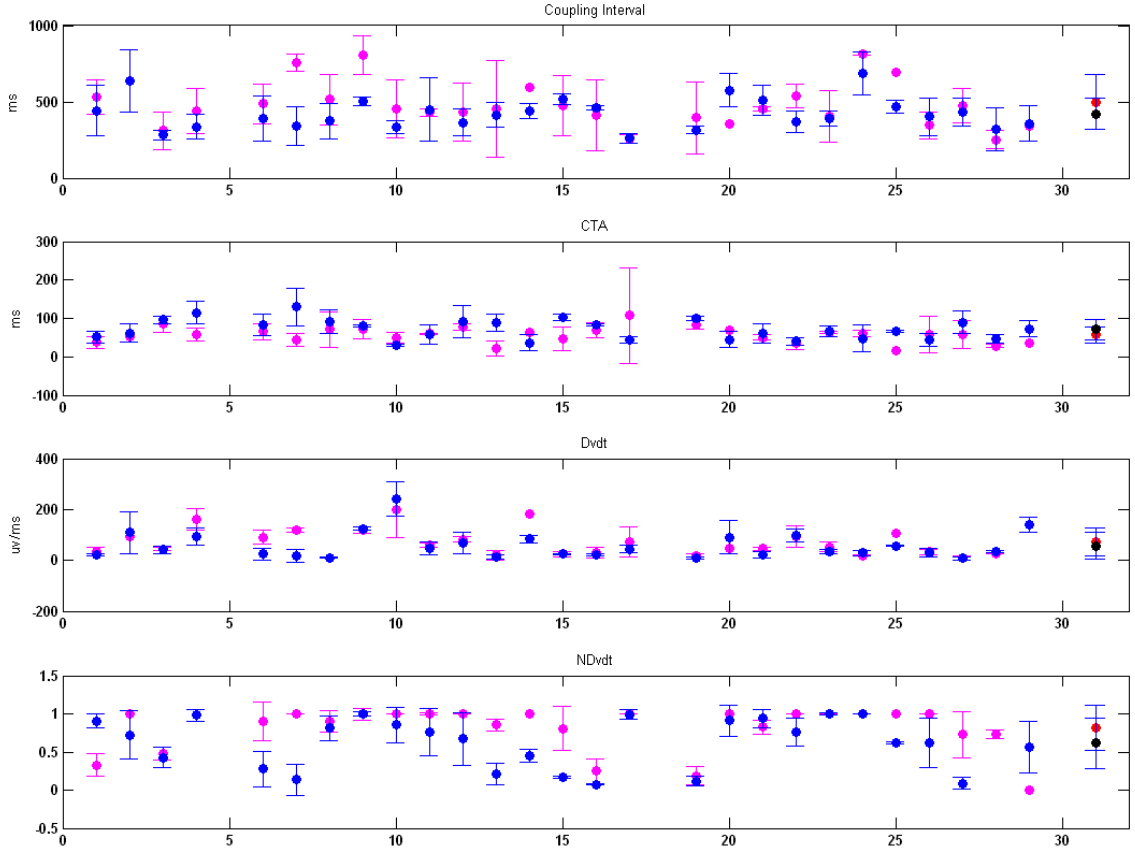

Figure 3.16 Mean value and standard deviation of *LPAA* (blue) and *RPAA* (pink) *CTA*, $Prem_{abs}$, *CTA*, *Dvdt* and *NDvdt*. The rightmost points in each panel are the average and standard deviation of the individual mean values.

Table 3.5 P value of Anova of Premabs, CTA, Dvdt and NDvdt, excluding patients with less than 2 LPAA and RPAA. For *CTA*, *Dvdt*, *NDvdt* analysis were repeated with (C) and without (N.C.) Prematurity as covariate. The analyses were done with patient effect considered as a random effect. However, the distribution of the patients *CTA*, *Dvdt* and *NDvdt* mean values were far from normal, with or without covariate.

	$Prem_{abs}$	*CTA*		*Dvdt*		*NDvdt*	
		N.C.	C.	N.C.	C.	N.C.	C.
Origin(L or R)	0.027	0.004	0.115	0.036	0.203	0.145	0.155
Patient	<0.001	<0.001	<0.001	<0.001	<0.001	0.304	0.456
Origin* Patient	<0.001	<0.001	<0.001	<0.001	<0.001	<0.001	<0.001

If the relation of speed to prematurity was the same across the tissue and if the pathway of propagation was also identical irrespective of the origin of the ectopic, then, following a sinus beat, *CTA* should be shorter for a *LPAA* than for a *RPAA* with the same level of prematurity. As it can be understood from Figure 3.17, this follows from the fact that the front created by the *LPPA* would be moving toward locations that were depolarized sooner than the position where the ectopic is created. In this simple model, a way to get a longer *CTA* for *LPAA* would be to assume that the speed of propagation, in addition to prematurity, also depends on position. This is shown in Figure 3.18, where

$$\theta(x) = \frac{1}{(1+kx)(1+e^{-\alpha P(x)})} \qquad (3.1)$$

where P is the coupling time at each location. Assuming a slower propagation would also be consistent with lower *Dvdt*. Our results suggest that, in patients experiencing prolonged AF, *LPPA*, beside the fact that they present greater prematurity, are often associated to some level of enhanced depression of excitability of the left atrium (Seen the analytical resolution in Annexe II). This is consistent with the finding that

preoperative impairment of left atrial function such as a larger LA, larger LA appendage and lower LA ejection fraction, increases the risk of post-operative AF [96].

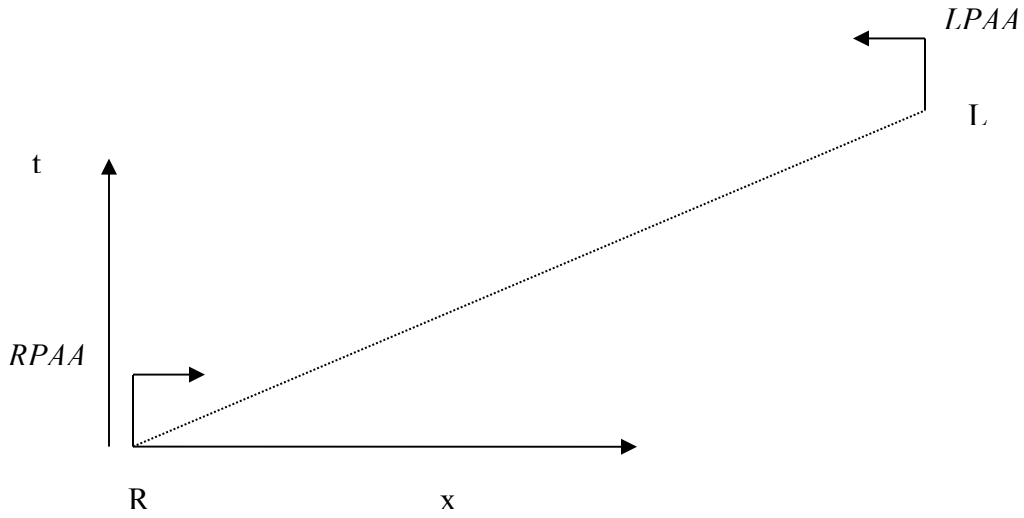

Figure 3.17 Diagram of pulse propagation either from *RPAA*, or from *LPAA*, assuming propagation at constant speed for the activation before the premature activation

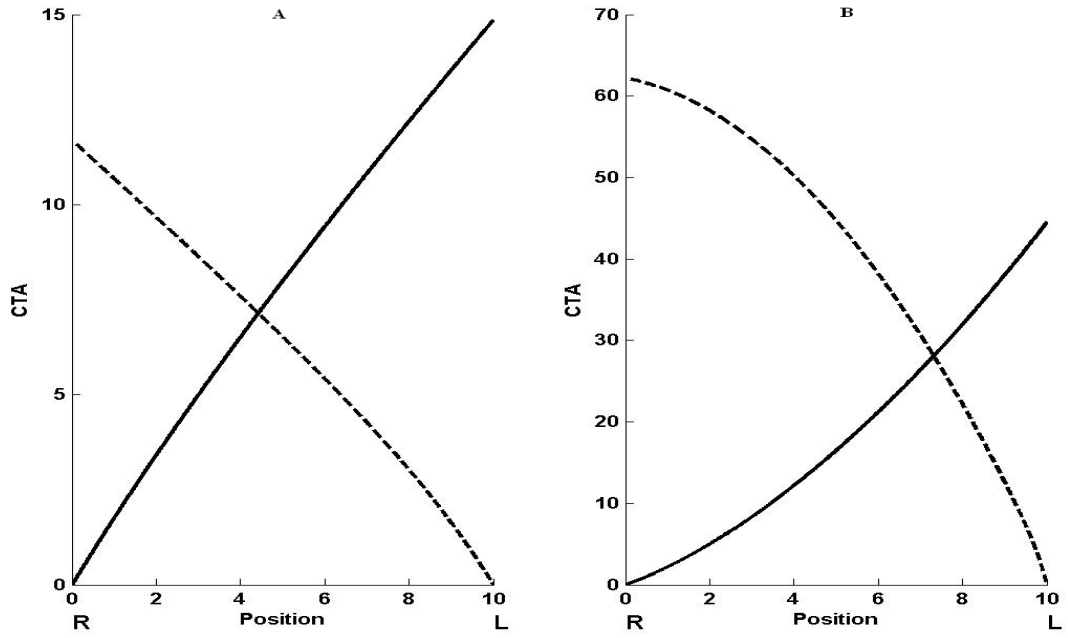

Figure 3.18 Simulation of eq. 3.1, with α=0.2, and k=0 (left) and k=0.5 (right). The premature impulse was applied at both end, with a coupling time P=1. Propagation of the

first front was done by stimulation at position 0 in a resting medium (i.e. $P(x) \rightarrow \infty$) The solid line is the conduction time vs. position of pulse from the right, and dot line for from the left applied with the prematurity =1.

Globally, there was an increase of R_{PAA} in last hour before the onset of the AF, coming essentially from an upsurge in *LPAA* (Figure 3.3). This is similar to the previous observations that the number of ectopic beats tends to increase before the start of paroxysmal AF [189] [33, 201]. The analysis of the temporal R_{PAA} evolution showed diverse of profiles (Figure 3.4), with 18 patients displaying some sustained increase of the number of *LPAA* in the last 40 to 15 minutes before AF. Hence, AF is not always preceded by an increasing trend of PAA or *LPAA*.

Logistic regression analysis indicated that four variables were contributing more often to distinguish the last time periods (5, 10, 15, 20 and 30 minutes) before AF from the other time periods: higher heart rate, higher *LFPortion*, increase density of PAA and short-transient arrhythmias.

Higher heart rate is in accordance with the results of different groups that suggested that postoperative patients with higher heart rate were more prone to AF [24, 71, 202]. However, Hogue et al. rather concluded that heart rate dynamics before AF could be either lower, higher or even constant. [136]. Our observations did not contradict either of these statements. As seen in figure 3.5 A, which is a population-based approach, there is indeed a gradual acceleration of the heart rate before AF. However, cluster analysis of figure 3.5 B reveals that only 15/29 patients follow this trend. As for PAA rate, there is no unique pattern that could be alone predictive of impending AF. The heart rate variability measures were calculated in five minutes intervals. This time frame was considered as a tradeoff between the stationary needed for FFT to be significant and its frequency resolution. Heart rate variability might be useful as a measure of the modulation of autonomic tone even though the connection between may sometime become ambiguous. Indeed, Movement and vascular perturbations that may be unrelated to the autonomic tone might alter the heart rate variability.

As discussed in Section 1.2.1 (Chapter 1), the LF component of heart rate variability is often considered to be a marker of sympathetic modulation, although this point of view remains somewhat controversial. In both raw data and position data, we found an increasing trend of the population mean *LFPortion*, in last 30 minutes, reaching a peak in last 10 minutes before AF (Figure 3.6 B). The increase of both *AAMean* and *LFPortion* might be explained as an augmentation of the sympathetic and/or decrease of the parasympathetic tone in last half hour. However, the study of correlation between *AAMean* and *LFPortion* trend did not support that point of view because the correlation was widely distributed among the patients (correlation between 5 min. values, [min,max, mean ± std,]: 2hr=[-0.77,0.45,-0.12 ± 0.37]; last hr=[-.74,0.59,-0.12 ± .035];last ½ hr=[-0.84,0.73,-0.06 ± 0.51]). That's to say, the two variables could not be equivalent since *LFPortion* and *AAMean* represents two different physiological meanings. The higher or lower *AAMean* is caused by the increase of sympathetic or the decreased of parasympathetic tone. *LFPortion* reflects the fluctuation of heart rate, so it is also more related to the temporal fluctuation of sympathovagal action. Therefore, both variables entered into the final logistic regression model.

Dimmer et al. reported an increase *LF/HF* ratio before AF, which they attributed to a loss of vagal tone ($0.16<HF<0.4$) and a moderate increase in sympathetic tone (*LF*) [71]. In our case, there was no significant time effect for *LF* or *HF* alone. As for heart rate, Hogue et al. observed divergent autonomic conditions before AF onset: heightened sympathetic tone in some patients, but either higher vagal tone or dysfunctional autonomic heart rate control in others [136]. This is consistent with the huge variability in *LFPortion* time course found in cluster analysis (Figure 3.6 B).

Although the same variables had significant time effects and were selected in the final logistic regression model for either raw or normalized data, the latter always had higher level of statistical significance and correct classification. This comes from the huge variations of mean level and amplitude of changes observed for every variable among the patients. The normalization, based on the distribution of the values in each patient,

removes these differences of scale. It suggests that a relative threshold, adapted to the state of the patient, can be a better predictor of impending AF.

3.6.2 Triggering vs. Non-triggering PAA

Prematurity (coupling interval) is believed to be an important index of the pro-arrhythmic potential of a PAA [186, 190, 199, 203]. The triggering PAAs were among the 10% most premature PAA experienced by each individual for ~40% of the patients, while prematurity was uniformly distributed for the others (Figure 3.11 A). The triggering PAA with long coupling time were not necessarily associated with periods with high density of PAA or transient arrhythmias (Figure 3.11 B). This suggests that the state of the tissue in which the PAA takes place must also be taken into account

Figure 3.11 shows that the distribution of *CTA* was variant and multimodal, which suggests the existence of multiple foci and/or conduction paths. As a consequence, the correlation between prematurity and *CTA* was erratic among patients (*LPAA*, from -0.78 to 0.65, -.21±0.36), as well as the position of the trigger PAA in the distribution (from 0.017 to 1, .44 ±0.36). Although related, *CTA* is not completely equivalent to the duration of the P wave that was found to be prolonged in patients developing AF [28, 30, 127, 128].

As mentioned earlier, *Dvdt* obtained from AEG characterizes local propagation. *Dvdt* of the trigger PAAs had a lower relative value than other PAA, even when correcting for prematurity and previous sinus rhythm (Figure 3.13), which suggests that that the substrate of local tissue was with enhanced depressed excitability.

AAMean, the AA of sinus beat, and *LFPortion* of five minutes preceding each PAA were analyzed. There was a significant proportion of patients for which the triggering PAA was associated with lower *AAMean* and higher *LFPortion* (Figure 3.13A). However, few patients possessed both properties (Figure 3.13B), which suggests that these indices may

qualify different properties of the substrates. Temporal analysis suggested the same conclusion.

Forward logistic regression, in conjunction with bootstrapping, identified four stable independent predictors of triggering PAA: $Prem_{abs}$(or $Prem_{rel}$), *NDvdt*, *LFPortion*, *ArrhyDuration* (Figure 3.14). Together, they achieved a sensitivity and specificity ~ 80%. The model indicates that more premature PAA with smaller *Dvdt*, preceded by sinus rhythm with higher *LFPortion* and more transient arrhythmias, are more likely to trigger prolonged AF. The model brings together properties of the PAA per se (prematurity), of the substrate in which it occurs (*Dvdt*) and of the dynamics (*LFPortion*, *ArrhyDuration*).

The same logistic model was obtained when including only *LPAA* for the 26 patients for which the trigger was also from the left atrium. Whilst prematurity appears as a stable discriminator of the trigger, the predictive power of the other variables differs contingent to the PAA density of the patient. For low PAA density patient, longer *ArrhyDuration* and, to some extent, shorter *AAMean*, are associated with the trigger. For high density PAA patients, the risk factors rather become *Dvdt* and *LFPortion*. The contribution of Dvdt might be explained by the fact that, when many PAA occur close to the onset of AF, the state of the tissue for each PAA may become more important to discriminate the trigger.

3.7 Summary

1. AF was always immediately preceded by a premature atrial PAA mainly originating from the left Atrium. The number of PAA and the fraction of *LPAA* among the patients were very inhomogeneous. *LPAA* was more prone to elicit arrhythmia than *RPAA*.

2. PAA rate, arrhythmia duration time, sinus heart rate, LF portion of heart rate variability showed significant changes over the time in last hours before the onset of AF.

3. Prematurity, *Dvdt* of the PAA, as well as LF portion and unsustained arrhythmia duration time in the preceding five minutes were predictors of the model to discriminate triggering from non-triggering PAA.

Chapter 4 Preoperative Risk Factor Analysis of AF and Non-AF Patients

Pre-CABG clinical data were available for 137 patients, 108 patients from Hôpital du Sacré-Coeur de Montréal, and 29 patients from Institut de cardiologie de Montréal (ICM).

The following clinical data were available for all patients and included in the analysis: age, sex, left ventricular ejection insufficiency (insufficient if LVEF<60%), hypertension(HT), diabetes, chronic obstructive pulmonary disease (COPD), history of stroke, former myocardial infarct(MI), serum creatinine level, number of vessels at CABG surgery, beating heart or extra-corporal circulation, duration of extra-corporal circulation, duration of clamp time, preoperative Beta-blocker administration, preoperative calcium inhibitor administration, and preoperative vasopressors/inotropes administration.

Incidence of Atrial Fibrillation

41 (41/137=29.9%) patients experienced a first >10 minutes AF episode during the second and third 24hrs after CABG surgery. This incidence was on the same level as that reported in the United States (33.7%), Canada (36.6%), Europe (34.0%), United Kingdom (31.6%), lower than for Middle East (41.6%), but higher than South America (17.4%) and Asia (15.7%) [77].

Statistical Methods:

Univariate associations between potential predictors and AF were investigated using chi-test (category variable), t-test, ANOVA (scale variable), logistic regression modeling and survival analysis (for both kind of variables).

All variables with significant univariate effect were further analyzed with multivariate logistic regression using a combinative stepwise forward conditional selection method. The analysis, repeated with choice among all variables, gave the same results. Model entry and retention criteria were set at $p<0.1$ and $p<0.15$. The final logistic models were evaluated using the Hosmer-Lemeshow goodness-of-fit test [146]. The receiver operating characteristic (ROC) was used to compare the strength of the different models. Because of the disproportion between men and women (104 vs. 33), weighted logistic regression was used for some analyses, in which the contribution of the women to the likelihood function was multiplied by the male vs. female ratio.

Cox regression (proportional hazards model) was used to investigate the effect of clinical variables upon the post-operative time of AF [149].

4.1 Univariate Analysis Result

4.1.1 Univariate Logistic Regression

The baseline characters of the 137 patients of our study population, is listed in Table 4.1. The predictive power of the variables to discriminate AF from Non-AF patients was firstly assessed by univariate logistic regression. The analysis was repeated using unweighted (UW) or sex-weighted (W) logistic regression. As seen in Table 4.2, four variables were either significant or close to be significant for both analyses: age, previous myocardial infarct, and hypertension and serum creatinine. The next sections provide a detailed analysis of these four variables.

Table 4.1 Baseline characters of the 137 patients of the study population

Group	AF	Non-AF
Number (%, among total)	41(29.93%)	96(70.07%)
Age (mean±std), years	68.54±7.40	62.42±9.19
Sex (n, % among men/women) Men Women	 31(29.8%) 10(30.3%)	 73(70.2%) 23(69.7%)
LVEF (n, %)	7 (17.07%)	11(11.46%)
Stroke (n, %)	4(9.75%)	4(4.16%)
MI (n, %)	23(56.09%)	39(40.62%)
COPD (n, %)	4(9.75%)	10(10.42%)
Hypertension (n, %)	30(73.17%)	56(58.33%)
Serum Creatinine (mean±std, mmol/L)	101.08±38.170	89.29±28.793
Diabetes (%)	13(31.71%)	31(32.29%)
Mean Number of Vessels of CABG surgery (Mean)	2.63	2.63
Beating Heart vs. Extra-Corporal Circulation	4(9.75%)	10(10.42%)
Duration of Extra-Corporal (mean±Std), minutes	71.07±38.89	66.27±34.54
Cross-clamp(mean±Std), min.	44.05±26.09	42.94±25.66
Preop. Treatment (n, %) Beta-Blockers Calcium channel blockers Vasopressor/Inotropes	 28(68.29%) 11(26.83%) 2(4.87%)	 77(80.21%) 23(23.96%) 3(3.13%)

% represents the rate among the AF or Non-AF group if not specified

Table 4.2 P value of variables in univariate unweighted and sex weighted logistic regression

	UW	W
Age	0.000	0.000
Gender	0.927	0.896
LVEF	0.311	0.229
Former History of Stroke	0.219	0.230
Previous Myocardial Infarct(MI)	0.043	0.007
Hypertension(HT)	0.057	0.072
Diabetes	0.642	0.433
COPD	0.989	0.814
Serum Creatinine	0.065	0.032
Number of Vessels of CABG surgery	0.924	0.581
Beating Heart vs. Extra-Corporal Circulation	0.829	0.549
Duration of Extra-Corporal	0.624	0.700
Duration of Clamp	0.987	0.838
Preoperative Beta-blocker	0.372	0.423
Preoperative Calcium Inhibitor	0.408	0.294
Preoperative Vasopressor/Inotropes	0.642	0.681

4.1.2 Age/Gender

As seen in Figure 4.1, the patients were rather uniformly distributed among 50 to 80 age groups, with a few patients below 50 and over 80. However, the proportion of AF patients clearly increased with age. There was also three times more male than female patients (104 vs. 33), but the proportion of AF was the same in the two groups (M: 29.81%, F: 27.27%, p=0.830).

Figure 4.2 shows the age distribution across the (AF vs. Non-AF) and (Male vs. Female) groups. Two-way ANOVA indicated a significant AF vs. Non-AF effect (p=.001), with an estimated AF-Non-AF difference of 6.15 years (95% conf. inter.: 2.7-9.7 y.), as well as a significant sex effect (p<.001), with an estimated Female-Male difference of 6.8 years (95% confidence interval: 0.9-12.8), but no interaction (p=0.957). However, the age dispersion of the male and female Non-AF patients was very large.

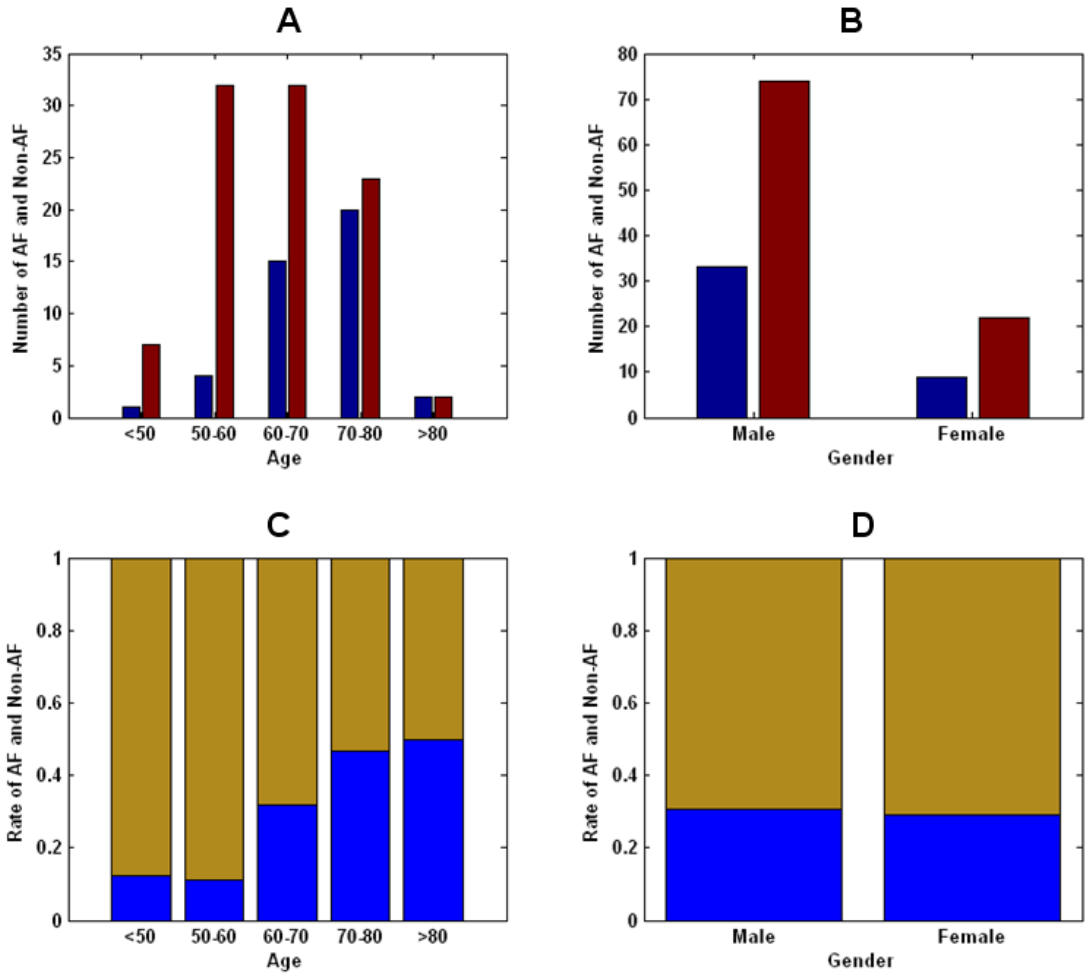

Figure 4.1 Number of AF (blue) and Non-AF (red) patients in the different A) age groups and B) sex groups; Proportions of AF (blue) and Non-AF (golden) patients in C) age groups and D) sex groups.

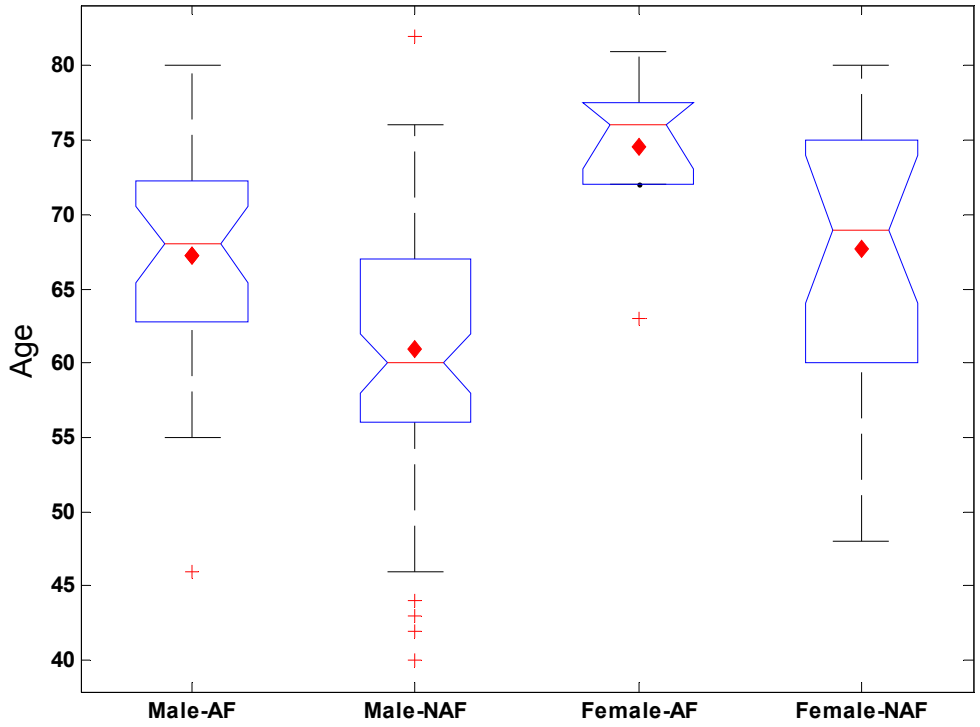

Figure 4.2 Age distribution across AF vs. Non-AF and Male vs. Female groups. The lower and upper lines of each box are the 25th and 75th percentiles, whose separation defined the inter-quartile range. The middle line is the median and red diamond the mean. The upper and lower 'whiskers', the lines extending above and below the boxes, are located either at 1 inter-quartile from the top and bottom of the box, or at the position of the minimum and maximum if they are within these limits. Outliers beyond these limits are indicated by the +. The notches in the box are the 95% confidence interval of the median. All following box plot figures follow the same formula.

4.1.3 Artery Hypertension (HT)

Table 4.3 R (AF): Risk of AF in the group without (Non-HT) and with (HT) hypertension. RR: relative risk

	N	Non-HT	R(AF)	HT	R(AF)	RR(HT/Non-HT)	P(χ^2)
Total	137	51(37.2%)	0.196	86(62.8%)	0.349	1.78	.057
Men	104	41(39.4%)	0.195	63(60.6%)	0.365	1.87	.081
Women	33	10(30.3%)	0.200	23(69.7%)	0.304	1.52	.434

As seen, in Table 4.3, the ratio of hypertensive to non-hypertensive patients is approximately 2 to 1 in both sex groups, with a relative risk of AF greater than 1.5 for hypertensive patients.

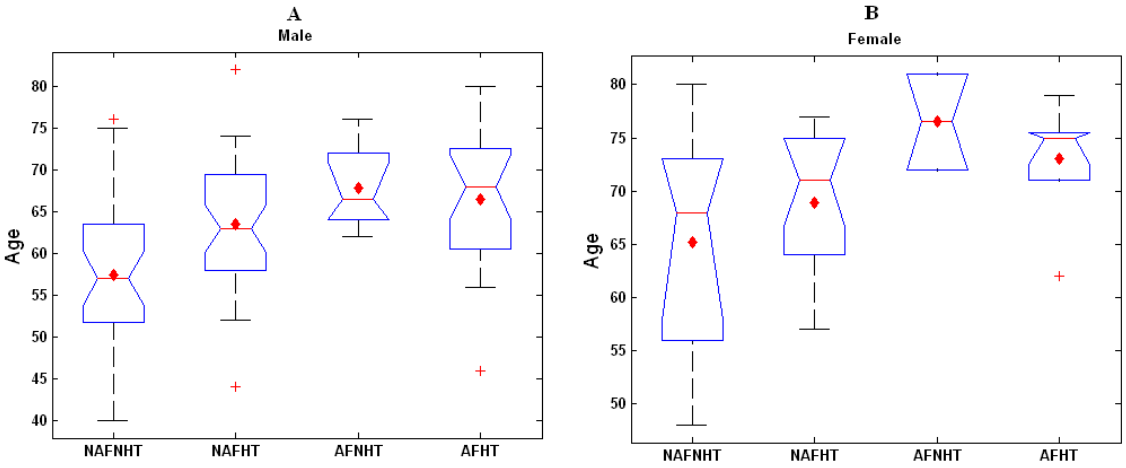

Figure 4.3 Distribution of Age as a function HT and AF among. A) male and B) female. The symbols of four groups: NAFNHT, Non-AF without HT; NAFHT, Non-AF with HT; AFNHT, AF without HT; AFHT, AF with HT.

However, the interplay of hypertension and age made its real AF predictive power harder to assess (See Figure 4.3). On one hand, hypertensive patients tended to be older in both sex groups (Male: 64.57 vs. 59.5, Female 70.2 vs. 67.8), which made them more prone to AF. Were the differences simply a consequence of age promoting both AF and

hypertension, or rather the expression of a risk factor whereby hypertensive patients became more liable to AF at a lower age? Upon 3-ways ANOVA of age, Sex (p=0.001) and AF (p=0.001) effects were diagnosed as significant, but not HT (p=0.576). There was also an indication of a potential HT*AF interaction (p=0.076), patients without hypertension and AF having a propensity to be younger. The small differences of age existing between hypertensive and non-hypertensive AF patients (HT vs. Non-HT, Men: 66.5 ± 8.0 vs. 67.9 ± 5.1, Women= 73.3 ± 5.5 vs. 76.5 ± 6.4) somewhat mitigated to the role of hypertension as an independent risk factor, at least in the male group.

4.1.4 Prior Myocardial Infarct (MI)

Table 4.4 R(AF): Risk of AF in the group without (Non-MI) and with (MI)

(RR: relative risk)

	N	Non-MI	R(AF)	MI	R(AF)	RR (MI/Non-MI)	P(χ^2)
Total	137	75(54.7%)	0.227	62(45.3%)	0.371	1.64	.064
Men	104	60(57.7%)	0.233	44(42.3%)	0.386	1.66	.092
Women	33	15(45.5%)	0.200	18(54.5%)	0.333	1.66	.392

The patients were almost equally divided between the groups with and without prior myocardial infarct (MI), but the former had a 2/3 increase of risk. Figure 4.4 details the relation between age, sex, AF and MI. In the men group, Age remained the main predictor of AF in both the MI and Non-MI groups. For women, the AF vs. Non-AF age difference was much reduced in the MI group, suggesting that it could be an age-independent AF predictor for this group.

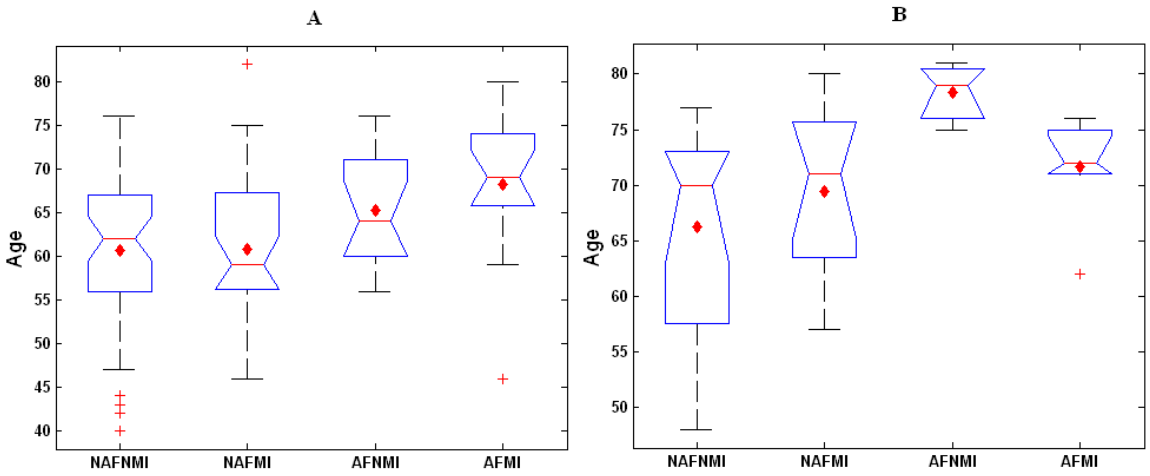

Figure 4.4 Distribution of age in the groups with and without previous MI and AF for A) male and B) female. NAFNMI, Non-AF without MI; NAFMI, Non-AF with MI; AFNMI, AF without MI; AFMI, AF with MI.

4.1.5 Serum Creatinine

A simple T-test indicated a different serum creatinine levels (Non-AF: 89.29±28.793 vs. AF: 101.08±38.170 mmol/L, p=.05). However, upon closer scrutiny, the situation was more complex. There was a marked difference between sexes (Figure 4.5 A), and two-ways (AF, Sex) ANOVA diagnosed only the sex effect to be significant (p=.01). However, the Non-AF vs. AF differences varied among the different age groups (Figure 4.5 B). Since age was a predictor of AF, the level of serum creatinine could be helpful to reduce the number of false positive among older age groups. HT has a significant effect on serum creatinine level. ANOVA analysis on the two effects of HT and AF, neither of them is significant (HT: 0.102, AF: 0.135, HT*AF: 0.986). In Figure 4.6 B, it seemed there is effect of HT between Non-AF and AF. The non-significance might be caused by the confounding of serum creatinine level of HT, Non-AF patients with Non-HT, AF patients.

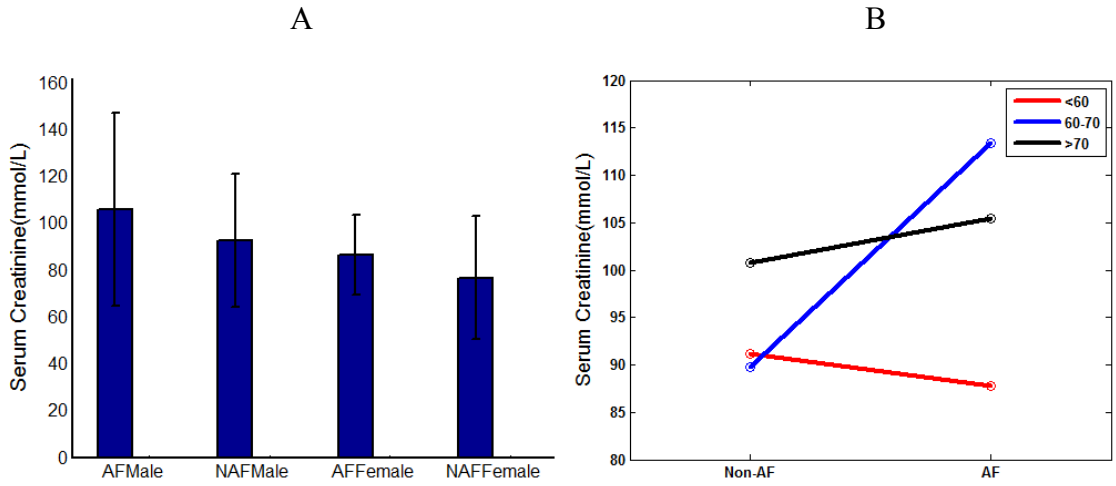

Figure 4.5 A) Bar plot of mean and standard deviation of serum creatinine level in AF vs. Non-AF according to gender. AFMale: AF and Male; NAFMale: Non-AF and Male; AFFemale: AF and Female; NAFFemale: Non-AF and Female (Sex effect=0.01). B) Mean serum creatinine of different age groups. The ordinate of both panels is the serum creatinine level.

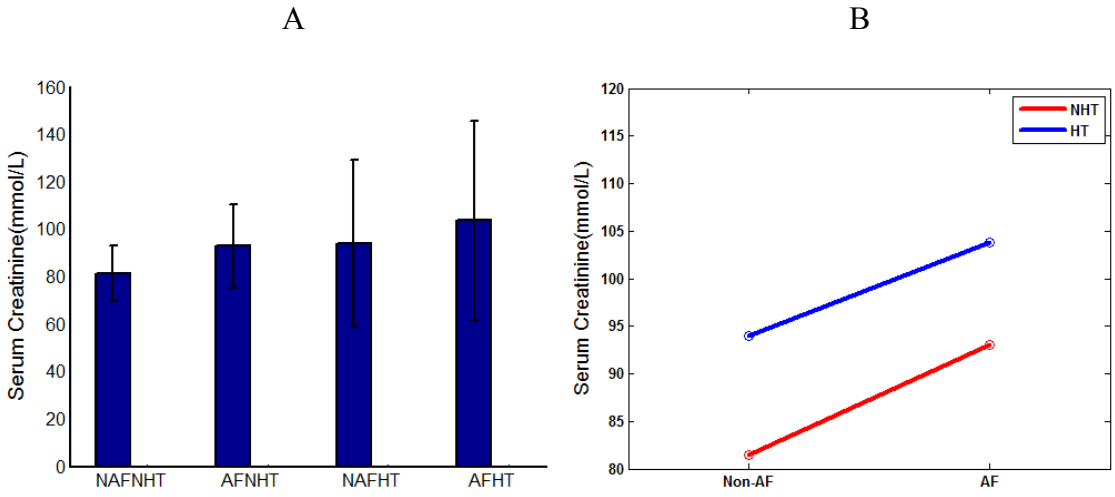

Figure 4.6 A) mean and standard deviation of serum creatinine level as function of HT and AF. NAFNHT:Non-AF and Non-HT, AFNHT: AF and Non-HT, NAFHT: Non-AF and HT, NAFHT: AF and HT (Effect: HT: 0.102, AF: 0.135, HT*AF: 0.986). B) Mean of serum creatinine level in AF vs. Non-AF according to HT. The ordinate of both panels is the serum creatinine level.

4.2 Multivariate Logistic Regression Analysis

Both weighted and unweighted stepwise forward multivariate logistic regressions were finally applied using the complete set of variables that was analyzed with univariate regression. The regression was run using a p=0.1 liberal criteria of inclusion. Table 4.5 summarizes the final results. Age and serum creatinine were included with similar β in both multivariate models, age always entering as the first and most important predictor. Preoperative myocardial infarct was included in the weighted model, but was less significant in the unweighted analysis model, meaning that its discriminative power was slightly more important for women. HT was never included in the multivariate models, a consequence of its correlation with age as discussed in the above section.

Table 4.5 Beta values and probability of the variables included in the logistic regression models. Weighted(W) and unweighted (Non-W) univariate (U) and multivariate (Mv) models. The numbers in parenthesis is the order of entry of each variable in the stepwise models. For variables not included in a model, the significance of the variable evaluated at the last step of the iteration is indicated.

		Uv. Non-W	Uv. W.	Mv UW	Mv W
Age	β	0.086	0.0847	0.086 (1)	0.101 (1)
	p	<0.001	<0.001	0.001	<0 .001
Infarct	β	0.768	0.8331		0.711 (2)
	p	0.043	.0077	0.145	0.036
Creatinine	β	0.012	0.0123	0.011 (2)	0.012 (3)
	p	0.065	0.0317	0.066	0.025
HT	β	0.795	0.6318		
	p	0.057	0.072		

Because AF proportions in men and women were similar, sex was not a significant univariate predictor. However, results of section 4.2.2, showing about 5 years difference between men and women for both AF and Non-AF patients, suggested that the predictive power of age could be improved by introducing a correction for sex. However, the gain was not sufficient for sex to be included in the models, probably because of the wide dispersion of age among Non-AF women. The same result was obtained in complementary analyses in which an additional age*sex variable was also considered.

A logistic regression model provided score for each patient, which was used to build a receiver operating characteristic (ROC) curve. It supplied a global assessment of the model and a procedure to select an optimal threshold for discrimination [204]. The ROC of three models (I: Age, II: Age+Serum Creatinine, III: Age+ Previous myocardial infarct + Serum Creatinine) pictured the improvement of prediction brought by the introduction of each variable. Since the β values of age and serum creatinine were similar for both the unweighted and weighted models, the β values from the weighted regression were used for Model III. The threshold to compute the sensitivity and specificity was selected as the level associated to the shortest distance to (1-specifity, sensitivity) = (0, 1) (see Figure 4.7).

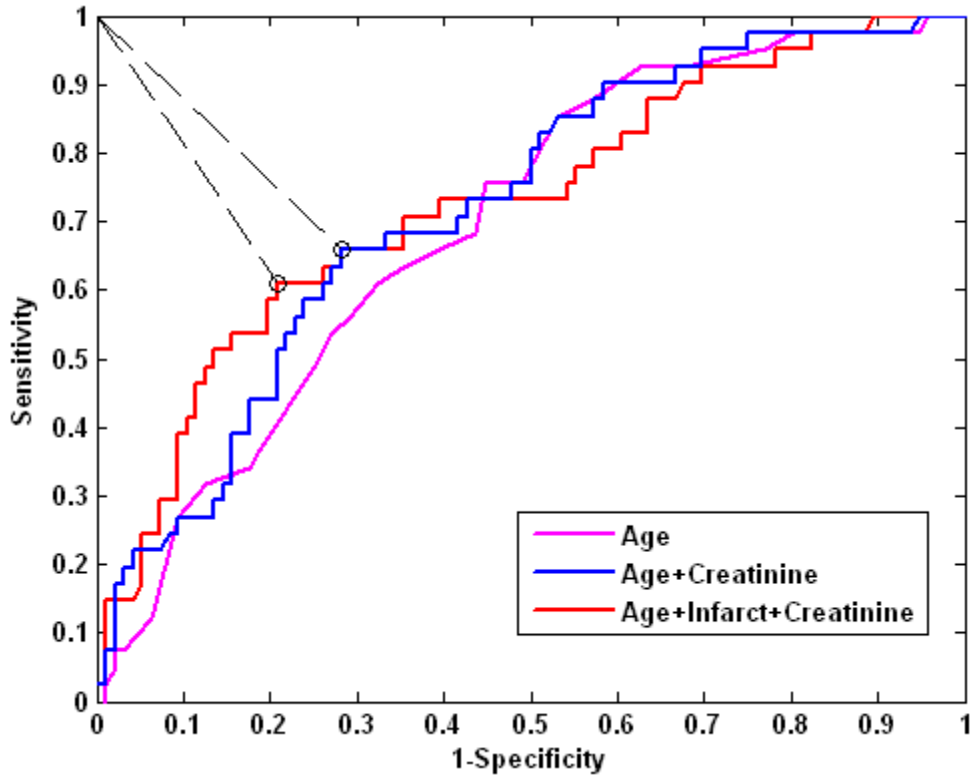

Figure 4.7 ROC curves from logistic regression Model I, II and III. The circles of the curves correspond to the optimal sensitivity and specificity for each model.

Table 4.6 presents the results of the three models for total population, as well as men (M) and women (W) separately. The men and women indices were calculated using the same cut-off thresholds. Serum creatinine yielded an around 5% increase of sensitivity and specificity. Previous myocardial infarct improved the specificity, but did not change (vs. Model I, II) and even reduced (vs. Model II) the sensitivity. However, it improved much the specificity and accuracy for women, which was expected since it was included in the weighted logistic regression model only. In summary, Model II had the highest sensitivity and medium, whilst Model III had the highest specificity.

Table 4.6 Indices of Model I, II, and III on men, women and total population

	Model I		Model II		Model III	
Sensitivity	60.98%		65.85%		60.98%	
	51.61% (M)	90% (W)	58.07% (M)	90% (W)	51.61% (M)	90% (W)
Specificity	67.71%		71.88%		79.17%	
	78.08% (M)	34.78% (W)	76.71% (M)	56.52% (W)	80.82% (M)	73.91% (W)
Accuracy	65.69%		70.07%		73.72%	
	70.19% (M)	51.52% (W)	71.15% (M)	66.67% (W)	72.11% (M)	78.79% (W)
Miss-Classification	34.31%		29.93%		26.28%	
	29.81% (M)	48.48% (W)	28.85% (M)	33.33% (W)	27.89% (M)	21.21% (W)
Positive Predictive Test	44.64%		50%		55.56%	
	50% (M)	37.5% (W)	51.43% (M)	47.37% (W)	53.33% (M)	60% (W)
Negative Predictive Test	80.25%		83.13%		82.61%	
	79.17% (M)	88.89% (W)	81.16% (M)	92.86% (W)	79.73% (M)	94.44% (W)
ROC Area	0.69792		0.71989		0.72726	

M: Male; F*: Female;*

Sensitivity=True Positive/ (True Positive+False Negative);

Specificity=True Negative/ (True Negative+False Positive);

Accuracy=(True Positive+True Negative)/(True Positive+ True Negative + False Positive + False Negative);

Miss-Classification=1-Accuracy;

Positive Predictive Test=True Positive/ (True Positive + False Positive);

Negative Predictive Test=True Negative/ (True Negative+False Negative);

Model I was equivalent to putting a threshold on age. When logistic regression was run for men only, age was the single significant predictor. As seen in Figure 4.8, the errors of Model I came from old patients without AF (F^+: False positive, 31 patients) or young patients with AF (F^-: False negative, 16 patients), showed in Figure 4.8. Ideally, supplementary variables should act to decrease the scores of the F^+ and increase that of F^-, without altering the classification of the true positives (T^+) and negatives (T^-).

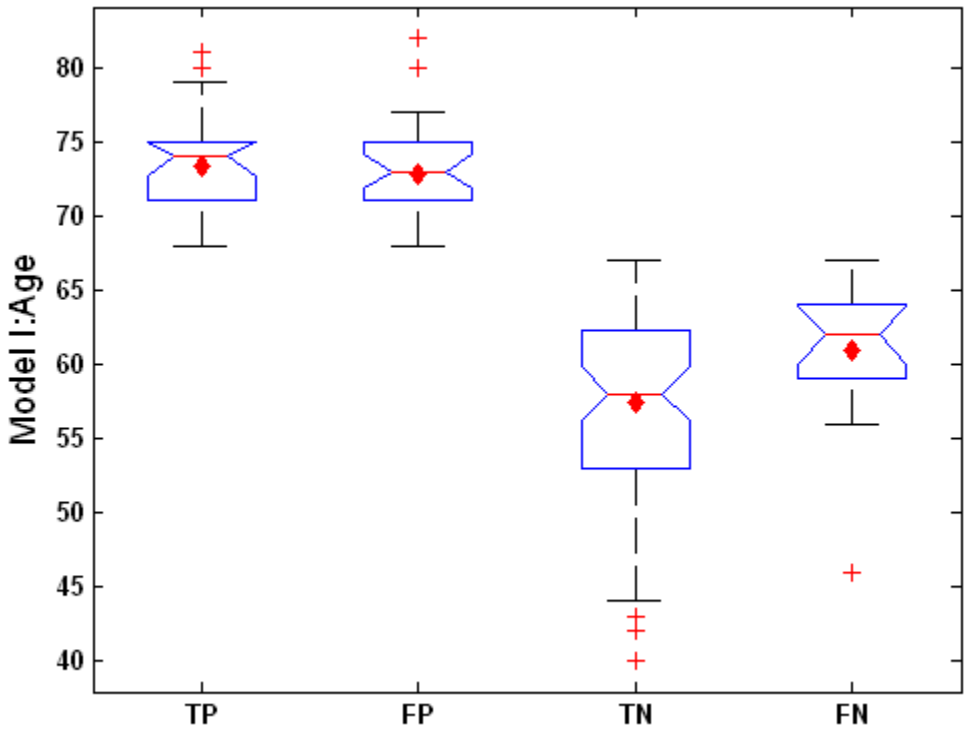

Figure 4.8 Distribution of age of TP, FP, TN and FN obtained by Model I. The diamond square points indicate the mean value of each group. TP: True Positive; FP: False Positive; TN: True Negative; FN: False Negative.

Model II introduced serum creatinine. Classification was improved for 6 F^+ (becoming T, 1 man and 5 women) and 2 F^- (becoming T^+, 2 men). Figure 4.9 shows the distribution graph of serum creatinine of TP, FP, TN and FN obtained by Model II. The diamond square points indicate the mean value of serum creatinine in each group. However, it also created 2 F^+ (2 men). This explains why the variable was not included in the model if

only men were considered. The main effect was increasing the specificity for women from 34.78% to 56.5%. A new variable of multiplication of creatinine and age was generated to repeat the regression analysis. In Model II, this variable was also entered into the model, but the ROC curve remained almost the same, and the sensitivity and specificity were not improved.

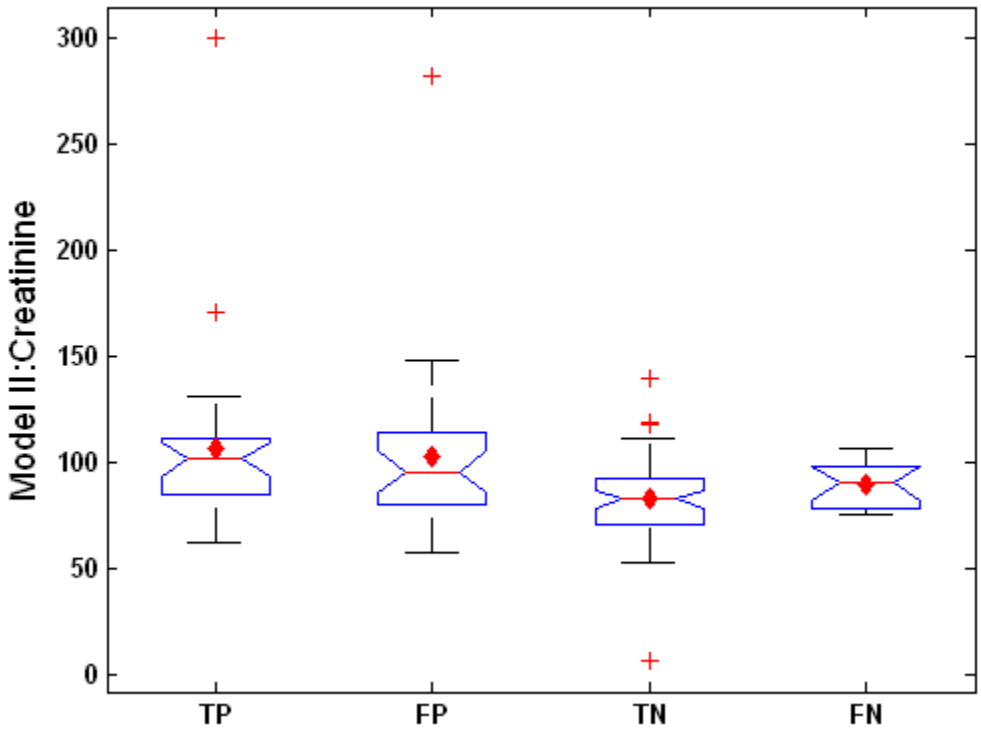

Figure 4.9 Distribution of serum creatinine of TP, FP, TN and FN obtained by Model II. The diamond square points indicate the mean value of serum creatinine in each group.

Model III added the variable of myocardial infarct. Compared to Model II, it improved the classification of 9 T^-, (4 men ,5 women); 1 T^+ (a man), at the expense of two 2 F^+, (1 man and 1 woman) and 3 F^- (3 men). Figure 4.10 shows the proportion of history infarct in four groups TP, FP, TN and FN. The specificity of women increased from 56.52% to 73.91%, and men from 76.71% to 80.92%, while sensitivity of men decreased from 58.07% to 51.61%.

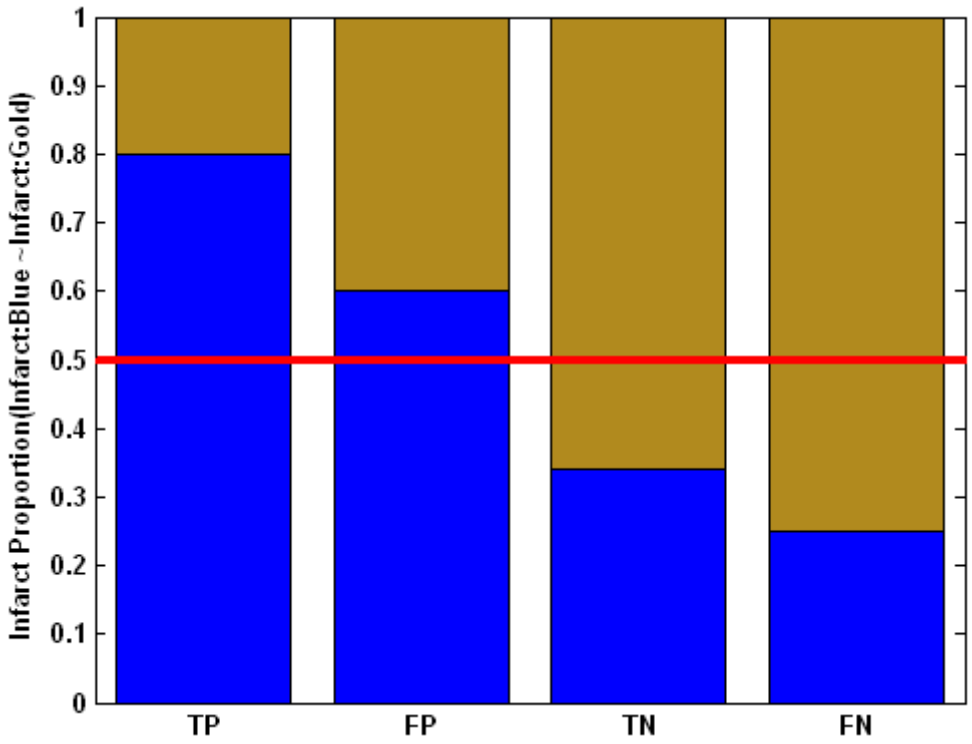

Figure 4.10 Pervious myocaridal infarct proportion in four groups TP, FP, TN and FN.

To summarize, serum creatinine improved the female specificity and male sensitivity, and the myocardial infarct mainly improved the female specificity. Initial analyses suggested that sex could be a predictor in the model. However, the variables of myocardial infarct and serum creatinine had more significant role than sex.

4.3 Cox Regression

It might be presumed that patients with higher preoperative risk could develop AF sooner after surgery. Figure 4.11 shows the post-operative without AF Kaplan-Meier survival curve and cumulative hazard functions for all patients [205, 206]. There was a quasi-exponential increase of the number of AF from the second to the fourth post-operative day.

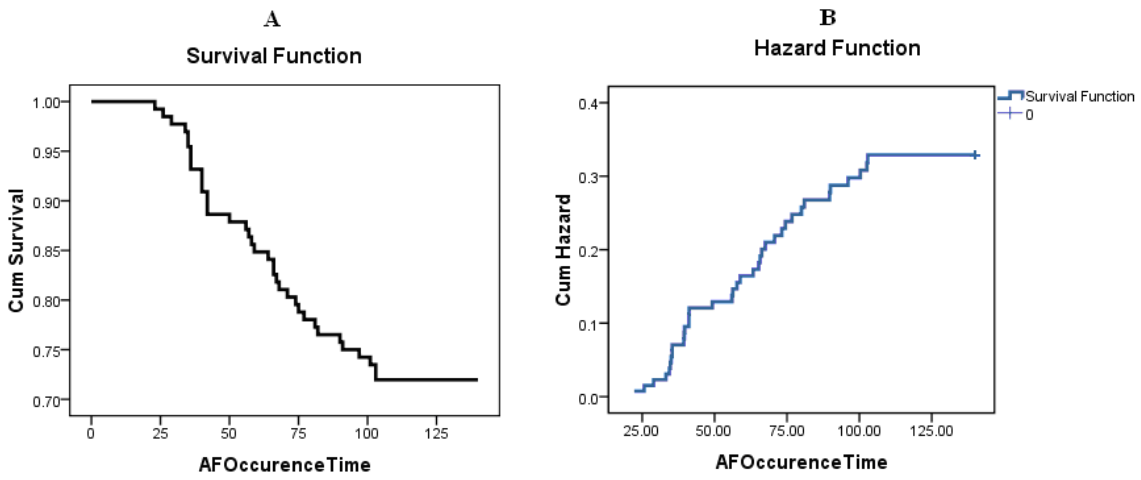

Figure 4.11 Survival curve and cumulative hazard function of AF with respect post-operative time (A: Survival function, B: Hazard Cumulative Hazard function).

The baseline hazard function measures survival independently of the covariates. Forward and backward stepwise Cox regression was applied to the same set of variables that were considered for the logistic regression in the previous section. The analysis was performed with entry and removal probability, i.e. 0.05 and 0.10 respectively. As for unweighted logistic regression, both age (β=0.081, p<0.001), serum creatinine (β=0.009, p=0.026) were the variables included in the both forward and backward final models. This has been expected since the preoperative risk was related to the final probability of surviving without AF.

Figure 4.12 shows the survival curves for three groups defined by the AF probabilities of the logistic regression model, Model III, presented in the previous section : 1) P $\leq$0.2; 2) 0.2< P $\leq$0.4; 3) P> 0.4. As expected, the final survival proportion was lower for the higher AF probability groups. However, the initial onset of AF was not delayed among the three groups. Among AF patients, the correlation between the AF onset time and the preoperative probability was weak and non-significant (r=-0.107, p=0.535). This suggests that the preoperative variables can to a certain extent predict who will get AF, but does not seem to be predictive on the time when AF will occur. A similar analysis of patients

classified by age groups (40, 50, 60, 70 and 80) produced the same results, which is not surprising since age was the main contributor to the probability (Figure 4.13, left panel). The same kind of conclusion was also drawn by examining the survival curve as a function of gender (Figure 4.12, right panel).

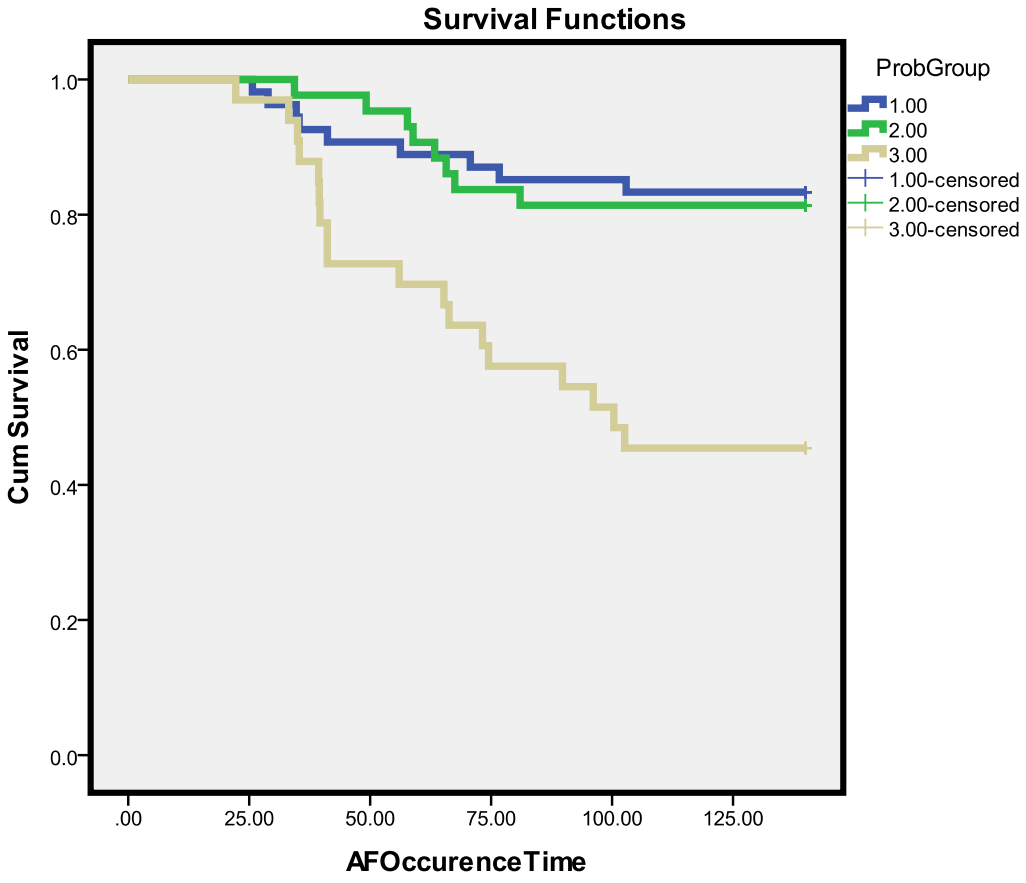

Figure 4.12 Survival curves of three groups of Patients with different preoperative risk score classified in three groups.

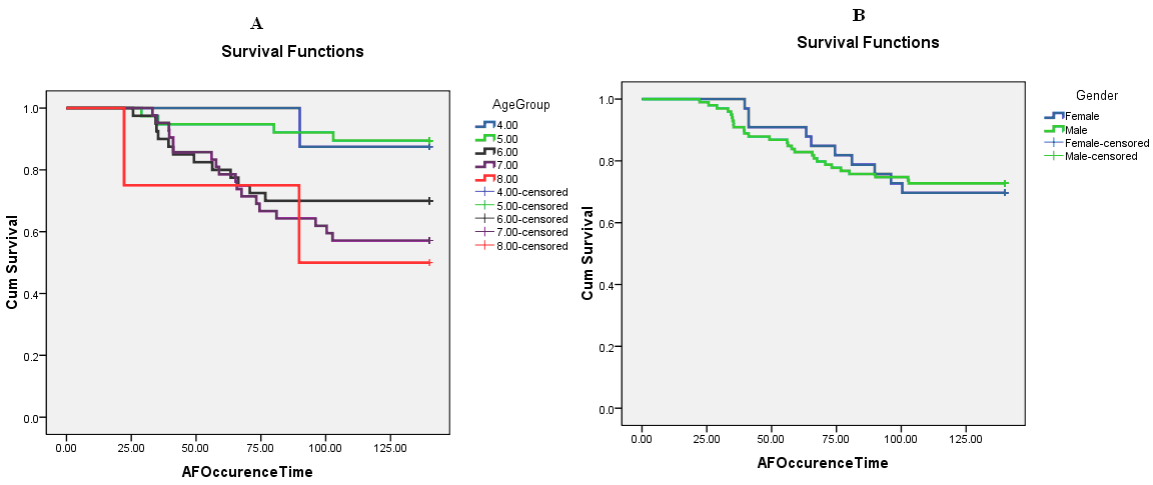

Figure 4.13 Survival curves by the functions of age group and sex

In addition, the risk score also presented very low correlation with the total PAA number, arrhythmia duration time among AF patients. This also indicated that the preoperative risk score plays the role of static risk factor in the occurrence of postoperative AF.

4.4 Discussion

Age appeared as the most important predictor of postoperative atrial fibrillation after CABG surgery, the mean age of the AF patients being around 6 years older than Non-AF patients (Men: ~67 vs. ~61 years, women: ~68 vs. ~75 years). Different studies of post-CABG AF have reached the same conclusion [74, 81, 97, 100, 117, 207]. The association has been attributed to age-related changes such as shorter effective refractoriness, longer atrial conduction times, atrial stiffening, and splitting of the atrial excitation waveform caused by the pectinated trabecula [4, 208]. It has also been suggested that unavoidable trauma to sympathovagal fibers originating from the deep or superficial cardiac plexus during surgery may enhance the pro-AF effect of preexisting atrial electrical changes caused by aging [81].

There was around 3 times more men than women in our sample (104 vs. 33), but the incidence of AF was the same in the two groups. Despite the fact that women patients

were on average older, and that the difference of age between AF and Non-AF patients was the same in the two groups (ANOVA and Figure 4.12), sex did not appear as independent predictor in univariate or multivariate (as sex*age) logistic regression model. Our results concurred with Auer et al. who concluded that sex was not an independent risk factor, but contradict Zaman et al. who reached the inverse conclusion results [80, 100, 209]. However, it cannot be said that gender has absolutely no effect. The main improvement in predictive power from logistic regression model from Model I to Model III appeared in the specificity for women (Table 4.5). Many women were false positive with the model incorporating age only because the average age of the women Non-AF group was the same than the AF men group.

Hypertension is associated with left ventricular hypertrophy, which impair ventricular filling, induce left atrial enlargement, and slow down atrial conduction velocity [210]. The changes in cardiac structure and physiology leading to hypertension also predispose to a higher risk of developing AF. Conventional therapy of atrial fibrillation currently focuses on interventions to control heart rate, rhythm, and the prevention of stroke by anticoagulant medications, rather than treatment of hypertension. In patients with AF, aggressive treatment of hypertension may reverse the structural changes in the heart, reduce thromboembolic complications, and retard or prevent the occurrence of AF [210]. Nevertheless, our study concluded that the role of hypertension in the occurrence of post-CABG AF is for the less dubious. Hypertensive patients had indeed a 78% increased risk to of AF, an effect close to significance in univariate analyses (Table 4.2 and 4.3). However, it did not appear as a predictor in the final logistic model, contradicting the conclusion of Svedjeholm et al. [117]. In our sample, the effect of HT was confounded by age.

To some extent, the same age confounding effect was also present for pervious myocardial infarct (MI) (Figure 4.4), though it was still present particularly in the weighted version of the final logistic model (Table 4.3, 4.4 and 4.5). Many studies have demonstrated that MI has the potential to provoke AF (for review [211], [212]), although the mechanism is still not clearly understood. In this setting, the risk of AF is increased

by elevated heart rate, left ventricular dysfunction and impaired hemodynamic. High heart rate suggested that the cardiac autonomic nervous system might be involved. Left ventricular dysfunction and impaired hemodynamic hinted to a mechanical effect. Reduced ejection fraction coming from left ventricular dysfunction or hypertension could result in an additional expansion of the atria before opening of the atrio-ventricular valves that may induce pro-AF remodeling Reversely, AF can often complicate MI acute myocardial infarction (AMI) by reducing the pump function of the heart

Serum creatinine is the commonly used indicator of renal function. Renal dysfunction is defined by a serum creatinine level of at least 177 μmol/L, accompanied by an increase of at least 61.9 μmol/L from baseline [77]. Serum creatinine is usually higher in male patients than female patients whether developing AF or not [94, 95, 213]. Radmehr evaluated the effect of preoperative increased level of serum creatinine. It was found that higher serum creatinine level group had higher frequent postoperative atrial fibrillation, so he proposed that serum creatinine level preoperatively is a marker of increased early mortality and outcome after CABG [94] . In our sample, the level of creatinine was higher for AF group for patients older than 60 years, whereas the relation was even inversed for younger patients (Figure 4.5). This result is difficult to explain, and may result from the limited size of our study population.

The purpose of using weighted likelihood logistic regression was to circumvent the disproportion of the male and female population in our sample. Sex did not show up as an independent predictor in our analysis, but it showed some level of interplay with other factors such of age, previous MI, serum creatinine. The difference between the unweighted and weighted model was the higher level of significance of previous MI in the latter. MI mainly improved the prediction specificity for women, at the expense of sensitivity for men. The final complete model achieved a sensitivity of around 60%, and specificity of around 80%.

It is natural to think that AF should occur sooner in patients with higher preoperative risk. However, the survival curves rather showed that AF occurs at the end of the first operative days irrespective of the preoperative risk. However, the hazard rate was both higher and more sustained in the high risk group (Figure 4.11, 4.12). As suggested in chapter 3, some changes, beyond preoperative risk, might condition the appearance of AF, which is the topic of the next chapter.

4.5 Summary

1. Age was the most important predictor of postoperative atrial fibrillation after CABG surgery. The level of serum creatinine and prior myocardial infarct were also preoperative predictors. Serum Creatinine played the role to improve the female specificity and male sensitivity, and the myocardial infarct mainly improved the female specificity.

2. The preoperative risk score could to a certain extent predict who would develop AF, but were not predictive on the time when AF would occur.

Chapter 5 AF vs. Non-AF Clinical Predictor Analysis

In this chapter, we compare AF and Non-AF patients to find predictors that can discriminate the two groups. AF and Non-AF patients are compared with respect to the preoperative risk factors obtained in chapter 4 and the time series considered in chapter 3. For each AF patient, the last 2 hours before AF were retained as in chapter 3. Each AF patient was matched with two Non-AF patients. For these, the two hours corresponding to the same post-operative time were selected (Figure 5.1)

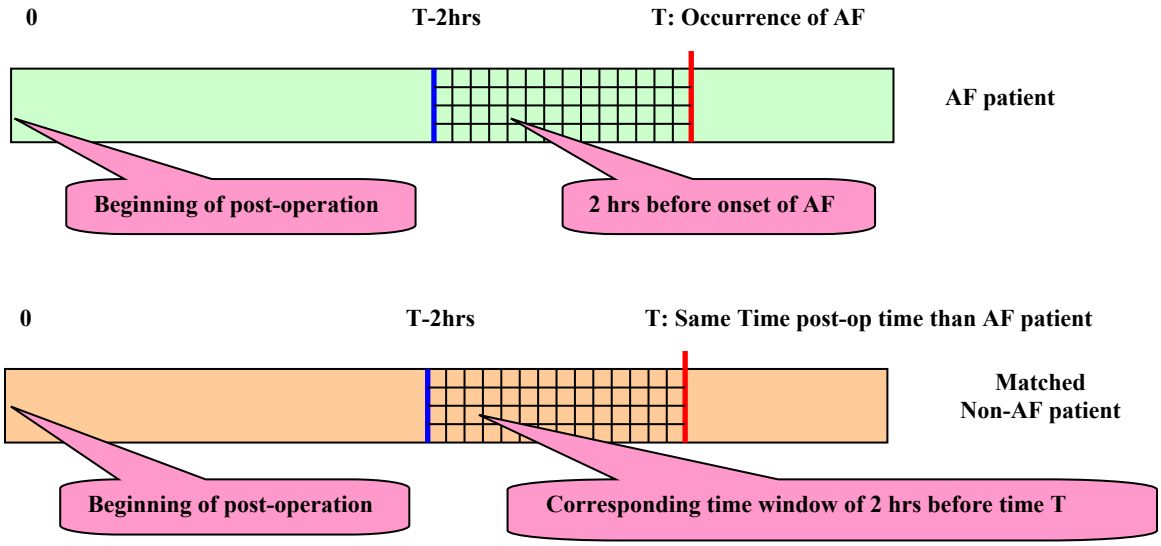

Figure 5.1 Time windows of AEG signals for an AF patient and its matched Non-AF control. 0 represents the time of beginning of post-surgery. T for AF patient is the time of occurrence of AF, T for control (Non-AF) patient is the same post-operative time.

The AF group of 29 patients was the same that was analyzed in Chapter 3. After excluding the noisy and incomplete recordings, 87 Non-AF patients were available. Ideally, each AF patient should have been matched according to sex, preoperative risk

and date of surgery. The second criterion was intended to get the same distribution of preoperative risk in both groups. The third criterion was aimed at bringing homogeneity in the surgery and post-surgery handling.

The matching procedure was the following

1. Sort the AF patients in risk ascending order ($[R_i^{AF}, i=1,29,\ R_i^{AF} < R_{i+1}^{AF}]$);
2. Starting from the first AF patient, find the 10 closest non-AF patients with $R^{\sim AF} \geq R_i^{AF}$. If less the 10 are available, include the closest patients with $R^{\sim AF} < R_i^{AF}$;
3. Among these 10 Non-AF patients, find the two patients whose date of surgery is the closest to that of the AF patient. For close surgery date, select the patient that has the same sex than the AF patient.
4. Remove the AF and matched Non-AF patients.
5. Repeat steps 1 to 4 until the last AF patient.

The dates of the surgery were spread over a period of 64 months. The analyses of chapter 4 had shown a significant difference of age and pre-operative risk between AF and Non-AF patients. Our set of Non-AF patients was not large enough to reach an equal distribution of preoperative risk score in the two groups (p_{t-test} =0.0070). The characteristics of the final control group were as following: 58 control patients (Sex: Male 45, Female 13, Age: 65 ± 8.2, *PreopScore* 0.2964 ± 0.1503) to be compared with the AF group (Male 23, Female 6, Age: 68.8 ± 6.3, *PreopScore*: 0.3911 ± 0.1514).

5.1 Univariate Analysis

We firstly present detailed analyses of the variables that were shown in chapter 3 to display significant temporal changes prior to the onset of AF, namely R_{PAA}, *ArrhyDuration*, *AAMean* and *LFPortion*. It is followed by the results of the multivariate analyses to discriminate between AF and Non-AF patients.

In some analyses, we introduced the concept of Relative Difference (*RD*) variables. It measures the change of a variable x_i at time *i* relative to a reference value x_0 as:

$$\mathrm{RDx_i} = \frac{x_i - x_o}{x_o + 0.001} \qquad (5.1)$$

where 0.001 avoids divergence when $x_0 = 0$.

5.1.1 Analysis of PAA

As in AF group (section 3.1.1), the total number of PAA varied widely among Non-AF patients (Min. 0, Max. 811, Median. 5, mean 49). It should be mentioned that 77% of the PAA were concentrated in 4 patients ((444+445+500+811=2200)/2843), while 24 patients have only 3 or less PAA. As shown in Figure 5.2 and confirmed by the Kolmogorov-Smirnov test (P< .001), the distribution of the PAA number in the two groups (AF: Min. 3, Max. 4539, Median 87, mean 575) was different, The main dissimilarities between the two groups came from the ~30% of Non-AF patients with 0 or 1 PAA, and from ~20% of the AF patients with more than 1000 PAA. There were no correlation between the preoperative risk and the number of PAA, neither in the AF (r=.187, p =.33) nor the control group (r = -0.001, p=.996).

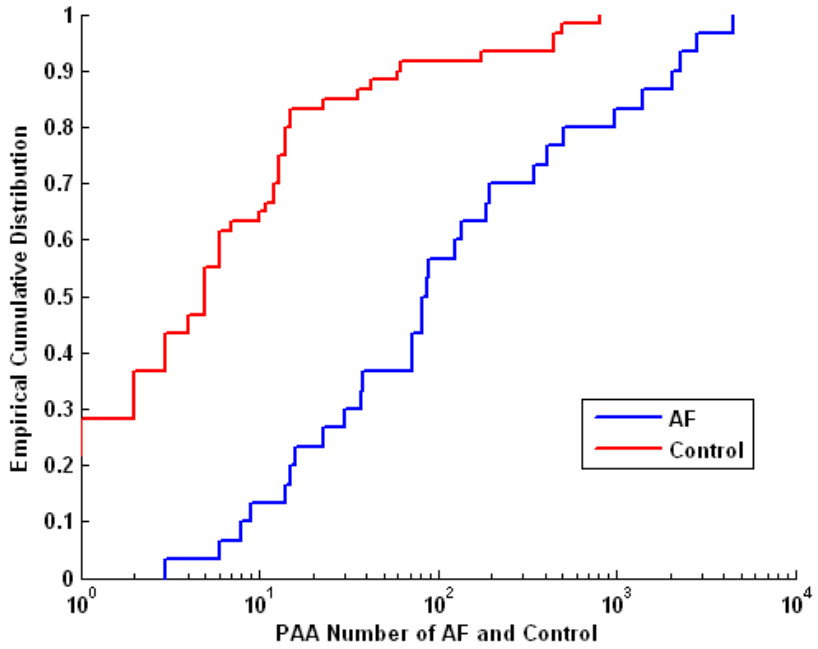

Figure 5.2 Cumulative distribution of the PAA number in AF and Control group. The distribution of the PAA number in the two groups, AF (blue line) and Control (red line) was quite different.

5.1.1.1 LPAA and RPAA

Also as for AF patients (section 3.1.1), the fractions of LPAA and RPAA (*LPAAFraction* and *RPAAFraction*, total number of LPAA or RPAA divide the total number of PAA of 2 hours) were very inhomogeneous among the control patients (Figure 5.2).

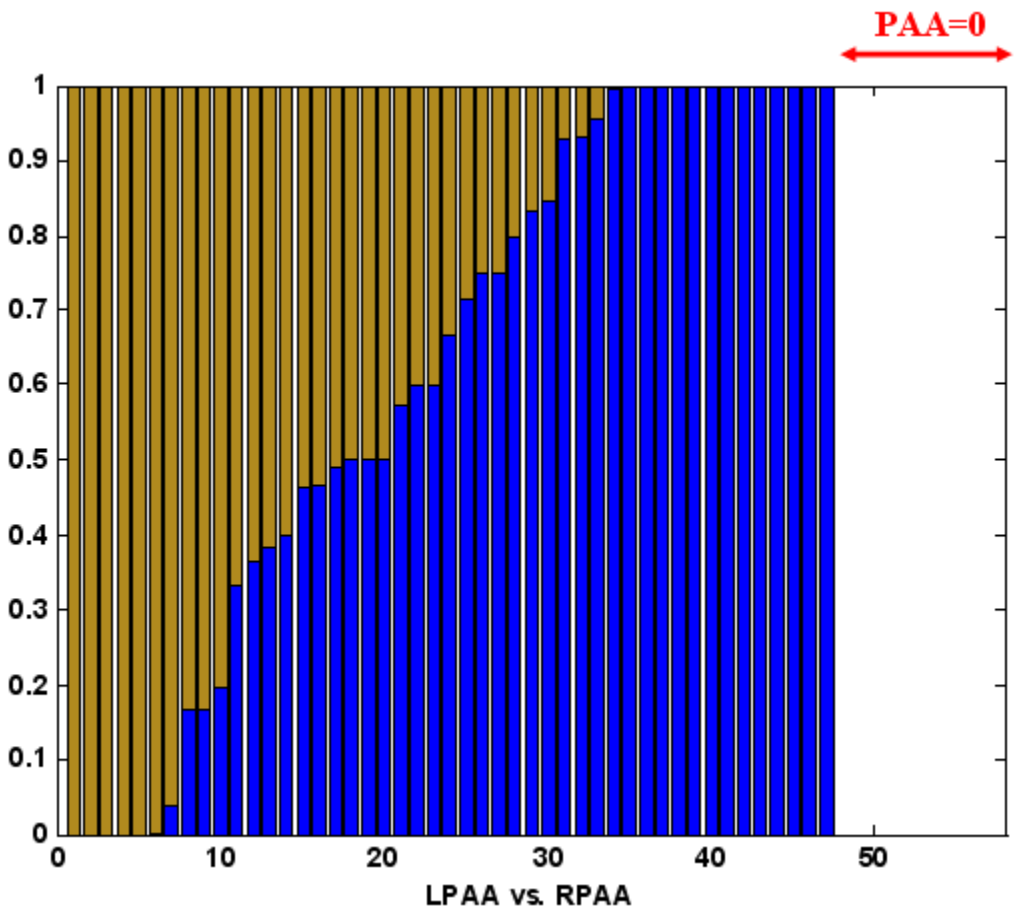

Figure 5.3 Fraction of LPAA (blue color) and RPAA (golden color) for each patient of the control group. Patients 48 to 58: no PAA detected. Homogeneity of the proportions was rejected by χ^2 test (<0.001) using either the mean number (all patients) or the mean proportion (patients 1-47) of left and right PAA.

It is noteworthy that 92% of the RPAA occurred in three patients (811,499,426) that had respectively none, one and 18 LPAA, while 47% (445) of the LPAA were concentrated in one patient that did not have any RPAA. Among the 47 patients with a number of PAA >0, 64% had a LPPA proportion >.5, which is a slight but not significant excess, in contrast with what we found in AF patients.

In the forward stepwise logistic regression model, both the total number of *PAA* and *LPAAFraction* (set to .5 for patient without *PAA*) brought a significant contribution to the discrimination of AF and Non-AF patient (P=.017 and .001 respectively, Figure 5.4), while the preoperative risk (*PreopRisk*), which was highly significant alone, was not included in the final model (P=.135, if added to the final model). Hence both the number of PAA and *LPAAFraction* can partly discriminate AF from control patients (Non-AF). The fact that an increase of PAA rate was often detected prior to the onset of AF in the previous analyses (section 3.1.2) calls for a comparison of the dynamics in the two groups.

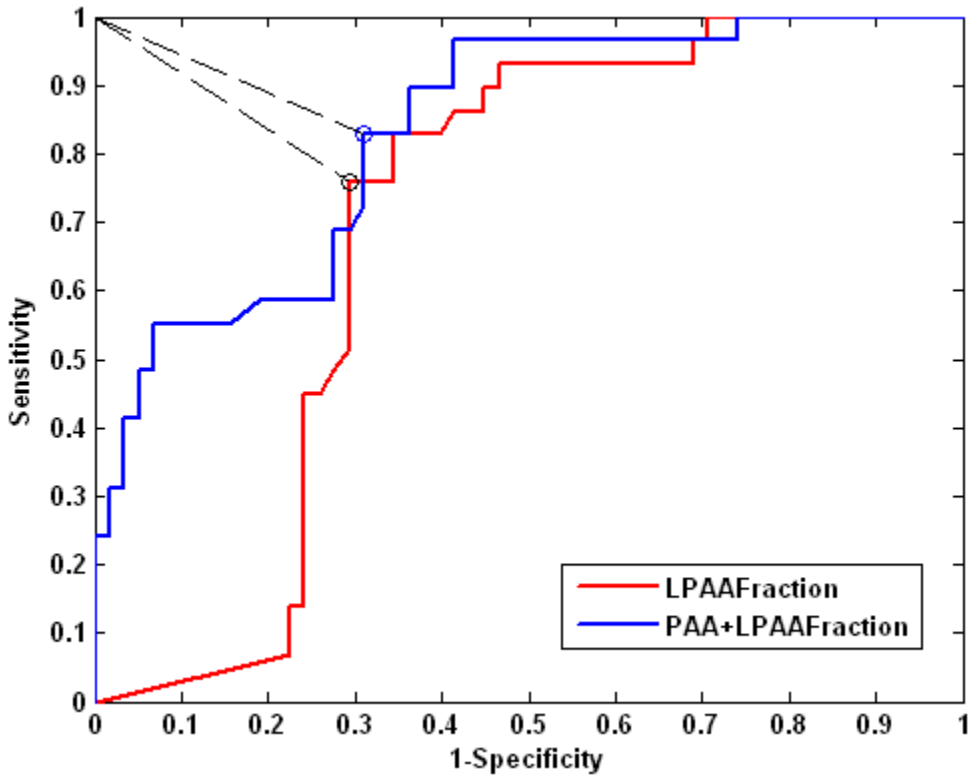

Figure 5.4 ROC curves from a logistic model including the total number of PAA and the *LPAAFraction.* In the forward stepwise logistic regression model, the total number of PAA and *LPAAFraction* both brought a significant contribution to the discrimination of AF and Non-AF patient. For the first mode l (red ROC curve), the predictor is *LPAAFraction*; for the second model (blue ROC curve), the two predictors are *LPAAFraction* and PAA are included.

5.1.1.2 PAA Rate (R_{PAA}) and Proportion (P_{PAA}) Analysis

As in section 3.1.2, PAA temporal evolution was studied by calculating PAA rate (R_{PAA} = number of PAA within 5 minutes interval/5 minutes minus non sustained arrhythmia duration) and proportion (P_{PAA} = number of PAA within 5 minutes/total number PAA in two hours, set to 1/24 if total number PAA=0). The evolution trends of R_{PAA} and P_{PAA} of AF and control patients are shown in Figure 5.5.

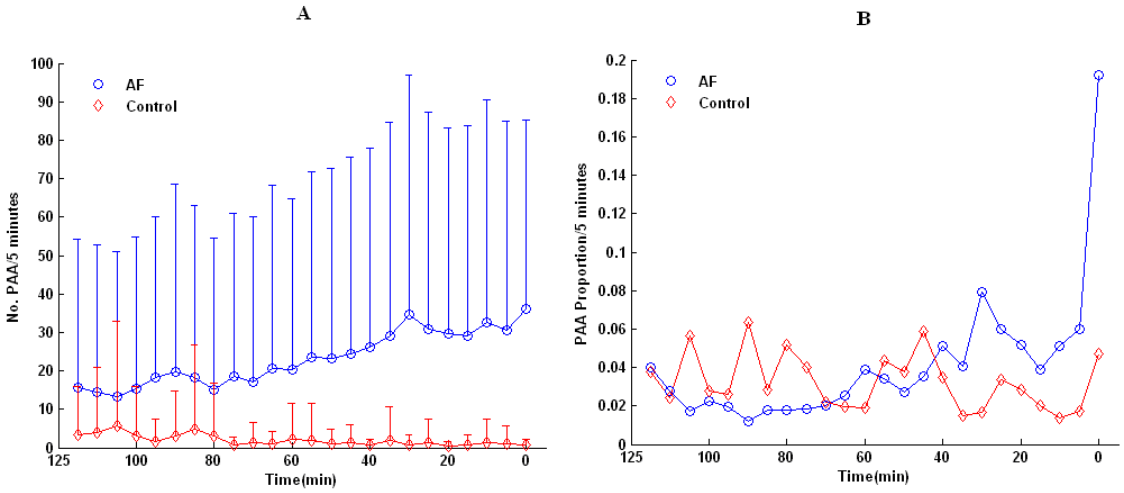

Figure 5.5 A) Mean value and standard deviation of PAA rate (R_{PAA}) within each 5 minutes for the 2 hrs of Control (Non-AF) and AF Group. B) Mean value of PAA proportion (P_{PAA}) within each 5 minutes for the 2 hrs. Control (Non-AF, diamond shape, red line); AF(circle shape, blue line).

As expected from the results of the section 5.1.1.1 logistic regression, ANOVA analysis of R_{PAA} showed significant group (AF vs. Non-AF) effect (AF: 23.2 ± 4.7 vs. Non-AF: 2.0 ± 3.3 PAA/5 min., P< .001). However, both R_{PAA} and P_{PAA} also had a significant time*group (AF vs. Non-AF) interaction effect, stemming from the lack of time effect in the control group.

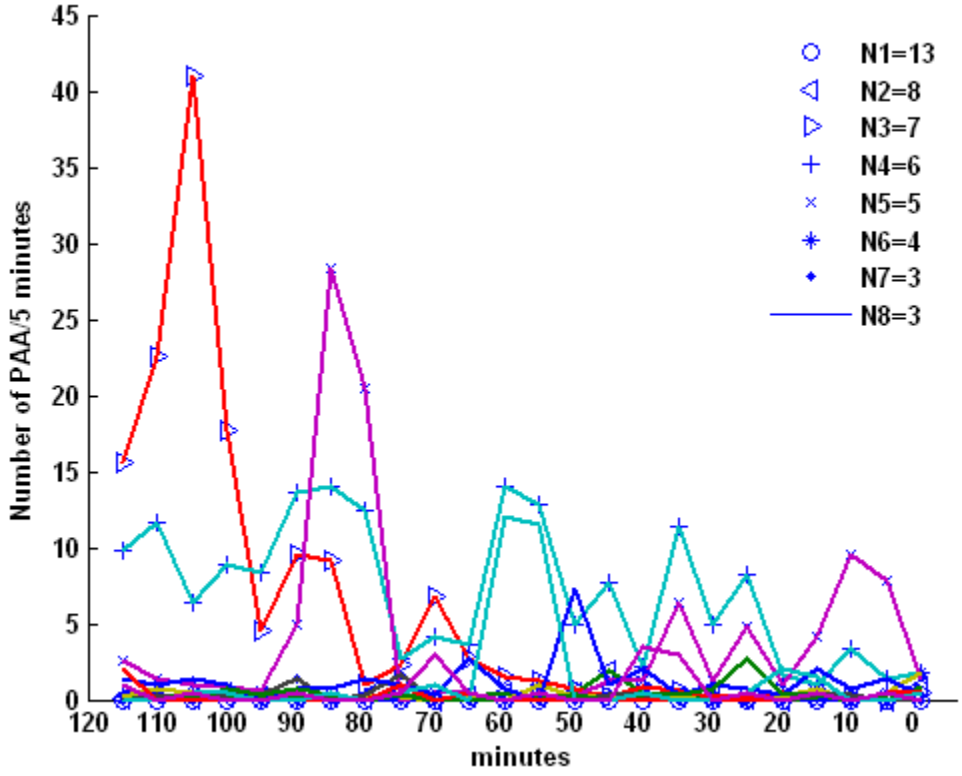

Figure 5.6 The 8 biggest groups from cluster analysis of PAA rate in control group (Patients without PAA were excluded).

Figure 5.6 presents the results of the cluster analysis of the control R_{PAA} temporal evolution. Most patterns displayed minor isolated burst over a constant trend. Some patients showed long lasting period of sustained PAA rates.

5.1.1.3 LPAA Analysis

Our previous analyses have demonstrated the importance of LPAA as trigger of AF. Figure 5.7 displays the temporal evolution of the LPPA rate (R_{PAA}^{L}) and LPAA Fraction (*LPAAFraction*= number of LPAA/ number of PAA within each 5 minutes interval, set to .5 if no PAA in the interval). Both variables showed a significant group and

group*time effect (p< .0001). In fact, the time effect was significant in AF group (p<.001), but not in Non-AF group.

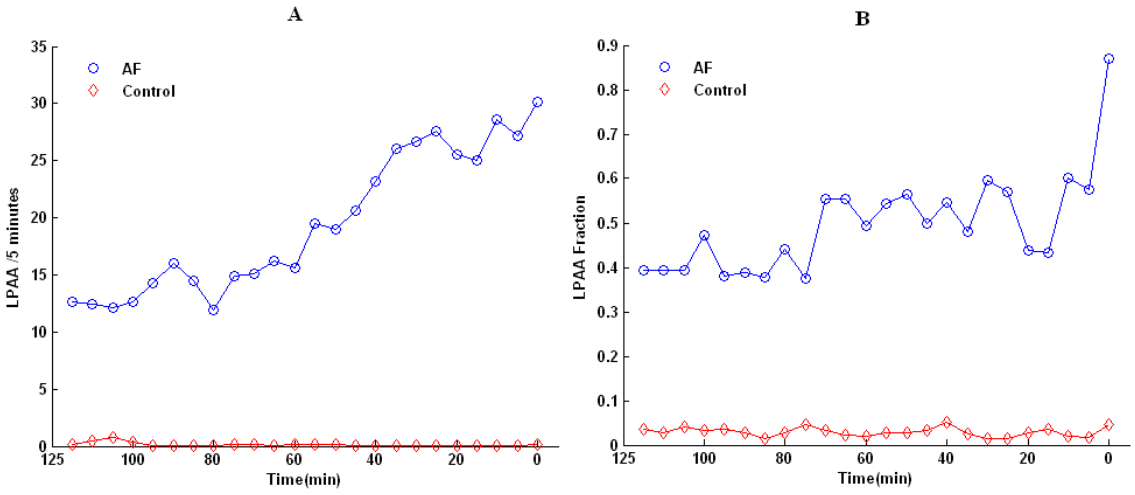

Figure 5.7 A) mean value of LPAA number within each 5 minutes during 2 hrs. B) Mean value of LPAA Fraction within each 5 minutes during the 2 hrs. (AF: blue line and circle shape; Control: red line and diamond shape).

5.1.2 Non-sustained Arrhythmia

The evolution of the arrhythmia duration (*ArrhyDuration*) is shown in the left panel of Figure 5.8. ANOVA showed again significant group and group*time (P< .001) effects. Post-hoc analysis showed that there were significant contrast between the [120 60] vs. [60 0], and [10 5] vs. [5 0] periods in AF group, but none in the control group. The analysis of RD (Relative Difference) of arrhythmia duration time (using the first 5 minutes as reference) yielded to the same conclusion.

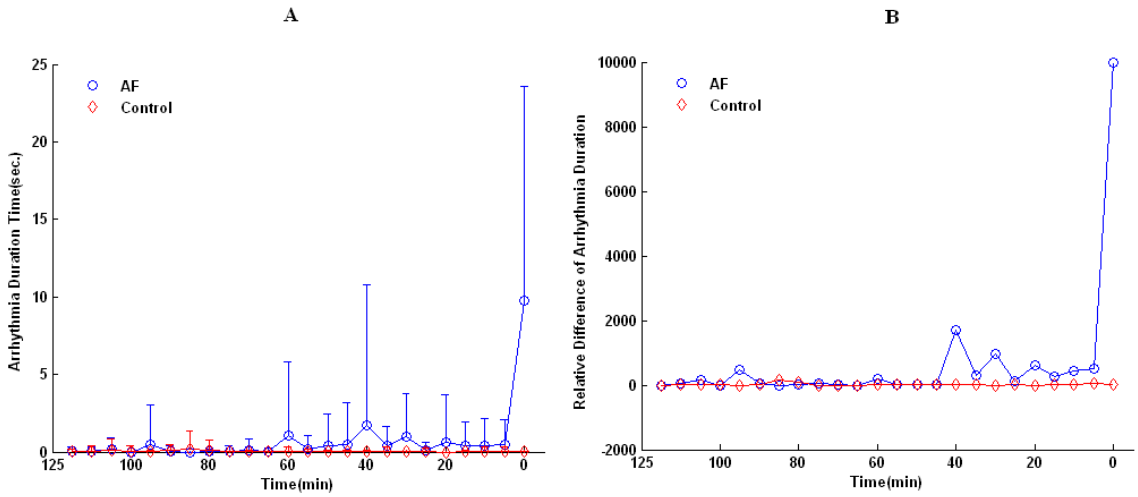

Figure 5.8 A) The mean value and standard deviation of arrhythmia duration time (sec.) in each five minutes; B) The mean value of relative difference value of arrhythmia duration for AF and Control. The relative difference (eq. 5.1) was calculated using the value of the first 5 minutes as reference. (AF: blue line and circle shape; Control: red line and diamond shape).

5.1.3 AA Trend and AA Relative Difference Trend

The analysis of AA trend (calculated from normal sinus beats) in AF patients showed a subset of patient with an increase heart rate preceding the onset of AF (Section 3.2 & Fig. 3.5). Such a trend did not exist in the control group (Fig. 5.9 and 5.10). ANOVA showed that the time (p=0.001, Huynh-Feldt), time*group (p=0.055) effects were significant or closely significant, while the group effect was not significant (p=0.761), meaning that the mean heart rate was the same in the two groups. No significant time contrast existed in Non-AF group.

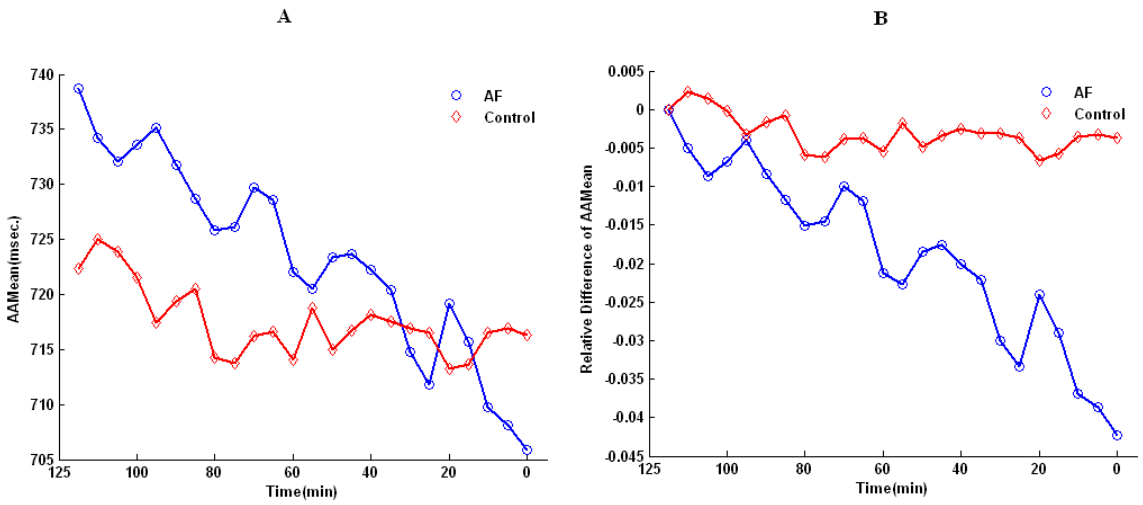

Figure 5.9 The trend of raw AA (A) and relative difference (B) AA, the latter calculated using the time period of the first 5 minutes as the reference. AF: red and diamond; Non-AF: blue and circle. As in chapter 3, only normal sinus beats were considered.

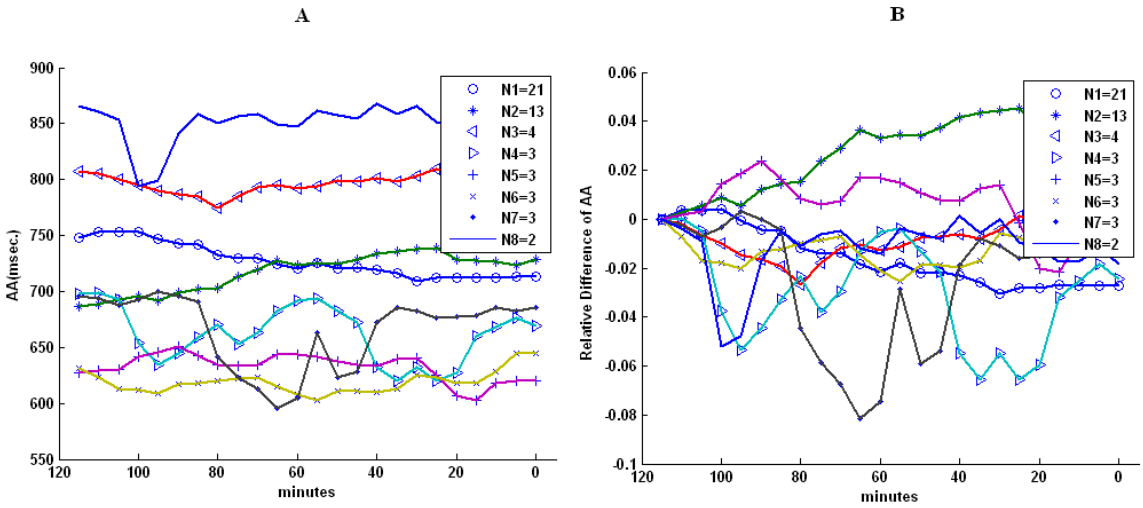

Figure 5.10 Cluster analysis of AA raw (Panel A) and relative difference data (Panel B). In panel A and B the mean trends of 8 more populated groups were plotted respectively.

5.1.4 LFPortion of AF and Control Patients

In the analysis of the pre-AF temporal evolution (Section 3.3) and of the trigger PAA (Section 3.5), *LFPortion* ($LF/(LF+HF)$) was a predictor of the onset of AF. The evolution of mean of *LFPortion* and of its relative in the AF and Control group are plotted in Panel A and B of Figure 5.11, respectively. The analysis was done with ANOVA. Except for the last 5 minutes interval, the mean *LFPortion* was always slightly higher in the control group, although the group effect was not significant (p=.11). There was again no significant time effect in the control group.

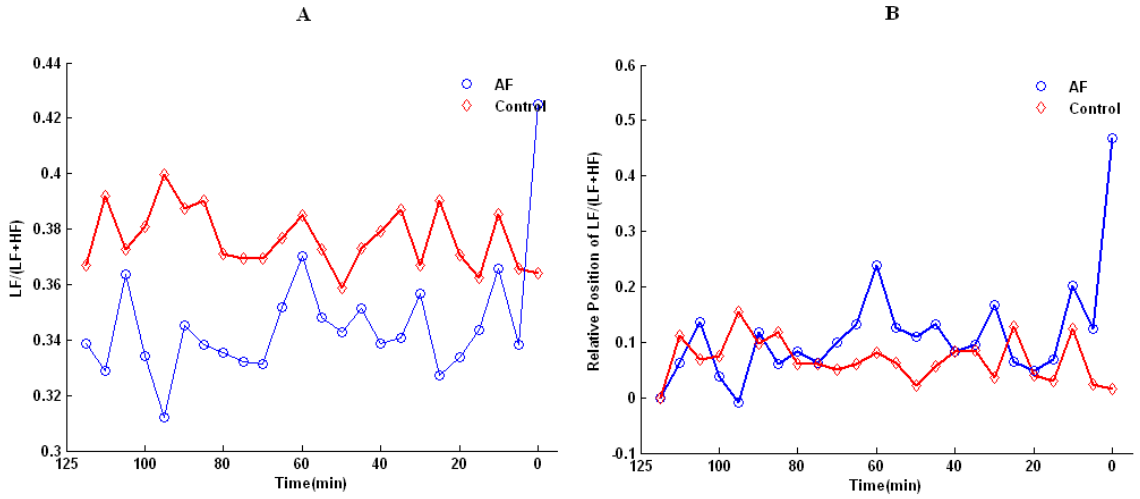

Figure 5.11 The trend of mean of *LFPortion* (A) and of its relative difference (B). (AF: blue, circle; Control: red, diamond)

5.2 Model Building to Discriminate AF from Non-AF Patients

This section investigates whether and to which extent the preoperative risk and the variables extracted from AEG can discriminate AF from Non-AF patients. The following variables were considered: *PreopRisk*, R_{PAA} , R_{PAA}^{L} , *LPAAFraction*, *AAMean* , *AAStd* , *rMSSD* , $pNN50$, *CTAMean* , *CTAVMean* , *CTAStd* , *CTAVStd* , *LFPortion* , $CorrAA\_AV$, $CorrAA\_CTA$, $CorrAV\_CTA$ (the definition each variable was given in chapter 2.). The AEG variables were computed over 5, 10 and 15 minutes periods.

Logistic regression was performed with different choices of time intervals (i.e. BTI= 5 to 15 minutes).

5.2.1 Logistic Regression Based on BTI (Basic Time Interval) Data

In the first type of analysis, all time intervals were classified as AF (1) for AF patients and Non-AF (0) for control patients, and then analyzed together by logistic regression. As aforementioned, the preoperative risk score (*PreopRisk*) was also included. Forward and backward regressions were applied with entering and removing criteria of 0.05 and 0.10 respectively. Only the variables entered in both instances were kept and a final forward model was run with these variables. The same set of variables was selected for all BTI. The only exception was *LFPortion*, which was kept because it was significant for the 5 and 10 min. BTI, but not in 15 BTI.

Table 5. 1 Beta value of predictors in the final forward logistic regression model for 5, 10, 15 minutes intervals

	5 min.	10 min.	15 min.
PreopRisk	2.744	2.902	2.726
R_{PAA}	.143	.217	.235
LPAAFraction	1.398	2.222	2.286
LFPortion	-2.326	-1.978	
pNN50	-13.597	-14.154	-.774
CTAVMean	.014	.014	.013
CTAVStd	.032	.067	.083
CorrAA_AV	-1.006	-1.190	-1.046

Table 5.1 shows β values of the variables entered in the final models, a positive and negative corresponding to an increase and decrease AF occurrence risk respectively. The higher value of *LFPortion* (expected from Figure 5.11), *pNN50* and *CorrAA_AV* have protective effect. Inversely, the increase of R_{PAA} , *LPAAFraction*, *CTAVMean* and *CTAVStd* lead to higher risk. The temporal evolution of the scores for three BTI (Figure 5.12) as well as their sensitivity and specificity (i.e. nb. of time intervals correctly classified as 1 or 0, Table 5.2) show that the three models provided similar discrimination. Figure 5.12 shows that the separation between the groups increases as time gets closer to the onset of AF.

Table 5. 2 Sensitivity, specificity, and ROC area of models of 5, 10 and 15 minutes BTI

	Sensitivity	Specificity	ROC Area
5 min.	75.07%	70%	0.813
10 min.	79.64%	69.44%	0.821
15 min.	80.27%	67.32%	0.815

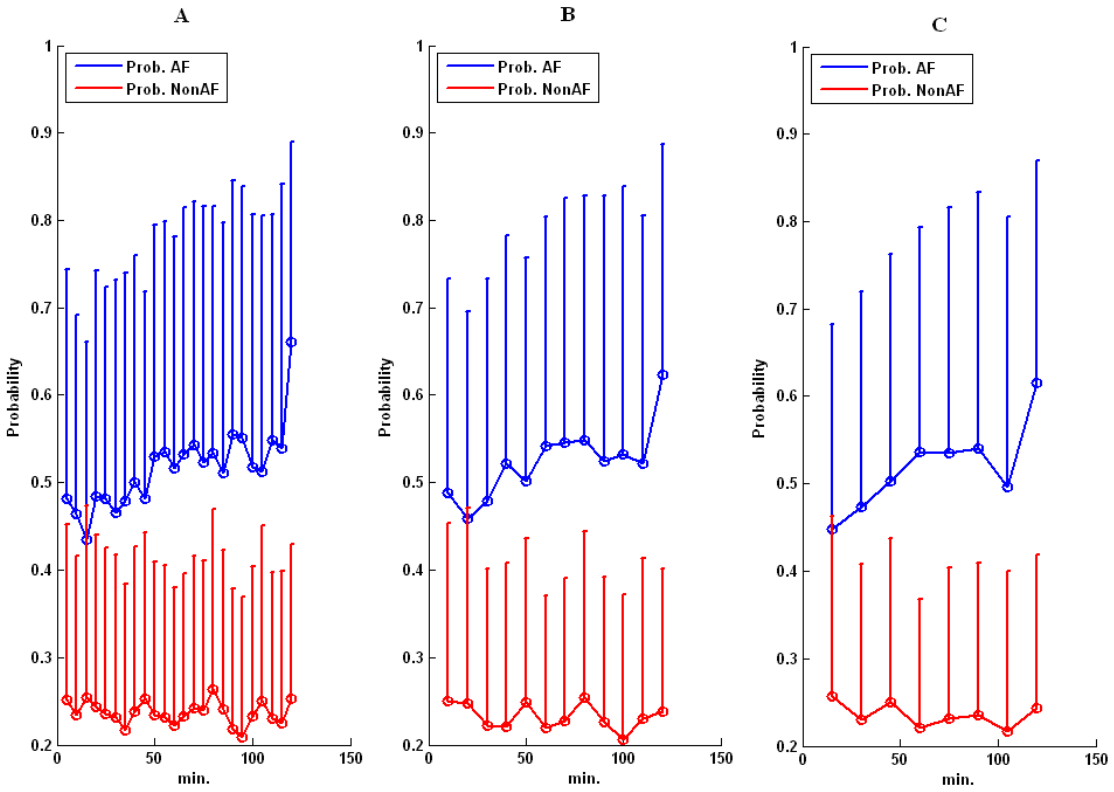

Figure 5.12 The time evolution of mean and standard deviation of the risk scores of 5, 10 and 15 minutes BTI (A, B, C) logistic regression model in AF (red) and Non-AF (blue) groups.

The left panels of Figure 5.13 show the temporal evolutions of *pNN50*, *CTAVMean*, *CTAVStd* and *CorrAA_AV* along the 2 hours time in each group for 10 minutes BTI. There are clear and sustained differences between the AF and Non-AF groups justifying the inclusion of these variables in the logistic regression models, as well as the sign of their contribution in the model. However, the cumulative distributions of the average within AF or Non-AF (right panels) reveal that the differences mainly result from an excess subset of Non-AF patients in the upper or lower range of values. This explains why no significant group effect was found upon ANOVA analysis, as documented in Table 5.3. The comparisons of the AUC (area under ROC curve) differences of the

successive models obtained in the eight steps of the logistic regression are presented in Table 5.4. It shows that most predictors produced significant changes.

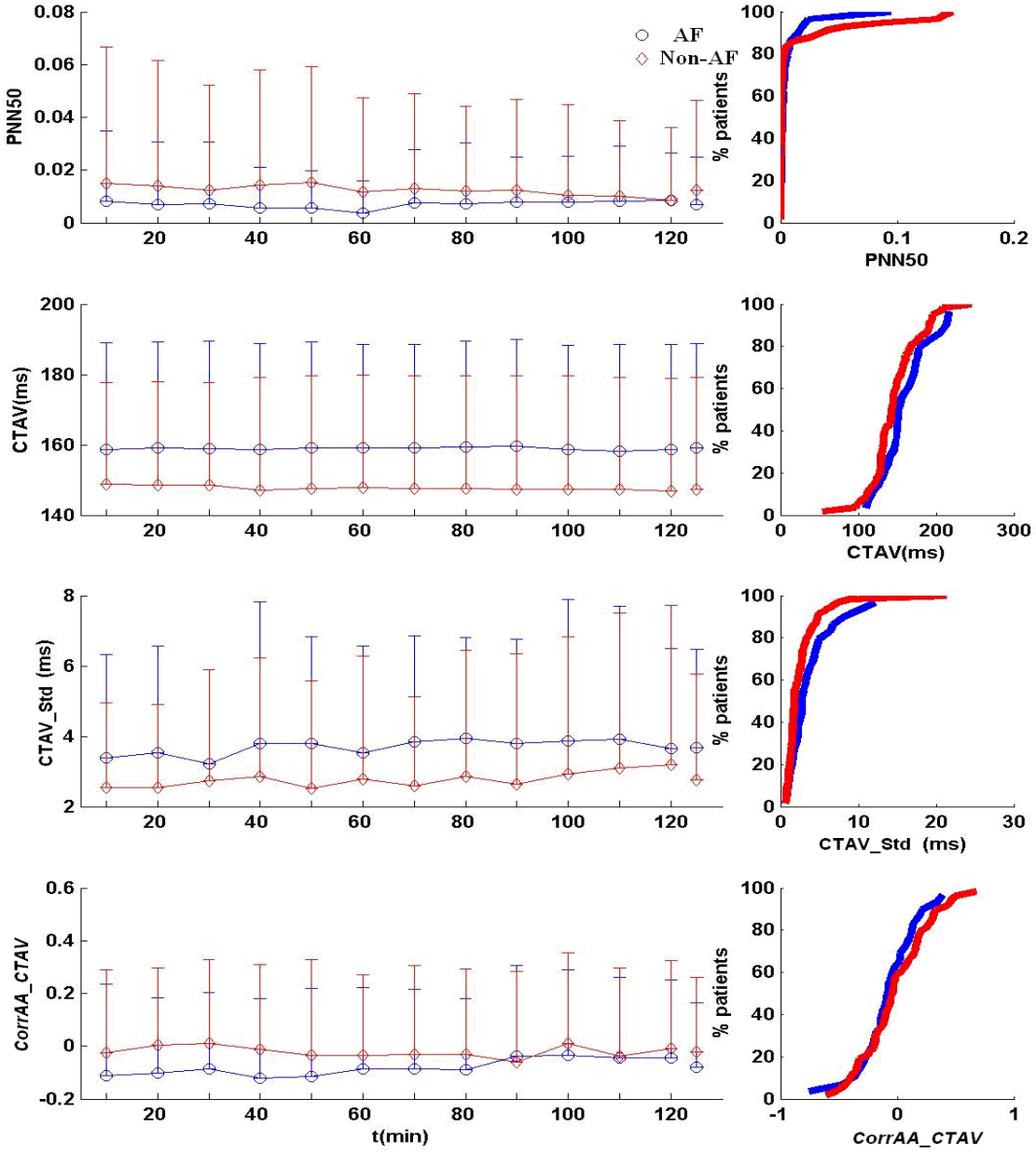

Figure 5.13 Left panels: temporal evolution of *pNN50*, *CTAVMean*, *CTAVStd* and *CorrAA_AV* (from top to bottom) in AF (blue circle) and NAF (red diamond) groups. All values were computed from normal sinus beats in each 10 minutes interval. The average values were also calculated for each patient. The last point in each panel shows the mean

and standard deviation of these averages in each group. The right panels show the cumulative distribution of these averages within each group.

Table 5. 3 p value of Group (AF vs. Non-AF), Time, and Group*Time effects upon ANOVA analysis of each variable of 10 minutes BTI data

	Group	Time	Group*Time
PreopRisk	.007		
R_{PAA}	.001	.04	<.001
LPAAFraction	<.001	.008	.113
sdLFPortion	.193	0.565	.005
pNN50	.423	.841	.650
CTAVMean	.173	.624	.832
CTAVStd	.174	.544	.805
CorrAA_AV	.342	.700	.494

Figure 5.14 shows that the stepwise evolution ROC curves according to the predictors entering order into logistic regression model of 10 minutes BTI data. The main improvements come from the first four variables as R_{PAA} , *PreopRisk* score, and *LPAAFraction*, and *CTAVMean*. The index of likelihood of the 8 stepwise models shows increase when new predictor enters (Table 5.5). The sensitivity refers to the ratio of the number of BTI correctly classified as AF over the number of BTI of all AF patients together, while specificity is a similar measure for Non-AF patients.

.

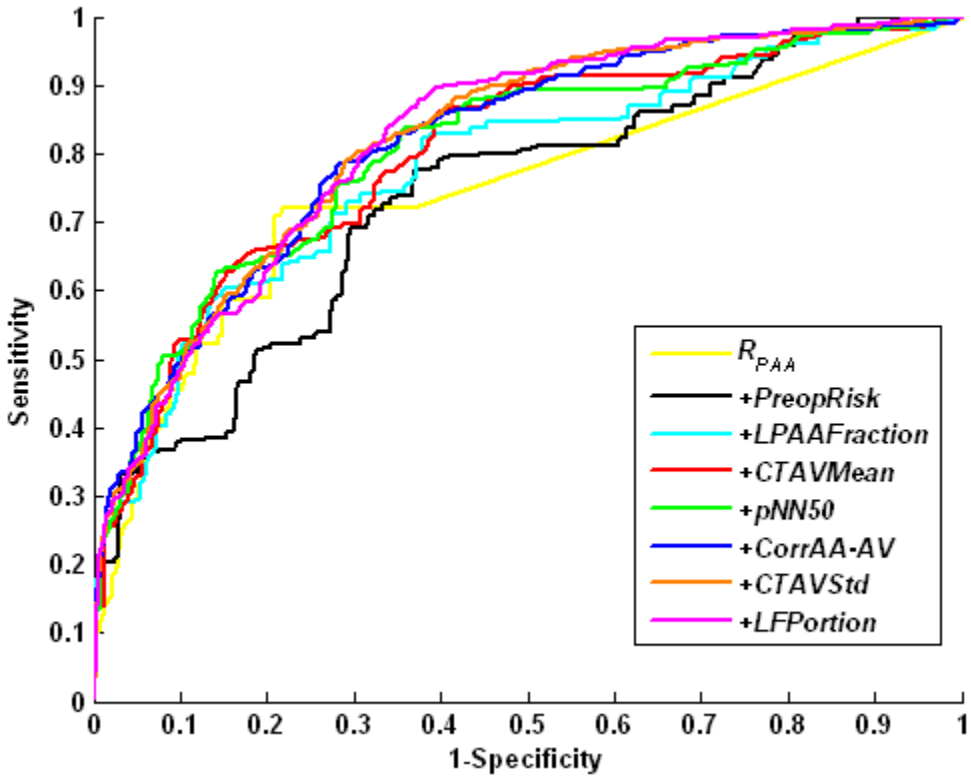

Figure 5.14 ROC curves of stepwise logistic regression models for 10 minutes BTI by the order of predictors entering into the models: R_{PAA}, *PreopRisk*, *LPAAFraction*, *CTAVMean*, *pNN*50, *CorrAA_AV*, *CTAVStd*, *LFPortion*.

Table 5. 4 Comparison of AUC (area under ROC curve) among the successive models obtain in the eight steps of the logistic regression

	I vs. II	II vs. III	III vs. IV	IV vs. V	V vs. VI	VI vs. VII	VII vs. VIII
Difference	0.00973	0.0401	0.0214	0.00369	0.00423	0.00568	0.00145
S.E.	0.0184	0.0106	0.00671	0.00454	0.00291	0.00389	0.00248
95% Confidence Interval	-0.0264 to 0.0459	0.0193 to 0.0608	0.00828 to 0.0346	-0.00521 to 0.0126	-0.00148 to 0.00994	-0.00195 to 0.0133	-0.00342 to 0.00632
Significance	0.5794	0.0002	0.0014	0.0187	0.1467	0.1447	0.5598

The following variables were successively entered in the model: RPAA, PreopRisk, LPAAFraction, CTAVMean, pNN50, CorrAA_AV, CTAVStd and LFPortion, in model I to VIIII. Line 1 and 2: Difference of AUC and its standard deviation, line 3: 95% confidence interval of the difference, line 4: significance of the difference.

Table 5. 5 Sensitivity, specificity, and ROC area of stepwise logistic regression models by the order of variables entering into the models

	Sensitivity	Specificity	ROC Area	-2Log likelihood
R_{PAA}	0.721557	0.783626	0.74839	1180.251
PreopRisk	0.691617	0.703216	0.73865	1095.245
LPAAFraction	0.730539	0.709064	0.77873	1035.528
CTAVMean	0.658683	0.817251	0.80015	1014.186
pNN50	0.754491	0.719298	0.80384	1000.350
CorrAA_AV	0.784431	0.719298	0.81574	982.955
CTAVStd	0.790419	0.710526	0.81997	975.811
LFPortion	0.796407	0.694444	0.82141	970.039

Finally, the stability of the logistic regression modeling was tested by bootstrap applied 10 minutes BTI data. Random samples were constructed from the 1440 (12*(29+58)) time intervals of all patients with samples sizes of [150 240 330 420 510 600 690 780 870 960]. 100 different random samples were produced for each sample size, which were analyzed with forward conditional logistic regression. Then, the fraction of the 100 samples in which each variable was selected as a significant predictor ($p<0.05$) was computed and is displayed in Figure 5.15. We considered a variable to be stable predictor if it was selected in more 70% of the samples with the last and larger 960 sample size of (960/1440). According this criterion, the stable predictors were PreopRisk, R^{L}_{PAA} , R_{PAA} , *LPAAFraction*, *pNN50*, *CTAVMean*, *CorrAA_AV*. In the following, the logistic regression model, including these 7 variables is referred as Model 0.

We also gathered the β coefficients of these stable predictors of all samples in which they were selected. The mean and standard deviation of these β are shown in figure 5.16 for each sample size. The beta coefficients converged to rather stable values as the sample size was enlarged. The final Model 0 was computed using for each variable the mean β value obtained from the larger sample size.

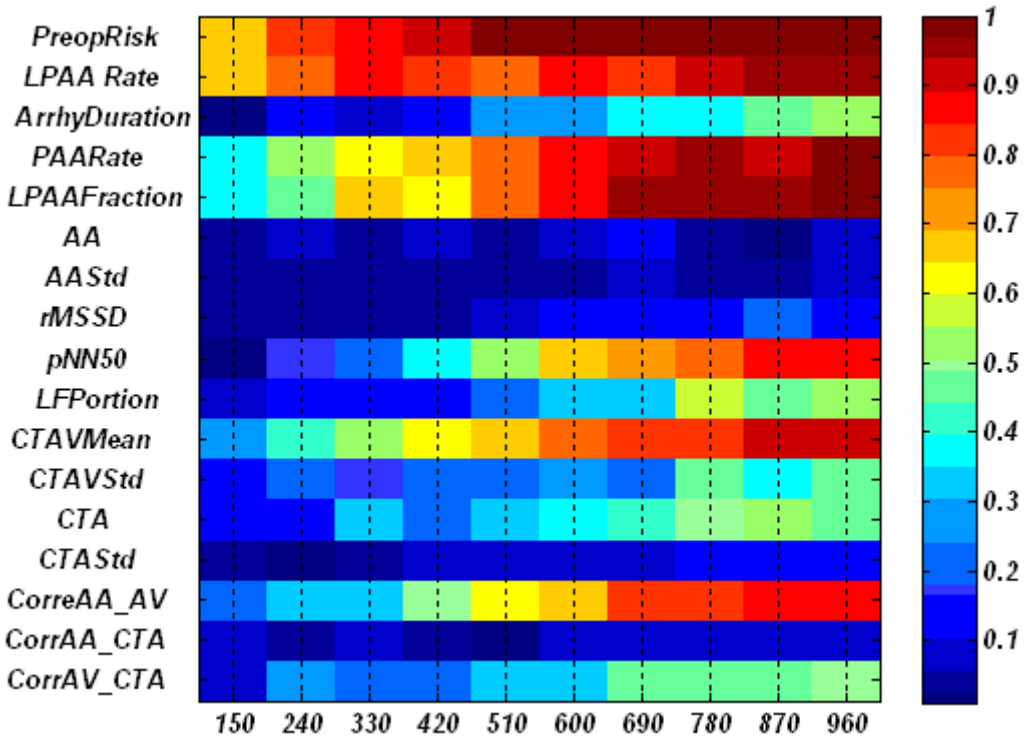

Figure 5.15 For each sample size (represented by the abscissa value), the fraction of 100 random samples in which each variable was selected as a significant predictor ($p<0.05$).

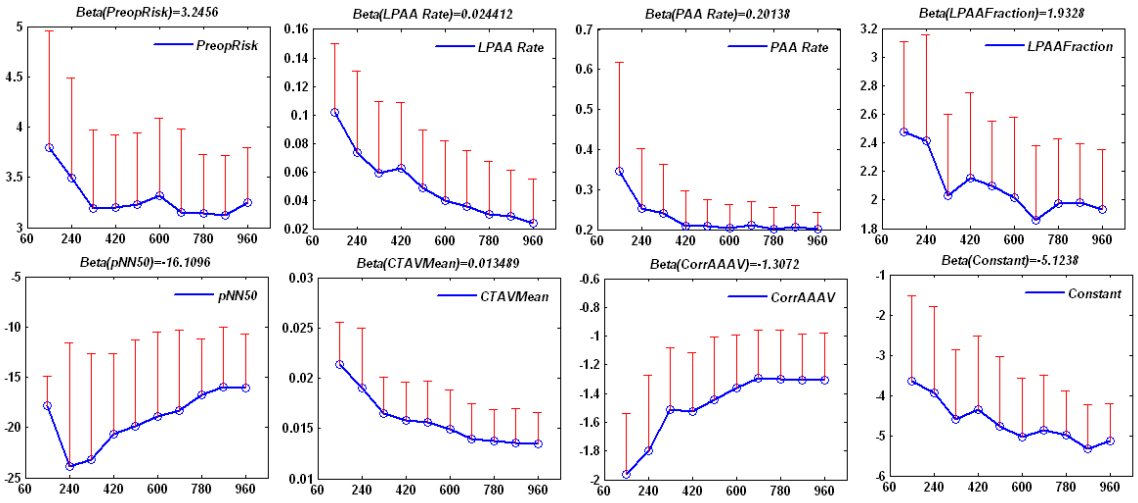

Figure 5.16 mean and standard deviation of the β coefficients of the 7 stable predictors as a function of the sample size. (The value of the constant was added). For each sampling size, the mean and standard deviation of the β value of each variable were computed from all the samples in which it was included as a significant predictor.

5.2.2 Modified Models for AF and Non-AF Prediction

Model 0 had two characteristics: 1) the number of Non-AF patients was twice that of AF; 2) all time intervals were labeled as 1 (i.e. AF) for AF patients, which favours variables with group difference that are not or are weakly time-dependent. Four additional logistic regression models were considered to study the robustness of the discrimination and take into account time-dependent change. In order to balance the contribution of AF and Non-AF patients, the weight of all intervals belonging to AF patient were doubled to even the contributions of the two groups. This model is referred as Model I. The analyses of chapter 3 have shown that there were temporal changes in AF patients. Three other models were examined to investigate whether better discrimination could be achieved by trying to take these changes into account. In Model II, the status variable was set to 0 for time intervals belonging to the first hour, and 1 for those in the second hour for AF patients. In Model III and Model IV, the time intervals of AF patients were assigned to different weights. For Non-AF patient, the weight of each

interval was set to 1/N (N= number of time intervals for each patient). For time intervals from AF patients, weights either increased linearly (Model III) or followed a hyperbolic tangent (Model IV, Figure 5.17), with a sum equal to 1. These weights were chosen to assess how rewarding more a prediction of AF closer could change the selection of predictors and the quality of the discrimination. Results are presented for 10 minutes BTI data.

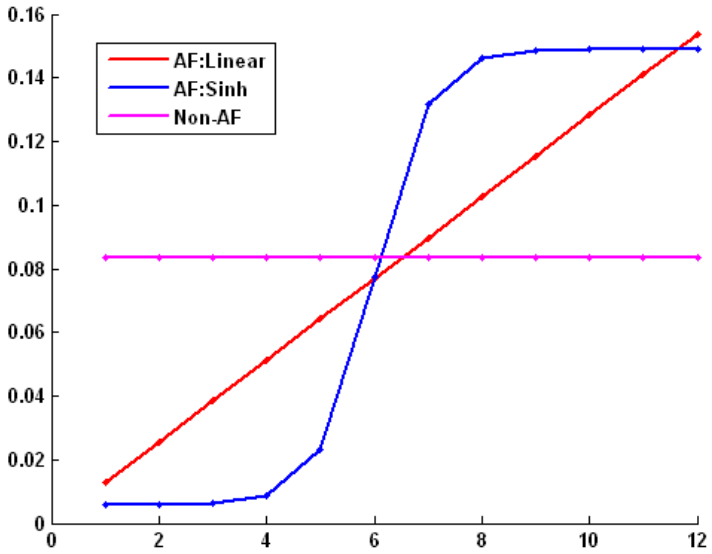

Figure 5. 17 Weights assigned to AF and Non-AF time intervals in Model III and Model IV. Linear (red, model III) and hyperbolic tangent (blue, model IV) weights for AF time intervals, constant weights (magenta) for Non-AF time intervals. The data is 10 minutes BTI data. The sum of the weights is 1 for all cases.

Bootstrapping method was applied to the four models in order to study the stability of the models as it was done in Model 0. 100 realisations were done for each sample size, and figure 5.18 shows the fraction of these in which each variable was selected as a significant predictor: Model I (A), Model II (B), Model III (C) and Model IV (D).

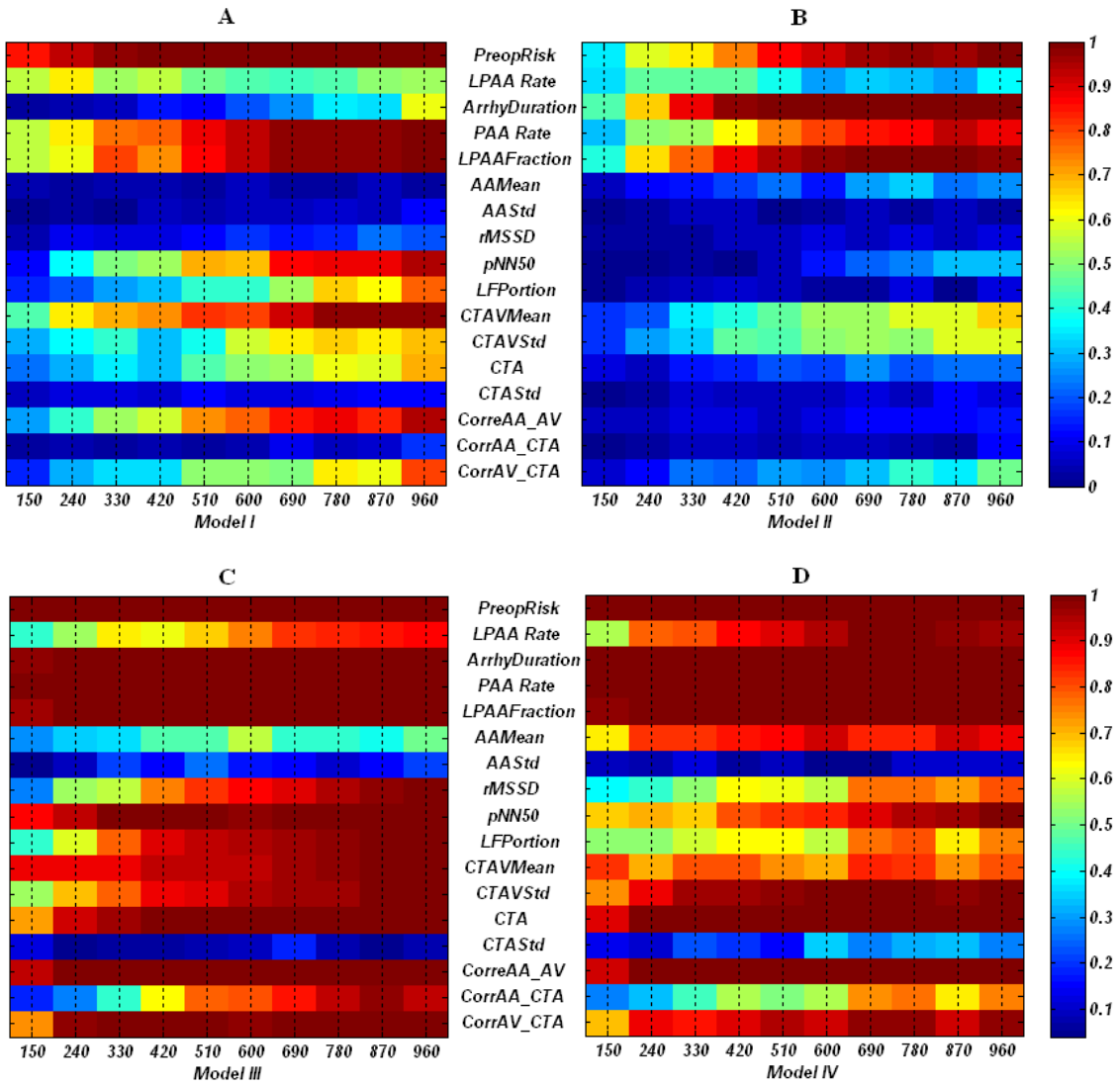

Figure 5.18 For each sample size, appearing in the abscissa, 100 random samples were constructed from the full set of intervals. The figure show the fraction of these in which each variable was selected: Model I (A), Model II (B), Model III (C) and Model IV (D).

As for model 0, the variables appearing in more than 70% of the highest sample size realizations were selected and were considered to be stable predictor. In Table 5.6, the mean beta coefficients (the same calculation method as Model 0) of these stable predictors are showed. In Table 5.6, Model 0 and Model I almost had the same predictors. The common ones, which had also very similar beta values, were: *PreopRisk*, *PAARate*, *LPAAFraction*, *pNN50*, *CTAVMean*, *CorrAA_AV*. *LPAARate* appeared in

Model 0 and not Model 1, while it was the inverse for *LFPortion* and *CorrAV_CTA*. The difference of Model 0 and Model I laid in the weights of AF time intervals, which were doubled in Model 1. Since all time intervals of AF patients were classified AF and had the same weights, the predictors were variables with stable group difference.

For Model II (AF patients intervals of the first hour classified as 0, but all intervals with the same weight), the number of stable predictors was reduced to 4: *PreopRisk*, *ArrhyDuration*, *PAARate*, *LPAAFraction*. Because the samples were constructed from a set where the number of intervals coming from Non-AF patients was twice that of AF patients, *PreopRisk* was still selected. Nevertheless, because AF patients intervals of the first hour classified as 0, the selection of the predictors was biased toward those having not only group difference (AF vs. Non-AF), but also significant time effect.

Model III and Model IV were constructed as alternative to highlight the variables with time-dependant changes in the AF group. Many new variables were selected as predictors. The stable ones of both models were *PreopRisk*, *LPAARate*, *ArrhyDuration*, *PAARate*, *pNN50*, *rMSSD*, *LFPortion*, *CTAVMean*, *CTA*, *CorrAA_AV*, *CorrAA_CTA*, *CorrAV_CTA*. Among those predictors, some were reflecting the group differences, but many were linked to change occurring before onset of AF. Compared to Model 0, I, and II, the last two models were more complicated. All the predictors appearing in two or more models showed identical function, either proarrhythmic or protective.

In order to compare the prediction performance of five modeling methods, the stable predictors and the mean β values of the stable predictors were employed to build the prediction model. The mean β values were calculated as the same way as in Model 0 analysis in section 5.2.1. The prediction indices were evaluated by the prediction model running over the complete data set. Table 5.6 shows the comparison of the prediction performance of the five models. The five models had similar sensitivity, specificity, and ROC curve area, but Model III provided the poorest performance for all the three indices.

The Sensitivity and specificity measured the classification of the time intervals, irrespective of which group the patients came from. We introduced an alternative index, prediction accuracy, pertaining to the discrimination of the patients, which brings a more appropriate measure of the performance from the monitoring point of view. It was calculated by assuming that a patient became classified as AF as soon as a first time intervals was classified as such. Model 0 to Model IV all achieved 100% accuracy for AF patients, whereas the accuracy for Non-AF patients always remained around 40%, a bad performance of prediction for Non-AF patients.

Table 5. 6 The mean value of beta coefficients of stable predictors of Model 0,I,II,III,IV

	Model 0	Model I	Model II	Model III	Model IV
PreopRisk	3.2456	3.2259	1.7693	3.3663	3.4492
PAARate	0.20138	0.19586	0.087225	0.18203	0.17814
LPAARate	0.024412			0.014696	0.012062
ArrhyDuration			0.25511	0.15763	0.1885
LPAAFraction	1.9328	1.9239	1.5909	1.9343	
AA					-0.0029401
pNN50	-16.1096	-16.388		-20.7817	-17.9611
rMSSD				0.033205	0.043766
LFPortion		-2.4539		-1.5424	-1.2832
CTAVMean	0.013489	0.013127		0.01012	0.01035
CTAVStd				0.044525	0.040076
CTA				0.011708	0.01376
CorrAA_AV	-1.3072	-1.3066		-0.85636	-0.58995
CorrAA_CTA				-0.36647	-0.33485
CorrAV_CTA		-0.76795		-0.58638	-0.44437
Constant	-5.1238	-4.6291	-3.8176	-4.3322	

Table 5. 7 Indices of five models (excluding the missing value periods, and missing value patients)

	Sensitivity	Specificity	ROC	AF Accuracy	Non-AF Accuracy
Model 0	77.54%	72.58%	0.8193	100%	41.38%
Model I	75.15%	75.18%	0.8158	100%	41.38%
Model II	72.89%	72.13%	0.7766	100%	36.21%
Model III	79.04%	71.28%	0.8363	100%	39.66%
Model IV	79.64%	70.13%	0.8337	100%	39.66%

5. 3 WMAM (Weighted Moving Average Method) For Model Prediction Improvement and Monitoring

The reason for the low Non-AF patient prediction accuracy was that there were many sparse, isolated alarms. It was hypothesized that a weighted moving average method (WMAM) could improve the accuracy for Non-AF prediction. We consider a WMAM model in which the final score was a function of the current and two previous time intervals. To the select the weights ($[\beta(i) \quad \beta(i-1) \quad \beta(i-2)]$), the method of the odds ratio maximization of in logistic regression, gave us the way to calculate a set of optimal weights of WMAM method. First, the score of each time interval was computed from each prediction model. Then, logistic regression was run, using the scores of the current and two previous intervals as independent variables. The dependant variable was set to 0 or 1 depending on the time interval of Non-AF or AF patients, i.e., all the time interval status of each AF were set as 1, and those of Non-AF were set as 0. The normalized beta

values (i.e., $\beta(j)/\min(\{\beta(i),\beta(i-1),\beta(i+1)\}$ and then rounded to nearest tenth decimal values) obtained for each model for 10min BTI data are given in Table 5.8.

Table 5. 8 Normalized beta coefficients obtained by logistic regression

	β (i)	β (i-1)	β (i-2)
Model 0	3	0	1
Model I	2.5	1	1
Model II	4	2	1
Model III	2.2	1	1
Model IV	2.6	1	1

To simplify the calculation, the final score assigned to each interval was calculated as:

$$Final\_Score(i) = \frac{\beta(i) * score(i) + \beta(i-1) * score(i-1) + \beta(i-2) * score(i-2)}{\beta(i) + \beta(i-1) + \beta(i-2)} \qquad (5.1)$$

, which corresponds to the logarithm of the odds ratio divided by the sum of the beta.

As in the previous section, the prediction accuracy of AF and Non-AF was calculated by assuming that a patient was classified as AF as soon as the score of one interval was above the threshold. The evolutions of the accuracy vs. cut-off point value are shown in Figure 5.19. These curves were turned to ROC curves by plotting the accuracy of AF vs. 1- accuracy of Non-AF. The rule of ROC analysis was then be used to select optimal thresholds, which are plotted as magenta dots in Figure 5.19. However, the slope of the curves around the operation point, which measures the dependability of the prediction as a function of the threshold, should also be minimal. As seen in Figure 5.19, Model II would be rejected in the light of this criterion.

Figure 5.20 shows the classification provided for each patient and each time interval using the optimal ROC threshold for each model (panels A, B, C, D, E corresponding to Model 0, I, II, III, IV, respectively). The ordinate is the time from 100 minutes to the

onset of AF, or the corresponding monitoring time Non-AF. The abscissa is the patients ID (1-29, AF; 30-87, Non-AF). The correctness of the prediction is indicated by a color code: red, true positive (i.e. interval from AF patient classified as AF); green: false negative; white, true negative; magenta, false positive; black, missing independent variables because of insufficient sinus beats.

The temporal evolution of the accuracy of AF and Non-AF are shown in Figure 5.20. Ideally, the Non-AF accuracy should remain relatively high and constant, while the AF accuracy should increase as the onset of arrhythmia get closer, but reach a high level soon enough to allow a prophylactic intervention. Taking into account the stability of the accuracy vs. the value of threshold (robustness of the model), the high value requirement of prediction accuracy for both AF and Non-AF patients, as well as the simplicity of the model (the less number of predictors, the better under the same performance circumstances), Model 0 and Model I appeared as the two best choices. Model II, III and Model IV were discarded because either they were too sensitive to the cut-off point, or had lower AF accuracy or were too complicated. One hour before the end of monitoring, around 70% Non-AF patients were correctly classified by Model 0 and I, while around 75% of AF patients were correctly predicted.

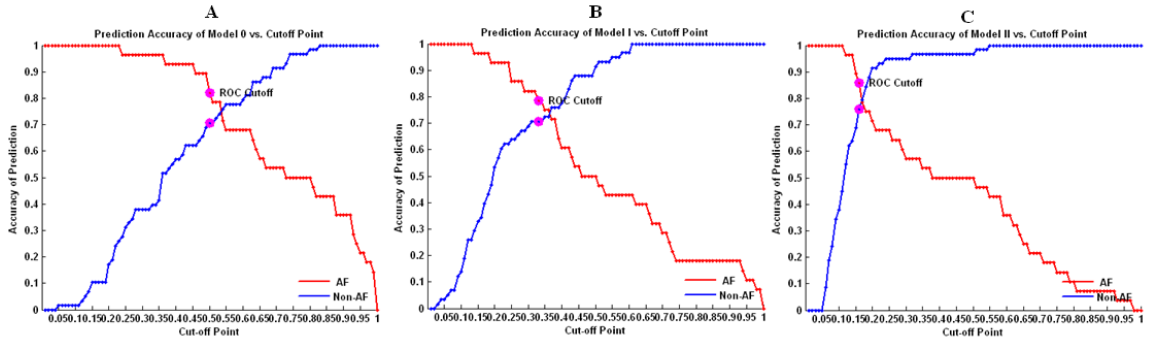

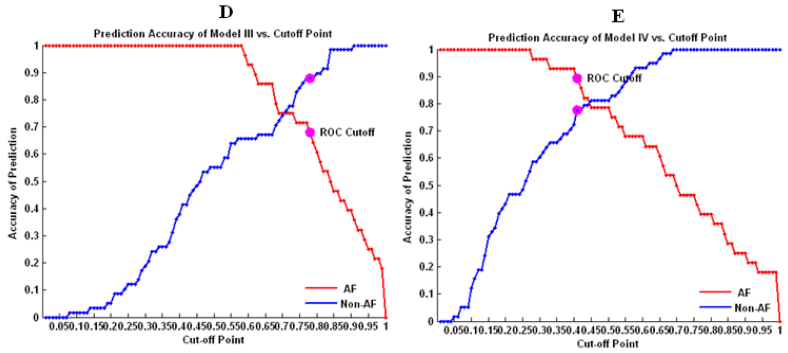

Figure 5.19 Prediction accuracy of AF and Non-AF vs. cut-off point. The magenta points are the optimal ROC cut-off points and their corresponding prediction accuracy values.

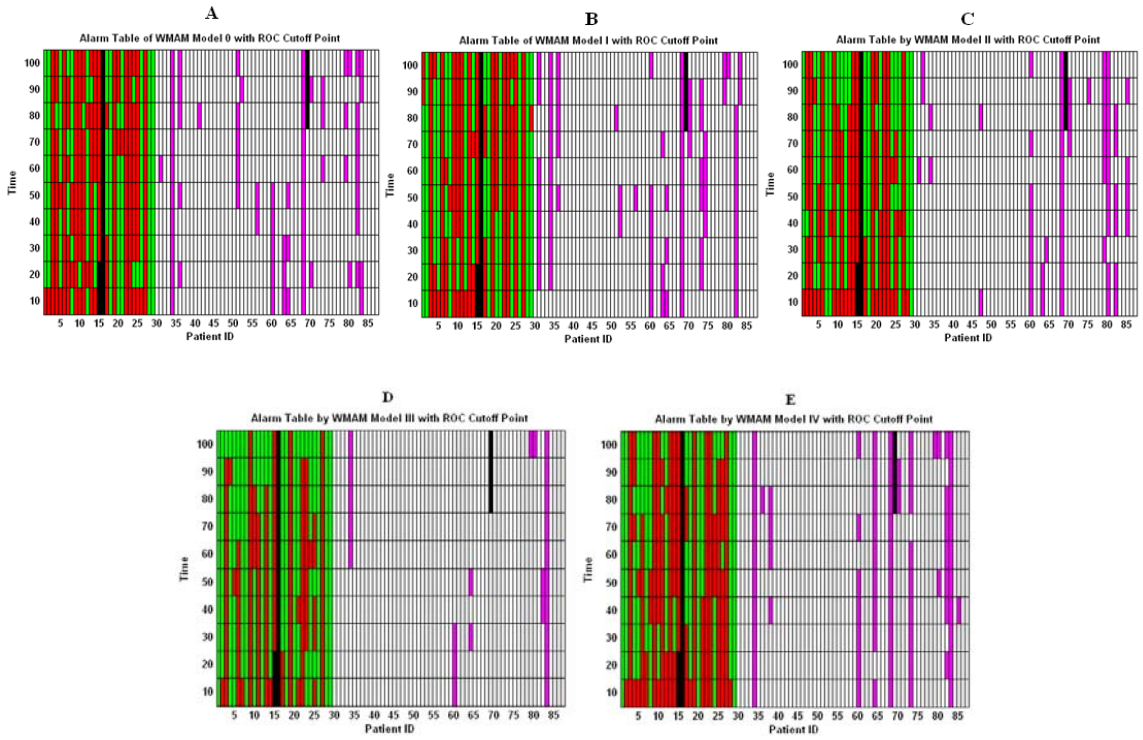

Figure 5.20 Classification of each time interval for Model 0, I, II, III, IV, (A to E) using the optimal threshold shown in Figure 5.19. The ordinate is the time from 100 minutes to the onset of AF, or corresponding monitoring time for Non-AF. The abscissa is the patients ID (1-29, AF; 30-87, Non-AF). Color code: red, true positive; green: false negative; white, true negative; magenta, false positive; black, missing independent variables because of insufficient sinus beats.

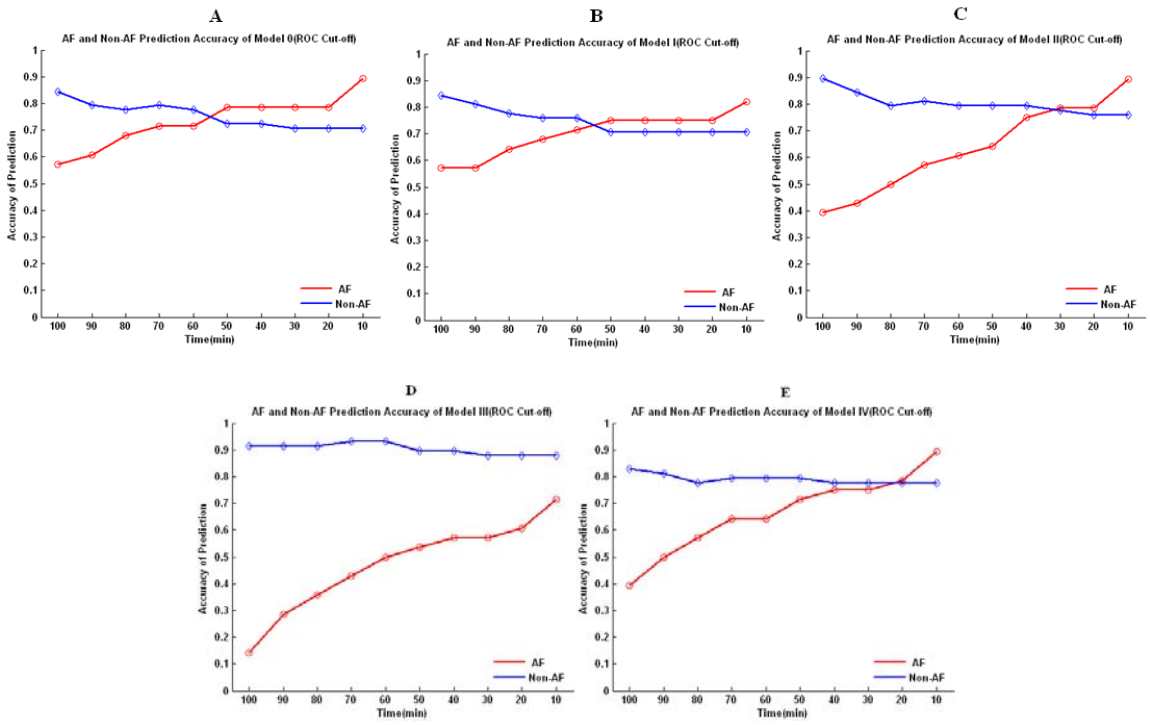

Figure 5.21 Prediction accuracy of AF and Non-AF prediction over the time based on ROC threshold for Model 0, I, II, III and IV. The abscissa is the time before the onset of AF, or the corresponding monitoring time for Non-AF. The ordinate is prediction accuracy for AF (red) and Non-AF (blue).

5.4 Discussion

In this chapter, different weighted and unweighted methods were used to construct logistic regression models. A final WMAM logistic regression approach, combining the scores of neighbouring time intervals, was used to improve the accuracy of the prediction. In contrast with the position data used in Chapter 3, raw data and relative difference variables were considered in the analysis. In chapter 3, there was a triggering PAA and a triggering time period for each AF patient. Position data strengthened the differences between the trigger PAA or time period and the others within each patient, irrespective of the amplitude of these differences. In the modeling process, the dependant

variable of the trigger PAA/Time period was assigned the value 1, and all others a value 0. However, the calculation of position data was based on the distribution of data over the complete monitoring interval, which makes this method inapplicable in a context of monitoring. As an alternative, we used the normalized data in which all differences were expressed relative to an initial reference period. Result of the logistic and cumulative logistic regressions with normalized data were not reported because it did not help to improve the discrimination between AF and Non- patients. The specificity and sensitivity of the models were either too poor, or too complex including as much as 20 variables.

Five methods were investigated, differing by the weights allocated either to AF and Non-AF patients or to the different time intervals for AF patients. In all instances, the preoperative risk was a significant predictor. The preoperative risk, specified by the patient age, previous infarct, and serum creatinine, has a long term impact on the occurrence of postoperative AF, a point on which there is no dispute [74, 97, 100, 207, 214-216].

Bootstrapping was used to evaluate the stability of the predictors. Predictors were considered as stable if there were appearing in a large fraction of the samples, herein 70% for the larger sampling rate. This was done to alleviate the limitation coming from the smallness of the database and provide robustness to the final model since it became relatively insensitive to the choice of subsets of observations. A second measure of robustness, which was considered for the final WMAM models, was the slope of the accuracy around the optimal threshold. A robust model should maintain a high and stable AF and Non-AF prediction accuracy for some range of threshold around the optimal choice. Besides being robust and accurate, a good model should also include a minimal number of significant predictors.

Among the five models, Model 0 and Model I were best in fulfilling the three criteria. Besides the preoperative risk score, their common predictors were *PAARate*, *LPAAFraction*, *pNN50, CTAVMean*, *CorrAA_AV*. *LFPortion,* was in Model I only, but was also appearing in Model 0 when it was run over the complete set of patients. It will

nevertheless be discussed because its importance in the analysis of AF patients in Chapter 3.

Before trying to infer what each predictor might mean in term of physiological difference between AF and Non-AF patients, it must be remind it would be misleading to consider that all predictors contributed equally among the patients and that the difference between AF patients from Non-AF patients is homogeneous. As shown in the cluster analyses of Chapter 3, specific changes were usually restricted to distinct and restricted subsets of AF patients, and different predictors were found to reflect the changes before the onset of AF. Thereby, many variables ended up being included in the logistic regression model. Relating the changes indicated by the different predictors to all patients might lead to controversial arguments. Therefore, the following attempt to explain the mechanism of change between AF and Non-AF associated to each predictor can only applicable to a subset of patients.

Two of these predictors were related *PAA*: *PAARate*, *LPAAFraction*. Repetitive measure ANOVA analysis showed that *PAARate* had significant group effect as well as a time effect restricted to the AF group. Since the analysis of Chapter 3 found that *LPAA* were more prone to initiate AF, it was not surprising that *LPAAFraction* appeared as a predictor.

pNN50 is the ratio of the number of consecutive sinus beats with *AA* >50ms to the total number of sinus beats in five minutes intervals. The concept was first proposed by Ewing to study the neural autonomic balance from ECG recordings [217, 218]. Mietus et al. also proposed that enhanced discrimination between a variety of normal and pathological conditions could be obtained by using various *pNN* thresholds. In their study, there found higher *pNN50* in healthy control versus congestive heart failure patients, healthy young subjects versus healthy old subjects [219]. In our study, lower *pNN50* appeared to increase the risk in a subset of patients to develop AF, which is consistent with their results. Vikman et al. also proposed that decreased complexity of sinus beats interval dynamics played the role of marker of both altered regulation of sinus node behavior and

an increased possibility of atrial firing from a single ectopic focus before the spontaneous onset of AF, which together predispose the spontaneous onset of AF [201]. Ewing et al. proposed *pNN50* to be more likely a measure cardiac vagal integrity and that lower *pNN50* in patients with altered hearts came from parasympathetic damages [218]. According to this point of view, lower *pNN50* in AF patients, associated to parasympathetic tone withdraw, should lead to an increase of the *LFPortion*. However, this would contradict the observation that AF group had a lower *LFPortion* than Non-AF group. In fact, there was no strong correlation between *pNN50* and *LFPortion* in the AF group, thereby explaining why the two variables might be included in the model. Herein, we can only conclude that low *pNN50*, which occurred in a subset of AF patients, could be related to impaired neural autonomic interaction, especially low level of parasympathetic tone.

In the models, the heart rate variability was not a significant predictor to differentiate AF from Non-AF patients although a subset of AF patients showed brief periods of sudden changes in heart rate variability, which possibly reflected transient fluctuations of the autonomic control. These abrupt changes might make the substrate more prone to develop atrial fibrillation, primarily in individuals predisposed to arrhythmia by virtue of preoperative factors and frequent PAA.

In Chapter 3, the results showed an increase of *LFPortion* before the AF onset in a subgroup of patient, suggesting in these an increased of the sympathetic tone fluctuation. In this chapter, Figure 5.11 showed *LFPortion* to be slightly lower in AF group except for the last five minutes. Even though this difference came from a subset of patient as mentioned in Section 5.2.1, high *LFPortion* appeared as a stable, protective predictor in Model I, II, III, and IV. The two results seemed contradictory. This might be explained as follows: There was indeed an increase of the *LFPortion* in a subset of patients close to the onset of AF, but globally, its mean value over the two hours remains higher in the Non-AF group. It should be mentioned that, because the onset of AF is often preceded by PAA and transient episodes of arrhythmia, the FFT spectrum calculation, which relies on

deletion of PAA and arrhythmia and interpolation, may enhance the low frequency portion of the spectrum.

Longer *CTAVMean* appeared as a risk factor in both Model 0 and I. *CTAV* is known to be modulated by cardiac autonomic nervous and to be related to the electrophysiological properties of the AV conduction pathways [220-226]. The cardiac autonomic nervous system simultaneously regulates SA and AV node. Indirectly, the change of the heart rate also influenced the variability of AV conduction time [227-230]. Increased parasympathetic tone or decreased sympathetic tone usually leads to an augmentation of the AV conduction time. Besides, an increase of the inhomogenity of action potential propagation would also prolong the AV conduction time. Reduced coronary blood flow can result in a prolongation of the myocytes action potential [231] and to impaired propagation of the sinus impulses through the atria and the auriculo-ventricular conduction system [232, 233] . Therefore, longer *CTAVMean* may results from structural difference, lower sympathetic (or higher parasympathetic) tone or perfusion defect.

Many studies on ECG proposed that a prolonged signal-averaged P-wave duration has been shown to be an independent predictor of AF after cardiac surgery [24, 234, 235]. However, Amar did not find P wave duration time to discriminate between AF and Non-AF patients [236]. We found *CTA* to be longer in the AF group (mean, AF: 56.5 msec., Non-AF: 52.65 msec.). However, the difference was not large enough to be significant upon repeated measures ANOVA, as well as univariate or multivariate logistic regression. Detailed analysis showed that the longer *CTA* for AF patients was caused by only a subset and lead to a higher group mean value. Some studies proposed that the P wave dispersion was predictor to AF patients [30, 32, 237, 238]. As for *CTA*, we found a slightly larger CTA standard deviation in the AF groups, which was not large enough to become significant in any of the analyses.

The correlation between the *AA* (sinus beat interval) and *CTAV* (atrio-ventricular conduction time), was found to be a predictor, with slightly more negative value in the AF (mean: -.082 vs. -.021). This correlation translates the rhythm dependence of the

atrio-ventricular conduction time, which was more important in a subset of AF patients. If the change of atrial rhythm depends mainly on neural inputs, then their concordant influence on both *AA* and *CTAV* (i.e. either should be reduced or increased together) acts to erase the negative rhythm dependant correlation. This suggests that an imbalance between the neural input to the atrial and atrio-ventricular node might exist is some AF patients.

Above all, the mechanisms leading to post-CABG AF appears to be very complex, with contribution of different interacting physiological factors. Our study suggests that patients developing AF may have a vulnerable substrate, which might result from different factors such as age or prior structural heart diseases. The conduction property of atrium tissue is widely influenced by the autonomic neural balance and heart rate variability can reflect the autonomic modulation. This modulation may create a more vulnerable substrate. The trigger of AF is a premature atrial activation, but its ability to initiate an AF depends on the vulnerability of the atrial substrate.

5.5 Summary

1. Five models were proposed to discriminate AF from Non-AF patients. The choice of predictors and the values of their coefficients for score computation were made using a bootstrap method to enhance the robustness of the models. They had similar sensitivity, specificity, and ROC curve area, while with a poor performance for Non-AF patients;
2. The Accuracy of Non-AF prediction was improved by a moving average extension of these models. Two models were selected, based on the stability of accuracy with respect to change in threshold;
3. The common predictors of the two best models were *Preoprisk, PAARate*, *LPAAFraction*, *pNN50, CTAVMean* and *CorrAA_AV*;

4. There was no correlation between *Preoprisk* and *PAARate*. High *PAARate* and *LPAAFraction* were both predictors of AF group despite their wide distributions among both Non-AF and AF patients;
5. Reduced *pNN50* and more negative *CorrAA_AV* were AF risk factor, both suggesting reduced autonomic tone;
6. Longer *CTAVMean* was also a risk factor, which could be linked to depressed or inhomogeneous substratum for conduction.

Chapter 6 Originality, Limitation and Future Development of the Study

6.1 Originality of the Study

Using three-channel AEG instead of the standard Holter ECG recordings can provide information that are difficult or even impossible to obtain from the latter, such as the origin of premature atrial activation (*LPAA* or *RPAA*), the precise duration of atrial arrhythmias, the local coupling time between atrial activations or their local derivatives. However, it has necessitated the development of a new timing algorithm that proved to be reliable and effective. The adaptive filtering of the signals and adjustment of the detection threshold, the utilization of global and individual channel pseudo- energy, as well the A-V distinction based on dual band pass filtering are the most innovative aspect of the method. The reliable detection and discrimination of atrial and ventricular activations is a problem that also come up with the sensing electrode of devices such as pacemaker and implantable defibrillator, for which the algorithm could be eventually adapted. The project also required the development of validation software to validate markers, as well as to define and validate beats. It encompasses different options available in commercial software such as Burdick Vision Premier, and Spike, and brings some innovative ideas, for instance the classification module, the modification and suspicious detection showing, or the find module which make the software very convenient in doing validation. This software system is already used for other projects in our laboratory.

The analysis proceeds in three steps: 1) preoperative discrimination of AF and Non-AF patients; 2) temporal evolution in AF patient and discrimination of trigger versus non-trigger PAA; 3) discrimination of AF and Non-AF patients AF using preoperative risk and the different time series.

1. Preoperative risk factors

The preoperative risk score could to a certain extent predict who will get AF, but was not predictive on the time when AF occurred. Age appeared as the main preoperative predictor, complemented by the level of serum creatinine and prior myocardial infarct. Creatinine improved the female specificity and the male sensitivity, while the history of myocardial infarct mainly impacted the female specificity.

2. Analysis of AF patients

Position data, whereby data were normalized with respect the distribution within each patient, were more effective in discriminating both the time interval closest to the AF and the triggering PAA. AF was always immediately preceded by a PAA mainly originating from the left Atrium. However, the number of PAA and the fraction of LPAA among the patients were very inhomogeneous, LPAA being more prone to elicit the arrhythmia than RPAA. The time interval close to AF was characterized by increased transient arrhythmias, PAA rate, sinus heart rate and LF portion of heart rate variability. However, these changes were not homogeneous in the AF population, each occurring in a subset of the patients as illustrated by cluster analysis. Trigger PAAs were characterized by shorter prematurity, depressed Dvdt and the higher incidence of non-sustained arrhythmias in the few minutes before the trigger PAA.

3. Comparison of AF and non-AF patients

Five logistic regression models to discriminate AF from Non-AF patients were compared, differing in the weights given either to AF and Non-AF patients or to the different time intervals before the AF onset. A bootstrap method was used to identify the more stable predictors, and a moving average formulation was introduced to improve the accuracy of the discrimination. Two models were finally selected, based on the criteria of robustness, accuracy, and practicability. In these, around 70% Non-AF and 75% of AF patients were correctly classified in the last hour before AF. The common AF predictors of these

models were increased *PAA* rate and fraction of *PAA* initiated in the left atrium, lower *pNN50* and correlation of atrio-ventricular conduction time vs. AA, as well as prolonged of atrio-ventricular conduction time.

6.2 Study Limitation

Ideally, the development of the logistic regression models should have been as that of the timing algorithm: choice of variable and parameter determination through a test set of data, assessment an independent validation set. However, the limited number of available patients precludes from using this procedure. Bootstrapping was used to somewhat get around this shortcoming, but the pitfall of over-fitting still remains. We consider that results are fairly indicative of the characteristics of AF and Non-AF patients, but the accuracy of the model should still be tested on a larger and different population.

The building of the model was based on off-line validated data. Validated data would obviously not be available for online monitoring. Therefore, the robustness to noise and false detection still needed to be tested.

6.3 Future Development

The construction of the prediction model was based on multiple time series extracted from the AEG. However, it is possible that other variables that can be computed from AEG could improve the accuracy. One interesting variable, which has been proposed Pagé et al., is that the integral surface subtended by unipolar atrial waveform. [143, 239]. It was used as a measure of neural modification of action potential duration in canine preparation. In these studies, the dogs were in atrio-ventricular block, such the ventricular activation was not interfering with the atrial signal. In patients, the atrial repolarization is at least partially masked by the ventricular activation. When part of the atrial repolarization is available, as in Figure 6.1, the area could still bring relevant information about local neural input, particularly for site close the origin of PAA. It could be also

interesting to investigate if a method could be devised to restitute the complete atrial repolarization, as it was done for ECG T-wave in a context of atrial flutter [240].

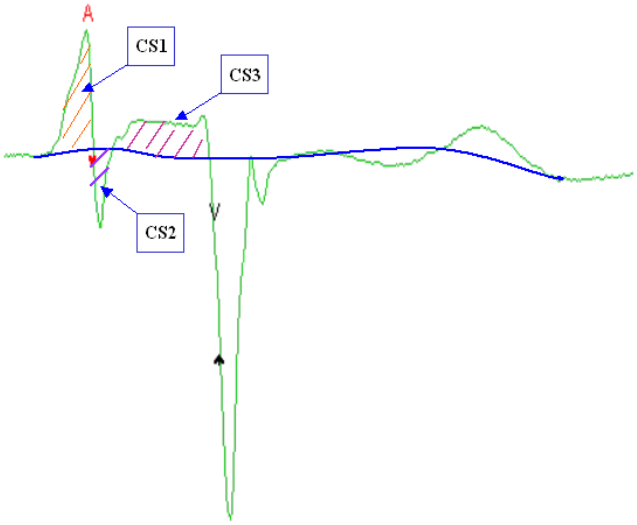

Figure 6.1 Activation integral surfaces of wave

Other variables might also be considered, such as fractal dimension that measures the heart rate complexity and for which patients with various cardiac pathology has been shown to differ from normal subjects [136]. Moreover, other time series could also bring significant contribution. Our guess is that the monitoring of the pressure could be particularly useful, particularly in association with heart rhythm. In some case, fluctuations of the hearth rhythm could be a response to vascular events that must certainly occur after an open-heart surgery.

Finally, a moving average version of the logistic regression model was introduced to take into account with the temporal evolution of the AF vs. Non-AF discrimination. Other methods, such as Bayesian survival analysis could offer interesting alternative [241]. In fact static Bayesian network has been used in the context of beat classification and fibrillation [242-245] . Adapting this algorithm for time changing prediction could be interesting.

Reference:

[1] L. H. Opie, Ed., *Heart Physiology: From Cell to Circulation*. Lippincott Williams & Wilkins, 2004.

[2] M. N. L. Robert M. Berne, Ed., *Cardiovascular Physiology*. Mosby Inc., 2001.

[3] G. K. Moe and J. A. Abildskov, "Atrial fibrillation as a self-sustaining arrhythmia independent of focal discharge," *Am Heart J,* vol. 58, pp. 59-70, Jul 1959.

[4] M. J. Davies and A. Pomerance, "Pathology of atrial fibrillation in man," *Br Heart J,* vol. 34, pp. 520-5, May 1972.

[5] S. Nattel, "From guidelines to bench: implications of unresolved clinical issues for basic investigations of atrial fibrillation mechanisms," *Can J Cardiol,* vol. 27, pp. 19-26, Jan-Feb 2011.

[6] E. J. Benjamin*, et al.*, "Impact of atrial fibrillation on the risk of death: the Framingham Heart Study," *Circulation,* vol. 98, pp. 946-52, Sep 8 1998.

[7] S. Nattel*, et al.*, "Basic mechanisms of atrial fibrillation--very new insights into very old ideas," *Annu Rev Physiol,* vol. 62, pp. 51-77, 2000.

[8] G. H. Sohn*, et al.*, "The incidence and predictors of postoperative atrial fibrillation after noncardiothoracic surgery," *Korean Circ J,* vol. 39, pp. 100-4, Mar 2009.

[9] J. K. Ryu, "Postoperative atrial fibrillation after noncardiothoracic surgery: is it different from after cardiothoracic surgery?," *Korean Circ J,* vol. 39, pp. 93-4, Mar 2009.

[10] P. Rossi*, et al.*, "Post-operative atrial fibrillation management by selective epicardial vagal fat pad stimulation," *Journal of Interventional Cardiac Electrophysiology,* vol. 24, pp. 37-45, 2009.

[11] K. Jongnarangsin and H. Oral, "Postoperative atrial fibrillation," *Cardiol Clin,* vol. 27, pp. 69-78, viii, Feb 2009.

[12] S. B, "Decling CABG rate means fewer jobs for surgeons," *Canadian Medical Association Journal,* vol. 173, p. 2, Sep 13 2005.

[13] N. Echahidi*, et al.*, "Obesity and metabolic syndrome are independent risk factors for atrial fibrillation after coronary artery bypass graft surgery," *Circulation,* vol. 116, pp. I213-9, Sep 11 2007.

[14] L. L. Creswell and R. J. Damiano, Jr., "Postoperative atrial fibrillation: an old problem crying for new solutions," *J Thorac Cardiovasc Surg,* vol. 121, pp. 638-41, Apr 2001.

[15] T. Hakala*, et al.*, "Prediction of atrial fibrillation after coronary artery bypass grafting by measuring atrial peptide levels and preoperative atrial dimensions," *Eur J Cardiothorac Surg,* vol. 22, pp. 939-43, Dec 2002.

[16] G. Filardo*, et al.*, "New-onset postoperative atrial fibrillation and long-term survival after aortic valve replacement surgery," *Ann Thorac Surg,* vol. 90, pp. 474-9, 2010 2010.

[17] M. F. El-Chami, *et al.*, "New-onset atrial fibrillation predicts long-term mortality after coronary artery bypass graft," *J Am Coll Cardiol,* vol. 55, pp. 1370-6, 2010 Mar 2010.
[18] A. E. Contreras, *et al.*, "Atrial fibrillation in postoperative cardiac surgery. Prevalence and hospitalized period.," *Medicina (B Aires),* vol. 70, pp. 339-42, 2010 2010.
[19] S. Bramer, *et al.*, "The Impact of New-Onset Postoperative Atrial Fibrillation on Mortality After Coronary Artery Bypass Grafting," *Annals of Thoracic Surgery,* vol. 90, pp. 443-450, 2010.
[20] C. W. Hogue, Jr., *et al.*, "Epidemiology, mechanisms, and risks: American College of Chest Physicians guidelines for the prevention and management of postoperative atrial fibrillation after cardiac surgery," *Chest,* vol. 128, pp. 9S-16S, Aug 2005.
[21] W. H. Maisel, *et al.*, "Atrial fibrillation after cardiac surgery," *Ann Intern Med,* vol. 135, pp. 1061-73, Dec 18 2001.
[22] P. L. Page and J. Pym, "Atrial fibrillation following cardiac surgery," *Can J Cardiol,* vol. 12 Suppl A, pp. 40A-44A, Jan 1996.
[23] P. Comtois, *et al.*, "Mechanisms of atrial fibrillation termination by rapidly unbinding Na+ channel blockers: insights from mathematical models and experimental correlates," *Am J Physiol Heart Circ Physiol,* vol. 295, pp. H1489-504, Oct 2008.
[24] S. Sovilj, *et al.*, "ECG-based prediction of atrial fibrillation development following coronary artery bypass grafting," *Physiol Meas,* vol. 31, pp. 663-77, 2010 May (Epub 2010 Mar 2010.
[25] F. Roshanali, *et al.*, "Prediction of atrial fibrillation via atrial electromechanical interval after coronary artery bypass grafting," *Circulation,* vol. 116, pp. 2012-7, 2007 Oct 30 (Epub 2007 Oct 2007.
[26] D. Kaireviciute, *et al.*, "Atrial fibrillation following cardiac surgery: clinical features and preventative strategies," *European Heart Journal,* vol. 30, pp. 410-425, 2009.
[27] T. Acil, *et al.*, "Value of preoperative echocardiography in the prediction of postoperative atrial fibrillation following isolated coronary artery bypass grafting," *Am J Cardiol,* vol. 100, pp. 1383-6, Nov 1 2007.
[28] P. J. Stafford, *et al.*, "Signal averaged P wave compared with standard electrocardiography or echocardiography for prediction of atrial fibrillation after coronary bypass grafting," *Heart,* vol. 77, pp. 417-22, May 1997.
[29] J. R. Ehrlich, *et al.*, "Prediction of early recurrence of atrial fibrillation after external cardioversion by means of P wave signal-averaged electrocardiogram," *Z Kardiol,* vol. 92, pp. 540-6, Jul 2003.
[30] C. M. Chang, *et al.*, "The role of P wave in prediction of atrial fibrillation after coronary artery surgery," *Int J Cardiol,* vol. 68, pp. 303-8, Mar 15 1999.
[31] V. Vassilikos, *et al.*, "Novel non-invasive P wave analysis for the prediction of paroxysmal atrial fibrillation recurrences in patients without structural heart disease A prospective pilot study," *Int J Cardiol,* Sep 11 2010.

[32] O. Ceylan*, et al.*, "[Value of interatrial conduction time and P wave dispersion in the prediction of atrial fibrillation following coronary bypass surgery]," *Anadolu Kardiyol Derg,* vol. 10, pp. 495-501, Dec 2010.
[33] D. Amar*, et al.*, "Competing autonomic mechanisms precede the onset of postoperative atrial fibrillation," *J Am Coll Cardiol,* vol. 42, pp. 1262-8, Oct 1 2003.
[34] P. Comtois and S. Nattel, "Impact of tissue geometry on simulated cholinergic atrial fibrillation: a modeling study," *Chaos,* vol. 21, p. 013108, Mar 2011.
[35] D. Chamchad*, et al.*, "Nonlinear heart rate variability analysis may predict atrial fibrillation after coronary artery bypass grafting," *Anesth Analg,* vol. 103, pp. 1109-12, Nov 2006.
[36] T. Raman*, et al.*, "Preoperative left atrial dysfunction and risk of postoperative atrial fibrillation complicating thoracic surgery," *J Thorac Cardiovasc Surg,* Sep 26 2011.
[37] L. W. Lo*, et al.*, "Neural mechanism of atrial fibrillation: insight from global high density frequency mapping," *J Cardiovasc Electrophysiol,* vol. 22, pp. 1049-56, Sep 2011.
[38] D. C. Shah*, et al.*, "Toward a mechanism-based understanding of atrial fibrillation," *J Cardiovasc Electrophysiol,* vol. 12, pp. 600-1, May 2001.
[39] M. S. Spach, "Mounting evidence that fibrosis generates a major mechanism for atrial fibrillation," *Circ Res,* vol. 101, pp. 743-5, Oct 12 2007.
[40] O. Berenfeld, "Ionic and substrate mechanism of atrial fibrillation: rotors and the exitacion frequency approach," *Arch Cardiol Mex,* vol. 80, pp. 301-314, oct-dec 2010.
[41] H. Oral, "Post-operative atrial fibrillation and oxidative stress: a novel causal mechanism or another biochemical epiphenomenon?," *J Am Coll Cardiol,* vol. 51, pp. 75-6, Jan 1 2008.
[42] L. L. Mackstaller and J. S. Alpert, "Atrial fibrillation: a review of mechanism, etiology, and therapy," *Clin Cardiol,* vol. 20, pp. 640-50, Jul 1997.
[43] S. B. Olsson, "Atrial fibrillation--new aspects on mechanism and treatment," *J Intern Med,* vol. 239, pp. 3-15, Jan 1996.
[44] J. Jalife*, et al.*, "Mother rotors and fibrillatory conduction: a mechanism of atrial fibrillation," *Cardiovasc Res,* vol. 54, pp. 204-16, May 2002.
[45] G. R. Mines, "On dynamic equilibrium in the heart," *J Physiol,* vol. 46, pp. 349-83, Jul 18 1913.
[46] W. E. Garrey, "The nature of fibrillary contraction of the heart.—Its relation to tissue mass and form," *Am. J. Physiol.,* p. 18, 1914.
[47] W. E. Garrey, "Auricular fibrillation," *Physiol. Rev.,* pp. 215-50, 1924.
[48] M. J. Janse, "Focus, reentry, or "focal" reentry?," *Am J Physiol Heart Circ Physiol,* vol. 292, pp. H2561-2, Jun 2007.
[49] G. K. Moe*, et al.*, "A Computer Model of Atrial Fibrillation," *Am Heart J,* vol. 67, pp. 200-20, Feb 1964.
[50] M. A. Allessie*, et al.*, "Circus movement in rabbit atrial muscle as a mechanism of tachycardia. III. The "leading circle" concept: a new model of circus movement in cardiac tissue without the involvement of an anatomical obstacle," *Circ Res,* vol. 41, pp. 9-18, Jul 1977.

[51] A. T. Winfree, "Electrical turbulence in three-dimensional heart muscle," *Science,* vol. 266, pp. 1003-6, Nov 11 1994.
[52] V. Zykov, *Simulation of wave processes in excitable media*. Manchester: Manchester University Press, 1987.
[53] P. Comtois*, et al.*, "Of circles and spirals: bridging the gap between the leading circle and spiral wave concepts of cardiac reentry," *Europace,* vol. 7 Suppl 2, pp. 10-20, Sep 2005.
[54] V. A. Courtemanche M, *Nonlinear dynamics in medicine and physiology, Reentry in excitable media*: Springer-Verlag, 2003.
[55] J. L. Cox, "A perspective on postoperative atrial fibrillation," *Semin Thorac Cardiovasc Surg,* vol. 11, pp. 299-302, Oct 1999.
[56] J. L. Cox, "The role of surgical intervention in the management of atrial fibrillation," *Tex Heart Inst J,* vol. 31, pp. 257-65, 2004.
[57] A. Vinet, Ed., *Cardiac Electrophysiology: from Cell to Bedside, Non-linear Models of Propagation in Excitable Tissues*. Philadelphia: W.B Saunders, 1995, p.^pp. Pages.
[58] J. Han*, et al.*, "Temporal dispersion of recovery of excitability in atrium and ventricle as a function of heart rate," *Am Heart J,* vol. 71, pp. 481-7, Apr 1966.
[59] J. Han and G. K. Moe, "Nonuniform Recovery of Excitability in Ventricular Muscle," *Circ Res,* vol. 14, pp. 44-60, Jan 1964.
[60] J. Pellman*, et al.*, "Extracellular matrix remodeling in atrial fibrosis: mechanisms and implications in atrial fibrillation," *J Mol Cell Cardiol,* vol. 48, pp. 461-7, Mar 2010.
[61] A. Y. Tan and P. Zimetbaum, "Atrial Fibrillation and Atrial Fibrosis," *J Cardiovasc Pharmacol,* Dec 4 2010.
[62] L. Jideus*, et al.*, "The role of premature atrial contractions as the main triggers of postoperative atrial fibrillation," *J Electrocardiol,* vol. 39, pp. 48-54, Jan 2006.
[63] M. H. Hsieh*, et al.*, "Mechanism of spontaneous transition from typical atrial flutter to atrial fibrillation: role of ectopic atrial fibrillation foci," *Pacing Clin Electrophysiol,* vol. 24, pp. 46-52, Jan 2001.
[64] C. F. Tsai*, et al.*, "Initiation of atrial fibrillation by ectopic beats originating from the superior vena cava: electrophysiological characteristics and results of radiofrequency ablation," *Circulation,* vol. 102, pp. 67-74, Jul 4 2000.
[65] W. S. Lin*, et al.*, "Catheter ablation of paroxysmal atrial fibrillation initiated by non-pulmonary vein ectopy," *Circulation,* vol. 107, pp. 3176-83, Jul 1 2003.
[66] A. Vincenti*, et al.*, "Onset mechanism of paroxysmal atrial fibrillation detected by ambulatory Holter monitoring," *Europace,* vol. 8, pp. 204-10, Mar 2006.
[67] J. E. Olgin*, et al.*, "Heterogeneous atrial denervation creates substrate for sustained atrial fibrillation," *Circulation,* vol. 98, pp. 2608-14, Dec 8 1998.
[68] G. Katsouras*, et al.*, "Differences in atrial fibrillation properties under vagal nerve stimulation versus atrial tachycardia remodeling," *Heart Rhythm,* vol. 6, pp. 1465-72, Oct 2009.
[69] M. Oliveira*, et al.*, "Effects of vagal stimulation on induction and termination of atrial fibrillation in an in vivo rabbit heart model," *Rev Port Cardiol,* vol. 29, pp. 375-89, Mar 2010.

[70] J. Wang, *et al.*, "Regional and functional factors determining induction and maintenance of atrial fibrillation in dogs," *Am J Physiol,* vol. 271, pp. H148-58, Jul 1996.
[71] C. Dimmer, *et al.*, "Variations of autonomic tone preceding onset of atrial fibrillation after coronary artery bypass grafting," *Am J Cardiol,* vol. 82, pp. 22-5, Jul 1 1998.
[72] C. Dimmer, *et al.*, "Initiating mechanisms of paroxysmal atrial fibrillation," *Europace,* vol. 5, pp. 1-9, Jan 2003.
[73] Z. Lu, *et al.*, "Atrial fibrillation begets atrial fibrillation: autonomic mechanism for atrial electrical remodeling induced by short-term rapid atrial pacing," *Circ Arrhythm Electrophysiol,* vol. 1, pp. 184-92, Aug 2008.
[74] M. Budeus, *et al.*, "Prediction of atrial fibrillation after coronary artery bypass grafting: the role of chemoreflex-sensitivity and P wave signal averaged ECG," *Int J Cardiol,* vol. 106, pp. 67-74, Jan 4 2006.
[75] S. F. Aranki, *et al.*, "Predictors of atrial fibrillation after coronary artery surgery. Current trends and impact on hospital resources," *Circulation,* vol. 94, pp. 390-7, Aug 1 1996.
[76] C. W. Hogue, Jr. and M. L. Hyder, "Atrial fibrillation after cardiac operation: risks, mechanisms, and treatment," *Ann Thorac Surg,* vol. 69, pp. 300-6, Jan 2000.
[77] J. P. Mathew, *et al.*, "A multicenter risk index for atrial fibrillation after cardiac surgery," *JAMA,* vol. 291, pp. 1720-9, Apr 14 2004.
[78] C. T. Tran, *et al.*, "Atrial Na,K-ATPase increase and potassium dysregulation accentuate the risk of postoperative atrial fibrillation," *Cardiology,* vol. 114, pp. 1-7, 2009.
[79] R. G. Silva, *et al.*, "Risk factors, morbidity, and mortality associated with atrial fibrillation in the postoperative period of cardiac surgery," *Arq Bras Cardiol,* vol. 83, pp. 105-10; 99-104, Aug 2004.
[80] J. Auer, *et al.*, "Risk factors of postoperative atrial fibrillation after cardiac surgery," *J Card Surg,* vol. 20, pp. 425-31, Sep-Oct 2005.
[81] D. Amar, *et al.*, "Older age is the strongest predictor of postoperative atrial fibrillation," *Anesthesiology,* vol. 96, pp. 352-6, Feb 2002.
[82] A. Rybicka-Musialik, *et al.*, "Predictors of long-term outcome in patients with left ventricular dysfunction following coronary artery bypass grafting," *Kardiol Pol,* vol. 66, pp. 1260-6, Dec 2008.
[83] F. Bernet, *et al.*, "Impact of female gender on the early outcome in off-pump coronary artery bypass surgery," *Eur J Med Res,* vol. 11, pp. 114-8, Mar 27 2006.
[84] D. Kalavrouziotis, *et al.*, "The impact of new-onset atrial fibrillation on in-hospital mortality following cardiac surgery," *Chest,* vol. 131, pp. 833-9, 2007 2007.
[85] D. L. Reich, *et al.*, "Intraoperative tachycardia and hypertension are independently associated with adverse outcome in noncardiac surgery of long duration," *Anesth Analg,* vol. 95, pp. 273-7, table of contents, Aug 2002.
[86] G. H. Almassi, *et al.*, "Stroke in cardiac surgical patients: determinants and outcome," *Ann Thorac Surg,* vol. 68, pp. 391-7; discussion 397-8, Aug 1999.

[87] E. M. Mahoney, *et al.*, "Cost-effectiveness of targeting patients undergoing cardiac surgery for therapy with intravenous amiodarone to prevent atrial fibrillation," *J Am Coll Cardiol,* vol. 40, pp. 737-45, Aug 21 2002.
[88] L. A. Mendes, *et al.*, "Right coronary artery stenosis: an independent predictor of atrial fibrillation after coronary artery bypass surgery," *J Am Coll Cardiol,* vol. 25, pp. 198-202, Jan 1995.
[89] X. Sun, *et al.*, "Association of body mass index with new-onset atrial fibrillation after coronary artery bypass grafting operations," *Ann Thorac Surg,* vol. 91, pp. 1852-8, Jun 2011.
[90] M. A. Arias and J. Sanchez-Gila, "Obesity as a risk factor for developing postoperative atrial fibrillation," *Chest,* vol. 129, pp. 828; author reply 828-9, Mar 2006.
[91] J. Osorio, "Atrial fibrillation: Obesity increases risk of AF in women," *Nat Rev Cardiol,* vol. 7, p. 417, 2010.
[92] M. Banach, *et al.*, "Obesity and postoperative atrial fibrillation. Is there no connection? Comment on: Wanahita et al. "atrial fibrillation and obesity--results of a meta-analysis"," *Am Heart J,* vol. 156, p. e5, Jul 2008.
[93] M. A. Arias, *et al.*, "Postoperative atrial fibrillation and obesity," *Am J Cardiol,* vol. 97, pp. 1551-2, May 15 2006.
[94] H. Radmehr, *et al.*, "Relation between preoperative mild increased in serum creatinine level and early outcomes after coronary artery bypass grafting," *Acta Med Iran,* vol. 49, pp. 89-92, 2011.
[95] M. Najafi, *et al.*, "Is preoperative serum creatinine a reliable indicator of outcome in patients undergoing coronary artery bypass surgery?," *J Thorac Cardiovasc Surg,* vol. 137, pp. 304-8, Feb 2009.
[96] J. M. Leung, *et al.*, "Impairment of left atrial function predicts post-operative atrial fibrillation after coronary artery bypass graft surgery," *Eur Heart J,* vol. 25, pp. 1836-44, Oct 2004.
[97] M. Haghjoo, *et al.*, "Predictors of postoperative atrial fibrillation after coronary artery bypass graft surgery," *Indian Pacing Electrophysiol J,* vol. 8, pp. 94-101, 2008 Apr 2008.
[98] V. Ducceschi, *et al.*, "Perioperative clinical predictors of atrial fibrillation occurrence following coronary artery surgery," *Eur J Cardiothorac Surg,* vol. 16, pp. 435-9, Oct 1999.
[99] C. R. Asher, *et al.*, "Analysis of risk factors for development of atrial fibrillation early after cardiac valvular surgery," *Am J Cardiol,* vol. 82, pp. 892-5, Oct 1 1998.
[100] A. G. Zaman, *et al.*, "Atrial fibrillation after coronary artery bypass surgery: a model for preoperative risk stratification," *Circulation,* vol. 101, pp. 1403-8, Mar 28 2000.
[101] J. M. Kalman, *et al.*, "Atrial fibrillation after coronary artery bypass grafting is associated with sympathetic activation," *Ann Thorac Surg,* vol. 60, pp. 1709-15, Dec 1995.
[102] A. Valtola, *et al.*, "Does coronary artery bypass surgery affect metoprolol bioavailability," *Eur J Clin Pharmacol,* vol. 63, pp. 471-8, May 2007.

[103] R. J. Alves, *et al.*, "Prevention of atrial fibrillation with moderate doses of amiodarone in the postoperative period of cardiac surgery is safe and effective in patients with high risk for developing this arrhythmia," *Arq Bras Cardiol,* vol. 89, pp. 22-7, Jul 2007.
[104] D. Amar, *et al.*, "Clinical prediction rule for atrial fibrillation after coronary artery bypass grafting," *J Am Coll Cardiol,* vol. 44, pp. 1248-53, Sep 15 2004.
[105] S. Bramer, *et al.*, "New-Onset Postoperative Atrial Fibrillation Predicts Late Mortality After Mitral Valve Surgery," *Ann Thorac Surg,* Oct 4 2011.
[106] G. J. Murphy, *et al.*, "Operative factors that contribute to post-operative atrial fibrillation: insights from a prospective randomized trial," *Card Electrophysiol Rev,* vol. 7, pp. 136-9, 2003.
[107] A. E. Topal and M. N. Eren, "Predictors of atrial fibrillation occurrence after coronary artery bypass graft surgery," *Gen Thorac Cardiovasc Surg,* vol. 59, pp. 254-60, Apr 2011.
[108] J. P. Mathew, *et al.*, "Atrial fibrillation following coronary artery bypass graft surgery: predictors, outcomes, and resource utilization. MultiCenter Study of Perioperative Ischemia Research Group," *JAMA,* vol. 276, pp. 300-6, Jul 24-31 1996.
[109] V. Salaria, *et al.*, "Role of postoperative use of adrenergic drugs in occurrence of atrial fibrillation after cardiac surgery," *Clin Cardiol,* vol. 28, pp. 131-5, Mar 2005.
[110] E. V. Tselentakis, *et al.*, "Inflammation effects on the electrical properties of atrial tissue and inducibility of postoperative atrial fibrillation," *J Surg Res,* vol. 135, pp. 68-75, Sep 2006.
[111] A. Kourliouros, *et al.*, "Substrate modifications precede the development of atrial fibrillation after cardiac surgery: a proteomic study," *Ann Thorac Surg,* vol. 92, pp. 104-10, Jul 2011.
[112] M. Kestelli, *et al.*, "[The role of inflammation in atrial fibrillation/The comparison between the efficiency of different anti-arrhythmic agents in preventing postoperative atrial fibrillation after open-heart surgery]," *Anadolu Kardiyol Derg,* vol. 8, pp. 394; author reply 394-5, Oct 2008.
[113] R. B. Tang, *et al.*, "Inflammation and atrial fibrillation: is Chlamydia pneumoniae a candidate pathogen of atrial fibrillation?," *Med Hypotheses,* vol. 67, pp. 462-6, 2006.
[114] G. Lamm, *et al.*, "Postoperative white blood cell count predicts atrial fibrillation after cardiac surgery," *J Cardiothorac Vasc Anesth,* vol. 20, pp. 51-6, Feb 2006.
[115] I. Savelieva and J. Camm, "Statins and polyunsaturated fatty acids for treatment of atrial fibrillation," *Nat Clin Pract Cardiovasc Med,* vol. 5, pp. 30-41, 2008.
[116] A. J. Ahlsson, *et al.*, "Postoperative atrial fibrillation is not correlated to C-reactive protein," *Ann Thorac Surg,* vol. 83, pp. 1332-7, Apr 2007.
[117] R. Svedjeholm and E. Hakanson, "Predictors of atrial fibrillation in patients undergoing surgery for ischemic heart disease," *Scand Cardiovasc J,* vol. 34, pp. 516-21, Oct 2000.
[118] M. V. Podgoreanu and J. P. Mathew, "Prophylaxis against postoperative atrial fibrillation: current progress and future directions," *JAMA,* vol. 294, pp. 3140-2, Dec 28 2005.

[119] E. N. Deliargyris, *et al.*, "Preoperative factors predisposing to early postoperative atrial fibrillation after isolated coronary artery bypass grafting," *Am J Cardiol,* vol. 85, pp. 763-4, A8, Mar 15 2000.
[120] J. Price, *et al.*, "Current use of prophylactic strategies for postoperative atrial fibrillation: a survey of Canadian cardiac surgeons," *Ann Thorac Surg,* vol. 88, pp. 106-10, Jul 2009.
[121] R. A. Ott, *et al.*, "Reduced postoperative atrial fibrillation using multidrug prophylaxis," *J Card Surg,* vol. 14, pp. 437-43, Nov-Dec 1999.
[122] P. R. Kowey, *et al.*, "Physician stated atrial fibrillation management in light of treatment guidelines: data from an international, observational prospective survey," *Clin Cardiol,* vol. 33, pp. 172-8, Mar 2010.
[123] V. Fuster, *et al.*, "[ACC/AHA/ESC 2006 guidelines for the management of patients with atrial fibrillation--excutive summary]," *Rev Port Cardiol,* vol. 26, pp. 383-446, Apr 2007.
[124] H. Cao, *et al.*, "Natriuretic peptides and right atrial fibrosis in patients with paroxysmal versus persistent atrial fibrillation," *Peptides,* vol. 31, pp. 1531-9, Aug 2010.
[125] M. B. Yilmaz, *et al.*, "Atrial natriuretic peptide predicts impaired atrial remodeling and occurrence of late postoperative atrial fibrillation after surgery for symptomatic aortic stenosis," *Cardiology,* vol. 105, pp. 207-12, 2006.
[126] L. Jordaens, *et al.*, "Signal-averaged P wave: predictor of atrial fibrillation," *J Cardiovasc Electrophysiol,* vol. 9, pp. S30-4, Aug 1998.
[127] M. Budeus, *et al.*, "Long-term outcome after cardioversion of atrial fibrillation: prediction of recurrence with P wave signal averaged ECG and chemoreflexsensitivity," *Int J Cardiol,* vol. 112, pp. 308-15, Oct 10 2006.
[128] M. Budeus, *et al.*, "Prediction of atrial fibrillation in patients with cardiac dysfunctions: P wave signal-averaged ECG and chemoreflexsensitivity in atrial fibrillation," *Europace,* vol. 9, pp. 601-7, Aug 2007.
[129] C. Dimmer, *et al.*, "Analysis of the P wave with signal averaging to assess the risk of atrial fibrillation after coronary artery bypass surgery," *Cardiology,* vol. 89, pp. 19-24, 1998.
[130] K. Aytemir, *et al.*, "Prediction of atrial fibrillation recurrence after cardioversion by P wave signal-averaged electrocardiography," *Int J Cardiol,* vol. 70, pp. 15-21, Jul 1 1999.
[131] K. Sakabe, *et al.*, "Relation of gender and interatrial dyssynchrony on tissue Doppler imaging to the prediction of the progression to chronic atrial fibrillation in patients with nonvalvular paroxysmal atrial fibrillation," *Heart Vessels,* vol. 25, pp. 410-6, 2010.
[132] M. Budeus, *et al.*, "[The prediction of atrial fibrillation recurrence after electrical cardioversion with P wave signal averaged EKG]," *Z Kardiol,* vol. 93, pp. 474-8, Jun 2004.
[133] R. Abe and T. Nishida, "[The criteria for the prediction of paroxysmal atrial fibrillation by time domain analysis of the P wave-triggered signal-averaged electrocardiogram]," *Nihon Rinsho,* vol. 53, pp. 496-502, Feb 1995.
[134] S. Poli, *et al.*, "Prediction of atrial fibrillation from surface ECG: review of methods and algorithms," *Ann Ist Super Sanita,* vol. 39, pp. 195-203, 2003.

[135] E. S. Task Force, "Heart rate variability. Standards of measurement, physiological interpretation, and clinical use. Task Force of the European Society of Cardiology and the North American Society of Pacing and Electrophysiology.," *Eur Heart J,* vol. 17, pp. 354-81, Mar 1996.
[136] C. W. Hogue, Jr*., et al.*, "RR interval dynamics before atrial fibrillation in patients after coronary artery bypass graft surgery," *Circulation,* vol. 98, pp. 429-34, Aug 4 1998.
[137] M. Bettoni and M. Zimmermann, "Autonomic tone variations before the onset of paroxysmal atrial fibrillation," *Circulation,* vol. 105, pp. 2753-9, Jun 11 2002.
[138] C. K. Peng, "Quantification of scaling exponents and crossover phenomena in nonstationary heartbeat time series," *Chaos: An Interdisciplinary Journal of Nonlinear Science,* vol. 5, pp. 82-87, 1995.
[139] A. M. Pichlmaier*, et al.*, "Prediction of the onset of atrial fibrillation after cardiac surgery using the monophasic action potential," *Heart,* vol. 80, pp. 467-72, Nov 1998.
[140] S. M. Dogan*, et al.*, "Predictors of atrial fibrillation after coronary artery bypass surgery," *Coron Artery Dis,* vol. 18, pp. 327-31, 2007 2007.
[141] T. Akazawa*, et al.*, "Preoperative plasma brain natriuretic peptide level is an independent predictor of postoperative atrial fibrillation following off-pump coronary artery bypass surgery," *J Anesth,* vol. 22, pp. 347-53, 2008.
[142] Y. Shingu*, et al.*, "Postoperative atrial fibrillation: mechanism, prevention, and future perspective," *Surg Today,* vol. 42, pp. 819-24, Sep 2012.
[143] R. Nadeau*, et al.*, "Cervical vagosympathetic and mediastinal nerves activation effects on atrial arrhythmia formation," *Anadolu Kardiyol Derg,* vol. 7 Suppl 1, pp. 34-6, Jul 2007.
[144] C. S. Davis, *Statistical Methods for the Analysis of Repeated Measurements*: Springer, 2002.
[145] P. R. Hinton, *Statistics Explained*. New York: Routledge, 2004.
[146] S. L. David B. Hosmer. (2000). *Applied Logistic Regression*.
[147] D. W. Hosmer Jr*, et al.*, "A computer program for stepwise logistic regression using maximum likelihood estimation," *Computer Programs in Biomedicine,* vol. 8, pp. 121-134, 1978.
[148] M. S. Pepe, *The statistical evaluation of medical tests for classification and prediction*. New York, USA: Oxford University Press, 2004.
[149] S. L. David W. Hosmer. (1999). *Applied survival analysis: regression modeling of time to event data*.
[150] P. J. R. Leonard Kaufman, *Find Groups in Data An Introduction to Cluster Analysis*. Hoboken, New Jersey: John Wiley & Sons, Inc., 2005.
[151] B. Dube*, et al.*, "Automatic detection and classification of human epicardial atrial unipolar electrograms," *Physiol Meas,* vol. 30, pp. 1303-25, Dec 2009.
[152] G. Tremblay and A. R. LeBlanc, "Near-optimal signal preprocessor for positive cardiac arrhythmia identification," *IEEE Trans Biomed Eng,* vol. 32, pp. 141-51, Feb 1985.
[153] J. Pan and W. J. Tompkins, "A real-time QRS detection algorithm," *IEEE Trans Biomed Eng,* vol. 32, pp. 230-6, Mar 1985.

[154] X. Tang, *et al.*, "[A strategy of ECG classification based on SVM]," *Sheng Wu Yi Xue Gong Cheng Xue Za Zhi,* vol. 25, pp. 246-9, Apr 2008.
[155] M. I. Owis, *et al.*, "Study of features based on nonlinear dynamical modeling in ECG arrhythmia detection and classification," *IEEE Trans Biomed Eng,* vol. 49, pp. 733-6, Jul 2002.
[156] Y. H. Chen and S. N. Yu, "Subband features based on higher order statistics for ECG beat classification," *Conf Proc IEEE Eng Med Biol Soc,* vol. 2007, pp. 1859-62, 2007.
[157] Y. P. Meau, *et al.*, "Intelligent classification of electrocardiogram (ECG) signal using extended Kalman Filter (EKF) based neuro fuzzy system," *Comput Methods Programs Biomed,* vol. 82, pp. 157-68, May 2006.
[158] V. Krasteva and I. Jekova, "Assessment of ECG frequency and morphology parameters for automatic classification of life-threatening cardiac arrhythmias," *Physiol Meas,* vol. 26, pp. 707-23, Oct 2005.
[159] J. Kim, *et al.*, "Robust algorithm for arrhythmia classification in ECG using extreme learning machine," *Biomed Eng Online,* vol. 8, p. 31, 2009.
[160] R. Alcaraz, *et al.*, "Classification of paroxysmal and persistent atrial fibrillation in ambulatory ECG recordings," *IEEE Trans Biomed Eng,* vol. 58, pp. 1441-9, May 2011.
[161] E. D. Ubeyli, "Adaptive neuro-fuzzy inference system for classification of ECG signals using Lyapunov exponents," *Comput Methods Programs Biomed,* vol. 93, pp. 313-21, Mar 2009.
[162] C. D. Nugent, *et al.*, "An intelligent framework for the classification of the 12-lead ECG," *Artif Intell Med,* vol. 16, pp. 205-22, Jul 1999.
[163] N. Mahalingam and D. Kumar, "Neural networks for signal processing applications: ECG classification," *Australas Phys Eng Sci Med,* vol. 20, pp. 147-51, Sep 1997.
[164] W. Jiang and S. G. Kong, "Block-based neural networks for personalized ECG signal classification," *IEEE Trans Neural Netw,* vol. 18, pp. 1750-61, Nov 2007.
[165] Y. H. Hu, *et al.*, "Applications of artificial neural networks for ECG signal detection and classification," *J Electrocardiol,* vol. 26 Suppl, pp. 66-73, 1993.
[166] J. Feng, *et al.*, "[A multi-lead ECG classification network system based on modified LADT]," *Sheng Wu Yi Xue Gong Cheng Xue Za Zhi,* vol. 23, pp. 956-9, Oct 2006.
[167] L. Edenbrandt, *et al.*, "Neural networks for classification of ECG ST-T segments," *J Electrocardiol,* vol. 25, pp. 167-73, Jul 1992.
[168] Y. Cao and Z. Fan, "[ECG pattern classification by feature searching algorithm based on maximal divergence]," *Sheng Wu Yi Xue Gong Cheng Xue Za Zhi,* vol. 25, pp. 53-6, Feb 2008.
[169] S. L. Brian S. Everitt, Morven Leese, Daniel Stahl, "Cluster Analysis," ed: John Wiley & Sons, Ltd, 2011.
[170] D. G. Altman. (1999). *Practical Statistics For Medical Research*.
[171] M. Rangayyan, *Biomedical signal analysis : a case-study approach*. New York: Wiley-Interscience, 2002.
[172] R. C. Dorf. (2006). *Circuits Singals and Speech and Image Processing*.

[173] C. Y. Frederick Mosteller, "Tables of the Freeman-Tukey Transformations for the Binomial and Poisson Distributions," *Biometrika,* vol. 48, pp. 433-440, Dec. 1961.
[174] J. D. Drake and J. P. Callaghan, "Elimination of electrocardiogram contamination from electromyogram signals: An evaluation of currently used removal techniques," *J Electromyogr Kinesiol,* vol. 16, pp. 175-87, Apr 2006.
[175] A. Pichon*, et al.*, "Spectral analysis of heart rate variability: interchangeability between autoregressive analysis and fast Fourier transform," *J Electrocardiol,* vol. 39, pp. 31-7, Jan 2006.
[176] D. Grimaldi*, et al.*, "Spectral analysis of heart rate variability reveals an enhanced sympathetic activity in narcolepsy with cataplexy," *Clin Neurophysiol,* vol. 121, pp. 1142-7, Jul 2010.
[177] R. H. Fagard*, et al.*, "Power spectral analysis of heart rate variability by autoregressive modelling and fast Fourier transform: a comparative study," *Acta Cardiol,* vol. 53, pp. 211-8, 1998.
[178] D. Chemla*, et al.*, "Comparison of fast Fourier transform and autoregressive spectral analysis for the study of heart rate variability in diabetic patients," *Int J Cardiol,* vol. 104, pp. 307-13, Oct 10 2005.
[179] F. Eberhardt*, et al.*, "Atrial near-field and ventricular far-field analysis by automated signal processing at rest and during exercise," *Ann Noninvasive Electrocardiol,* vol. 11, pp. 118-26, Apr 2006.
[180] P. Langley*, et al.*, "Principal component analysis as a tool for analyzing beat-to-beat changes in ECG features: application to ECG-derived respiration," *IEEE Trans Biomed Eng,* vol. 57, pp. 821-9, Apr 2010.
[181] A. Krisciukaitis*, et al.*, "Efficiency evaluation of autonomic heart control by using the principal component analysis of ECG P-wave," *Methods Inf Med,* vol. 49, pp. 161-7, 2010.
[182] J. Lee*, et al.*, "Development of a new signal processing algorithm based on independent component analysis for single channel ECG data," *Conf Proc IEEE Eng Med Biol Soc,* vol. 1, pp. 224-6, 2004.
[183] M. K. Stiles*, et al.*, "Wavelet-based analysis of heart-rate-dependent ECG features," *Ann Noninvasive Electrocardiol,* vol. 9, pp. 316-22, Oct 2004.
[184] J. A. Crowe*, et al.*, "Wavelet transform as a potential tool for ECG analysis and compression," *J Biomed Eng,* vol. 14, pp. 268-72, May 1992.
[185] M. J. Burke and M. Nasor, "Wavelet based analysis and characterization of the ECG signal," *J Med Eng Technol,* vol. 28, pp. 47-55, Mar-Apr 2004.
[186] L. Frost*, et al.*, "Premature atrial beat eliciting atrial fibrillation after coronary artery bypass grafting," *J Electrocardiol,* vol. 28, pp. 297-305, Oct 1995.
[187] L. Frost*, et al.*, "Atrial ectopic activity and atrial fibrillation/flutter after coronary artery bypass surgery. A case-base study controlling for confounding from age, beta-blocker treatment, and time distance from operation," *Int J Cardiol,* vol. 50, pp. 153-62, Jun 30 1995.
[188] M. Zimmermann and D. Kalusche, "Fluctuation in autonomic tone is a major determinant of sustained atrial arrhythmias in patients with focal ectopy originating from the pulmonary veins," *J Cardiovasc Electrophysiol,* vol. 12, pp. 285-91, Mar 2001.

[189] J. E. Waktare*, et al.*, "The role of atrial ectopics in initiating paroxysmal atrial fibrillation," *Eur Heart J,* vol. 22, pp. 333-9, Feb 2001.
[190] L. F. Hsu*, et al.*, "Atrial fibrillation originating from persistent left superior vena cava," *Circulation,* vol. 109, pp. 828-32, Feb 24 2004.
[191] A. G. Kleber and Y. Rudy, "Basic mechanisms of cardiac impulse propagation and associated arrhythmias," *Physiol Rev,* vol. 84, pp. 431-88, Apr 2004.
[192] L. L. Hill*, et al.*, "Management of atrial fibrillation after cardiac surgery--part I: pathophysiology and risks," *J Cardiothorac Vasc Anesth,* vol. 16, pp. 483-94, Aug 2002.
[193] L. L. Hill*, et al.*, "Management of atrial fibrillation after cardiac surgery-part II: prevention and treatment," *J Cardiothorac Vasc Anesth,* vol. 16, pp. 626-37, Oct 2002.
[194] E. R. DeLong*, et al.*, "Comparing the areas under two or more correlated receiver operating characteristic curves: a nonparametric approach," *Biometrics,* vol. 44, pp. 837-45, Sep 1988.
[195] D. Bamber, "The area above the ordinal dominance graph and the area below the receiver operating characteristic graph," *Journal of Mathematical Psychology,* vol. 12, pp. 387-415, 1975.
[196] F. Helie*, et al.*, "Spatiotemporal dynamics of reentrant ventricular tachycardias in canine myocardial infarction: pharmacological modulation," *Can J Physiol Pharmacol,* vol. 81, pp. 413-22, May 2003.
[197] C. Cabo*, et al.*, "Activation in unipolar cardiac electrograms: a frequency analysis," *IEEE Trans Biomed Eng,* vol. 37, pp. 500-8, May 1990.
[198] S. Scacchi*, et al.*, "A reliability analysis of cardiac repolarization time markers," *Math Biosci,* vol. 219, pp. 113-28, Jun 2009.
[199] M. S. Ashar*, et al.*, "Localization of arrhythmogenic triggers of atrial fibrillation," *J Cardiovasc Electrophysiol,* vol. 11, pp. 1300-5, Dec 2000.
[200] S. W. Rha*, et al.*, "Mechanisms responsible for the initiation and maintenance of atrial fibrillation assessed by non-contact mapping system," *Int J Cardiol,* vol. 124, pp. 218-26, Feb 29 2008.
[201] S. Vikman*, et al.*, "Altered complexity and correlation properties of R-R interval dynamics before the spontaneous onset of paroxysmal atrial fibrillation," *Circulation,* vol. 100, pp. 2079-84, Nov 16 1999.
[202] P. M. Okin*, et al.*, "Incidence of atrial fibrillation in relation to changing heart rate over time in hypertensive patients: the LIFE study," *Circ Arrhythm Electrophysiol,* vol. 1, pp. 337-43, Dec 2008.
[203] A. D. Taylor*, et al.*, "New insights into onset mechanisms of atrial fibrillation and flutter after coronary artery bypass graft surgery," *Heart,* vol. 88, pp. 499-504, Nov 2002.
[204] M. S. Pepe, *The statistical evaluation of medical tests for classification and prediction*: Oxford University Press, 2004.
[205] J. M. Bland and D. G. Altman, "Survival probabilities (the Kaplan-Meier method)," *BMJ,* vol. 317, p. 1572, Dec 5 1998.
[206] V. S. Stel*, et al.*, "Survival analysis I: the Kaplan-Meier method," *Nephron Clin Pract,* vol. 119, pp. c83-8, 2011.

[207] D. Amar, "Postoperative atrial fibrillation," *Heart Dis,* vol. 4, pp. 117-23, Mar-Apr 2002.
[208] M. S. Spach and P. C. Dolber, "Relating extracellular potentials and their derivatives to anisotropic propagation at a microscopic level in human cardiac muscle. Evidence for electrical uncoupling of side-to-side fiber connections with increasing age," *Circ Res,* vol. 58, pp. 356-71, Mar 1986.
[209] J. Auer*, et al.*, "Postoperative atrial fibrillation independently predicts prolongation of hospital stay after cardiac surgery," *J Cardiovasc Surg (Torino),* vol. 46, pp. 583-8, Dec 2005.
[210] J. S. Healey and S. J. Connolly, "Atrial fibrillation: hypertension as a causative agent, risk factor for complications, and potential therapeutic target," *Am J Cardiol,* vol. 91, pp. 9G-14G, May 22 2003.
[211] K. R. Nilsson, Jr.*, et al.*, "Atrial fibrillation management strategies and early mortality after myocardial infarction: results from the Valsartan in Acute Myocardial Infarction (VALIANT) Trial," *Heart,* vol. 96, pp. 838-42, Jun 2010.
[212] J. Schmitt*, et al.*, "Atrial fibrillation in acute myocardial infarction: a systematic review of the incidence, clinical features and prognostic implications," *Eur Heart J,* vol. 30, pp. 1038-45, May 2009.
[213] C. A. Jones*, et al.*, "Serum creatinine levels in the US population: third National Health and Nutrition Examination Survey," *Am J Kidney Dis,* vol. 32, pp. 992-9, Dec 1998.
[214] A. Sedrakyan*, et al.*, "Recursive partitioning-based preoperative risk stratification for atrial fibrillation after coronary artery bypass surgery," *Am Heart J,* vol. 151, pp. 720-4, Mar 2006.
[215] N. Ad*, et al.*, "Potential preoperative markers for the risk of developing atrial fibrillation after cardiac surgery," *Semin Thorac Cardiovasc Surg,* vol. 11, pp. 308-13, Oct 1999.
[216] H. R. Gibbs*, et al.*, "Postoperative atrial fibrillation in cancer surgery: preoperative risks and clinical outcome," *J Surg Oncol,* vol. 50, pp. 224-7, Aug 1992.
[217] D. J. Ewing*, et al.*, "Irregularities of R-R interval cycle length during 24 hour ECG tape recording. A new method for assessing cardiac parasympathetic activity," *Scott Med J,* vol. 29, pp. 30-1, Jan 1984.
[218] D. J. Ewing*, et al.*, "New method for assessing cardiac parasympathetic activity using 24 hour electrocardiograms," *Br Heart J,* vol. 52, pp. 396-402, Oct 1984.
[219] J. E. Mietus*, et al.*, "The pNNx files: re-examining a widely used heart rate variability measure," *Heart,* vol. 88, pp. 378-80, Oct 2002.
[220] J. C. Geller*, et al.*, "Changes in AV node conduction curves following slow pathway modification," *Pacing Clin Electrophysiol,* vol. 23, pp. 1651-60, Nov 2000.
[221] F. Hegbom*, et al.*, "Dual AV nodal pathways and conduction during atrial fibrillation," *Scand Cardiovasc J,* vol. 37, pp. 199-204, Sep 2003.
[222] M. R. Warner and J. M. Loeb, "Beat-by-beat modulation of AV conduction. I. Heart rate and respiratory influences," *Am J Physiol,* vol. 251, pp. H1126-33, Dec 1986.

[223] M. R. Warner, *et al.*, "Beat-by-beat modulation of AV conduction. II. Autonomic neural mechanisms," *Am J Physiol,* vol. 251, pp. H1134-42, Dec 1986.
[224] D. W. Wallick, *et al.*, "Dynamic interaction of vagal activity and heart rate on atrioventricular conduction," *Am J Physiol,* vol. 262, pp. H792-8, Mar 1992.
[225] D. W. Wallick, *et al.*, "Effects of autonomic activity and changes in heart rate on atrioventricular conduction," *Am J Physiol,* vol. 243, pp. H523-7, Oct 1982.
[226] K. W. Hewett, *et al.*, "Changes in atrioventricular conduction properties with refractory-period modulation," *J Cardiovasc Pharmacol,* vol. 28, pp. 824-32, Dec 1996.
[227] J. Billette, *et al.*, "Mechanisms of conduction time hysteresis in rabbit atrioventricular node," *Am J Physiol,* vol. 269, pp. H1258-67, Oct 1995.
[228] D. Medkour, *et al.*, "Anatomic and functional characteristics of a slow posterior AV nodal pathway: role in dual-pathway physiology and reentry," *Circulation,* vol. 98, pp. 164-74, Jul 14 1998.
[229] J. Billette and M. Lavallee, "From selective parasympathetic modulation of AV node to rate control therapy," *J Cardiovasc Electrophysiol,* vol. 16, pp. 1368-9, Dec 2005.
[230] R. Tadros and J. Billette, "Rate-Dependent AV Nodal Function: Closely Bound Conduction and Refractory Properties," *J Cardiovasc Electrophysiol,* Sep 28 2011.
[231] K. Mubagwa, *et al.*, "Resting and action potentials of nonischemic and chronically ischemic human ventricular muscle," *J Cardiovasc Electrophysiol,* vol. 5, pp. 659-71, Aug 1994.
[232] D. Sinker, *et al.*, "Sinus and A-V nodal dysfunction following myocardial infarction," *J Electrocardiol,* vol. 8, pp. 281-3, Jul 1975.
[233] R. Childers, "The AV node: normal and abnormal physiology," *Prog Cardiovasc Dis,* vol. 19, pp. 361-84, Mar-Apr 1977.
[234] R. H. Falk and A. Pollak, "Signal-averaged P wave duration and atrial fibrillation," *J Am Coll Cardiol,* vol. 23, pp. 549-50, Feb 1994.
[235] M. Rosiak, *et al.*, "Usefulness of prolonged P-wave duration on signal averaged ECG in predicting atrial fibrillation in acute myocardial infarction patients," *Med Sci Monit,* vol. 9, pp. MT85-8, Aug 2003.
[236] D. Amar, *et al.*, "Signal-averaged P-wave duration does not predict atrial fibrillation after thoracic surgery," *Anesthesiology,* vol. 91, pp. 16-23, Jul 1999.
[237] O. Turgut, *et al.*, "Association of P wave duration and dispersion with the risk for atrial fibrillation: practical considerations in the setting of coronary artery disease," *Int J Cardiol,* vol. 144, pp. 322-4, Oct 8 2010.
[238] J. Chandy, *et al.*, "Increases in P-wave dispersion predict postoperative atrial fibrillation after coronary artery bypass graft surgery," *Anesth Analg,* vol. 98, pp. 303-10, table of contents, 2004 2004.
[239] P. Page, *et al.*, "Differential effects of cervical vagosympathetic and mediastinal nerve activation on atrial arrhythmia formation in dogs," *Auton Neurosci,* vol. 128, pp. 9-18, Jul 30 2006.
[240] V. Jacquemet, *et al.*, "Extraction and analysis of T waves in electrocardiograms during atrial flutter," *IEEE Trans Biomed Eng,* vol. 58, pp. 1104-12, Apr 2011.

[241] M.-H. C. Joseph G. Ibrahim, Debjyoti Sinha, *Bayesian survival analysis*: Springer, 2001.
[242] A. Owen, "Antithrombotic treatment for the primary prevention of stroke in patients with non valvular atrial fibrillation: a reappraisal of the evidence and network meta analysis," *Int J Cardiol,* vol. 142, pp. 218-23, Jul 23 2010.
[243] A. Mak*, et al.*, "Bisphosphonates and atrial fibrillation: Bayesian meta-analyses of randomized controlled trials and observational studies," *BMC Musculoskelet Disord,* vol. 10, p. 113, 2009.
[244] G. Karraz and G. Magenes, "Automatic classification of heartbeats using neural network classifier based on a Bayesian framework," *Conf Proc IEEE Eng Med Biol Soc,* vol. 1, pp. 4016-9, 2006.
[245] H. Chrystyn and S. Dean, "An assessment of population-based and Bayesian methods to individualize digoxin doses shortly after the start of therapy for atrial fibrillation," *J Clin Pharm Ther,* vol. 16, pp. 177-85, Jun 1991.

ANNEXE I

Automatic detection and classification of human epicardial atrial unipolar electrograms

2009 Physiol. Meas. 30 1303

(http://iopscience.iop.org/0967-3334/30/12/002)

IOP PUBLISHING PHYSIOLOGICAL MEASUREMENT

Physiol. Meas. **30** (2009) 1303–1325 doi:10.1088/0967-3334/30/12/002

Automatic detection and classification of human epicardial atrial unipolar electrograms

B Dubé[1,2], A Vinet[1,2], F Xiong[1,2], Y Yin[1], A-R LeBlanc[1,2] and P Pagé[1,3]

[1] Research Center, Hôpital du Sacré-Cœur de Montréal, Université de Montréal, Canada
[2] Biomedical Engineering Institute, Université de Montréal, Canada
[3] Department of Surgery, Faculty of Medicine, Université de Montréal, Canada

Received 14 May 2009, accepted for publication 18 September 2009
Published 20 October 2009
Online at stacks.iop.org/PM/30/1303

Abstract

This paper describes an unsupervised signal processing method applied to three-channel unipolar electrograms recorded from human atria. These were obtained by epicardial wires sutured on the right and left atria after coronary artery bypass surgery. Atrial (A) and ventricular (V) activations had to be detected and identified on each channel, and gathered across the channels when belonging to the same global event. The algorithm was developed and optimized on a training set of 19 recordings of 5 min. It was assessed on twenty-seven 2 h recordings taken just before the onset of a prolonged atrial fibrillation for a total of 1593697 activations that were validated and classified as normal atrial or ventricular activations (A, V) and premature atrial or ventricular activations (PAA, PVA). 99.93% of the activations were detected, and amongst these, 99.89% of the A and 99.75% of the V activations were correctly labelled. In the subset of the 39705 PAA, 99.83% were detected and 99.3% were correctly classified as A. The false positive rate was 0.37%. In conclusion, a reliable fully automatic detection and classification algorithm was developed that can detect and discriminate A and V activations from atrial recordings. It can provide the time series needed to develop a monitoring system aiming to identify dynamic predictors of forthcoming cardiac events such as postoperative atrial fibrillation.

Keywords: Unipolar electrogram, human, atrium, automatic activation detection, classification

(Some figures in this article are in colour only in the electronic version)

1. Introduction

Atrial fibrillation (AF) occurs frequently as a complication of open heart surgery, with incidence generally reported of 15–40% (Creswell *et al* 1993, Maisel *et al* 2001, Villareal

et al 2004). It typically manifests 48–72 h after surgery. Perioperative, intraoperative and postoperative clinical information as well as standard ECG information have contributed to identifying some risk factors or the so-called predictors of AF after cardiac surgery (Maisel *et al* 2001, Svedjeholm and Håkanson 2000, Zaman *et al* 2000, Amar *et al* 2004, Magee *et al* 2007, Mathew *et al* 2004, Ak *et al* 2005, Asher *et al* 1998, Dupont *et al* 2001). For example, the analysis of P-wave duration and dispersion from preoperative ECG has been reported (Tsikouris *et al* 2001, Hayashida *et al* 2005, Passman *et al* 2001). Moreover, tentative predictive characteristics have been documented with the analysis of heart rate variability and nonlinear dynamics of RR intervals prior to postoperative AF, as well as in not surgically related paroxysmal AF (Amar *et al* 2003, Chamchad *et al* 2006, Hogue *et al* 1998, Tuzcu *et al* 2006, Vikman *et al* 2005). All these analyses were done off-line on relatively short episodes of signals and had a limited predictive power.

Intracardiac atrial signal can provide information that cannot be extracted from the surface ECG. Significant change of monophasic action potential waveforms has been reported prior to the onset of AF (Pichlmaier *et al* 1998) that might possibly be detected by unipolar atrial cardiac electrograms (Pagé *et al* 1995, Vigmond *et al* 2009). Furthermore, AF is often preceded by multiple atrial premature activations (Taylor *et al* 2002). Simultaneous recording of unipolar electrograms from different sites may provide information on the origin of these premature activations. For these reasons, it became critical to develop a reliable method of signal processing of atrial electrograms. Since unipolar atrial electrograms include waveforms related to both the local atrial activation (A) and the far-field ventricular activation (V), these events must be detected and distinguished. The purpose of the study was to develop an automatic and unsupervised detection method capable to analyse continuous three-channel recordings collected for period lasting as long as 4 days. The aims were to detect the A and V activations on each channel and to group together the activations belonging to the same A or V event. The main challenge was to overcome the non-uniformity of the waveforms amongst the channels, as well as their variations within each channel owing to single or multiple premature A (PAA) or V (PVA) activations. The detection was done by amending the classical energy-based detectors with nonlinear pre-conditioning. The identification of activation as A or V was achieved by an unsupervised algorithm based on adaptive comparison of high- and low-frequency content.

2. Method

2.1. Signal recording

Recordings were made continuously in 140 patients during the first 4 consecutive days following coronary artery bypass surgery using a modified (class III) three-channel Holter digital recorder with 16 bits encoding, providing a ± 5 mV input range with 0.16 μV resolution (Burdick, model 6632). The sampling rate was set at 500 Hz per channel. This setting, which is barely appropriate for atrial electrograms, was chosen such that batteries and the storage memory card had to be changed only once every 24 h. Three atrial unipolar electrodes (ETHICON model TPW40) were sutured on the epicardium of the atria and connected to the positive poles of the Holter by wires fixed on the patient's thoracic wall. The three negative poles of the Holter were connected together to serve as a reference electrode positioned on the left lateral side of the thigh. The recordings were transferred to a PC for off-line analysis. A short stretch of the signal is shown in figure 1, in which A and V activations are identified. The protocol was approved by the Ethics Committee of Hôpital du Sacré-Coeur de Montréal. To develop the detection algorithm, a training set was constructed by taking

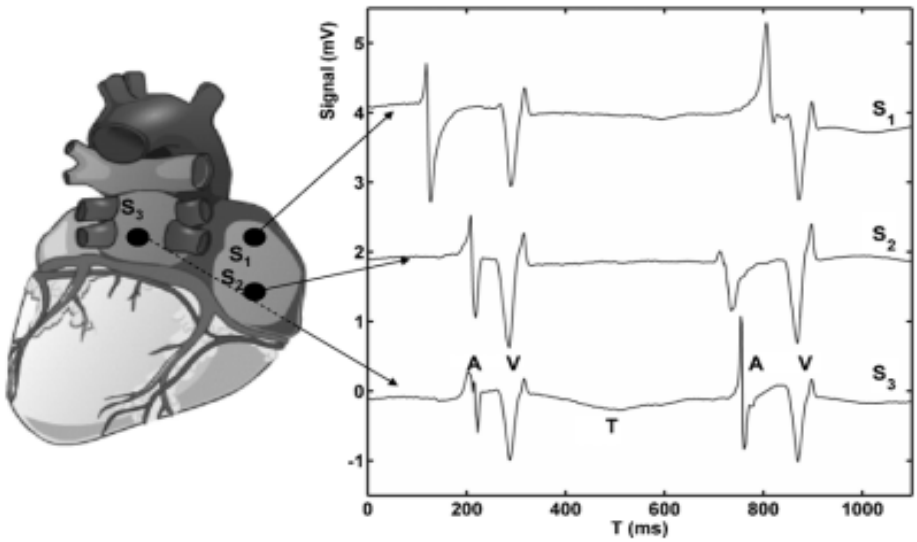

Figure 1. Posterior view of the heart showing the three electrodes sutured to the right (S_1, S_2) and left (S_3) atrium and their electrograms. The atrial (A) and ventricular activations (V) are indicated for two beats, as well as the ventricular T wave (T). The first is a normal sinus beat, while the second is an ectopic, as shown by the change of firing sequence of the A activations.

5 min episodes from 19 patients selected to represent typical examples of the more complex rhythms encountered throughout the recordings. All activations and their labels were validated by an expert cardiologist using an in-house interactive program developed for that purpose. Afterwards, 2 h recordings from 27 patients taken just before the onset of a prolonged (>30 min) episode of AF were used as a validation set.

2.2. *Constraints and methodological choice*

In the course of the development process, an array of difficulties and constraints had to be overcome through specific methodological choices.

(i) The requirement to pool together the activations of the channels belonging to the same atrial or ventricular event, allowing calculation such as intra-atrial and atrio-ventricular conduction times as well as the identification of the site of the origin of PAA, led to the concept of global and local activation and energy, the latter built from the derivative of the signals (Tremblay and LeBlanc 1985, Pan and Tompkins 1985). In the following, 'global event' refers to an activation detected on the sum of the energy of the three channels, while 'local event' stands for an activation detected on the energy of a single channel. We found that it was much easier to detect global events and determine afterwards the local members than to start from the individual channels and group activations subsequently.

(ii) For global events, activations across the channels had to be encompassed in a single continuous high-amplitude energy segment. Appropriate averaging windows had to be found to cope with the wide spread of intra-atrial conduction times both within and between the patients (e.g. figures 1, 3 and 5), which stems from the variation in the activation sequences amongst the beats and from the change in the location of the electrodes and in the pathways of propagation across the patients. These variations also conditioned the algorithm to find the limits of the global events within which local events were to be searched.

(iii) Events detection was based on energy thresholds. Since noise and amplitude of the activations were seen to vary widely even in 5 min recordings (e.g. figure 5(c)), thresholds had to be adaptive. The problem of non-stationarity was particularly critical with regard to the detection of atypical events such as isolated ectopic beats and short episodes of arrhythmia, which becomes imperative in the context of monitoring where these events can be particularly consequential (Taylor *et al* 2002).

(iv) The typical ten-fold difference between peak energies of A and V activations required a dual threshold, leading to a two-pass detection algorithm. The threshold of the second pass had to be set low enough for maximum detection, while avoiding false detection by being too close to the noise level. This led to the introduction of functions to monitor the quality of the signal (QoS) that directed both the local filtering of the signals and the value of the thresholds.

2.3. Detailed algorithm

The flowchart of the detection algorithm is shown in figure 2. The main steps of the method are explained, followed by the description of the QoS functions.

2.3.1. Detection method and fiducial activation time

Step 1. QoS functions, described later, are calculated from the raw signals (S_i (n) $i = 1, 2, 3$, channel number, $n = 1$, N, sample number). The calculation of these functions and all the steps of the algorithm are performed in successive 300 s windows (the width can be chosen anywhere from a minimum value of 15 s without consequence) with 3–6 s overlap to ensure detection continuity.

Step 2. The derivative function D_i° is calculated as

$$D_i^\circ(n) = (S_i(n+2) + S_i(n+1) - S_i(n-1) - S_i(n-2))/(6^*T_s), \qquad T_s = 2\,\text{ms}. \tag{1}$$

It corresponds to the mean of the backward and forward derivatives after a three-point moving average of the signal. The frequency response of this derivative function (i.e. gain as a function of the frequency of the input signal) has a maximum around 75 Hz and fades out at higher frequencies. As explained later, $D_i^\circ(n)$ is processed according to the value of the QoS functions to yield $D_i^b(n)$.

Step 3. The amplitudes of the activations, which might be disproportioned across the channels, must be balanced. Otherwise, the events with the largest amplitudes may dominate the detection process, blurring the information of the other channels or, in the same channel, masking lower amplitude events. The balance is done by clipping all peaks for which $\left|D_i^b\right|$ is taller than a reference value calculated in successive 30 s intervals, which typically encompasses between 30 and 60 A and V activations. The reference maximum for each channel $\left(D_i^{\max}\right)$ is set at the value corresponding to 99% of the cumulative distribution of $\left|D_i^b(n)\right|$ within each 30 s window, with a minimum value of 50 μV ms^{-1}. A channel remaining everywhere <20 μV ms^{-1} is considered disconnected and is ignored. A channel is tagged as disproportioned if $\left|D_i^{\max}\right| > 2\ \min(\{|D_j^{\max}|_{j=1,\mathrm{M}} \leqslant 3, M = \text{the number of active channels}\})$. All its peaks that are beyond the limits $\pm 1/2\left(\left(\sum_{i=1,M} \boldsymbol{D_i^{\max}}\right) - \mathbf{min}\left(\left\{\boldsymbol{D_{i=1,M}^{max}}\right\}\right)\right)$ are then trimmed off at these values to produce the final derivative $D_i(n)$.

Steps 4 and 5. Two band-pass filtered signals are constructed from $D_i(n)$, with a high cut-off frequency of 90 Hz $\left(D_i^{90}(n)\right)$ and 25 Hz $\left(D_i^{25}(n)\right)$, respectively, and a common low cut-off frequency of 6 Hz.

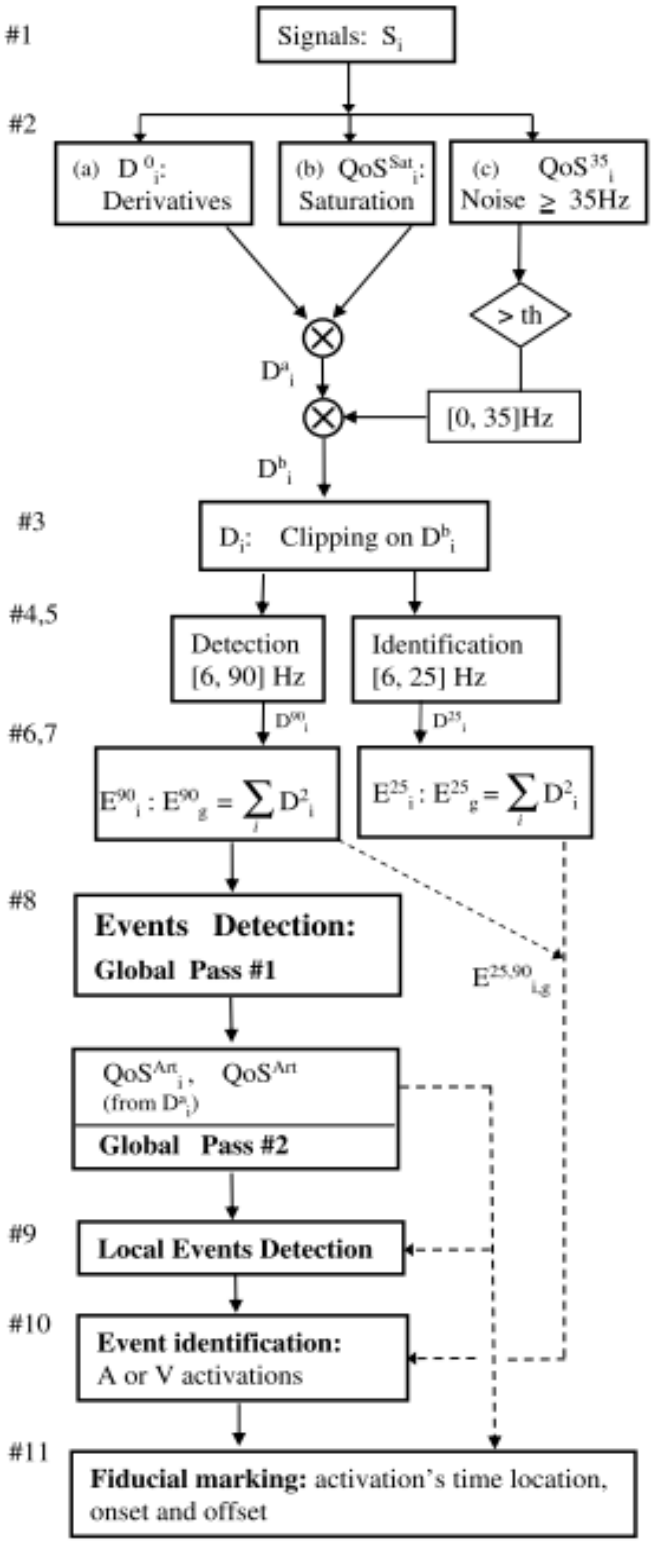

Figure 2. Detection and labelling algorithm. See the text for details.

Steps 6 and 7. Four energy functions are calculated from both D_i^{25} and D_i^{90}: one for each channel $\left(E_i^{25,90}, i = 1, 3\right)$ and a global energy $\left(E_g^{25,90}\right)$. $E_{i,g}^{90}$ are used for detection (steps 8 and 9) and compared to $E_{i,g}^{25}$ to discriminate A from V events (step 10).

The calculation of E_i^{90} begins with the intermediate quantity,

$$M_i^{90}(n) = \frac{1}{13}\sum_{k=n-6}^{k=n+6}\left(D_i^{90}(k)\right)^2, \tag{2}$$

which is a mean over a 24 ms sliding window, and

$$E_i^{90}(n) = \frac{1}{15}\sum_{k=n-7}^{k=n+7} M_i^{90}(k), \tag{3}$$

an average over a 28 ms sliding window. This calculation (sum followed by average), based on the Tremblay–LeBlanc oesophageal A-wave and QRS detector (Tremblay and LeBlanc 1985) and the Pan–Tompkins QRS detector (Pan and Tompkins 1985), removes notches around the points where $D_i^{90}(n)$ changes sign and maintains high amplitude along the entire interval over which local activation takes place. E_i^{25} is calculated the same way using D_i^{25}.

The global energy is given by

$$M_g^{90}(n) = \frac{1}{35}\sum_{k=n-17}^{k=n+17}\left(D_1^{90}(k)\right)^2 + \left(D_2^{90}(k)\right)^2 + \left(D_3^{90}(k)\right)^2, \tag{4}$$

$$E_g^{90}(n) = \frac{1}{15}\sum_{k=n-7}^{k=n+7} M_g^{90}(k). \tag{5}$$

The windows used for global energy are larger to embed the asynchronous atrial activations of the three channels within a single high-amplitude segment (figure 3(b)).

Step 8: detection of global events. $E_g^{90}(n)$ is used to detect A and V global events. The detection proceeds in two steps that are illustrated in figure 3. First, all the large energy events are detected. They are then removed from $E_g^{90}(n)$ to find out potential remaining events, which are most often V activations or atypical low amplitude A's.

2.3.2. *Peak detection and peak delineation (onset and offset)*

Pass 1. A threshold function $\mathrm{Thresh}_1(n)$ is calculated from the time course of maximum ($\mathrm{MAX}_1(n)$) and minimum ($\mathrm{MIN}_1(n)$) functions constructed from $E_g^{90}(n)$. First, in each successive 100 ms interval, $\mathrm{MAX}_1(n)$ is set to the maximum of E_g^{90} encountered in a ± 1 s window centred on the middle of the interval. The resulting staircase function is then smoothed with a moving average over a ± 100 ms window. The $\mathrm{MIN}_1(n)$ function, which tracks the local floor level, is constructed in a similar way, but with minimum taken over windows of ± 250 ms for each 20 ms interval and a final moving average over ± 50 ms. An intermediate sample-by-sample detection threshold is defined as

$$\mathrm{Thresh}_o(n) = \mathrm{MIN}_1(n) + 0.20\ \mathrm{MAX}_1(n). \tag{6}$$

The final threshold is taken as

$$\mathrm{Thresh}_1(n) = \max([0.01\ \mathrm{Thresh}_o(n) + 0.99\ \mathrm{Thresh}_1(n-1), 1000(\mu\mathrm{V/ms})^2]). \tag{7}$$

Thresh_1 adapts exponentially to an abrupt but sustained jump of the energy, but damps transient short variations. Any segment along which $E_g^{90}(n)$ remains $\geqslant \mathrm{Thresh}_1(n)$ for at least 40 ms is

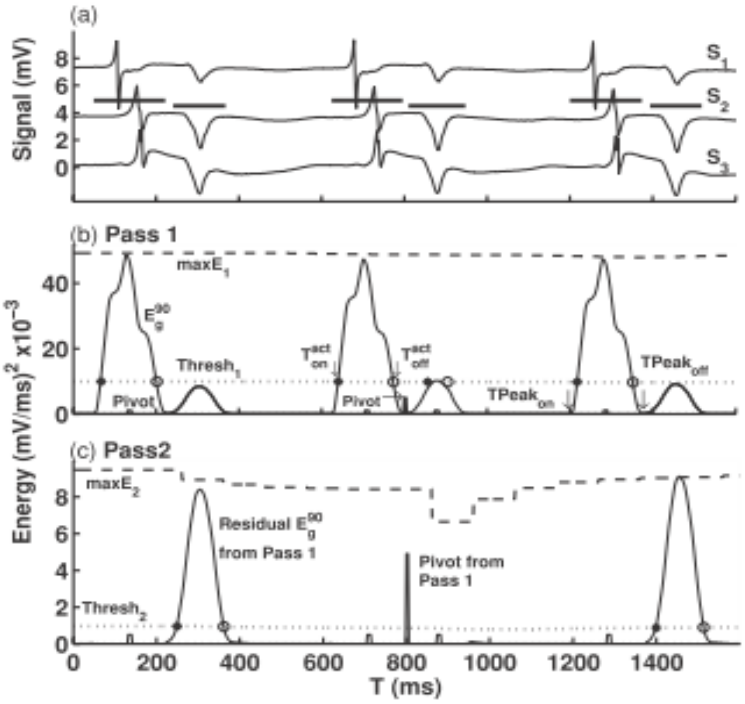

Figure 3. Detection of global activations (step 8). (a) Original signals S_1, S_2 and S_3. The horizontal lines show the extent of the global activations, from their onset ($TPeak_{on}$) and to their offset ($TPeak_{off}$). (b) Pass 1: global events are segments with $E_g^{90} \geqslant Thresh_1$ (grey line) for at least 40 ms, from $T^{act}{}_{on}$ (*) to $T^{act}{}_{off}$ (o). The upper dash line is MAX_1 used to calculate $Thresh_1$ (equation (6)). $TPeak_{on}$ and $TPeak_{off}$ are the minimum before $T^{act}{}_{on}$ and after $T^{act}{}_{off}$, respectively. Each event is removed and replaced by a three sample pivot with an amplitude = 5% of energy at $T^{act}{}_{on}$. If the limits of two events are separated by less than 50 ms, as the two events in the middle of the panel, a pivot is inserted in the middle, with an amplitude = 50% of energy at the first $T^{act}{}_{on}$. (c) Pass 2: the residual E_g^{90} is analysed as in Pass 1, with the new threshold $Thresh_2$ (grey line), calculated from the updated MAX_2 function (upper dash line, equation (8)).

considered as a global event (figure 3(b)). A global atrial event is associated with activations of the individual channels that occur in a sequence reflecting the propagation of the electrical wave across the atria (figure 3(a)). Hence, markers defining the onset and termination of each global event are needed to set the limits for the later search of the related local activations. The onset time of the event ($TPeak_{on}$) is determined by a stepwise backward search starting from $T^{act}{}_{on}$, the time of the initial up-crossing of $Thresh_1$ (figure 3(b)). The search continues as long as $E_g^{90}(T < T_{on}^{act})$ remains greater than a floor value plus 2% of $Thresh_1(T_{on}^{act})$. The floor value is updated at each step as the minimum of E_g^{90} in the interval [T-40 ms, T]. Once $TPeak_{on}$ has been found, additional tests are performed to avoid a local minimum. Typically, E_g^{90} local minimum may occur when one channel is activated much before or after the others. A similar stepwise forward search is performed from T_{off}^{act}, the final time of down-crossing of $Thresh_1$, to find $TPeak_{off}$, the end of the global event.

Pass 2. Typically, events associated with atrial activations, which have higher energy content, are detected in the first pass (figure 3(b)). The aim of the second pass is to detect the remaining events, which might be V activations or sequences of fast A and/or PAA for which energy can be depressed. All events found in pass 1 are removed from E_g^{90}, being substituted by a

line extending from $E_g^{90}(\text{TPeak}_{on})$ to $E_g^{90}(\text{TPeak}_{off})$. To avoid that the new threshold reaches the noise level when there is no true remaining event, a three-sample peak is left in the middle of each removed event (the pivot in figure 3(b)). The amplitude of the pivot is set to 0.05 $E_g^{90}\left(T_{on}^{act}\right)$ unless the beginning of the next detected event (TPeak_{on}) is less than 50 ms ahead of the end (TPeak_{off}.) of the current event. In that case, it is likely that all events have already been detected and a ten-fold increased pivot is introduced between TPeak_{off} and the next TPeak_{on} (figure 3(b), middle). The transformed E_g^{90} is then processed as in pass 1 to obtain a new $\text{MAX}_2(n)$ function ($\text{MIN}_1(n)$ is kept unchanged), and $\text{Thresh}_0(n)$ is recalculated as

$$\text{Thresh}_0(n) = \text{MIN}_1(n) + X(n)\text{MAX}_2(n). \tag{8}$$

In pass 1 (equation (6)), $X(n)$ was fixed to 0.20. In pass 2, to avoid false detections, $X(n) \in [0.15, 1.25]$ is set proportional to a QoS function ($\text{QoS}^{Art}(n)$ that quantifies the level of noise). Finally, the new $\text{Thresh}_2(n)$ function is calculated as

$$\text{Thresh}_2(n) = \alpha(n)\ \text{Thresh}_0(n) + (1 - \alpha(n))\ \text{Thresh}_2(n-1). \tag{9}$$

α is increased linearly from 0.01, the value in pass 1, to 0.05 according to the level of noise (QoS^{Art}) to speed up the adaptation of the threshold when the signal becomes noisy. Events detection and delineation are then performed on the transformed E_g^{90} as in pass 1 (figure 3(c)).

Step 9: detection of local events. E_i^{90} is used to find the activations of the individual channels within the [TPeak_{on}, TPeak_{off}] interval delineating each global event. The threshold within the borders of each global event is the constant value:

$$\begin{aligned}\text{Th}_i = {} & \max\left(\left[\min\left(E_i^{90}([\text{TPeak}_{on}, \text{TPeak}_{off}]\right)\right]\right) \\ & + a\ c\ \max\left(\left[E_g^{90}(\text{TPeak}_{on}, \text{TPeak}_{off}), 100(\mu\text{V/ms})^2\right]\right)\end{aligned} \tag{10}$$

with $c = 0.01$ and 0.02, for global activations found in pass 1 and pass 2, respectively; $a \in [1, 3]$ depending linearly on QoS^{Art}.

Because it sometimes occurs that the A and V activations of a cardiac beat are gathered in the same global event, up to two local activations by the channel can be accepted within each global event. Typically, this occurs when A and V activations become unrelated, as when a spontaneous PVA is produced during or close to an atrial activation. For each channel, all maxima > Th_i within the [TPeak_{on}, TPeak_{off}] limits of the global event are collected, with a list of their times of occurrence $\left(\left\{T_{Max}^i(j),\ j = 1, k\right\}\right)$ sorted in descending order of amplitude. The largest maximum, at time $T_{Max}^i(1)$, is kept as an activation. Then, the remaining members of the list are scanned for a second activation. Their amplitudes are recalculated relative to the closest minimum in the interval extending from the time of their maximum to $T_{Max}^i(1)$. The largest of these corrected maxima > Th_i is kept as a second activation. The rationale is that two activations in a channel must be separated by a period during which energy is depressed. If no local event is found, the search procedure is repeated once with $\text{Th}_i = \text{Th}_i/2$.

Finally, the limits of each local activation $\left(T^{act}{}_{on}{}^i(k), T^{act}{}_{off}{}^j(k)\right)$ are determined, providing the interval in which the final fiducial marker will be positioned (step 11). This is done through a forward and backward search around $T_{Max}^i(k)$ to find the positions where E_i^{90} reaches γ^* $E_i^{90}(T_{\text{Max}}(k))$, with $\gamma \in [0.01, 0.1]$ proportional to QoS^{Art}. At the end of this step, there is a sequence of global and related local events, with the time intervals defining their respective boundaries.

Step 10: *waveform labelling*. Because the electrodes are sutured to the atria, deflections associated with the atrial activations, which correspond to the propagation of an activation front close to the electrode, are most often brisker than those associated with ventricular activations (figure 1). Figure 4 shows that the peaks of E_g^{25} are much lower than those of E_g^{90}

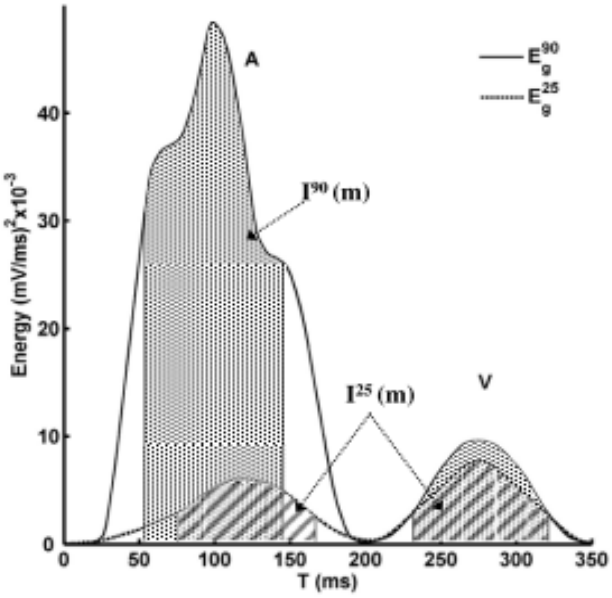

Figure 4. E_g^{90} (continuous line) and E_g^{25} (dash line). I^{90} and I^{25} are the integrals over ±40 ms around the maximum of E^{90} and E^{25}, respectively. The ratio $R = 100\, I^{25}/I^{90}$ is used to discriminate A and V events.

for A than for V events. As a consequence, the ratio of the low-to-high-frequency energy content of A events is smaller. This feature is used to label each global (comparing E_g^{25} and E_g^{90}) and local event (comparing E_l^{25} and E_l^{90}). For each event m, the E^{25} and E^{90} energies are integrated over a 41 sample window centred on their respective maximum to get $I^{25}(m)$ and $I^{90}(m)$ (figure 4) and a classification ratio R is computed as

$$R(m) = 100\frac{I^{25}(m)}{I^{90}(m)}. \tag{11}$$

Since the properties of the activations may change in time, the threshold value of R to discriminate between A and V events must be updated continuously. The discrimination value for the mth event in a sequence is set to

$$\mathrm{DF}\,(m) = \frac{\mathrm{DF}(m-2) + \mathrm{DF}(m-1) + \beta_m R(m) + \beta_{m+1} R(m+1)}{2 + \beta_m + \beta_{m+1}} \tag{12}$$

with default $\beta_{m,m+1} = 1$.

The algorithm first proceeds to the labelling of the global events, whose ratios are calculated from E_g^{25} and E_g^{90}. The principle of the DF calculation is based on the alternation of A and V activations in normal cardiac cycles (figure 4). DF, with $\beta_{m,m+1} = 1$, is a weighted average with sizeable contributions from ∼6 consecutive R values. The averaging provides the inertia to maintain discrimination for short sequences in which alternation is broken (figure 5). For longer abnormal sequences where a single type of events dominates, DF must be avoided to fluctuate randomly in a range of R values associated with similar events. Long-lasting abnormal sequences were most often found when the A and V activations were embedded in the same global event for successive cardiac beats. In normal cases, the systolic time interval (A to next V) is much shorter than the diastole (V to next A). In that sense, consecutive

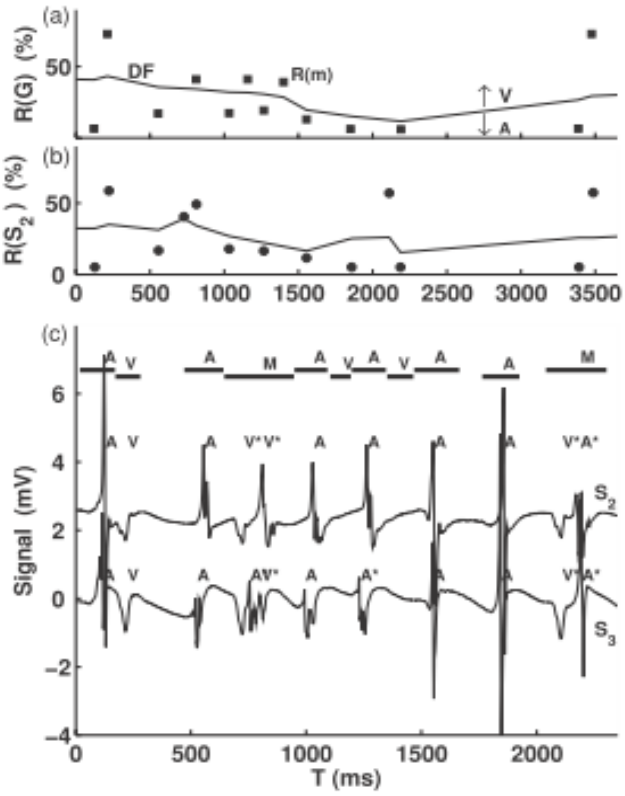

Figure 5. Labelling of a sequence of events (shown in (c)) containing a salvo of PAA. (a) Discriminating function (continuous line, DF) and sequence of the R ratio (described in figure 4) for global events, showing discrimination of A (under DF) and V (over DF). When an activation is missed (3 V in that example), DF, which also depends on past values, maintains the discrimination. (b) The DF function for channel S_2 shown in 5 c. Even if only one V is detected after four successive A, the discrimination is maintained. (c) A and V detection and discrimination for a salvo of PAAs whose energy was highly depressed. All the PAA were correctly detected and labelled as A, even when much depressed as in channel S_3 (only 2 channels shown for clarity). In S_2, the first fusion beat was detected, but the depressed A was labelled as a possible V. In S_3, the three fusion beats were labelled as A. In the first one, the V is misplaced and generates a (F−, F+) pair.

global events containing both the A and V activations become isolated, since only the diastolic intervals are maintained. Besides, in such a global event, A and V activations are usually detected on at least one channel such that the global contains at least four local activations. Under these conditions, a global event k is considered isolated if (1) $\mathrm{TPeak}_{\mathrm{on}}(k)$- $\mathrm{TPeak}_{\mathrm{off}}(k-1)$ > 300 ms and $\mathrm{TPeak}_{\mathrm{on}}(k+1)$- $\mathrm{TPeak}_{\mathrm{off}}(k) > 300$ ms, and if 2) it contains at least four local activations. A global event fulfilling these two criteria is ignored in the calculation of DF (its $\beta = 0$ in equation (12)). After five successive isolated global events, the update of DF is interrupted and its value is set to the mean of the 5 closest normal DF values (i.e. updated with $\beta_{m,m+1} = 1$, equation (12)). If these do not exist, DF is set to 50%, as long as the events remain isolated. The labelling rule for global events is

$$\begin{aligned} R(m) &\leqslant \mathrm{DF}(m) \Rightarrow A \text{ events} \\ R(m) &> \mathrm{DF}(m) \Rightarrow V \text{ events.} \end{aligned} \tag{13}$$

Once global events have been labelled, the procedure is repeated for local events (figure 5(b)). $R(m)$ is recomputed over a 21-sample window around the $E_i^{25,90}$ maximum

and DF in equation (12) is recalculated for each channel. However, since a local event contains a single activation by construction, the second criterion to define isolated activation and to change the calculation of DF is ignored.

The labelling process is completed with tests of coherence. Local V events belonging to a global identified as A are labelled as A^*, except that if their ratio $R_i(m) > 75\%$, in which case they are labelled as V^* (figure 5(c)). On the other hand, local A in a global V are labelled as V^* unless their ratio $R_i(m) < 25\%$, in which case they are labelled as A^*. Afterwards, if all channels have a single activation in a global and if only one of these has a type differing from that of the global, it is changed. Finally, global events that contain some mismatched local activations (V^* in global A, or A^* in global V) are relabelled as a mixed (M) (figure 5(c)).

Step 11: final fiducial marker. To position the final fiducial marker associated with each activation, E_i^{90} is integrated from ${T^{\text{act}}}_{\text{on}}{}^i$ to ${T^{\text{act}}}_{\text{off}}{}^i$ and the marker is put down at the time where the cumulative energy reaches 50% of the total.

2.3.3. Noise monitoring: conditional filtering and threshold modulation. Three QoS functions are computed from the raw signal S_i: $\text{QoS}^{\text{Sat}}{}_i(n)$, acting to eliminate saturation episodes and to damp high-amplitude baseline wandering; $\text{QoS}_i{}^{35}(n)$, to measure medium (>35 Hz) to high-frequency flickering noise and trigger local low-pass filtering; $\text{QoS}_i{}^{\text{Art}}$, measuring the unfiltered low-to-medium frequency noise to modulate the detection thresholds. These functions provide a sample per sample evaluation of different features of the signals.

QoS_i^{Sat}. $\text{QoS}_i^{\text{Sat}}(n) \in [0, 1]$ (default value = 1) is a multiplicative function convoluted with the raw derivative (to produce D_i^a from D_i°, step 2 in figure 2). It is meant to detect both saturation and large amplitude baseline wandering. First, $\text{QoS}_i^{\text{Sat}}$ is set to 0 along each segment where S_i is outside 95% of the ±5 mV quantification limits. If two saturation epochs are closer than 100 ms, they are joined as a continuous saturated interval. Afterwards, to deal with baseline wandering, S_i is low-pass filtered at 2 Hz and each point where $\text{QoS}_i^{\text{Sat}}(n) \neq 0$ receives amplitude ($B(n)$) calculated as the difference between the maximum and the minimum in a window of 250 ms centred on sample n. $\text{QoS}_i^{\text{Sat}}$ is then calculated as

$$\text{QoS}_i^{\text{sat}}(n) = 1 - \max\left(0, \frac{B(n) - 700\ \mu V}{500\ \mu V}\right) * 0.25. \tag{14}$$

Finally, $\text{QoS}_i^{\text{Sat}}$ is smoothed by taking a moving average on a ±50 ms window. Thanks to the multiplication of the raw derivative by $\text{QoS}_i^{\text{Sat}}$, detection is maintained for short saturation intervals that may occur during real atrial activation, but is suppressed within and close to long-lasting saturation episodes. In addition, low-frequency large fluctuations of the baseline, which may interfere with the detection process, are damped.

QoS_i^{35}. $\text{QoS}_i^{35}(n)$ aims at reducing the local medium to high-frequency content of the derivative to avoid false detection in a noisy part of the signal while preserving the energy of real activations to maintain A versus V discrimination. S_i is first smoothed with a [1 2 3 2 1] moving average and then scanned to generate the list of all extrema with amplitude greater than 30 μV (in reference to the closest extremum on either side). In addition to its amplitude, each extremum is characterized by a local frequency, calculated as the inverse of the time from the previous to the next nearest extremum in the list. It is an instantaneous frequency that does not correspond to a sustained oscillation. Extrema with a frequency <35 Hz are discarded from the list, because the times between these peaks and their neighbours are in the range of those seen in real activations. To keep only extrema that can perturb the

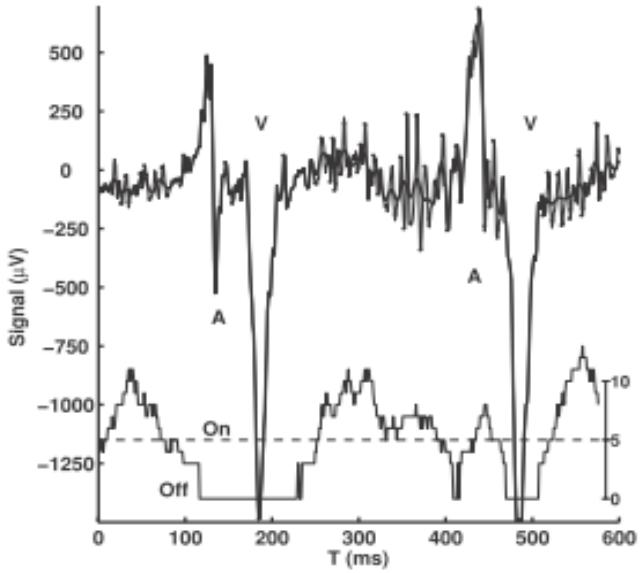

Figure 6. Conditional low-pass filtering. The extrema with a local frequency >35 Hz (dots on the signal, upper trace) are counted to obtain the function QoS^{35} (lower trace). Where $\mathrm{QoS}^{35} > 5$ (dashed line), local filtering is applied. The filtering remains off during most of the interval over which each activation occurs. The thick line on the upper trace is the signal after filtering.

energy significantly, the mean amplitude of the remaining peaks is computed over a 30 s window slid by 5 s steps. For each of these windows, a threshold is set at half this mean, with lower and upper limits of 30 and 100 μV, respectively. All extrema with amplitude less than this threshold are considered harmless and are removed from the list. Finally $\mathrm{QoS}_i^{35}(n)$ is defined as the number of remaining extrema in a centred window of 70 ms, which provides a measure of the local density of a high-frequency artefact. $\mathrm{QoS}_i^{35}(n) \geqslant 5$ indicates that the point lies in a region where fluctuations with frequency $\geqslant$35 Hz have been detected (figure 6). Within each such segment, D_i^a is low-pass filtered with a 35 Hz FIR (−6db cut-off, FIR1 function in Matlab) to produce D_i^b (step 2, figure 2). To avoid abrupt discontinuities at the ends of the filtered interval, each boundary is flanked by an interval of 7 samples on which a moving-average filter is applied. As seen in figure 6, filtering is most often not activated during activation, thereby preserving the energy of the event.

QoS_i^{Art}. $\mathrm{QoS}_i^{\mathrm{Art}}$ measures the density of harmful artefacts in the range of frequencies (<35 Hz) that were ignored by QoS^{35}. It serves to adjust the threshold of the second pass of detection on E_g^{90} (step 8) and the threshold for local activations (step 9). Ideally, only the peaks that do not correspond to real activation but are high enough to be potentially detected as false activations in the second pass should be counted. S_i is filtered with a nine sample moving filter ([123454321], −3db cut-off at 33 Hz), all the extrema are extracted and their amplitude and frequency are computed as for $\mathrm{QoS}_i^{35}(n)$. Those with a frequency of $\geqslant$35 Hz are ignored. The mean value ($\overline{A}$) and the standard deviation (σ) of the amplitude of the remaining peaks are computed in 30 s windows moved by 5 s steps. $\overline{A}$ is either increased to 40 μV or decreased to 100 μV if it is outside the [40, 100] μV interval. Then all the peaks with amplitude less than $\overline{A}$ are discarded, since they are too low to interfere with the detection. Besides, within each global found in pass 1 (from $\mathrm{TPeak}_{\mathrm{on}}$ to $\mathrm{TPeak}_{\mathrm{off}}$), the mean amplitude of the remaining peaks is calculated, and all those which are greater than this mean plus σ are also ignored. These are

potentially real activations that should not be used to measure noisy fluctuation in the signal. Finally, $QoS_i^{Art}(n)$ is computed as 100*(the number of remaining peaks in a centred $\pm$100 ms window)/(the number of samples in the window). QoS_i^{Art} is used to adjust the threshold for each channel (step 9, equation (10)), and $QoS^{Art} = \sum QoS_i^{Art}$ acts on the threshold of the second pass of detection of the global (step 8, equation (9)).

2.4. Method used to set the value of the parameters

The choice of the parameters' value in different steps of the detection method was based on a compromise between T+ and F− rates, with an emphasis on the detection of PAA specific to the context of monitoring for FA. It was done through an iterative process involving repeated detailed examination of all false and missed detections in the training set, as well as of the characteristics of the signals in the region where these were occurring. A large validation set was constructed to test the validity of the final set of parameters. Regarding the method for labelling activations, the limits of the band width (6–90 Hz, 6–25 Hz) of the two filters to discriminate *A* and *V* activations were changed systematically to determine the optimal values.

3. Results

3.1. Training set and optimization

The development and optimization of the algorithm was based on a training set of 19 recordings of 5 min from distinct patients, selected to be representative of the various waveforms and hindrances that could be encountered in the timing process. In addition to usual problems such as saturation, noise and baseline wandering, they include isolated and burst of PAA and PVA, as well as complex rhythms that often precede the onset of atrial fibrillation. The activation markers and their labels (A, V, PAA, PVA) were manually edited and validated by an expert in cardiology, for a total of 46014 events: 23246 A and 22768 V, including 2366 PAA and 472 PVA. To compare the training set validated markers (TM) with those obtained by the program (PM), the TMs were handled successively in time increasing order. The closest PM to a TM in a $\pm$10 ms window was considered as a true positive (T+). At the end of the procedure, the TMs not associated with a PM and the PMs not associated with a TM were counted as false negative (F−) and false positive (F+), respectively.

The first and second rows of table 1(A) show the performance that was reached by optimizing the parameters of the different steps of the method without the QoS functions. Their comparison illustrates the gain brought by the second pass of detection: an overall 21.5% increase in T+, with 7%, 26% and 11% improvement in the detection of A's, V's and PAA's, respectively, at the expense of 5% more F+. The two-pass method still produced 1.6% of F−, and 8.5% F+. On a 24 h recording of similar complexity ($\sim$173 000 activations at 60 bpm), this would still bring $\sim$3000 missed and $\sim$15 000 false events. Besides, 8.8% of the PAA were undetected.

At this point, it became clear that further improvement had to come from the pre-processing of the derivatives based on continuous indices quantifying the quality of the signal. Lines 3–5 of table 1 show the evolution of the performance as the different pre-processing procedures were activated. Baseline wandering correction and saturation detection (QoS^{Sat}) followed by [6, 90] Hz band-pass filtering reduced the number of F+ by 3.3% (line 3). Conditional low-pass filtering (QoS^{35}, line 4) brought an additional 1.7% decrease of F+. These functions, which remove false peaks in the local and global energy functions, act on F+ with minimal effect on F−.

Table 1. Performance of the detection in the test set. (A) Detection of activations with the different pre-processing functions on or off. NbP = 1, first pass of detection only, 2, two-pass; PBand refers to [5–90] Hz pass-band filtering. In the last three lines, coloured noise was added (see the text). (B) Labelling of T+ activations obtained at line six of A.

(A) Detection performance on the training set

							Detect	% T+	% F−	% F+	%T+ A	%T+ V	%T+ PAA
	Activations in the reference						**46014**				23246	22768	2366
	NbP	QSat	PBand	Q35	Clip	Q_Art					100%	100%	100%
(1)	1	Off	Off	Off	Off	Off	37005	76.9	23.2	3.6	90.7	62.7	80.2
(2)	2	Off	Off	Off	Off	Off	49174	98.4	1.6	8.5	97.7	99.0	91.4
(3)	2	On	On	Off	Off	Off	47598	98.2	1.78	5.23	97.6	98.8	90.8
(4)	2	On	On	On	Off	Off	46829	98.2	1.8	3.57	97.5	98.9	90.7
(5)	2	On	On	On	On	Off	47631	99.48	0.52	4.03	99.47	99.5	96.79
(6)	2	On	On	On	On	On	**46818**	**99.42**	**0.58**	**2.51**	**99.4**	**99.4**	**96.24**
(7)	1	On	On	On	On	Off	43107	91.43	8.57	2.25	93.6	89.2	92.5
(8)	N(0, 100 μV)			All_On			47941	98.83	1.17	5.35	98.7	98.95	94.3
(9)	N(0,100 μV)Q35			On	Q_Art	Off	49920	98.98	1.02	9.51	98.7	99.1	95.3
(10)	N(0100 μV) Q35			Off	Q_Art	Off	89016	99.64	0.36	93.8	99.8	99.5	99.1

(B) Labelling

	Activation in reference	% T+	% labelled as A	% labelled as V
A	23 246	99.41	95.91	4.09
V	22 768	99.42	1.0	99.0
PAA	2 366	96.24	92.71	7.29

A large fraction of the remaining F− was coming from recordings where the energy of some channels was disproportionate, leading to tall global energy peaks. These peaks, picked in the first stage of the detection, were leaving pivots of such large amplitude that the threshold of the second pass was too high. This problem was solved by clipping the derivatives to diminish the disproportion between the amplitudes. As seen in line 5 of table 1, this lessens the number of F− by a factor of 3.5. However, this major improvement in F− and PAA detection (90.7–96.8%) came at the expense of a higher number of F+. The comparison of lines 5 and 7 shows both the necessity and the problem brought by the second pass of detection. It is needed, even after pre-processing, since there is still 8.57% of F− after the first pass (line 7). It decreased the F− to 0.52%, but doubled the number of F+.

The remaining F+ came mainly from noisy portions of the signals, with spurious crossings of the second pass threshold that had been lowered by the clipping. To correct this problem, we introduced a modulation of the thresholds by the QoS^{Art} function, active only on noisy portions of the signal. This last improvement reduced (line 6 of table 1(A)) the F+ number by a factor of 1.6 without much effect on the other indices, thereby preserving the low F− and the high PAA detection performance achieved by clipping the derivatives. It represents the final setting that was used to process the validation set. The comparison of lines 2 and 6 shows the total benefit of preconditioning the signals and their derivatives and of modulation of the thresholds. The F− and F+ numbers are improved by a factor of 2.8 and 3.4, respectively, with an additional 5% detection of PAA events. The best performances for the F− and PAA were obtained at line 5, with derivatives clipping and without threshold correction for low-frequency artefacts, but at the expense of greater F+. Around 60% of the final remaining F+ and F− came from 2 files, in which the fusion of A and V activations was the main source of error.

The labelling specificity for T+ A's, V's and PAAs is presented in table 1(B). The %T+ (99.4%) are the same for A and V activations, confirming the efficiency of the double-pass threshold. Moreover 95.9% and 99% of the A's and V's were correctly labelled. The 93% proportion of correctly labelled PAAs was also acceptable. Figure 5 illustrates a case of PAA in which strong sinus activations are followed by a burst PAAs with less amplitude and derivatives close to those of the V activations. Nevertheless, the algorithm was able to detect and label these activations correctly.

3.2. Validation set

The final optimized algorithm was tested on a larger set of data taken just before the onset of an AF, which is a moment where the heart rhythm is known to become more irregular and complex (Taylor *et al* 2002). Twenty-seven patients had a prolonged episode of AF (>30 min). A 2 h recording taken just before the onset of AF was extracted for each of these patients. Markers were determined with our algorithm and then validated successively by two persons supervised by an expert. From the original 81 segments available (27 patients*3 channels *2 h recordings), 2 were rejected because the electrodes were not attached to the atrium, providing electrograms similar to an ECG, and 1 because it was too noisy to be validated. The final validation set gathered 1593697 activations: 796913 A, 796784 V containing, respectively, 39705 PAA and 3157 PVA. As expected, the rate of PAAs over normal sinus beats (∼1/20) was very large, while the rate of PVA, which was ten times lower, nevertheless remained substantial. The comparison of the original and validated markers was done as for the training set.

The first line of table 2(A) summarizes the performance of the detection algorithm on the validation set. The %T+ is 99.93% for all events together and 99.83% for PAA. The method fulfils the objective of reaching a high level of V, A and PAA detection, while maintaining acceptable count of F+ (0.37%). Lines 2 and 3 confirm on the larger scale of the validation

Table 2. (A) Performance of the detection in the validation set. Same as table 1. In line 7, all functions were on, but each channel was processed alone. (B) Labelling of T+ activations obtained at line 1 of A.

(A) Detection performance on the validation set

							Detect	% T+	% F−	% F+	%T+ A	%T+ V	%T+PAA
		Activation in the reference					1593697				796913	796784	39705
	NbP	QSat	PBand	Q35	Clip	Q_Art					100%	100%	100%
(1)	2	On	On	On	On	On	**1598621**	**99.93**	**0.07**	**0.37**	**99.97**	**99.89**	**99.83**
(2)	1	Off	Off	Off	Off	Off	1171053	73.3	26.7	0.2	99.0	47.5	84.9
(3)	2	Off	Off	Off	Off	Off	1611807	99.63	0.37	1.5	99.7	99.56	97.3
(4)	2	On	On	Off	Off	Off	1600672	99.82	0.18	0.62	99.76	99.89	97.0
(5)	2	On	On	On	Off	Off	1596238	99.79	0.21	0.37	99.69	99.89	96.97
(6)	2	On	On	On	On	Off	1600962	99.94	0.06	0.52	99.97	99.9	99.84
(7)	Individual channels						1584860	98.78	1.22	0.67	98.63	98.93	98.35
(8)	N(0, 100 μV)						1635020	99.61	0.39	2.98	99.94	99.58	99.45

(B) Labelling

	Activation in reference	% T+	% labelled as A	% labelled as V
A	796 913	99.97	**99.89**	0.11
V	796 784	99.89	0.25	**99.75**
PAA	39 705	99.83	**99.30**	0.70
PVA	3 157	88.28	20.81	79.19

set the absolute necessity of the 2 passes/2 thresholds approach. For these two lines, all QoS functions were inactivated. Even if the rates of F+ (1.5%) and F− (%0.37) may already appear acceptable, they still represent ∼30 000 activations that would have to be corrected. In the training set, the %F+ was at 8.5% at this stage of the analysis because problematic cases were over-represented.

Lines 4–6 of table 2(A) document the effects of the different mechanisms of the pre-processing. As for the training set, clipping (line 6) yielded an additional three-fold reduction in F−, a 2% improvement in PAA. It was also highly recurrent since, for each patient, at least one channel was clipped in 28.5% of the normal A activations and in 37.2% of the PAA. However, it increased the number of F+. This detrimental effect was corrected by the modulation of the threshold by QoS^{Art} (i.e. line 6 versus line 1).

Table 2(B) demonstrates similar %T+ in the different classes of activation (99.97–99.83%) except PVA's, for which %T+ drops to 88.28%. The missed PVAs represent ∼1/3 of the missed V (366/992). Nearly all missed V arose from the fusion of the ventricular and the atrial activations, in which the V deflection was not detected within the simultaneous high amplitude A. It could come from the superposition of A and PVA, of a non-causal PAA and a V, or from instances where the intra-atrial and atrio-ventricular conduction times were close to one another. In fact, the length of integration windows for both global and local energies (equations (3) and (5)) set the limits below which distinct activations cannot be separated.

The two rightmost columns of table 2(B) sum up the performance of the labelling of the T+ activations. Globally, the percentage of correct labelling is beyond 99.75% for both A and V activations, and is 99.3% for PAA. Incorrectly labelled PAAs most often belonged to fast bursts of ectopy where some A's with depressed amplitude were coincident with V activation. In these cases, a single activation was detected, which might end up being classified as a V. Hence, these fusion events also created F− V activation in the table. The percentage of PVAs labelled as V was lower (79.2%). 86% of these labelling errors occurred in a single file, and were coming in a majority from A–V fusions in which a single activation was detected.

4. Discussion

The robustness of the algorithm was confirmed by comparing more than 1.5 million validated markers taken in 2 h before the onset of a prolonged FA, a period with unusual complex rhythms. To perform the huge validation task, an interactive program was developed. It can display on windows of adjustable time durations, the three channels, their activation markers, as well as different time series (e.g., AA, AV, VV) to locate and correct wrong or missing markers.

4.1. Noise filtering and detection threshold

A proper filtering method would aim to discard all fluctuations that do not correspond to activations, while preserving the energy content of real activation. The nature of the problem can be illustrated by comparing the 'false extrema', lying outside the limits of the global activation, to those occurring inside these limits. In the training set, 30% of these 'false extrema' had amplitude $>200\ \mu$V. For each 10 s intervals, the ratio of the mean amplitude of the activations to the mean amplitude of the 'false activations' was calculated for all channels in the training set, providing a measure of the signal-to-noise ratio. The cumulative distribution of these ratios is shown in figure 7(a). 7.5% of the activations had a ratio lower than 2, meaning that the rejection of 'false extrema' without losing real activations and creating of F− could not be based only on a criterion of amplitude. However, as shown in figure 7(b), the distribution of the local frequency of the 'false extrema' was also very different, with peaks around 5 Hz

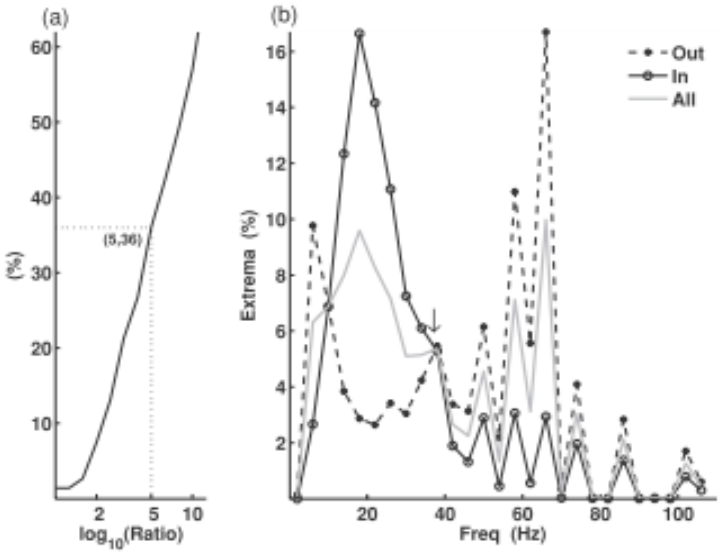

Figure 7. (a) Cumulative distribution (%) in the training set of the ratio of the amplitude of the activations to the amplitude of the extrema lying outside the global activations. The scale of the abscissa is logarithmic. (b) Distribution of the local frequency (defined in section 2.3.2) of all the extrema in the training set. Solid grey line: all extrema (Nb ∼229000). Solid dark line: extrema lying inside the limits of the global activations, from $T^{\text{act}}_{\text{on}}$ to $T^{\text{act}}_{\text{off}}$. Dash line: 'false extrema' outside the global activations. Ideally, these last ones should be filtered to avoid F+. To prevent the filtering of extrema potentially associated with real activation (dark line), filtering was triggered for extrema with a frequency above 35 Hz (arrow) if their local density was beyond a threshold.

and 60 Hz. The peak at 5 Hz was found to be associated with the T wave, corresponding to the repolarization of the ventricles. These extrema were eliminated by the uniform application of the [5–90] Hz pass-band filter. Comparing the distribution of frequencies inside and outside the global activations, we elected to filter the extrema with a frequency >35 Hz, provided that their density was high enough. As illustrated in figure 6, the conditional triggering of the filter governed by QoS^{35} indeed protected the section of the signal associated with activations. For the extrema in [5–35] Hz frequency range, potentially associated with real activations, the QoS^{Art} mechanism was introduced to adjust the threshold of the second pass depending on the density of low-frequency fluctuations.

The effect of QoS^{35} and QoS^{Art} was further investigated by adding coloured noise in all channels of the training set ($N(\mu = 0, \sigma = 100\ \mu\text{V})$ Gaussian noise, [0.05–120] Hz pass-band filtered). Deactivating both QoS^{35} and QoS^{Art} yielded to a shocking 93.8% of F+ (table 1, line 10), a consequence of the second pass threshold that was designed to detect low-amplitude events, but made the process highly sensitive to noise. QoS^{35} was highly effective, bringing a ten-fold reduction of the F+ (table 1, line 9, 9.51% F+). QoS^{Art} further halved the number of remaining F+.

4.2. Dynamic threshold

The statistics of tables 1 and 2 confirm that a two-pass detection algorithm is necessary. The activations undetected by the first pass, but identified by the second past, represent ∼50% of the V and ∼15% PAA. The ratio of the threshold of the first pass to the second pass ($\text{Thr}_1/\text{Thr}_2 = 11.1 \pm 0.7$) illustrates the huge variation of energy that makes this procedure indispensable.

The dynamical adjustment of the Thr_1 was also found to be essential. Amongst the patients, the ratio of maximum to minimum Thr_1 within the 2 h recordings was uniformly distributed between 2 and 15. There was also a 15-fold variation of the mean value of Thr_1, which shows that Thr_1 must be adapted in time within each patient, as well as between patients. This was even truer for Thr_2. The ratio of maximal to minimal Thr_2 was found to vary from 14 to 120 amongst the patients, with a 12-fold variation of the mean Thr_2 value.

4.3. Reduction of the number of active channels

Multi-channel recordings permit more robust event detection in particular when some channels become noisy or depressed. However, in a long-lasting recording, the signal of some leads may become transiently or permanently lost or degraded. The algorithm was tested in the worst situation where only one signal is left. In that case, the clipping of disproportionate activations (step 3) and the difference between local and global energy both disappear.

Line 7 of table 2(A) shows the detection performance for each channel analysed alone. The rate of detection remains excellent (T+ = 98.78% overall, 98.35% for PAA), but, as expected, the numbers of F+ and F− increase. The 17-fold increase of F− (from.07 to 1.22%) is misleading because 82% of these came from two electrodes, bringing 49% and 33% of the F−, respectively. The first of these channels had long intervals in which the signal was behaving as an ECG, with high amplitude V and very low amplitude A activations that were missed. The situation was inverted in the second channel, where V's were missed because their amplitude was very low with respect to A's. When a second channel was added, most of these F− were detected because they were embedded in global activation within which the low-threshold search was performed for each channel.

4.4. Final fiducial marker

The time of occurrence of the minimum temporal derivative (dV/dt_{min}) is the usual marker of activation for unipolar electrograms because it corresponds to the moment where the activation front travels beneath the electrode (Hélie *et al* 2003). However, it is less appropriate for a remote signal such as the V deflection where it depends on the position of the electrode relative to ventricular activation fronts (Gulrajani 1998). We have chosen to position the final fiducial marker at the time of median cumulative energy within each activation. For A activations, the difference between the median energy marker and the position of dV/dt_{min} was stable with a difference of the order of the 2 ms sampling time (2.7 ± 1.4 ms, median 2.4 ms). Hence, if dV/dt_{min} is needed, it can be taken as the minimum closest to median energy marker. The method also stabilizes the time markers associated with V activations when these are shallow, biphasic or with multiple notches. In these cases, dV/dt_{min} markers were often associated with spurious fluctuations of the AV and VV intervals that were suppressed with the median energy markers.

4.5. Source of errors and potential improvement

The major part of the residual 0.07% F− in the validation set was from events where the A and V activations were too close to be separated (most often a PAA and V, or a PVA and A). The global energy, which is a weighted average over an interval of ∼80 ms, was constructed to encompass all A activations of a cardiac beat together. Consequently, A and V activations closer than this interval ended up inevitably in the same global. However, they could still be detected in the search for local activation, which uses the local energies. The local energy is

a weighted average with sizeable contribution over an interval of ~40 ms, such that *A* and *V* events separated by less than ~50 ms can hardly be distinguished. In fact, this condition rarely occurs simultaneously on all channels, such that the two events were always detected on at least one channel. This was not reflected on the statistics of tables 1 and 2, which shows the performance for all channels taken together. In mixed globals in which A and V activations have been found in at least one channel, a deeper search could be performed on channels in which only one activation has been found. A higher sampling rate will certainly be helpful for these cases.

Clipping and the second pass make the system highly sensitive to noise, because it decreases the detection threshold to capture smaller activations. This problem was quite successfully dealt with by adjusting the threshold with $\mathrm{QoS}^{\mathrm{Art}}$. The function measures the local density of extrema in a range of amplitudes. In some cases, activations were missed in the second pass because the presence of high-density low-amplitude noise led to a large increase of the $\mathrm{QoS}^{\mathrm{Art}}$ function that raised too much the threshold. This largely explains the 2.98% F+ rate that was obtained when coloured noise was added to all channels of the validation set (line 8 of table 2(A)). $\mathrm{QoS}^{\mathrm{Art}}$ could be improved by weighting the contribution of each extremum by a measure of the local signal-to-noise ratio. The latter could be evaluated from the portions of the signal outside the global events found in the first pass of detection.

4.6. Comparison with other methods

Our problem of detection and labelling is somewhat similar to that encountered in the analysis of signals recorded by an implantable cardioverter defibrillator or pacemaker although their waveforms are different since their casing served as a reference electrode. Despite the high sampling rate usual in these devices, the low detection threshold, required to capture activations during atrial ectopy, tachycardia and fibrillation, often leads to false detections caused by noise or far-field R-waves (FFRW) (Kolb *et al* 2006).

To discriminate FFRW from activations, clustering-based methods using amplitude and minimum derivative have been proposed (Lewalter *et al* 2007, Padeletti *et al* 2005, Van Hemel *et al* 2004). Although often appropriate, this approach was clearly failing for some of our patients. In figure 8(a), the plot of activation amplitude versus $\mathrm{d}V/\mathrm{d}t_{\mathrm{min}}$ shows a continuous spectrum, thus invalidating separation by clustering. However if PAAs were removed, A and V events could indeed be separated. This is not the case in figure 8(b), where V activations fall in between two separated clusters of A activations. In both cases, our method based on energy frequency content was able to correctly label most of the activations.

Another study proposed to use A and V wave templates to detect and label the activations (Eberhardt *et al* 2006). The main goal of this study was to show that the activations were stable in sinus rhythm despite highly changing conditions (i.e. rest, supine and four levels of exercise), even if inter-individual variability was important. *A* and *V* templates were speculated to remain stable and different enough for the approach to be possible. Whereas the condition of stationarity of the waveforms might be respected during exercise, it is often not the case for the complex rhythms that frequently arise just before AF (e.g. figure 5). This makes the template approach less appropriate for our work.

In our case, the problem of noise faulty detections was enhanced since detection of V far-field activations had to be identified without the assistance of an ECG or of a ventricular electrogram because the three available channels of your Holter device were used to record the atrial electrograms. Convolution of the signal with a noise-driven filter has been proposed to reduce faulty detection (Eberhardt *et al* 2006). Unsteady noise level and energy content of the activations encountered in many of our recordings also hampered adaptive filtering approaches

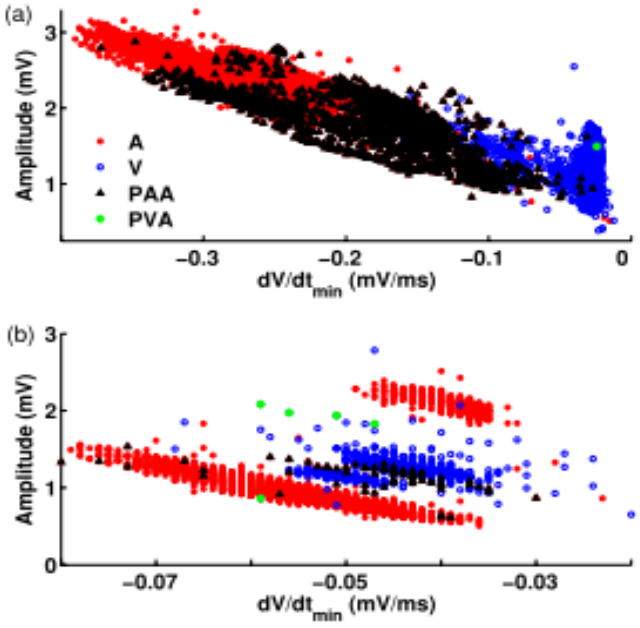

Figure 8. Dispersion of the amplitude and dV/dt_{min} of the activations from two channels from different patients. All activations from 2 h recording prior to AF onset are shown. (a) The A (red dot), V (blue circle) and PAA (black triangle) distributions form a continuous cluster, with PAA spread out between A and V. (b) PAA and V fall in a cluster between two separated clusters of A. In both cases, the activations were correctly identified as A or V by the discriminating function.

using either noise or activation templates (Thakor and Zhu 1991, Theres *et al* 2000). We elected to perform a continuous monitoring of the quality of the signal to guide local filtering, as well as threshold functions. The signal was blanked and clipped during episodes of saturation and low-pass filtering and threshold adjustment were performed according to the local density of extrema. As shown in table 1(A), this brought an improvement of the %F+ and %F− by a factor of 3.3 and 2.8, respectively. The weighting functions translating the action of the QoS function on the threshold were tuned to detect PAA and PVA even at the expense of some F+. These can also be adjusted for other requirements or different types of signals. From lines 5 and 6 in table 1(A) and lines 1 and 6 table 2(A), an alternative way to use threshold modulation by the QoS^{Art} function might be to start detection without adjustment for the low-frequency artefacts, which would be activated only if the detection appears to become erratic. Some additional criterion to trigger threshold adjustment would then have to be introduced.

5. Conclusion

Development of an automatic algorithm to process (i.e. detection and proper identification) complex cardiac signals is a challenge. The adverse recording conditions resulting in long duration signals of highly variable quality with varying waveform morphologies are the main obstacles. Moreover, cardiac arrhythmias and the superposition of waveforms of different origins make the labelling even more complex in some situations. The heuristic solution presented reaches an excellent level of accuracy. It achieves a high detection rate of premature atrial activations, which is critical for the study of electrical events preceding AF onset. The algorithm is robust to noise and minimizes the so-called blanking period over which the algorithm stops to search for activations. The labelling of the events of atrial and ventricular

events also reaches a very high level of correctness. The method will be used to analyse atrial electrophysiological events leading to AF, thereby providing a unique new direction of research on the mechanism of this challenging cardiac arrhythmia.

Acknowledgment

The authors gratefully acknowledge grants from the Canadian Institutes of Health Research and The Mathematics of Information Technology and Complex Systems (Mitacs, Canada).

References

Ak K, Akgun S, Tecimer T, Isbir C S, Civelek A, Tekeli A, Arsan S and Cobanoglu A 2005 Determination of histopathologic risk factors for postoperative atrial fibrillation in cardiac surgery *Ann. Thorac. Surg.* **79** 1970–5

Amar D, Shi W, Hogue C W Jr, Zhang H, Passman R S, Thomas B, Bach P B, Damiano R and Thaler H T 2004 Clinical prediction rule for atrial fibrillation after coronary artery bypass grafting *J. Am. Coll. Cardiol* **44** 1248–53

Amar D, Zhang H, Miodownik S and Kadish A H 2003 Competitive autonomic mechanisms precede the onset of postoperative atrial fibrillation *J. Am. Coll. Cardiol* **42** 1262–8

Asher C R, Miller D P, Grimm R A, Cosgrove D M 3rd and Chung M K 1998 Analysis of risk factors for development of atrial fibrillation after cardiac valvular surgery *Am. J. Cardiol.* **82** 892–5

Chamchad D, Djaiani G, Jung H J, Nakhamchik L, Carroll J and Horrow J C 2006 Nonlinear heart rate variability analysis may predict atrial fibrillation after coronary artery bypass grafting *Anesth. Analg* **103** 1109–12

Creswell L L, Schuessler R B, Rosenbloom M and Cox J L 1993 Hazards of postoperative atrial arrhythmias *Ann. Thorac. Surg* **56** 539–49

Dupont E, Ko Y, Rothery S, Coppen S R, Baghai M, Haw M and Servers N J 2001 The gap-junctional protein connexin40 is elevated in patients susceptible to postoperative atrial fibrillation *Circulation* **103** 842–9

Eberhardt F, Bonnemeier H, Lipphardt M, Hoffmann U G, Schunkert H and Wiegand U K 2006 Atrial near-field and ventricular far-field analysis by automated signal processing at rest and during exercise *Ann. Noninvasive Electrocardiol* **11** 118–26

Gulrajani R 1998 *Biolectricity and Biomagnetism* (New York: Wiley) chapter 7

Hayashida N, Shojima T, Yokokura Y, Hori H, Yoshikawa K, Tomoeda H and Aoyagi S 2005 P-wave signal averaged electrocardiogram for predicting atrial arrhythmia after cardiac surgery *Ann. Thorac. Surg* **79** 859–64

Hélie F, Vinet A and Cardinal R 2003 Spatiotemporal dynamics of reentrant ventricular tachycardias in canine myocardial infarction: pharmacological modulation *Can. J. Physiol. Pharmacol.* **81** 413–22

Hogue C W Jr, Domitrovitch P P, Stein P K, Despotis G D, Re L, Schuessler R B, Kleiger R E and Rottman J N 1998 RR interval dynamics before atrial fibrillation in patients after coronary artery bypass graft surgery *Circulation* **98** 429–34

Kolb C, Wille B, Maurer D, Schuchert A, Weber R, Schibgilla V, Klein N, Hummer A, Schmitt C and Zrenner B 2006 Management of far-field R wave sensing for the avoidance of inappropriate mode switch in dual chamber pacemakers: results of the FFS-test study *J. Cardiovasc. Electrophysiol.* **17** 992–7

Lewalter T, Tuininga Y, Frohlig G, Remerie S, Eberhardt F, Schmidt J, van Groeningen C and Wohlgemuth P 2007 Morphology-enhanced atrial event classification improves sensing in pacemakers *PACE* **30** 1455–63

Magee M J, Herbert M A, Dewey T M, Edgerton J R, Ryan W H, Prince S and Mack M J 2007 Atrial fibrillation after coronary bypass grafting surgery: development of a predictive risk algorithm *Ann. Thorac. Surg* **83** 1707–12

Maisel W H, Rawn J D and Stevenson W G 2001 Atrial fibrillation after cardiac surgery *Ann. Intern. Med* **135** 1061–73

Mathew J P, Fontes M L, Tudor I C, Ramsay J, Duke P, Mazer C D, Barash P G, Hsu P H and Mangano D T 2004 A multicenter risk index for atrial fibrillation after cardiac surgery *JAMA* **291** 1720–9

Padeletti L, Michelucci A, Frohlig G, Corbucci G, van Oort G and Barold S S 2005 Digital technology in cardiac pacing: methods for morphology analysis of sensed endocavitary signals *J. Intervent. Cardiac. Electrophysiol.* **14** 9–16

Pagé P, Dandan N, Savard P, Nadeau R, Armour J A and Cardinal R 1995 Regional distribution of atrial electrical changes induced by stimulation of extracardiac and intracardiac neural elements *J Thorac. Cardiovasc. Surg.* **109** 377–88

Pan J and Tompkins W J 1985 A real time QRS detection algorithm *IEEE Trans. Biomed. Eng.* **32** 230–6

Passman R, Beshai J, Pavri B and Kimmel S 2001 Predicting post-coronary bypass surgery atrial arrhythmias from the preoperative electrocardiogram *Am. Heart J.* **142** 806–10

Pichlmaier A M, Lang V, Harringer W, Heublein B, Schaldach M and Haverich A 1998 Prediction of the onset of atrial fibrillation after cardiac surgery using the monophasic action potential *Heart* **80** 467–72

Svedjeholm R and Håkanson E 2000 Predictors of atrial fibrillation in patients undergoing surgery for ischemic heart disease *Scand. Cardiovasc. J.* **34** 516–21

Taylor A D, Groen J G, Thorn S L, Lewis C T and Marshall A J 2002 New insights into the onset mechanisms of atrial fibrillation and flutter after coronary artery bypass graft surgery *Heart* **88** 499–504

Thakor N V and Zhu Y S 1991 Applications of adaptative filtering to ACG analysis: noise cancellation and arrhythmia detection *IEEE Trans. Biomed. Eng.* **38** 785–94

Theres H, Sun W, Combs W, Panken E, Mead H, Baumann G and Stangl K 2000 P wave and far-field R wave detection in pacemaker patient atrial electrograms *PACE* **23** 434–40

Tremblay G and LeBlanc A R 1985 Near optimal preprocessing for positive cardiac arrhythmia identification *IEEE Trans. Biomed. Eng.* **32** 141–51

Tsikouris J P, Kluger J, Song J and White C M 2001 Changes in P-wave dispersion and duration after open heart surgery are associated with the peak incidence of atrial fibrillation *Heart Lung* **30** 466–71

Tuzcu V, Nas S, Borklu T and Urgur A 2006 Decrease in the heart rate complexity prior to the onset of atrial fibrillation *Europace* **8** 398–402

Van Hemel N M, Wohlgemuth P, Engbergs J G, Lawo T, Nebaznivy J, Taborsky M, Witte J, Boute W, Munneke D and van Groeningen C 2004 Form analysis using digital signal processing reliably discriminates far-field R waves form P waves *PACE* **27** 1615–24

Vigmond E J, Tso V, Ying Y L, Page P and Vinet A 2009 Estimating atrial action potential duration from electrograms *IEEE Trans. Biomed. Eng.* **56** 1546–55

Vikman S, Lindgren K, Makikallio T H, Yli-Mayry S, Airaksinen K E and Huikuri H V 2005 Heart rate turbulence after atrial premature beats before spontaneous onset of atrial fibrillation *J. Am. Coll. Cardiol.* **45** 278–84

Villareal R P, Hariharan R, Liu B C, Kar B, Lee V V, Elayda M, Lopez J A, Rasekh A, Wilson J M and Massumi A 2004 Postoperative atrial fibrillation and mortality after coronary artery bypass surgery *J. Am. Coll. Cardiol* **43** 742–8

Zaman A G, Archbold R A, Helft G, Paul E A, Curzen N P and Mills P G 2000 Atrial fibrillation after coronary artery bypasses surgery a model for postoperative risk stratification *Circulation* **101** 1403–8

Déclaration de tous les coauteurs autre que l'étudiant

1. Identification de l'étudiant

   Feng Xiong

2. Nom de l'unité académique

   Institut de génie biomédical, département de physiologie, faculté des médicine

3. Nom de programme

   Ph.D. en génie biomédical

4. Description de l'article

   Ordre des auteurs : B Dubé, A Vinet, F Xiong, Y Yin, A-R LeBlanc, P Pagé

   Titre de l'article : Automatic detection and classification of human epicardical atrial unipolar electrograms

   Revues de publication : Physiol. Meas. 20(009) 1303-1325

   État actuel de l'article : Publié

<u>Déclaration de tous les coauteurs autre que l'étudiant</u>

À titre de coauteur de l'article identifié ci-dessus, je suis d'accord pour que FENG XIONG inclue cet article dans sa thèse de doctorat qui a pour titre : Mechanism and Prediction of Post-Operative Atrial Fibrillation Based on Atrial Electrogram

ANNEXE II

Stimulation at x=0

$$T(x) = P + c\int_{o}^{x} \left(1 + e^{-\alpha(T(y)-cy)}\right)dy$$

Z=T(y)/c, Z(0)=P/c

$$Z(x) = \frac{P}{c} + \int_{o}^{x} \left(1 + e^{-\alpha c(Z(x)-y)}\right)dy$$

$$Z(x) = \frac{P}{c} + x + \int_{o}^{x} e^{-\alpha c(Z(x)-y)}dy$$

$$Z(x) - x = \frac{P}{c} + \int_{o}^{x} e^{-\alpha c(Z(x)-y)}dy$$

U(x)=Z(x)-x, U(0)=P/c

$$U(x) = \frac{P}{c} + \int_{o}^{x} e^{-\alpha cU(x)}dy$$

$$e^{\alpha cU(x)}\frac{dU(x)}{dx} = \frac{1}{\alpha c}\frac{de^{\alpha cU(x)}}{dx} = 1$$

$$e^{\alpha cU(x)} - e^{\alpha P} = \alpha cx$$

$$e^{\alpha cU(x)} = \alpha cx + e^{\alpha P}$$

$$U(x) = \frac{1}{\alpha c}\ln\left(\alpha cx + e^{\alpha P}\right)$$

$$T(x) = cx + cU(x) = \frac{1}{\alpha}\ln\left(\alpha cx + e^{\alpha P}\right) + cx$$

$$CTA_{RL}(x) = T(x) - T(0) = cx + \frac{1}{\alpha}\ln\left(\alpha c x + e^{\alpha P}\right) - P$$

$$CTA_{RL}(L) = cL + \frac{1}{\alpha}\ln\left(\alpha c L + e^{\alpha P}\right) - P$$

Stimulation at x=L

$$T(x) = P + c\int_0^x \left(1 + e^{-\alpha(T(y)+cy)}\right)dy$$

By the same procedure

Z=T(y)/c

$$Z(x) = \frac{P}{c} + x + \int_L^x e^{-\alpha c(Z(x)+y)}dy$$

U(x)=Z(x)-x, U(0)= P/c

$$U(x) = \frac{P}{c} + \int_L^x e^{-\alpha c(U(x)+2x)}dy$$

$$\frac{dU(x)}{dx} = e^{-\alpha c(U(x)+2x)}$$

$$\frac{de^{\alpha cU(x)}}{dx} = \alpha c e^{-\alpha c 2x}$$

$$e^{\alpha cU(x)} - e^{\alpha P} = -(e^{-\alpha c 2x} - 1)/2$$

$$e^{\alpha cU(x)} = \frac{(1 - e^{-\alpha c 2x})}{2} + e^{\alpha P}$$

$$U(x) = \frac{1}{\alpha c}\ln\left(\frac{(1 - e^{-\alpha c 2x})}{2} + e^{\alpha P}\right)$$

$$T(x) = cU(x) + cx = \frac{1}{\alpha}\ln\left(\frac{(1-e^{-\alpha c2x})}{2} + e^{\alpha P}\right) + cx$$

$$CTA_{LR} = T(x) - T(0) = \frac{1}{\alpha}\ln\left(\frac{(1-e^{-\alpha c2L})}{2} + e^{\alpha P}\right) + cL - P$$

Hence

$$CTA_{RL}(L) - CTA_{LR} = \frac{1}{\alpha}\ln\left(\alpha cL + e^{\alpha P}\right) - \frac{1}{\alpha}\ln\left(\frac{(1-e^{-\alpha c2L})}{2} + e^{\alpha P}\right) \geq 0$$

If

$$2\alpha cL \geq 1 - e^{-\alpha c2L}$$

which is always true.